

**FOSSIL
FUELS
MANAGEMENT**

**DOE/MC/08383-45
Vol. 1 of 2**

**LITTLE KNIFE FIELD CO₂ MINITEST, BILLINGS COUNTY, NORTH DAKOTA
Final Report
Volume I: Technical Report**

Work Performed for the Department of Energy
Under Contract No. DE-AC21-79MC08383

Date Published—July 1983

Gulf Oil Exploration and Production Company
Oklahoma City, Oklahoma



**National Petroleum Technology Office
U.S. DEPARTMENT OF ENERGY
Tulsa, Oklahoma**

DISCLAIMER

This report was prepared as an account of work sponsored by an agency of the United States Government. Neither the United States Government nor any agency thereof, nor any of their employees, makes any warranty, expressed or implied, or assumes any legal liability or responsibility for the accuracy, completeness, or usefulness of any information, apparatus, product, or process disclosed, or represents that its use would not infringe privately owned rights. Reference herein to any specific commercial product, process, or service by trade name, trademark, manufacturer, or otherwise does not necessarily constitute or imply its endorsement, recommendation, or favoring by the United States Government or any agency thereof. The views and opinions of authors expressed herein do not necessarily state or reflect those of the United States Government.

This report has been reproduced directly from the best available copy.

DOE/MC/08383-45
Vol. 1 of 2
Distribution Category UC-92a

LITTLE KNIFE FIELD CO₂ MINITEST, BILLINGS COUNTY, NORTH DAKOTA
Final Report
Volume I: Technical Report

James E. Upton, *Principal Investigator*
Gulf Oil Exploration and Production Company
P.O. Box 24100
Oklahoma City, Oklahoma 73124

Kenneth L. Spence, *Technical Project Officer*
Bartlesville Energy Technology Center
P.O. Box 1398
Bartlesville, Oklahoma 74005

Work Performed for the Department of Energy
Under Contract No. DE-AC21-79MC08383

Date Published—July 1983

UNITED STATES DEPARTMENT OF ENERGY

TABLE OF CONTENTS

	<u>Page</u>
ABSTRACT.....	1
HISTORY OF PROJECT	2
INTRODUCTION	3
DRILLING, COMPLETION, AND WELL TESTING PROCEDURES	4
Zabolotny Injection Well No. 1	4
Observation Wells	7
Zabolotny Observation Well No. 1	7
Zabolotny Observation Well No. 2	10
Zabolotny Observation Well No. 3	11
LABORATORY DETERMINATION OF CO ₂ -WATER DISPLACEMENT PARAMETERS	14
FOUR WELL MULTI-WELL PULSE TEST	16
RESERVOIR GEOLOGY	18
Lithology	18
Carbonate Cycles	20
Diagenesis	20
Reservoir Specific	24
Structure	24
Pore and Throat System	26
EQUIPMENT AND INSTRUMENTATION	29
CO ₂ Injection System	29
Water Injection System	30
Fluid Sampling System	30
SIMULATION MODELS	31
CO ₂ -WATER INJECTION DESIGN	32
FLUID INJECTION	34
LOGGING PROGRAM	35
FLUID SAMPLING PROGRAM	38
PRESSURE CORING	40
Zabolotny Observation Well No. 4	40
MINITEST SIMULATION	46
SWEEP EFFICIENCY	52

TABLE OF CONTENTS

	<u>Page</u>
COMMERCIALIZATION OF THE CO ₂ MISCIBLE DISPLACEMENT PROCESS	52
RESULTS OF SIMULATION STUDIES	53
OBSERVATION WELL SATURATION DATA ANALYSIS	54
CORROSION STUDY	57
CONCLUSIONS	60
ACKNOWLEDGEMENTS	60
REFERENCES	61

APPENDICES

1. Injection well no. 1 log suite.
2. Gulflog computation summary - injection well no. 1.
3. Core analysis report - injection well no. 1.
4. Fracture **detection: Core** vs. logs comparison Little Knife CO₂ project.
5. Temperature **log injection well no. 1.**
6. Results of **water injection** from cased hole log analysis in the injection well no. 1, **Little Knife Field CO₂** pilot test, North Dakota.
7. Dual spacing **thermal neutron** decay time (TDT log) - injection well no. 1.
8. Observation well no. 1 log suite.
9. Gulflog computation summary - observation well no. 1.
10. Core analysis report - observation well no. 1.
11. Interim report: Little Knife CO₂ minitest project multiwell pulse test report, Little Knife Field, North Dakota.
12. Dual spacing thermal neutron decay time (TDT log) - observation well no. 1.
13. Observation well no. 2 log suite.
14. Gulflog computation summary - observation well no. 2.
15. Core analysis report - observation well no. 2.
16. Dual spacing thermal neutron decay time (TDT log) - observation well no. 2.
17. Observation well no. 3 log suite.
18. Gulflog computation summary - observation well no. 3.
19. Core analysis report - observation well no. 3.
20. Dual spacing thermal neutron decay time (TDT log) - observation well no. 3.
21. Log-flow-log test results on observation wells no. 1, 2 and 3.
22. Reservoir and formation characterization Little Knife CO₂ minitest project.
23. Depositional facies, diagenesis and reservoir character of the Mission Canyon Formation (Mississippian) of the Williston Basin at Little Knife Field, North Dakota.
24. Semi-log plot of pore throat radii (microns) vs. percent of throats (48 analyses, 12 from each well).
25. Special core analysis - injection well no. 1.

26. Special core analysis - observation well no. 1.
27. Special core analysis - observation well no. 2.
28. Special core analysis - observation well no. 3.
- 29.* Little Knife Field CO₂ minitest water injection simulation, Billings County, North Dakota.
- 30.* Design of a CO₂-water injection program for the Little Knife CO₂ flood minitest.
- 31.* Little Knife CO₂ flood residual oil and CO₂-water relative permeability measurements.
32. Daily fluid injection data - rates, volumes, and pressures.
33. Little Knife CO₂ minitest - logging report.
34. Dual spacing thermal neutron decay time (TDT), gradiomanometer, and cased reservoir analysis logs - observation well no. 1.
35. Dual spacing thermal neutron decay time (TDT), gradiomanometer, and cased reservoir analysis logs - observation well no. 2.
36. Dual spacing thermal neutron decay time (TDT), gradiomanometer, and cased reservoir analysis logs - observation well no. 3.
37. Little Knife CO₂ minitest - fluid sampling report.
38. Daily drilling report for injection well no. 1 and observation wells no. 1, 2, 3 and 4.
39. Observation well no. 4 log suite.
40. Little Knife CO₂ minitest pressure-core well report.
41. Observation well no. 4 plug and donut analyses.
- 42.* Analysis of observation well no. 4 pressure-core data - Little Knife CO₂ project.
- 43.* Little Knife Field CO₂ minitest - compositional simulation report.
- 44.* An equation-of-state study on the fluid properties, phase behavior and multiple-contact miscibility in CO₂ displacement processes.
- 45.* Analysis of observation well saturation data, Little Knife CO₂ project.
46. Corrosion inspection of 2-7/8 inch tubing.
- 47.* Corrosion study for the Little Knife CO₂ minitest.

*APPENDICES AVAILABLE IN VOLUME II.

OTHER APPENDICES AVAILABLE ON OPEN FILE AT THE BARTLESVILLE ENERGY TECHNOLOGY CENTER, BARTLESVILLE, OKLAHOMA.

LIST OF FIGURES

	<u>Page</u>
FIGURE 1	Index map of the Williston Basin 65
FIGURE 2	Top of Mission Canyon Formation structure map 66
FIGURE 3	Little Knife CO ₂ minitest pattern 67
FIGURE 4	Little Knife CO ₂ minitest location 68
FIGURE 5	Casing and tubing settings in injection well no. 1 69
FIGURE 6	Modified tubing setting in injection well no. 1 70
FIGURE 7	Pressure history curve for injection well no. 1 71
FIGURE 8	Wellhead schematic of injection well no. 1 72
FIGURE 9	Wellhead schematic of observation wells 73
FIGURE 10	Casing and tubing setting in observation well no. 1 74
FIGURE 11	Pressure history curve for observation well no. 1 75
FIGURE 12	Casing and tubing settings in observation well no. 2 76
FIGURE 13	Pressure history curve for observation well no. 2 77
FIGURE 14	Casing and tubing settings in observation well no. 3 78
FIGURE 15	Pressure history curve for observation well no. 3 79
FIGURE 16	CO ₂ -water relative permeability, injection well no. 1. Extracted core, no oil present 80
FIGURE 17	CO ₂ -water relative permeability, injection well No. 1. Native state after CO ₂ flood 81
FIGURE 18	Four well multi-well pulse test response at observation well no. 1 82
FIGURE 19	Four well multi-well pulse test response at observation well no. 2 83
FIGURE 20	Four well multi-well pulse test response at observation well no. 3 84
FIGURE 21	Idealized depositional setting of Mission Canyon Formation at Little Knife Field 85
FIGURE 22	Basinal marine facies of the Mission Canyon Formation at Little Knife Field 85

LIST OF FIGURES

	<u>Page</u>
FIGURE 23	Open shallow marine facies of the Mission Canyon Formation at Little Knife Field 86
FIGURE 24	Transitional open to restricted marine facies of the Mission Canyon Formation at Little Knife Field 87
FIGURE 25	Restricted marine facies of the Mission Canyon Formation at Little Knife Field 87
FIGURE 26	Marginal marine facies of the Mission Canyon Formation at Little Knife Field 88
FIGURE 27	Intertidal buildup facies of the Mission Canyon Formation at Little Knife Field 89
FIGURE 28	Lagoon facies of the Mission Canyon Formation at Little Knife Field 90
FIGURE 29	Tidal flat/supratidal sabkha facies of the Mission Canyon Formation at Little Knife Field 91
FIGURE 30	Location of project interval within Mission Canyon Formation at Little Knife Field 92
FIGURE 31	North-south structural fence diagram of zones, A, B, C and D of the Mission Canyon Formation through cored wells in Little Knife Field 93
FIGURE 32	Type log of Mission Canyon Formation at Little Knife Field 94
FIGURE 33	Carbonate cycles of the Mission Canyon Formation at Little Knife Field 94
FIGURE 34	Events which deposited and modified the Mission Canyon Formation at Little Knife Field 95
FIGURE 35	Scanning electron micrograph of a pelletal ghost 96
FIGURE 36	Scanning electron micrograph of calcite crystals upon dolomite crystals 97
FIGURE 37	Simplified sequence of major events which are responsible for producing porous dolostones in the Mission Canyon Formation at Little Knife Field 98
FIGURE 38	Stratigraphic fence diagram of zones C and D of the Mission Canyon Formation through all minitest wells 99

LIST OF FIGURES

	<u>Page</u>
FIGURE 39	Close-up view of the reservoir rock in the Little Knife CO ₂ minitest 100
FIGURE 40	Photomicrographs of the reservoir rock in the Little Knife CO ₂ minitest in injection well no. 1 102
FIGURE 41	Photomicrographs of the reservoir rock in the Little Knife CO ₂ minitest in observation well no. 1 103
FIGURE 42	Photomicrographs of the reservoir rock in the Little Knife CO ₂ minitest in observation well no. 2 104
FIGURE 43	Core slabs of top of zone D reservoir rock from injection well no. 1 (9,817-9,819 feet) 105
FIGURE 44	Whole core porosity and permeability compared to lithology in each minitest well 106
FIGURE 45	Surface lineaments mapped throughout portions of Montana, western North Dakota and north- westernmost South Dakota 107
FIGURE 46	Surface lineaments from landsat photographs and aerial photographs in central and northern portions of Little Knife Field 108
FIGURE 47	Aerial view of nearest surface lineament next to the Little Knife CO ₂ minitest 109
FIGURE 48	Surface outcrop fractures measured at observation well no. 3 110
FIGURE 49	Fractures measured from oriented cores in the minitest project interval 111
FIGURE 50	Blocks of Sentinel Butte Formation illustrating surface fracture separation 112
FIGURE 51	Outcroppings of Sentinel Butte Formation, at observation well no. 3, where surface fracture strike directions and fracture separations were measured 113
FIGURE 52	Generalized illustration representing the average trends of fractures, not individual fractures, through the minitest area 114
FIGURE 53	Generalized illustration of the various pore types and associated throats in porous beds of Mission Canyon Formation 115

LIST OF FIGURES

	<u>Page</u>
FIGURE 54	Scanning electron micrographs of all four pore types in the Mission Canyon Formation at Little Knife Field 116
FIGURE 55	Scanning electron micrographs of relief pore casts of the four pore types in the Mission Canyon Formation at Little Knife Field 117
FIGURE 56	Scanning electron micrographs of relief pore casts from porous beds of Mission Canyon Formation at Little Knife Field 118
FIGURE 57	Scanning electron micrograph of a relief pore cast where two dolomite crystals grew toward each other, changing pore shape into a tetrahedral form 119
FIGURE 58	Average calculated pore throat radii and percent of throats, from core analysis, across the perforated interval in injection well no. 1 120
FIGURE 59	Average calculated pore throat radii and percent of throats, from core analysis, across the perforated interval in observation well no. 1 121
FIGURE 60	Average calculated pore throat radii and percent of throats, from core analysis, across the perforated interval in observation well no. 2 122
FIGURE 61	Average calculated pore throat radii and percent of throats, from core analysis, across the perforated interval in observation well no. 3 123
FIGURE 62	Representative individual samples of pore throat radii and percent of throats compared to the amount of porosity and permeability that is developed in injection well no. 1 124
FIGURE 63	Representative individual samples of pore throat radii and percent of throats compared to the amount of porosity and permeability that is developed in observation well no. 1 125
FIGURE 64	Representative individual samples of pore throat radii and percent of throats compared to the amount of porosity and permeability that is developed in observation well no. 2 126
FIGURE 65	Representative individual samples of pore throat radii and percent of throats compared to the amount of porosity and permeability that is developed in observation well no. 3 127

LIST OF FIGURES

		<u>Page</u>
FIGURE 66	Scanning electron micrographs of relief pore casts of each group of related pore throat radii sizes and their associated ranges of porosity and permeability	128
FIGURE 67	Pore-to-throat size ratios and pore-to-throat coordination numbers for porous beds of the Mission Canyon Formation	129
FIGURE 68	Layout of surface equipment of the Little Knife CO ₂ minitest site	130
FIGURE 69	CO ₂ injection system for the Little Knife CO ₂ minitest	131
FIGURE 70	Injection well no. 1 looking to the west	132
FIGURE 71	Fifty (50) ton capacity liquid CO ₂ truck	132
FIGURE 72	Line heater downstream of injection pump	133
FIGURE 73	CO ₂ gas meter shed downstream of the line heater	133
FIGURE 74	Manifold system at back of CO ₂ storage tanks	134
FIGURE 75	Water injection system for the Little Knife CO ₂ minitest	135
FIGURE 76	Salt water filter building and associated tanks	136
FIGURE 77	Injection well no. 1 looking to the east	136
FIGURE 78	Fluid sampling system for the Little Knife CO ₂ minitest	137
FIGURE 79	Pictorial representation of triangulation technique used in TDT log analysis	138
FIGURE 80	Fluid analysis results for observation well no. 1	139
FIGURE 81	Fluid analysis results for observation well no. 2	140
FIGURE 82	Fluid analysis results for observation well no. 3	141
FIGURE 83	Location of pressure core interval on observation well no. 4 sonic log	142

LIST OF FIGURES

		<u>Page</u>
FIGURE 84	Oil and water saturations from core analysis on injection well no. 1 and observation wells no. 1, 2, 3 and 4	143
FIGURE 85	Comparison of Gulflog vs. pressure-core oil saturations for observation well no. 4	144
FIGURE 86	Monitor log data (ϕ , S_o , S_w) at observation well no. 2 on June 30 th , 1981	145
FIGURE 87	Monitor log data (ϕ , S_o , S_w) at observation well no. 2 on July 14 th , 1981	146
FIGURE 88	Reservoir cross section grid based on whole-core porosity analysis	147
FIGURE 89	Oil differential formation volume factor and solution gas oil ratio at 245°F for Zabolotny 1-3-4A	148
FIGURE 90	Oil density and viscosity at 245°F, Zabolotny 1-3-4A	149
FIGURE 91	Phase boundary for oil-CO ₂ mixtures at 245°F, Zabolotny 1-3-4A	150
FIGURE 92	Pressure volume relationship at 245°F for oil-CO ₂ mixtures, Zabolotny 1-3-4A	151
FIGURE 93	Viscosity of oil-CO ₂ mixtures at 245°F, Zabolotny 1-3-4A	152
FIGURE 94	Density of oil-CO ₂ mixtures at 245°F, Zabolotny 1-3-4A	153
FIGURE 95	Coefficients of compressibility of reservoir oil with CO ₂ added at 245°F, Zabolotny 1-3-4A	154
FIGURE 96	Derived oil-water capillary pressure data	155
FIGURE 97	Relative permeability data for layer W	156
FIGURE 98	Relative permeability data for layer X	157
FIGURE 99	Relative permeability data for layer Y	158
FIGURE 100	Relative permeability data for layer Z	159
FIGURE 101	Coordinate system for the compositional simulation	160
FIGURE 102	Grid for the 11 x 11 x 4 simulator model	161

LIST OF FIGURES

	<u>Page</u>
FIGURE 103 Grid for the 16 x 15 x 4 simulator model	162
FIGURE 104 Simulator match of four-well pulse test response at observation well no. 1	163
FIGURE 105 Simulator match of four-well pulse test response at observation well no. 2	164
FIGURE 106 Simulator match of four-well pulse test response at observation well no. 3	165
FIGURE 107 Permeability-porosity relationship of core data and simulator data	166
FIGURE 108 Simulator match of the pressure-history at injection well no. 1	167
FIGURE 109 Simulator match of the pressure-history at observation well no. 1	168
FIGURE 110 Simulator match of the pressure-history at observation well no. 2	169
FIGURE 111 Simulator match of the pressure-history at observation well no. 3	170
FIGURE 112 Water saturation history match by layers for observation well no. 1	171
FIGURE 113 Water saturation history match by layers for observation well no. 2	172
FIGURE 114 Water saturation history match by layers for observation well no. 3	173
FIGURE 115 Simulator match of water saturation history for zone D at observation well no. 1	174
FIGURE 116 Simulator match of water saturation history for zone D at observation well no. 2	175
FIGURE 117 Simulator match of water saturation history for zone D at observation well no. 3	176
FIGURE 118 Measured CO ₂ contents from logs, separator gas analysis, and isotope analysis for observation well no. 1	177
FIGURE 119 Measured CO ₂ contents from logs, separator gas analysis, and isotope analysis for observation well no. 2	178

LIST OF FIGURES

	<u>Page</u>
FIGURE 120 Measured CO ₂ contents from logs, separator gas analysis, and isotope analysis for observation well no. 3	179
FIGURE 121 CO ₂ saturation history match (12-11-80 to 9-17-81) at observation well no. 1	180
FIGURE 122 CO ₂ saturation history match (12-11-80 to 9-17-81) at observation well no. 2	181
FIGURE 123 CO ₂ saturation history match (12-11-80 to 9-17-81) at observation well no. 3	182
FIGURE 124 Swelling factors of oil-CO ₂ mixtures at 245°F, Zabolotny 1-3-4A	183
FIGURE 125 Oil saturation history match by layers (12-11-80 to 9-17-81) for observation well no. 1	184
FIGURE 126 Oil saturation history match by layers (12-11-80 to 9-17-81) for observation well no. 2	185
FIGURE 127 Oil saturation history match by layers (12-11-80 to 9-17-81) for observation well no. 3	186
FIGURE 128 Oil saturation history match for zone D (12-11-80 to 9-17-81) in observation well no. 1	187
FIGURE 129 Oil saturation history match for zone D (12-11-80 to 9-17-81) in observation well no. 2	188
FIGURE 130 Oil saturation history match for zone D (12-11-80 to 9-17-81) in observation well no. 3	189
FIGURE 131 CO ₂ -free oil saturation profile (at reservoir conditions) on July 17, 1981, at observation well no. 4	190
FIGURE 132 Oil saturation profile (at stock tank conditions) on July 17, 1981, at observation well no. 4	191
FIGURE 133 Gas saturation distribution for layer Y at the end of CO ₂ injection (March 25, 1981)	192
FIGURE 134 Oil saturation distribution for layer Y at the end of CO ₂ injection (March 25, 1981)	193
FIGURE 135 Water saturation distribution for layer Y at the end of CO ₂ injection (March 25, 1981)	194

LIST OF FIGURES

		<u>Page</u>
FIGURE 136	Gas saturation distribution for layer Y on July 17, 1981	195
FIGURE 137	Oil saturation distribution for layer Y on July 17, 1981	196
FIGURE 138	Water saturation distribution for layer Y on July 17, 1981	197
FIGURE 139	CO ₂ -free oil saturation distribution (percentages) for layer Y on July 17, 1981	198
FIGURE 140	Oil recovery from the minitest by simulating production at the observation wells (four- layer model)	199
FIGURE 141	Water saturation history match for multiple- layer Y (12-11-80 to 9-17-81) at observation well no. 2 (six-layer model)	200
FIGURE 142	CO ₂ saturation history match for multiple- layer Y (12-11-80 to 9-17-81) at observation well no. 2 (six-layer model)	201
FIGURE 143	Oil saturation history match for multiple- layer Y (12-11-80 to 9-17-81) at observation well no. 2 (six-layer model)	202
FIGURE 144	Water saturation history match for combined layer Y (12-11-80 to 9-17-81) at observation well no. 2 (six-layer model)	203
FIGURE 145	Oil saturation history match for combined layer Y (12-11-80 to 9-17-81) at observation well no. 2 (six-layer model)	204
FIGURE 146	CO ₂ -free oil saturation profile (at reservoir conditions) on July 17, 1981 at observation well no. 4 (six-layer model)	205
FIGURE 147	Oil saturation profile (at stock tank conditions) on July 17, 1981 at observation well no. 4 (six-layer model)	206
FIGURE 148	Monitor log data (ϕ , S_o , S_w) at observation well no. 1 on August 25, 1981 (final monitor log)	207
FIGURE 149	Monitor log data (ϕ , S_o , S_w) at observation well no. 2 on September 16, 1981 (final monitor log)	208

LIST OF FIGURES

	<u>Page</u>
FIGURE 150 Monitor log data (\emptyset , S_o , S_w , S_g) at observation well no. 3 on September 17, 1981 (final monitor log)	209
FIGURE 151 Monitor log data (S_o , S_w , S_g , S_g -free) at a depth of 9,810 feet in observation well no. 1 vs. time	210
FIGURE 152 Monitor log data (S_o , S_w , S_g , S_g -free) at a depth of 9,813 feet in observation well no. 1 vs. time	211
FIGURE 153 Monitor log data (S_o , S_w , S_g , S_g -free) at a depth of 9,817 feet in observation well no. 1 vs. time	212
FIGURE 154 Monitor log data (S_o , S_w , S_g , S_g -free) at a depth of 9,860 feet in observation well no. 2 vs. time	213
FIGURE 155 Monitor log data (S_o , S_w , S_g , S_g -free) at a depth of 9,863 feet in observation well no. 2 vs. time	214
FIGURE 156 Monitor log data (S_o , S_w , S_g , S_g -free) at a depth of 9,867 feet in observation well no. 2 vs. time	215
FIGURE 157 Monitor log data (S_o , S_w , S_g , S_g -free) at a depth of 9,840 feet in observation well no. 3 vs. time	216
FIGURE 158 Monitor log data (S_o , S_w , S_g , S_g -free) at a depth of 9,843 feet in observation well no. 3 vs. time	217
FIGURE 159 Monitor log data (S_o , S_w , S_g , S_g -free) at a depth of 9,847 feet in observation well no. 3 vs. time	218

LIST OF TABLES

		<u>Page</u>
TABLE 1	Measurements of CO ₂ -water residual oil saturation and relative permeability, injection well no. 1	219
TABLE 2	Little Knife CO ₂ minitest fluid injection schedule	220
TABLE 3	Pre-injection waterflood residual-oil analysis, injection well no. 1	221
TABLE 4	Monitor log saturation data, layers X, Y and Z, for the observation wells	222
TABLE 5	Final monitor log saturation data, layers X, Y, and Z, for the observation wells	223
TABLE 6	Final monitor log saturation data, layer W, for the observation wells	224
TABLE 7	Sub-surface sample analysis, observation wells no. 2 and 3	225
TABLE 8	Separator gas analysis (N ₂ and H ₂ S free, mole percent) for observation well no. 1	226
TABLE 9	Separator gas analysis (N ₂ and H ₂ S free, mole percent) for observation well no. 1 (Continued)	227
TABLE 10	Separator gas analysis (N ₂ and H ₂ S free, mole percent) for observation well no. 2	228
TABLE 11	Separator gas analysis (N ₂ and H ₂ S free, mole percent) for observation well no. 2 (Continued)	229
TABLE 12	Separator gas analysis (N ₂ and H ₂ S free, mole percent) for observation well no. 3	230
TABLE 13	Separator gas analysis (N ₂ and H ₂ S free, mole percent) for observation well no. 3 (Continued)	231
TABLE 14	Water tracer analysis data for observation wells no. 1, 2 and 3	232
TABLE 15	CO ₂ isotope ratio analysis for injected CO ₂ , the three observation wells, and four field production wells surrounding the minitest	233
TABLE 16	Fluid properties of various coring fluid compositions with low slurry weight	234
TABLE 17	Spurt loss calculations for the coring fluids mentioned in Table 16	235

LIST OF TABLES

		<u>Page</u>
TABLE 18	Rheological and fluid-loss properties for various coring fluid compositions	236
TABLE 19	Spurt loss calculations for the coring fluids mentioned in Table 18	237
TABLE 20	Plug and donut analysis data for the observation well no. 4 pressure-core	238
TABLE 21	Pressure-core analysis, observation well no. 4	239
TABLE 22	Gulflog and core analysis comparison for all five minitest wells	240
TABLE 23	Oil composition and component parameters for the Peng-Robinson equation of state used in the simulator	241
TABLE 24	Binary interaction parameters for the Peng-Robinson equation of state used in the three-dimensional simulator	241
TABLE 25	Basic reservoir characteristic data, zone D of the Mission Canyon Formation in the Little Knife Field	242
TABLE 26	Physical properties of Little Knife Field reservoir fluids, Zabolotny 1-3-4A	242
TABLE 27	Distances and orientations of the production wells and observation wells relative to injection well no. 1	243
TABLE 28	Input data of reservoir rock properties of injection well no. 1 and observation wells no. 1, 2 and 3, as well pairs	244
TABLE 29	Percentages of oil displaced (at stock tank conditions) for layers W, X, Y and Z in the minitest area (radius = 283 feet)	245
TABLE 30	Input data of reservoir rock properties for layer Y in the six-layer model	246
TABLE 31	Carbon dioxide sweep efficiency	247
TABLE 32	Water analysis data from eight field production wells	248

LIST OF TABLES

		<u>Page</u>
TABLE 33	Physical properties and analysis of reservoir fluid from Zabolotny 1-3-4A	249
TABLE 34	Results of autoclave tests performed on various materials for corrosion study	250
TABLE 35	Results of autoclave tests performed on various materials for corrosion study (continued)	251
TABLE 36	Visual inspection results of surface and downhole tubulars and equipment	252
TABLE 37	Visual inspection results of surface and downhole tubulars and equipment (continued)	252
TABLE 38	Corrosion results of four (4) downhole flow-through racks, located throughout the field	253
TABLE 39	Corrosion results of two (2) downhole flow-through racks, located throughout the field and two (2) four inch (4") surface racks at the minitest site	254
TABLE 40	Corrosion results of six (6) four inch (4") surface racks located at a central production facility	255
TABLE 41	Corrosion results of seven (7) two inch (2") surface racks containing metal coupons, located throughout the field	256
TABLE 42	Corrosion results of one (1) two inch (2") surface rack containing metal coupons and four (4) two inch (2") surface racks containing coated coupons, located throughout the field	257
TABLE 43	Corrosion results of two (2) two inch (2") surface racks containing coated coupons at the minitest site	258
TABLE 44	Visual inspection results of tubing nipples recovered from observation well no. 3	258
TABLE 45	Independent laboratory results of pit-depth measurements made on corrosion nipples recovered from observation wells no. 2 and 3	259
TABLE 46	Corrosion results of wellhead equipment from observation well no. 1	260

FINAL REPORT
FOR THE
LITTLE KNIFE FIELD CO₂ MINITEST
BILLINGS COUNTY, NORTH DAKOTA

By

John B. Desch
Wayne K. Larsen
Robert F. Lindsay
Robert L. Nettle

Gulf Oil Exploration and Production Company
American First Tower
101 N. Robinson
P. O. Box 24100
Oklahoma City, Oklahoma 73124

ABSTRACT

A carbon dioxide (CO₂) minitest was conducted in the Mission Canyon Formation (lower Mississippian) at Little Knife Field, North Dakota. The Mission Canyon is a dolomitized carbonate reservoir which is undergoing primary depletion.

Four wells were drilled in an inverted four-spot configuration, covering five acres. The central well served as the injection well and was surrounded by three non-producing observation wells. Oriented cores were cut in each well for detailed reservoir characterization and laboratory testing. In addition, a well test program was conducted which involved two pulse tests and injectivity tests on the individual wells. Results from these tests were used as part of the input data for two reservoir simulation models. Various parameters in the computer models were varied to determine the most efficient injection plan for the specific reservoir characteristics.

A WAG-type injection sequence, selected on the basis of simulation studies, utilized five alternate slugs of formation water and CO₂. Preflush injection began December 11, 1980, followed by the WAG slugs from January 7 to March 25, 1981. Drive-water injection commenced immediately and was completed on September 24, 1981. Injection rates were maintained at 1,150 B/D during water injection and 40 T/D during CO₂ injection. Alcohol tracers were used during the waterflood preflush and with the water during the WAG injection period.

Fluid samples and cased-hole logs from each observation well, obtained on a periodic basis, were used to determine the advance of the injected fluids. In analyzing the data, it was evident that the injected waters and CO₂ did reach each

observation well. With the use of CO₂-isotope ratios, the arrival of the injected CO₂ at each observation well was accurately determined.

A pressure core behind the flood front was obtained to confirm residual oil saturations in the project interval. Overall rock recovery was excellent, 90 percent, but sample recovery under reservoir pressure was less than anticipated. Invasion of drilling fluids during coring was measured by introduction of a radioactive tracer into the coring fluid.

A compositional simulation model was used to history match the field performance of the CO₂ minitest. A detailed reservoir characterization was developed and used in the simulator to match bottom-hole pressures, water and CO₂ breakthrough times, and fluid saturation histories at the observation wells. The effects of gravity segregation, stratification and crossflow, and reservoir heterogeneity were also investigated.

The pattern sweep efficiency for carbon dioxide approached 52 percent in the minitest area. Displacement efficiency, as indicated by simulation study, was 50 percent of the oil-in-place at the start of the project, compared with an efficiency of 37 percent for waterflood. Thirty-one hundred (3100 SCF) cubic feet of CO₂ were required per incremental barrel of displaced oil. The absence of producing wells and the fact that only one zone within the Mission Canyon Formation was flooded, favorably influenced these figures.

The Little Knife CO₂ minitest confirmed, by field testing, the results of laboratory CO₂ miscible displacement tests. The minitest indicated that the CO₂ miscible displacement process has technical potential for commercialization in a dolomitized carbonate reservoir that has not been extensively waterflooded and has an indicated high remaining oil saturation.

HISTORY OF PROJECT

The United States Department of Energy on August 7, 1978, issued a request for proposal number EW-78-R-21-8383 entitled "Minitests of Carbon Dioxide Miscible Flooding Process". The objective of these minitests was to confirm by field testing the results of laboratory CO₂ miscible displacement tests and show that the CO₂ miscible displacement process had potential for commercialization in southwestern U. S. and Rocky Mountain area carbonate oil reservoirs that had not been extensively waterflooded and had a high remaining oil saturation. The Little Knife CO₂ minitest proposal was submitted after personnel from Gulf Science and Technology Company and Gulf Oil Exploration and Production Company verified that the CO₂ process was applicable. The cost-sharing contract was awarded on July 17, 1979. The project was anticipated to be completed in July, 1982.

A "Site Selection and Drilling Report" was presented to the DOE, as provided in the contract. Following acceptance of this report on August 10, 1979, an application was presented before the North Dakota Industrial Commission in August for approval of the project. Commission approval was granted on September 20. Under the National Environmental Policy Act of 1969 an environmental assessment was prepared and permit requests were then filed with the State of North Dakota and Billings County. Permission to drill the four minitest wells was given in September. The remainder of the first project year (July, 1979 - July, 1980) was utilized for design, laboratory work, and drilling of one injection well and three observation wells.

The first five months of the second project year involved surface facility construction, preparation for fluid injection, and submission of the "Well Test Report and CO₂ Injection Plan". Approval of the plan was given on November 19, 1980, and fluid injection began in early December. The balance of the second project year was spent injecting fluids.

Fluid injection continued through three months of the third project year and was finished on September 24, 1981. A fourth observation well was drilled within swept portions of the five-acre pattern. The surface equipment was dismantled and the wells plugged and abandoned during the next nine months. The final months were also used for compilation, interpretation, simulation, and documentation of the enormous amount of data collected during the previous two and one-quarter (2-1/4) years.

INTRODUCTION

Little Knife Field is located near the central portion of the Williston Basin (Fig. 1). The field is isolated within a broad, low lying, northward plunging anticlinal nose (Fig. 2). Closure on the east, north, and west is created by the gentle fold with stratigraphic entrapment forming closure to the south. Production is from dolomitized, porous beds of the Mission Canyon Formation. The primary recovery mechanism in the reservoir is fluid expansion with limited edge-water drive. Since discovery in January, 1977, to March, 1982, the field has produced 20.7 MMBO (41° API), 26.8 Tcf sour gas (1,250 GOR), and 3.4 MMBW.

The CO₂ minitest was a non-producing, five-acre field trial of the CO₂ miscible-displacement process, located in the center of the field (Fig. 2). The test pattern consisted of a single injection well offset by three observation wells in an inverted four-spot configuration (Fig. 3 and 4). The minitest involved time-lapse logging to monitor saturation changes as alternate slugs of water and CO₂ passed the three observation wells. A fourth observation well was drilled, pressure coring the project interval, within swept portions of the five-acre pattern. The resulting pressure-core saturations were used for comparison with log saturations. The minitest was designed to give the following information: 1) reduction in original oil saturation due to water injection, 2) reduction in waterflood residual-oil saturation due to alternate CO₂/water injection, 3) extent of gravity segregation, 4) effect of stratification and crossflow, and 5) influence of reservoir heterogeneity. This information will help assess the potential for a future field-wide fluid-injection project. Vertical and areal conformance of the injected slugs were determined as well as displacement efficiency. In lieu of actual production data, the day-to-day evaluation of project performance made use of a composition numerical reservoir-simulation model.

A large amount of work was done in support of this project by various groups within Gulf Oil Corporation. Each section in this final report represents a condensation of work reported by these groups on individual phases of the program. The appendices referred to throughout are the more detailed reports on each phase of the program.

DRILLING, COMPLETION AND WELL TESTING PROCEDURES

Zabolotny Injection Well No. 1

Zabolotny Injection Well No. 1 was spudded on December 5, 1979. A continuous directional survey was used to locate the bottom of the surface hole. Surface casing was cemented without difficulty. Drilling continued and coring depth was reached on December 28. The interval from 9,680-9,880 feet was cored. Coring operations were completed on January 1, 1980, and the hole was drilled to a total depth of 10,150 feet. Solids removal equipment was utilized in the drilling fluid program in all wells to reduce formation damage in order to obtain high quality, open-hole logs. The coring fluid and cement slurry programs were also designed to maximize test-data acquisition.

The open-hole logging suite for the injection well consisted of the following (Appendix 1):

1. Dual Laterolog-Micro-SFL with Gamma Ray and Caliper (DLL/MSFL).
2. Compensated Neutron-Formation Density with Gamma Ray and Caliper (CNL/FDC).
3. Borehole Compensated Sonic with Gamma Ray and Caliper (BHC).
4. Wave Forms-Variable Density (Wave Forms/VDL).
5. Fracture Identification Log with Gamma Ray (FIL).
6. Continuous Directional Survey (CDR).
7. Gyroscopic Multi-Shot Survey.

The gyroscopic multi-shot survey was run to total depth to compare with the continuous directional survey. Agreement between the two directional surveys was excellent. The multi-shot survey was used in the observation wells because it was judged to be more accurate.

The open-hole log calculations across the perforated interval 9,824 - 9,839 feet were:

$$\begin{aligned} S &= 23.1\% \\ S^w &= 76.9\% \\ \phi &= 20.0\% \end{aligned}$$

Whole-core porosity analysis across the same interval was:

$$\phi = 19.5\%$$

Log and core results on a foot-by-foot basis from this well are listed in appendices 2 and 3.

The fracture identification log (FIL) and wave forms-variable density log (wave forms-VDL) were both run to detect fractures in the Mission Canyon and were compared to oriented cores taken from the same interval. A fair comparison was obtained between oriented core fracture directions and fracture directions calculated from the logs. A summary of oriented core fracture directions and log calculated fracture directions, corrected for depth discrepancies, is presented in appendices 3 and 4.

Compared to the surface location, the bottom-hole location (at reservoir depth) in the injection well had a horizontal drift of 80 feet to the northwest, on an azimuth of 288° (Fig. 3).

After the well was circulated and cleaned up, a combination string of production casing was run and cemented. The casing was 5-1/2" OD, L-80, R-III, 8rd, LT&C. The weight below the DV collar was 23.0#/ft. and the weight above it was 17.0#/ft. (Fig. 5).

A completion rig was moved in on January 23, after the location was cleaned and covered with scoria. A cement bond log-variable density log with gamma ray (CBL-VDL-GR log) found good bonding throughout the Mission Canyon. A base thermal neutron decay time log (TDT) with gamma ray and casing collar locator, was run with five passes made to measure statistical variation. The casing was perforated at 9,824-9,839 feet, at a density of four shots per foot with 90-degree phasing, using the DLL/MSFL log for depth control. A perforation washer, with a mechanical collar locator, was run and each foot of perforations was swabbed and/or flowed until positive fluid entry was assured. The wellbore was cleaned by circulating with filtered salt water. The work string was laid down, and the production tubing string was run and set (Fig. 5).

The tubing was 2-7/8" OD, 6.5#/ft., C-75, R-2, CS-CB, coated internally with TK-2. Premium threads were used in order to get a bubble-tight seal. If any CO₂ were to leak into the casing, which was loaded with water, a severe corrosion problem would be likely. The tubing was coated for the same reason. The coating recommendation resulted from testing and prior field usage. Both Gulf and consulting service company personnel concurred on the coating. The various tubing nipples on the bottom of the packer assembly were run for a corrosion study. The nipples had been weighed and were to be reweighed after they were recovered at the end of the test. The nipples were isolated by special couplings so there would be no galvanic corrosion. The reentry guide was put on so that logging tools would be less likely to hang and/or damage the nipples. The landing nipples were made of Inconel 718. This alloy was one of the most corrosion-resistant materials tested. There were two landing nipples in the packer assembly and two in the tubing string. This arrangement permitted testing of the various components for leaks and provided a safe means for working on the well.

The packer and seal assembly had several features that were necessary. The packer had Nitrile packing elements and Viton O-rings. The seals were made of bonded Viton. These materials were used to combat the effects of CO₂. Additional seal units were used to allow the tubing to stretch and contract, depending on the type and temperature of the fluid injected.

Only one PTS (Pressure Transmission System) concentric chamber was run in the injection well. Two had been planned but "tight" spots in the casing made it

advisable to run only one (Fig. 6). The chamber was made of J-55 stock and was coated internally with TK-2. Capillary tubing, .094" OD, was run from the chamber to the surface. The capillary tubing was strapped to the 2-7/8" OD tubing, above and below every connection, and was connected directly to a recorder on the surface which gave a continuous reading and an intermittent printout of the chamber pressure. The pressure history for the injection well is shown in Figure 7. The capillary tubing was loaded with helium and a correction for this was made.

The contacted components of the casing fittings of the injection well were class "D" which was corrosion resistant in the presence of H₂S (Fig. 8). The tree had an Inconel-clad bore, which was NACE (National Association of Corrosion Engineers) rated for an H₂S atmosphere. The difference in design was possible because the fluid in the casing was static.

The well test procedure for the injection well consisted of: 1) a temperature survey, 2) log-inject-log tests, and 3) two pulse tests. The log portion of the log-inject-log test utilized the TDT log². The TDT log is a pulsed neutron tool that uses a neutron generator (minitron), which is a particle accelerator, to generate neutrons. The decay rate of the neutrons is a direct relationship of the neutron absorbers surrounding the tool. When the formation contains chlorine, or traces of boron and/or lithium, the absorption rate is much faster than formations without these elements. The absence of chlorine in hydrocarbons allows a distinction to be made between porous rocks containing oil and gas and those containing salt water, as well as determining their porosity and water saturation. By knowing the tools response to the formation, injected fluids, and formation fluids, the residual oil saturation after waterflooding can be determined. In addition, the interval affected by the injected fluids can also be detected. As stated above, a base TDT log was run before the casing was perforated. This log observed the TDT response to filtrate contamination by drilling and completion fluids.

Fifteen days later, the casing was perforated and approximately 100 barrels of oil produced with a perforation washer. Following this, a second TDT log was run to observe the dissipation of mud filtrate and other formation damage as the formation returned to original conditions. Next, 10 barrels of filtered produced salt water were injected at a rate of 30 barrels/hour. Temperature surveys were run during injection, at 23 minutes, 105 minutes, 165 minutes, and 225 minutes after injection. These surveys indicated that the injected fluid was confined to the project interval, with the majority entering into approximately the center 10 feet (Appendix 5). This injection profile was in good agreement with the forecast from the open-hole logs which showed that portion of the project interval to be most porous and permeable.

After completing the temperature surveys, a third TDT log was run, 50 barrels of filtered salt water were injected, and followed by a fourth TDT log. Flushing had not stabilized so an additional 50 barrels were injected and a fifth TDT log run. When run number five (5) was compared to run number four (4) no change in sigma was apparent, thus indicating the end of oil flushing due to water injection.

The TDT residual oil analysis was determined by comparing run number two (2) and run number five (5), and resulted in a volumetric weighted average of 41.1

percent residual oil across the perforated interval. The open hole log analysis resulted in a volumetric weighted average of 42.4 percent, with fairly uniform flushing. The results of communication analysis indicated that during injection some fluid communication occurred to the zone from 9,806-9,824 feet, located directly above the perforations. Fluids, however, were confined within the interval 9,806-9,839 feet, the basal portion of zone C and top portion of zone D (zonation defined below), with no migration through the bottom or top of this interval. A detailed description of the procedure and analysis can be found in appendix 6. The TDT logs are located in appendix 7.

The injection well was used as the injector for multi-well pulse tests initially involving the first two wells and later involving all four wells. Results of the two pulse tests are presented later in this report.

Observation Wells

Zabolotny Observation Well No. 1 was spudded on January 18, 1980, followed by Zabolotny Observation Well No. 2, on May 15, and Zabolotny Observation Well No. 3, on July 5. The solids removal equipment, coring fluid, and cement slurry programs employed in drilling the observation wells were the same as those used in the injection well.

The three observation wells required additional drilling time because they were directionally drilled so that the bottom-hole locations were evenly spaced from the injection well bottom-hole location. Even though all of the wells were drilled with the same bottom-hole assemblies, bit weights, rotating speeds at comparable depths, and the same rig and mud specifications, each drilled differently. Each observation well had to be oriented in a different direction (Fig. 3).

There were only minor differences between the completions of the injection and observation wells. All observation wells were equipped with two PTS concentric chambers. The pressures were checked in both chambers and a fluid gradient was calculated. The type of fluid in the bottom of the well was then known. One chamber also served as a back-up as well as a means of injecting chemical down-hole, if necessary. Gas-lift mandrels with wireline retrievable gas-lift valves were employed in the observation wells. These valves were needed when injected water reached the observation wells because there was not enough formation pressure to initiate flow. The wells were gas-lifted in order to obtain samples. The coating used in the observation wells was TK-7, as opposed to TK-2 in the injection well. Prior field experience at the Sacroc CO₂ project was the basis for the coating recommendations. The wellheads on the observation wells contained the same metallurgy as the injection well wellhead, the only difference was the valve arrangement (Fig. 9).

Zabolotny Observation Well No. 1

Coring depth for observation well no. 1 was reached on February 21, 1980. The interval from 9,737-9,853 feet was cored. Coring was completed on March 5 and the hole was drilled to a total depth of 10,213 feet. The open-hole logging suite was run and consisted of the following (Appendix 8):

1. Dual Laterolog-Micro-SFL with Gamma Ray and Caliper (DLL/MSFL).
2. Compensated Neutron-Formation Density with Gamma Ray and Caliper (CNL/FDC).
3. Borehole Compensated Sonic with Gamma Ray and Caliper (BHC).
4. Wave Forms-Variable Density with Gamma Ray (Wave Forms/VDL).
5. Fracture Identification Log with Gamma Ray (FIL).
6. Gyroscopic Multi-Shot Survey.

Open-hole log calculations across the perforated interval 9,809-9,824 feet were:

$$\begin{aligned}
 S &= 23.0\% \\
 S^w &= 77.0\% \\
 \emptyset &= 19.3\%
 \end{aligned}$$

Whole-core porosity analysis across the same interval was:

$$\emptyset = 19.5\%$$

Log and core results on a foot-by-foot basis from this well are listed in appendices 9 and 10.

Compared to the surface location, the bottom-hole location (at reservoir depth) in observation well no. 1 had a horizontal drift of 94 feet to the west-southwest, on an azimuth of 258° (Fig. 3). This bottom-hole location was 258 feet from the injection well bottom-hole location (at reservoir depth), to the northeast on an azimuth of 49°.

A combination string of production casing was run and cemented after the well was circulated and cleaned up. The casing program in the observation wells was slightly different from the injection well. Below the DV collar the casing was 5-1/2" OD, 23#/ft, N-80, R-III, 8rd, LT&C and above the DV collar the casing was 5-1/2" OD, 17#/ft, L-80, R-III, 8rd, LT&C (Fig. 10).

A workover rig was moved in on March 17 to begin completing the well. The CBL-VDL-GR log response was almost the same as that from the injection well. A base TDT log was run from PBD of 10,126 feet to 9,600 feet. The casing was perforated from 9,809-9,824 feet, at a density of one shot per foot with 0-degree phasing. The perforation washer was utilized to swab each foot of perforations until oil production was verified. A bit was run to plugged-back total depth (PBD) and the well was circulated with filtered salt water. The work string was pulled, the production tubing string was run, and the PTS chambers were hooked-up to the recorder (Fig. 10). The pressure history for observation well no. 1 is shown in figure 11.

As part of a reservoir and formation characterization program, a multiwell pulse test was conducted in April and May, 1980³. The injection well and observation well no. 1 were used in this test.

Background pressure data had to be collected prior to the test. A plug choke was run and set in the landing nipple above the PTS chambers so that wellbore effects would be minimized. The bottom-hole pressures in the observation well indicated that the plug was leaking so the tubing was loaded with water. The leak continued so the plug was pulled. The tubing was gas-lifted using nitrogen but the well would not flow. Coiled tubing, with a special end fitting to protect the tubing coating, was run and the tubing was unloaded to a depth of about 9,000 feet. The well would not flow. The casing was re-perforated from 9,809-9,824 feet on April 30, 1980, using a 2" OD gun loaded with 6.5-gram charges. Density was one shot per foot with 0-degree phasing. The well was opened and flowed for clean-up.

By injecting filtered salt water into the injection well, at a rate of 1,964 BWPD for two hours, a pulse was created in the reservoir that was monitored in the observation well. The initial response from this pulse arrived at the observation well in 30 minutes and peaked in 175.8 minutes, with a maximum amplitude of 17.600 psi. The pressure system used a 0-15,000 psia quartz sonde which was totally electronic. It had a sensitivity (ability to detect a change in pressure) of 0.001 psi. The analysis of the response provided the following: 1) transmissibility = 3,587 md-ft/cp, 2) diffusivity ($k/u\phi c$) = 40.703×10^6 md-psi/cp, and 3) storage capacity (ϕch) = 88.138×10^{-6} ft/psi. The primary conclusions from the analysis of the pulse test were:

1. Fluid communication did exist between injection well no. 1 and observation well no. 1.
2. There was no fracture continuity between the wells.
3. The effective hydraulic thickness of the project interval included the perforated interval and a dolomitized lobe above. The interval had an average thickness of 26.0 feet between the injection well and observation well.
4. The project interval of the Mission Canyon in the minitest area (9,806-9,839 feet, injection well depths) would confine fluids, i.e., no vertical migration of fluids would occur through its top or base.

Additional information is contained in appendix 11.

As the pulse test was being completed, the observation well no. 1 wellhead was damaged which necessitated killing the well with filtered salt water. The capillary tubing and wellhead were repaired but the gas-lift valves would not work. The tubing string had to be pulled and the valves replaced.

As a result of these incidents, the log-flow-log test was delayed approximately one month. As previously mentioned, the first TDT log was run prior to perforating the casing. Since that time, a total of 1,168 barrels of fluid had been produced. The log-flow-log test procedure was then carried out as follows:

TDT log Run No. 2
Flow 29 barrels of fluid

TDT log Run No. 3
Flow 32 barrels of fluid

TDT log Run No. 4
Flow 98 barrels of fluid

TDT log Run No. 5

The well was flowed in order to clean the perforations, dissipate formation damage, and re-establish, as nearly as possible, original fluid saturations around the wellbore. By monitoring saturations changes with the TDT log, it was determined that the saturations did return to near original. A copy of the TDT logs can be found in appendix 12.

The surface locations for the remaining two observation wells were relocated to their present surface positions after the pulse test and oriented core data from the injection well and observation well no. 1 were analyzed (Fig. 3).

Zabolotny Observation Well No. 2

Drilling of observation well no. 2 progressed smoothly during the months of May and June. Coring depth was reached on June 23 and the interval from 9,775-9,893 feet was cored. Coring was completed on the 26th, and the hole was drilled to a total depth of 10,150 feet. The following logs were run (Appendix 13):

1. Dual Laterolog-Micro-SFL with Gamma Ray and Caliper (DLL/MSFL).
2. Compensated Neutron-Formation Density with Gamma Ray and Caliper (CNL/FDC).
3. Borehole Compensated Sonic with Gamma Ray and Caliper (BHC).
4. Gyroscopic Multi-Shot Survey.

The fracture identification log (FIL) and wave forms-variable density log (waveforms-VDL) were both run in the injection well and observation well no. 1. Sufficient data were obtained for comparison with the oriented cores; therefore, these logs were deleted from the log suite.

Open-hole log calculations across the perforated interval 9,855-9,871 feet were:

$$\begin{aligned} S &= 24.9\% \\ S^w &= 75.1\% \\ \emptyset &= 20.3\% \end{aligned}$$

Whole-core porosity analysis across the same interval was:

$$\phi = 20.9\%$$

Log and core results on a foot-by-foot basis from this well are listed in appendices 14 and 15.

Compared to the surface location the bottom-hole location (at reservoir depth), in observation well no. 2, had a horizontal drift of 221 feet to the northwest, at an azimuth of 298° (Fig. 3). This bottom-hole location was 250 feet from the injection well bottom-hole location (at reservoir depth), to the southwest on an azimuth of 208°.

After the well was circulated and cleaned up, a combination string of production casing was run. The 5-1/2" OD casing was set at 10,149 feet and cemented. The casing-string design is similar to the previous wells (Fig. 12).

After the drilling rig was moved out, the location was cleaned and a workover rig was moved in. The DV collar was drilled and a bit, casing scraper, and string mill were run to bottom. The CBL-VDL-GR log indicated a good cement bond. A base TDT log was run and the casing was perforated from 9,855-9,871 feet, at a density of one shot per foot with 0-degree phasing. A perforation washer was run and each perforation was straddled and produced. The packer assembly was run on tubing and set. The work string was laid down. The production string was run and landed (Fig. 12). The down-hole equipment and wellhead were essentially the same as those described in observation well no. 1. The pressure history for observation well no. 2 is shown in figure 13.

After the base TDT log was run, a total of 1,057 barrels of fluid were produced. The log-flow-log test was then performed as follows:

TDT log Run No. 2
Flow 127 barrels of fluid

TDT log Run No. 3
Flow 468 barrels of fluid

TDT log Run No. 4
Flow 198 barrels of fluid

TDT log Run No. 5

A copy of the TDT logs can be found in Appendix 16. Analysis of run number five (5) showed that the well did clean up and the saturations did return to near original.

Zabolotny Observation Well No. 3

Observation well no. 3 was drilled without difficulty. Coring depth was reached on August 15, and four cores were cut from 9,758-9,894 feet. The hole was deepened to a TD of 10,150 feet and the following logs were run (Appendix 17):

1. Dual Laterolog-Micro-SFL with Gamma Ray and Caliper (DLL/MSFL).

2. Compensated Neutron-Formation Density with Gamma Ray and Caliper (CNL/FDC).
3. Borehole Compensated Sonic with Gamma Ray and Caliper (BHC).
4. Circumferential Micro-Sonic with Gamma Ray and Caliper (CMS).
5. Gyroscopic Multi-Shot Survey.

Open-hole log calculations across the perforated interval 9,837-9,852 feet were:

$$\begin{aligned}
 S &= 27.5\% \\
 S^w &= 72.5\% \\
 \emptyset &= 19.3\%
 \end{aligned}$$

Whole-core porosity analysis across the same interval was:

$$\emptyset = 19.5\%$$

Log and core results on a foot-by-foot basis for this well are listed in appendices 18 and 19.

Compared to the surface location, the bottom-hole location (at reservoir depth) in observation well no. 3, had a horizontal drift of 70 feet to the north, on an azimuth of 7° (Fig.3). This bottom-hole location was 283 feet from the injection well bottom-hole location (at reservoir depth), to the northwest on an azimuth of 330°.

The casing was set at a depth of 10,143 feet. The string was 5-1/2" OD, 23#/ft, N-80, R-III, 8rd, LT&C on bottom and 5-1/2" OD, 17#/ft, L-80, R-III, 8rd, LT&C, on top with the DV collar at approximately 6,921 feet (Fig. 14). The casing was cemented in two stages, with the same composition that was used in previous wells.

After the drilling rig was moved out, the location was cleaned and covered with scoria. A workover rig was moved in and the DV drilled. Following this, a bit, casing scraper, and string mill were run to bottom. The well was circulated with filtered, produced salt water. A casing collar log (CCL-N-GR) was run from PBSD of 10,015 feet to 8,500 feet and a CBL-VDL-GR log from PBSD to 4,600 feet. The log showed excellent bonding throughout the Mission Canyon section. A base TDT log was run and the casing was perforated at 9,837-9,852 feet with a 4" OD casing gun loaded with 22-gram charges at a density of one shot per foot with 0-degree phasing. The perforation washer was run and each perforation was flowed with approximately 20 barrels of fluid swabbed and/or flowed during each setting. The packer assembly was run on tubing and the packer set. The assembly was tested to 1,600 psi. The work string was laid down and the production string was run and landed (Fig. 14). The pressure recording system was purged with helium and tested. The pressure history for observation well no. 3 is shown in figure 15. The well was gas-lifted using nitrogen, but it would not flow. Coiled tubing was run to a depth of 9,000 feet, and the production tubing was unloaded with

nitrogen. The well still would not flow continuously. The casing was then re-perforated on October 9, 1980, using a 2-1/8" HSC gun loaded with four shots per foot and 90-degree phasing. The well was shot in an under-balanced condition and started flowing immediately.

The log-flow-log test was performed once flow had stabilized. After re-perforating, a total of 1,375 barrels of fluid were produced. The log-flow-log test was then performed as follows:

TDT log Run No. 2
Flow 126 barrels of fluid

TDT log Run No. 3

Analysis of the TDT logs showed that the well had not cleaned up. The decision was made to run the pulse test and then resume the log-flow-log test. The pulse test was concluded in late November and the log-flow-log procedure for observation well No. 3 proceeded as follows:

Flow 520 barrels of fluid

TDT log Run No. 4
Flow 392 barrels of fluid

TDT log Run No. 5

Analysis of the last run showed that the saturations around the wellbore had finally normalized. A copy of the TDT logs can be found in appendix 20. A summary of the logging results from the log-flow-log test performed in all three observation wells is contained in appendix 21.

LABORATORY DETERMINATION OF CO₂-WATER DISPLACEMENT PARAMETERS

The CO₂ flood in Little Knife was carried out using alternating water and CO₂ slugs (WAG)² for mobility control so that displacement of oil occurred in the presence of a mobile water saturation. Two uncertainties in the ability to predict the performance of this type of displacement were: 1) the extent to which mobile water shields trapped oil from CO₂, causing incomplete displacement even above the miscibility pressure, and, 2) the effect of CO₂ flood residual oil on water-CO₂ relative permeabilities in the WAG bank. This section describes a sequence of CO₂ WAG flood residual oil saturation and relative permeability measurements in preserved cores at reservoir conditions obtained in order to resolve these uncertainties.

Cores were from the Mission Canyon Formation zone D, in injection well no. 1. This core was cut with a neutral, surfactant-free mud to maintain original reservoir wettability, was wrapped in saran and aluminum foil at the wellsite, and was sealed in plastic to prevent weathering. Separator oil and gas samples were obtained from the Zabolotny 1-3-4A well and were reconstituted to the measured separator GOR.

The apparatus used in these measurements consisted of a slim tube connected in series with a core holder. The slim tube was 64 feet long with a 1/4 inch ID and was packed with 8-120 mesh silica sand. The rubber sleeve core holder accommodated a stack of one-inch diameter plugs approximately nine inches long. This arrangement allowed a miscible bank to be developed in the slim tube and then to pass through the core plugs. In the WAG tests, water was injected into the core plugs only and not into the slim tube. Because the slim tube hydrocarbon pore volume was approximately an order of magnitude greater than that of the core plugs, miscibility development in the slim tube could be confirmed by an overall material balance.

CO₂ WAG floods were carried out at predetermined water-CO₂ ratios and pressure, with CO₂ injected into the slim tube and water injected into the core along with the effluent from the slim tube. The floods were continued until a steady-state was obtained in the core plugs after CO₂ breakthrough, as indicated by no further pressure gradient changes. The core plugs were then removed from the core holder and a Dean-Stark extraction was carried out.

Steady-state water and CO₂ relative permeabilities were calculated from the injection rates corrected to reservoir conditions and the pressure drop across the core plugs. Oil and water saturations corresponding to these relative permeabilities were calculated from the Dean-Stark data (assuming the original oil density) and the volume of fluids produced during blowdown. Oil recovery from the slim tube was calculated from the volume of oil produced in the separator minus the oil produced from the core plugs.

Table 1 gives the results of CO₂-water displacement tests at 3,500 psi and 245°F. Over the WAG ratio range of zero to 3.0 RBbl/RBbl, CO₂ flood residual oil saturations were very low -- 0.8 percent PV to 3.1 percent PV. In these tests, a material balance on the slim tube gave ~95% OIP recovery, confirming that miscibility was developed. Because the magnitude of the residual oil saturation resulting from water trapping was expected to be greatest at pressures just in excess of the 3,400 psi minimum miscibility pressure (CO₂ must be enriched to the

greatest extent with intermediate hydrocarbons, of the gasoline range, to develop miscibility at this point) higher pressures were not investigated. These results suggest there will be no effect of a high mobile water saturation on CO₂-flood displacement efficiency above the minimum miscibility pressure at Little Knife.

To investigate the effect of the residual oil, solvent-extracted core plugs were water saturated and CO₂-water drainage relative permeabilities were measured over the same WAG ratio range. The residual oil determinations are also drainage measurements in the sense that CO₂ saturation increases at the expense of liquid saturation. The steady-state saturations corresponding to these WAG ratios are given in Table 1, and the CO₂ water relative permeability curves are plotted in figure 16. To obtain a direct comparison with figure 16, preserved core plugs were CO₂-flooded to residual oil saturation. Next they were, without extraction, completely water saturated and then subjected to a sequence of CO₂-water drainage relative permeability measurements. The results of these are shown in figure 17.

A comparison of the data in table 1 shows a higher gas saturation at any WAG ratio where residual oil is present. A comparison of figures 16 and 17 shows a higher water relative permeability and a lower CO₂ relative permeability at any water saturation when residual oil is present. Both comparisons suggest that the core plugs are substantially less water-wet in the presence of the very low residual oil saturation than when the oil is extracted.

To summarize, the Mission Canyon zone D carbonate reservoir rock at Little Knife appears strongly water-wet in native state tests. This wettability seems to be altered in some way during a CO₂ flood so that when CO₂-flood residual oil saturation is reached, the rock is no longer water-wet even when CO₂ and water are the only mobile phases. The fact that cores can be restored to a water-wet state by extraction with polar solvents and the fact that the solvent extract was found to contain much more pigmentation (determined by light absorption) than would be contained in the solvent extract of the same amount of original Little Knife oil suggests that separation of a heavy hydrocarbon phase may be responsible for the wettability change.

If this wettability change occurs early enough in the sequence of events leading to miscibility (i.e., if the first dilution of oil with CO₂ causes a water-wet to oil-wet shift which is then followed by displacement of oil), it would provide a sufficient explanation for the observed lack of residual oil at high WAG ratio because of the absence of trapping of oil by water in oil-wet systems.

Additional information is contained in appendix 31.

FOUR WELL MULTI-WELL PULSE TEST

A multi-well pulse test involving the four minitest wells was conducted on November 15, 1980⁴. Three days of unhindered background pressure had been recorded in the three observation wells prior to the test. The test was conducted by pumping filtered salt water into the injection well for two hours while the response to this "pulse" was monitored downhole in the three observation wells. A pulse response was recorded at each observation well. The single pulse was started at 12:10 + .25 hours and stopped at 14:10 + .00 hours, at an average injection rate of 2,297.5 BWPD. In addition, drawdown/buildup tests were conducted in each observation well and static reservoir pressures were recorded in all four wells. The objective of this test was to determine if a preferential direction to flow existed through the project interval in the minitest area.

The maximum response from the pulse arrived at observation well no. 1 (258 feet away) in 175.0 minutes with a maximum amplitude of 21.180 psi (Fig. 18). Analysis of the response provided the following: 1) transmissibility = 3,482.5 md-ft/cp, 2) diffusivity ($k/u\phi c$) = 39.578×10^6 md-psi/cp, 3) storage capacity (ϕch) = 87.990×10^{-6} ft/psi, 4) effective hydraulic thickness = 25.2 ft., 5) effective permeability = 29.3 md, and 6) storage = 33,610 res. bbl/acre.

The maximum response from the pulse arrived at observation well no. 2 (the nearest well, 250 feet away) in 175.98 minutes, with a maximum amplitude of 15.835 psi (Fig. 19). Analysis of the response provided the following: 1) transmissibility = 4,712 md-ft/cp, 2) diffusivity ($k/u\phi c$) = 37.638×10^6 md-psi/cp, 3) storage capacity (ϕch) = 125.19×10^{-6} ft/psi, 4) effective hydraulic thickness 36.5 ft., 5) effective permeability = 27.4 md, and 6) storage = 47,820 res. bbl/acre.

The maximum response from the pulse arrived at observation well no. 3 (the farthest well, 283 feet away) in 217.5 minutes, with a maximum amplitude of 16.010 psi (Fig. 20). Analysis of the response provided the following: 1) transmissibility = 3,189.6 md-ft/cp, 2) diffusivity ($k/u\phi c$) = 32.054×10^6 md-psi/cp, 3) storage capacity (ϕch) = 99.507×10^{-6} ft/psi, 4) effective hydraulic thickness = 29.4 ft., 5) effective permeability = 23.0 md, and 6) storage = 38,010 res. bbl/acre.

The following conclusions were derived from results of the test:

1. All three observation wells were in good fluid communication with the injection well.
2. There were no continuous high permeability channels or fractures connecting the injection well with any of the three observation wells.
3. There was no evidence of a free-gas saturation within the confines of the four-well minitest pattern.
4. In situ effective permeabilities representing the average value between the injection well and each of the observation wells were quite similar, the maximum being 29 md and the minimum being 23 md.

5. Effective hydraulic thicknesses contacted by the pulse wave between the wells varied from 25 to 36 feet.
6. Several injection-temperature surveys in the injection well showed that injected water was not migrating out of the project interval near the wellbore.
7. The pulse test hydraulic thicknesses correlated well with the combined electric log gross thickness of the project interval. The hydraulic thickness between the injection well and observation well no. 2 was slightly greater than the log thicknesses.
8. The in situ effective storage values between the three observation wells varied from a low of 34,000 res. bbl/acre (injection well to observation well no. 1) to a high of 48,000 res. bbl/acre (injection well to observation well no. 2).
9. Pressure drawdown/buildup tests were performed on each of the observation wells with some of the transmissibilities being less than those from the pulse test. This difference was an indication that there was some local confinement of fluid flow near the wellbore by low porosity/permeability streaks. This confinement apparently "comes and goes" when traversing interwell distances, resulting in the higher pulse test transmissibilities.
10. All of the observation wells had severe skin damage probably due to drilling fluid invasion, low perforation density, and invasion of cement into porous intervals and micro-fractures near the wellbore.

Additional information about the test is contained in appendix 22.

RESERVOIR GEOLOGY

The Mission Canyon Formation (lower Mississippian) at Little Knife Field is a 465 foot thick regressive carbonate sequence⁵, analogous to the lime mud-to-sabkha cycle of Wilson⁶. Most of the carbonates were deposited in a subtidal setting by five sub-environments or facies (Fig. 21). Upsection, these sub-environments are: 1) basinal,⁷ below wave base, "deeper water" carbonates, basal zone F (energy zone X of Irwin⁷) (Fig. 22); 2) open shallow marine, zone F (energy zones X-Y of Irwin⁷) (Fig. 23); 3) transitional open to restricted marine, on a shallow protected shelf, in zones E, D, and lower C (energy zones Y-Z of Irwin⁷) (Fig. 24); 4) a protected shelf of restricted marine, in mid to upper zone C and basal to mid zone B (energy zone Z of Irwin⁷) (Fig. 25); and 5) a narrow marginal marine, in mid to upper zone B (energy zone Z of Irwin⁷) (Fig. 26). This subtidal setting was interrupted by several shoaling upward carbonate cycles which deposited major and minor carbonate cycles in the lower two-thirds of the Mission Canyon. Intertidal carbonate facies, in mid to upper zone B, cap the subtidal facies and form a thin, dense veneer of emergent limestone deposits which are variable in thickness (Fig. 27). Thin, dense lagoonal limestone beds (Fig. 28) interfinger with and overlie the intertidal facies with tidal flat/supratidal anhydrite beds overlying both (Fig. 29).

Lithology

Key beds were located throughout the Mission Canyon section and were used to divide the formation into six informal zones (Fig. 30). Lithologies of these six zones, A through F, within the Mission Canyon at Little Knife Field are:

1. Zone A is a 60-foot thick interval composed of thin to thick bedded anhydrite. These beds of anhydrite form several textures, including: 1) chicken-wire mosaic, 2) thin-bedded mosaic, 3) laminated to medium bedded, 4) ropey displacive, and 5) burrowed replacive. Most of the textural names describing these anhydrite beds are after Maiklem, et al.⁸. Both a dolomite matrix and laminated interbeds of dolomite are associated with the anhydrite beds. At the base of the zone and into uppermost portions of zone B, pseudomorphs of anhydrite after selenite gypsum crystals, anhydrite porphyroblasts, and localized laminated crusts are present. Interpreted depositional setting is supratidal.
2. Zone B is 70 feet thick and forms part of the reservoir interval. It is separated into:
 - a) An upper interval varying from 5-40 feet in thickness consisting of interbedded, thin, porous, and discontinuous, lenticular dolomitized skeletal wackestones. They are partly replaced by anhydrite, which was later leached, and set between thin to thick beds of dense cemented grainstones. Constituents included peloids, clotted and lumped micrite, ooids, pisolites, calcispheres and skeletal detritus. Interpreted depositional setting of the skeletal

wackestones is shallow, nearshore subtidal while the wackestone/grainstones are part of an intertidal barrier. In south and southeast portions of the field additional anhydrite beds, via lateral facies changes, form uppermost portions of this zone. Within this area supratidal deposition similar to zone A forms upper zone B as well.

- b) The lower two thirds of the zone is dolomitized burrowed, sparsely skeletal, pelletal wackestone/packstones. The carbonates were partially replaced by anhydrite, then leached and form an upper reservoir. Interpreted depositional setting is restricted shallow marine. In south and southeast portions of the field lateral facies changes have intertidal limestone, in middle zone B, in place of dolomitized restricted marine rocks.
3. Zone C is 65 feet thick and also forms a portion of the reservoir interval. It is medium to thick bedded and slightly porous at its top, becoming dense downward, in mid-portions, then becoming more porous progressively lower in the section. Upper portions are slightly dolomitized to dolomitized pelletal wackestone/packstones grading downwards into skeletal wackestones with some replacement by anhydrite. Dense beds in mid portion of this zone are either only slightly dolomitized limestone or where dolomitized form microcrystal dolostone with sparse to less than common amounts of chert occluding any intercrystal pore space. Upper portions of the zone have rare quartz silt laminations beneath porous upper reservoir intervals, set in dense dolomite. The lower porous portion forms part of a lower reservoir interval. Depositional setting is restricted marine to transitional marine.
4. Zone D is 50 feet thick, forming the lowest portion of the reservoir interval. It is a medium to thick bedded, partially dolomitized to near completely dolomitized, burrowed, skeletal wackestone interbedded with mudstones. A dolomitized skeletal wackestone bed at the top of the zone is where the WAG minitest was conducted. The facies exhibits some anhydrite replacement and leaching. The uppermost portion of the zone forms the major portion of a lower reservoir interval. Within this bed a lateral facies change controls porosity distribution, changing from porous skeletal wackestone into dense skeletal packstone. Depositional setting is the seaward portion of a protected shelf, transitional between the open marine and restricted marine.
5. Zone E is 50 feet thick and is composed of thick bedded sparsely dolomitized to dolomitized skeletal mudstone/

wackestones with irregular shaped incipient chert nodules. Porosity intervals in this zone are non-hydrocarbon bearing. Depositional setting is restricted to transitional marine. This zone is non-hydrocarbon bearing.

6. Zone F is 170 feet thick and composed of medium to thick bedded alternating mudstones and skeletal packstone/grainstones. The basal 10-15 feet is slightly argillaceous, interlaminated skeletal packstones and pelletal packstones which form a transitional zone of contact from the Mission Canyon into the underlying Lodgepole Limestone. This zone is also non-hydrocarbon bearing. Depositional setting is open marine with the basal 15 feet deposited in a basinal marine setting.

Hydrocarbon bearing porosity is isolated within beds deposited in both transitional open to restricted marine and restricted marine settings, zones B, C and D of the Mission Canyon (Fig. 31). These beds were partially-to-completely dolomitized to form fine-grained, sucrosic dolostone (Fig. 32). A field-wide study of Little Knife discussing the overall depositional settings, diagenesis and reservoir character is included in appendix 23.

Carbonate Cycles

Within the open shallow marine facies, several medium to thick bedded shoaling upward carbonate cycles are formed by beds of mudstone/skeletal wackestone which grade up into high energy beds of skeletal packstone/grainstone (Fig. 33). These are called major carbonate cycles. Lower portions of each cycle are composed of mudstone/skeletal wackestone, deposited as carbonate muds below wave base, while capping beds of each cycle are composed of skeletal packstone/grainstones deposited in wave base. These major carbonate cycles are located in zone F.

As open marine facies prograded basinward, deposition behind it layed down medium to thick bedded transitional open to restricted marine facies, positioned on the seaward portion of a protected shelf. Within this setting carbonate muds piled up, mud being supplied and swept back into this setting from the open marine. Storms passing over this portion of the basin washed crinoid fragments back into the seaward side of the protected shelf. These skeletal fragments probably formed storm layers but were not preserved due to intense bioturbation, and were eventually worked into the muds to form a bed of skeletal wackestone. This left lower energy, burrowed, pelletal mudstones which grade up into skeletal wackestones and are referred to as minor carbonate cycles (Fig. 33). Minor carbonate cycles extend from the top of zone F to the base of zone C. The capping skeletal wackestone portion at the uppermost last minor carbonate cycle, at the top of zone D, is the interval within which the CO₂ minitest was conducted (Figs. 30, 32 and 33).

Diagenesis

An essentially paragenetic sequence for the Mission Canyon Formation at Little Knife Field has been constructed, from initial deposition of sediments to the final end product of porous oil bearing dolostone (Fig. 34). This sequence is

divided into 22 events and each event is placed in one of four groups, which are: 1) initial processes, 2) porosity destruction, 3) porosity creation, and 4) hydrocarbon emplacement. Many of these events are of lesser and greater importance in their effect on the section to produce either porous or dense rock. Events of major importance have asterisks placed next to them and simultaneously occurring or overlapping events are connected by arrows (Fig. 34).

Event one (1) is initial deposition of the sediments which, once piled up, produce the stratigraphic section. Event two (2) is redeposition by storms. These effects are seen in the basinal marine, open marine, transitional open to restricted marine, intertidal, lagoon and tidal flat/supratidal sabkha facies, essentially redistributing sediments in the same facies or into an adjacent facies. Event three (3) is micritization and is most common in the intertidal. Many ooids have been micritized to structureless pelletoids while others have remnant ooid structures still present. Event four (4) is bioturbation. Extensive burrowing has homogenized subtidal muddy portions of the section, producing more uniform, though low, permeable pathways through which fluids could migrate. This is an important stage in preparing the subtidal muds to be dolomitized. Events two (2) thru four (4) were probably simultaneously occurring events but for convenience of illustrating were split into three separate listings.

Event five (5) is physical compaction. This occurred due to the weight of overlying sediments piling up, squeezing and dewatering the muddy carbonates. This process reduces originally muddy porosities of 60 to 70 percent down to approximately 40 percent. Within sabkha and lagoonal evaporites compaction may have played a key role, as a mechanism for expelling dolomitizing brines outward into the subtidal carbonates. Compaction probably continued on as later events occurred.

Cementation began to chemically compact the section. Event six (6) is calcite cementation. Within both open marine high energy packstone/grainstones and intertidal wackestone/grainstones early calcite cementation is very extensive. This cemented the originally most porous and permeable sediments in the section to form the most dense beds of rock, other than beds of anhydrite. In event seven (7), local dolomite cementation occurred in a few sparse locations in the intertidal. Within these areas packstones of ooids have isopachous rim cements of dolomite. Both event six (6) and seven (7) appear to have occurred at similar times and overlap in their diagenetic timings.

Event eight (8), anhydrite cementation, and event nine (9), anhydrite porphyroblast growth, occurred in the intertidal and lagoonal settings. Also, in the lagoon ax-head-shaped selenite gypsum crystals grew. Both of these events follow events six (6) and seven (7) very closely, but generally have cross cutting relationships to the earlier events. If any original interparticle pore space was not filled by calcite cement, anhydrite cement has infilled it. Sources of Ca^{2+} and SO_4^{2-} ions were from brines concentrated on the sabkha and perhaps in the lagoon, which then began to move out into intertidal buildups.

Event ten (10), partial anhydrite replacement of subtidal skeletal fragments, preferentially crinoid columnals, followed events eight (8) and nine (9), as the brine generated on the supratidal sabkha moved through the lagoon and intertidal buildups and on out into subtidal beds. This brine not only affected the nearest subtidal facies but swept through most of the Mission Canyon section.

Event eleven (11) is chert replacement of large, irregularly shaped burrows in one porous interval of the transitional open to restricted marine facies, in zone E. Event twelve (12), partial chert replacement of anhydrite cements in the intertidal, probably occurred at the same time as event eleven (11). Both chert replacement events occur in stratigraphically isolated intervals. Exact timing of these events and their interrelationship to other events is difficult to assign and were arbitrarily assigned these positions.

Event thirteen (13), dolomitization of subtidal muddy carbonates, is the most important diagenetic process to have affected the Mission Canyon. Open marine mudstone/skeletal wackestone facies, rich in mud, are dolomitized. Much of the transitional open to restricted marine facies is dolomitized, while the restricted marine facies is dolomitized the most.

In muds, with skeletal particles, once most carbonate mud had been dolomitized local sourcing of carbonate for continued dolomitization became the larger skeletal constituents, in addition to any remaining mud¹⁰. At approximately 60-70 percent conversion to dolostone, finer skeletal fragments were affected by leaching of their smaller calcite crystals with remaining larger skeletal fragments left to "float" in a matrix of fine, porous, sucrosic, euhedral dolostone, ringed by dolomite crystal necklaces. Muds that are pelletal rich dolomitize their muddy portions first with larger pelletoids surrounded by dolomite crystal necklaces. These necklaces formed around the grains prior to their being leached, as an additional carbonate source, so that subtle dolomite-crystal-rimmed, oval-shaped, very fine moldic pore space is produced (Fig. 35). Microcrystal dolomite formed preferentially where limited amounts of carbonate muds were available. Also, certain beds, though mud rich, are completely dolomitized to dense microcrystal dolostone, with very small interlocking dolomite crystals. This type of dolomitization may reflect sites of multiple closely-spaced crystal nucleation or where ambient pore waters had higher concentrations of magnesium. In other locations, large volumes of lime mud diluted fluids moving through them, becoming less concentrated with respect to magnesium, with nucleation sites spread farther apart, promoting the creation of porous, fine grained sucrosic dolostone¹¹.

Unfortunately, SO_4^{2-} ions in a brine system severely retard dolomitization^{12,13,14}. Therefore, most SO_4^{2-} ions had to be removed from the brine before dolomitization could occur. This appears to have occurred at Little Knife^{15,16}. As the brine, enriched in Ca^{2+} , SO_4^{2-} and Mg^{2+} ions, moved through outer portions of the sabkha, lagoon and the intertidal, gypsum or anhydrite precipitated out of the brine. This began to reduce concentrations of Ca^{2+} and SO_4^{2-} ions. As this brine swept out and through the subtidal it preferentially replaced skeletal fragments, an additional sink for SO_4^{2-} ions. When replaced by anhydrite, skeletal fragments which were high Mg^{2+} calcite, liberated additional Mg^{2+} to the brine. Eventually this brine, behind its front, chemically evolved from a spearhead of replacing anhydrite to a dolomitizing brine, with an increased $\text{Mg}^{2+}/\text{Ca}^{2+}$ ratio¹⁷, which dolomitized carbonate muds. Dolomitization was at a much slower rate. This process left anhydrite replaced and non-replaced skeletal fragments floating in dolostone.

Event fourteen (14), chert cementation of dolomite intercrystal pore spaces occurred in a specific horizon of the restricted marine facies, in middle zone C.

Dense chert cemented dolostone and laterally non-dolomitized beds isolate the oil column into an upper and lower interval.

All of the above-mentioned events, through event fourteen (14), are interpreted to have occurred early. The next series of events are interpreted as much later events affecting the Mission Canyon.

Event fifteen (15), leaching of replacing anhydrite in subtidal rocks, is the most important late diagenetic event, which occurred as Laramide uplifts began charging fresh water into the subsurface. Sources of fresh water include the Black Hills, to the south, and uplifts in central Montana, to the west. Fresh water ultimately reached the Williston Basin and swept through portions of the Mission Canyon at Little Knife. This water leached anhydrite, which originally replaced skeletal fragments, producing moldic pore space. Leaching produced more porous and permeable fine grained sucrosic dolostones.

Event sixteen (16), calcitization of dolostones and limestones in the subtidal facies, is a direct response to anhydrite leaching. Leaching set free Ca^{2+} and SO_4^{2-} ions, with Ca^{2+} ions combining with available carbonate ions to precipitate fresh water calcite crystals which sit upon and have eaten into dolomite crystals, starting to dedolomitize them (Fig. 36). Event seventeen (17), anhydrite replacement of dolomite crystals in the subtidal, is an equivalent event with event sixteen (16), where SO_4^{2-} ions replaced dolomite crystals. Anhydrite replacement is rare. Calcite replacement (calcitization) is variable from non-existent, to sparse, to slightly common. Event eighteen (18), saddle dolomite growth in moldic pores, is extremely rare and has only been viewed in a few thin sections. This event is interpreted as a late diagenetic effect which is possibly related to events sixteen (16) and seventeen (17).

At this point broad, subtle folding within the basin formed the structure at Little Knife. Hydrocarbons then migrated into and were trapped in the upper half of the Mission Canyon, forming event nineteen (19). All diagenetic effects from this point on, in the oil column, were subdued.

Event twenty (20), stylolitization, is post-hydrocarbon emplacement. Stylolites are found in all facies. One particular stylolitized horizon, about one foot thick, serves as the zone D marker. This marker is picked off the sonic log and can be correlated, without great difficulty, through the field.

Fracturing is event twenty-one (21). Cementation of fractures is the final recognized event, event twenty-two (22). Cement types are calcite or dolomite.

This rather lengthy list of events that have affected the Mission Canyon section of Little Knife Field have either enhanced or deteriorated porous beds in the formation, which are now within the oil column. A simplified sequence of events is proposed which are major events in the Mission Canyon's history that sequentially are responsible for producing porous dolostone within which hydrocarbons are now trapped (Fig. 37).

First, after all initial processes deposited a muddy carbonate, the original marine water trapped within the sediments was displaced by a sabkha-derived brine. This brine was enriched with respect to Ca^{2+} , Mg^{2+} , and SO_4^{2-} ions; and, as this brine displaced the original marine water, anhydrite began to replace skeletal

fragments, preferably crinoid columnals, which reduced the Ca^{2+} and SO_4^{2-} ion concentrations. Additional Mg^{2+} ions were then added from crinoid columnals to the system.

Second, ultimately this brine chemically evolved into a Mg^{2+} rich and Ca^{2+} and SO_4^{2-} poor fluid, and began dolomitizing the muddy matrix creating porous calcareous dolostone to dolostone.

Third, a much later event, was freshwater movement through the subsurface which leached anhydrite-replaced skeletal fragments. This is interpreted to be in response to Laramide uplifts nearest the basin, which caught and discharged freshwater into the subsurface. This leaching action helped to create more porous and permeable dolostones. This produced moldic pores which are connected with dolomite intercrystal pores, all of which are connected three-dimensionally.

Fourth, Laramide-related structural motions caused the very gentle structural nose to form. At a similar time within the Cretaceous, hydrocarbons began to reach maximum maturity, were expelled from source rocks, and eventually migrated into porous dolostones of the Mission Canyon and were trapped.

Reservoir Specific

Beds utilized for the CO_2 minitest project interval are located at the base of zone C and at the top of zone D, a total thickness of 31 feet (Fig. 30 and 31). These beds form the mid-to-basal portion of the reservoir interval within the field. They were deposited within a transitional open to restricted marine setting by an epeiric sea which occupied the Williston Basin, with large volumes of lime mud being deposited (Figs. 21 and 32).

Reservoir rock characteristics in the project interval are similar in each well (Fig. 38). The lower half (15-16 feet) is composed of highly porous and permeable rock that is partially dolomitized (70 percent), originally skeletal wackestone (Fig. 39, 40, 41 and 42). A stylolite is located at the top of this bed throughout the minitest area, reducing porosity for approximately one foot (Fig. 43). This stylolitized horizon serves as a key bed marker on sonic logs to divide the Mission Canyon into zone C above and zone D below. The upper half of the project interval is formed by two beds of rock. The intermediate bed is dolomitic limestone, containing low amounts of porosity and permeability. The uppermost bed is calcareous dolostone, which contains fair to good amounts of porosity and permeability. In observation well no. 3 only dolomitic limestone is present. This lack of a bed of calcareous dolomite is due to less dolomitization affecting uppermost portions of the project interval at this location. A comparison of porosity and permeability to lithology by whole core analysis, in the first four wells, is illustrated in fig. 44.

Structure

Little Knife Field is located within a broad, low lying anticlinal nose plunging gently to the north (Fig. 2). Beds dip to the west at approximately one-half degree and to the east at approximately one-quarter degree. Closure across the field is less than 100 feet. Several slightly structurally higher areas of the field are separated by low saddles along the axis of the field, at

approximately twenty foot differences. Closure is structural to the north, east and west with lateral facies changes creating stratigraphic entrapment southward.

Regionally, western North Dakota, eastern Montana, and north-westernmost South Dakota are divided by a series of northwest and northeast trending surface lineaments. These lineaments tend to form elongate, slightly rhombic blocks. Little Knife is located within the center of the junction of the northeast trending Yellowstone block and the northwest trending Watford block¹⁸ (Fig. 45). In central and northern portions of the field, surface lineaments were mapped using Landsat and aerial photographs¹⁹ (Fig. 46). Both northeasterly and northwesterly trends, similar to regional trends, are present within the field (Fig. 47).

Surface outcrop fractures in the Sentinel Butte Formation, surrounding observation well No. 3, were measured by one of the authors (Fig. 48). Sixty-nine apparent strikes were obtained which revealed a predominance of fractures in a northwesterly direction, maximum value N. 70-80°W., and a northeasterly direction, maximum value N. 60-70°E. Oriented cores were obtained in each of the four minitest wells, with strike and dip of all fractures recorded. Strikes of the fractures within the minitest interval revealed slightly differing fracture orientations from well to well (Fig. 49). However, the average fracture strike directions from the cores tend to be in either a northwesterly (N. 67°W.) or northeasterly (N. 69°E.) direction, similar to surface outcrop fractures.

Fracture separation (distance from one fracture to the next parallel fracture) could not be determined from cores. Surface outcrops were used to study fracture separations, assuming they are similar in the subsurface. These fracture separations were found to vary from one to six feet. Surface soil cover limited the extent of the study area (Figs. 50 and 51).

Cores reveal the vertical continuity of individual fractures to be approximately eighteen to twenty-four inches. Each individual fracture consists of small interconnected, vertical, hairline, en echelon planes. No lateral offset has been observed where fractures transect skeletal fragments, ooids or pisolites.

The fracture identification log (FIL) and wave forms variable density log (Wave Forms-VDL) were both run in the first two wells drilled. A comparison of fracture directions taken from the oriented cores to those calculated fracture directions obtained from logs revealed a fair comparison, with fracture detection by the logs appearing slightly pessimistic but generally good. The FIL was, however, rated superior to the Wave Forms-VDL as the best source of fracture information from logs²⁰.

Because the fractures observed propagate only short distances vertically, it is felt that their lateral continuity may also extend for short distances. Multi-well pulse testing revealed no major contribution by fractures, but did calculate higher average permeabilities. These average permeabilities were approximately twice the permeabilities measured from whole core analysis and are interpreted to be due to the slight effect of short non-continuous fractures dispersed somewhat uniformly across the minitest area (Fig. 52).

Pore and Throat System

Four types of pores are recognized in the Mission Canyon, they are: 1) moldic pores,²¹ 2) polyhedral pores, 3) tetrahedral pores, and 4) interboundary-sheet pores²¹ (Fig. 53). Moldic pores are the largest and are produced by leaching of anhydrite which replaced skeletal fragments, mostly crinoid columnals, and measure at least 200 micrometers down to 30 micrometers wide (Figs. 54A and 55A). These large moldic pores are connected by pore throats to other pores and pore throats associated with intercrystal pores between dolomite crystals. Polyhedral pores are the largest intercrystal pores (Figs. 54B, 55B and 56A). Each pore is surrounded by several dolomite crystals to form a complex polyhedral shape 50 to 10 micrometers wide. Tetrahedral pores are intermediate-sized intercrystal pores, where individual dolomite crystals began to grow together at intermediate angles, impinging into other dolomite crystals and reducing pore size to a smaller tetrahedral shape 10 to 3 micrometers wide (Figs. 54C, 55C, 56A and 57). Interboundary-sheet pores are the smallest and narrowest intercrystal pores, found between individual dolomite crystals where pore space has been reduced by continued crystal growth to thin, linear, approximately 1-1.5 micrometer widths (Figs. 54D, 55D, 56A and 56B). Small, narrow interboundary-sheet pores are essentially pore throats and are referred to as pore/pore throats. All intercrystal pore types are similar to those described by Wardlaw²² and Wardlaw and Taylor²³.

Pore throat size radii connecting the various pores are of two major sizes and types, they are: 1) interboundary-sheet pore/pore throat radii, 0.6-0.8 micrometers, and 2) larger pore throat radii, 1.5-3.5 micrometers, which connect tetrahedral, polyhedral and moldic pores (Figs. 58, 59, 60 and 61). Both sizes of pore throats contribute to permeability development. Narrow interboundary-sheet pores/pore throats, though forming only small amounts of total porosity, contribute to overall permeability development. This pore throat size is present in dolostones which have up to 22 percent porosity and are the only pore throats available for fluid movement through beds of rock having less than 17 percent porosity. Tortuous pathways are the result of having four pore types being connected by essentially two sizes of pore throat radii (Fig. 56C).

When pore throat radii size is compared to the amount of porosity and permeability in individual samples, five (5) diverging groups or relationships are found to exist (Figs. 62, 63, 64, 65). They are:

<u>Group</u>	<u>Pore Throat Radii</u>	<u>Porosity</u>	<u>Permeability</u>
1	0.21 um	2.5-9.9% (avg. 6.2%)	0.1-0.3 md (avg. 0.16 md)
2	0.6 um	8.3-13.0% (avg. 10.7%)	0.7-1.0 md (avg. 0.8 md)
3	0.8 um	10-17.2% (avg. 13.6%)	1-7 md (avg. 3.5 md)

<u>Group</u>	<u>Pore Throat Radii</u>	<u>Porosity</u>	<u>Permeability</u>
4	0.8 & 1.8-2.5 um	17.3-22.4% (avg. 19.6%)	7-48 md (avg. 22.3 md)
5	2.5 um	21.8-27.6% (avg. 24.1%)	48-146 md (avg. 85.4 md)

These pore throat radii, porosity and permeability calculations are all from mercury injection capillary pressure curve samples.

The first and narrowest group (1) of pore throat radii measured average 0.21 micrometers in width (Fig. 66A). The range of porosity associated with this throat size varies between 2.5-9.9 percent, averaging 6.2 percent. Permeability is very low, 0.1-0.3 millidarcys, averaging 0.16 millidarcys. These are pore throats associated with beds of such low porosity and permeability that they do not hold or contribute to the fluid flow of hydrocarbons. These beds of rock are commonly referred to as "dense beds", even though they do contain minor amounts of pore space.

The second group (2) is composed of pore throat radii which average 0.6 micrometers wide (Fig. 66B). Porosity associated with this group ranges between 8.3-13.0 percent, averaging 10.7 percent. Permeability is slightly increased, 0.7-1.0 millidarcys, averaging 0.8 millidarcys. A noticeable gap in pore throat radii size separates these first two groups, 0.21 micrometer throat radii in group one compared to 0.6 micrometer throat radii in group two. Also, there is an overlap of porosity ranges associated with these two groups, between 8.3-9.9 percent. Therefore, beds containing this range of porosity overlap will have pores connected by either very narrow pore throats or by pore throats with widths three times as wide. Beds containing the narrower pore throat radii are essentially dense beds, lacking the necessary permeability to effectively flow or drain fluids. While other beds, of similar porosity, containing the larger pore throat radii, in contrast, have better permeable pathways and are able to pass fluids, draining that particular rock. Because these rocks lie within an actively-producing oil field this subtle change in pore throat size characteristics, which determines whether they will or will not give up fluids (hydrocarbons preferably), at economic rates, is very important to not only detect and document but also to use as a means of determining at what point, in terms of porosity, little or no fluids can or will be produced.

The next, third, group (3) is associated with slightly wider pore throat radii and higher amounts of porosity and permeability. Maximum pore throat radii width is 0.8 micrometers (highest percentage) but has a range between 0.6-2.0 micrometers (Fig. 66C). Porosity ranges between 10-17.2 percent and averages 13.6 percent. Permeability within these beds increases significantly, between 1-7 millidarcys, averaging 3.5 millidarcys. Here, between group two and three, a slight overlap of porosity ranges exist, between 10-13 percent. Pore throat size and permeability, however, are separate and do not overlap. Rocks containing this overlap of porosity will have pore throat radii of either 0.6 or 0.8 micrometers (group two and three, respectively) connecting the pores. The larger pore throat

radii, one-third wider than the smaller throats, boost permeability, letting fluids pass from pore-to-pore with greater ease.

Within the fourth group (4) a bimodal distribution of two pore throat radii sizes develops and becomes common. This relationship does not exist in any of the first three groups. These pore throat radii disperse into a secondary maximum size range (least common) at 0.8 micrometers and a maximum size range (most common) at 1.8-2.5 micrometers (polymodal²⁴) with low numbers of other throat radii sizes between the two dominant throat sizes (Fig. 66D). Porosity ranges between 17.3-22.4 percent, averaging 19.6 percent. Permeability leaps to a range of 7-48 millidarcys, averaging 22.3 millidarcys. These group four porosities and permeabilities represent average reservoir rock properties in Little Knife Field. Due to bimodal distribution of pore throat radii and because reservoirs normally undergo secondary recovery operations (waterflooding), when applicable, a careful characterization has to be made to determine if injected water will migrate through both pore throat sizes or if only large pore throats will be swept by water.

The final, fifth, group (5) contains pore throat radii that have only one size range (maximum percentage) at 2.5 micrometers and have the widest throats (Fig. 66E). The smaller, 0.8 micrometer throat radii present in the other two groups (3 and 4) are reduced to only a few sparse throats. High porosities, 21.8-27.6 percent, averaging 24.1 percent are associated with this group. Also, the highest permeabilities, 48-146 millidarcys, averaging 85.4 millidarcys are associated with these wide pore throats. These larger pore throats tend to form triangular bar to elongate wedge shapes, connecting polyhedral and tetrahedral pores.

Pore-to-throat size ratios are highly variable. These range from 40:1 when large polyhedral pores are well developed, and the ratios are even larger when comparing moldic pores-to-throats, while they go down to 4:1 when not well developed. Average pore-to-throat size ratios are approximately 5-10:1. The average pore-to-throat coordination number, the average number of throats connected to each pore, is 3 to 5 in two-dimensional view (Fig. 67).

The most significant attribute that each of the four pore types and various pore throat sizes have in common is that all are three-dimensionally interconnected (Fig. 53 and 55). Therefore, an understanding is required of not only how well all pore types, each of different size, are distributed throughout a dolostone but also how well each pore is connected with the next by a particular size of pore throat. These pore throats may either be: 1) very narrow, 2) may be bimodal, having two pore throat sizes, the largest four or five times the width of the smallest, or 3) be very large.

Forty-eight pore throat radii measurements were made, 12 from each well, and are illustrated in appendix 24, 25, 26, 27, and 28. Mercury injection capillary pressure curves from which these above measurements were made are also included in appendix 25, 26, 27 and 28, along with standard whole core analysis in appendix 3, 10, 15, and 19.

EQUIPMENT AND INSTRUMENTATION

Figure 68 illustrates the layout of the minitest site. The water filter and associated pumps and tanks, along with the water transfer pump, were located at a central production facility. The rest of the equipment was located at the test site. The test site equipment was designed to operate primarily with propane fuel. Only a limited amount of electrical power was available.

The trailer was the central point of the operation. It served as the instrumentation center, office, and storage area.

The equipment and instrumentation used in the project were separated into four systems. Foremost was the hardware used in the well completions as previously described. The other three systems were: 1) the CO₂ injection system, 2) the water injection system, and 3) the fluid sampling system.

CO₂ Injection System

The CO₂ injection system consisted of storage, metering, pumping, and vaporizing sections (Figs. 69 and 70). All were located at the minitest site. All equipment upstream of the liquid meter was furnished by the CO₂ supplier.

The CO₂ was transported in a liquid state by truck to the minitest site from near Brandon, Manitoba (Fig. 71). It was stored as a liquid at 0°F and 300 psi. The storage tanks had a vaporizing system, which is not shown in Figure 69. A refrigeration system was not installed because the CO₂ injection phase was to be completed during the winter. It was anticipated that the ambient winter temperature would be sufficiently low to prevent significant CO₂ loss.

The storage section had a capacity of 200 tons. This storage was approximately one-half (1/2) of the volume of one cycle of CO₂ injection. This capacity ensured that the injection schedule would not be altered or interrupted by delays in getting CO₂ to the test site.

CO₂, in a liquid state, was vaporized in the line heater (Fig. 72). Numerous safety relief valves provided vents in case liquid CO₂ was trapped and began to vaporize. All vessels were equipped with safety relief valves, even though they are not illustrated.

The metering system consisted of both a liquid and a gas meter (Fig. 73). Metered volumes were compared to delivered volumes. The liquid meter performed adequately, with the recorded meter volumes correlating well with actual CO₂ tank gauges. The gas meter also performed adequately, but the determination of injected volumes from gas-chart reading became very tedious. This problem was due to the difficulty in reading the compressibility factor (Z-factor) from the CO₂ compressibility vs. pressure correlation chart. The steepness of the temperature line, in the chart, corresponding to the injected temperature made it extremely sensitive to small pressure variations. The liquid meter reading was preferred for this reason.

The pumping system was comprised of two pumps, a charge pump and an injection pump. The charge pump ensured that liquid was being supplied to the injection

pump (Fig. 74). The injection pump consisted of a triplex pump driven by an internal combustion engine.

A line heater was used to vaporize the CO₂. The CO₂ could not be injected as a liquid without freezing the packer fluid² and possibly rupturing the casing and/or collapsing the tubing. The gaseous CO₂ was heated in order to avoid hydrate formation when it contacted water, and² also to ensure it was above the critical temperature of CO₂ (approximately 87.7°F).

Water Injection System

The water injection system consisted of two main segments (Fig. 75). The first segment was the filtering system which was located at a central production facility. The second segment was the injection pump which was located at the test site. A fiberglass line connected the two. Water for the project was produced formation water. A 30-day test was conducted and the water density remained essentially constant, so there were no quality control problems.

The main component of the filter section was the filter unit. It was an upflow, graded sand unit. Two tanks and pumps were necessary to backwash or regenerate the filter. Gas was added to the flow stream during the backwash cycle. The entire system was enclosed and a gas blanket was maintained in the filter unit (Fig. 76).

The water injection pump was a triplex pump, powered by an internal combustion engine. The unit was skid-mounted and enclosed in an insulated structure (Fig. 77).

Fluid Sampling System

The heart of the fluid sampling system was a three-phase metering separator (Fig. 78). The nominal rating of the unit was 1,000 BPD and 2 MMscf/D at 200 psi. The vessel itself was rated at 250 psi. The horizontal 24" OD x 10' vessel was equipped with standard instrumentation: 1) back-pressure valve and control, 2) relief valve, 3) pressure gauge, 4) thermometer, and 5) gauge glass. In addition, there were level controls for both oil and water and meters for gas, oil, and water. A downstream fluid sampler was attached. Only a small amount of fluid was produced from each observation well to collect representative samples to be analyzed for tracers, CO₂ content, and fluid composition. The entire unit was skid-mounted and enclosed² in a steel structure. The building was insulated and the unit was equipped with catalytic heaters to prevent freezing.

The normal flow pattern was from the well being sampled, to the manifold, through the separator, and into the tanks. The separator could be by-passed in the event that there was insufficient wellhead pressure to satisfy the back-pressure of the separator. Flow from the wells was initiated and/or maintained by gas-lift. The liquid was collected in 400-barrel tanks and then hauled to a central production facility. Two tanks were used to check the meters. These tanks also simplified the transfer of the fluids to the tank battery.

SIMULATION MODELS

In order to predict current and future technical performance of the minitest, and as a means of incorporating the large amount of data accumulated from the logs, cores, and well tests, two simulation models were developed: 1) a black-oil simulator, in a three-dimensional mode, and 2) a compositional simulator, in one-dimensional, two-dimensional, and three-dimensional modes.

The three-dimensional black-oil simulator was used to characterize the reservoir, history match production, and compute the amount and rate of water injection needed to maintain pressure in the minitest area. Those wells surrounding the project area provided: 1) core analysis, 2) open-hole logs, 3) semi-annual bottom-hole pressures, and 4) production performance, and were used as a base for reservoir characterization. As the four minitest wells were drilled and additional core analyses and log data became available, the black-oil model was updated.

The compositional simulator in a one-dimensional mode was used to match the slim-tube results. By matching the miscibility test data, the one-dimensional mode was utilized to determine a very rough estimate of the slug design. The two-dimensional mode then expanded on this estimate to refine the slug design for optimizing oil recovery by CO₂ and water injection. The three-dimensional mode was used to history match the performance of the minitest, obtain a better reservoir characterization and compute the sweep efficiency in the minitest area. Also, the model was used to predict the expansion of the CO₂ test to a field-wide application. The three-dimensional compositional model will be discussed later in this report. These simulation model studies contributed significantly to test design as well as to the interpretation and extrapolation of test results.

CO₂-WATER INJECTION DESIGN

A study of the preflush water injection phase of the minitest was completed using the three-dimensional, three-phase, black-oil simulator²⁵ (Appendix 29). The study was designed to investigate the water injection requirements for repressurization and the effects of injection on the reservoir. Several prediction cases were run to simulate the effects of various injection plans on the minitest area. These cases included two injection start-up dates and two different future production-performance schedules in the field area surrounding the minitest site.

The following observations were made, based on the results of the study:

1. The pressure in the minitest area would be raised above the calculated minimum CO₂ miscibility pressure of 3,400 psig, if water injection was begun on either September 1, or October 1, 1980.
2. A water injection rate of 1,150 STB/D, for fifteen (15) days, would adequately repressure the pilot area if the above dates were observed.
3. The existing rate of reservoir fluid withdrawal would not adversely affect the pilot area if the aforementioned injection plan was utilized.
4. Water injection in the minitest area would not strongly affect the average reservoir pressure in zone D of Little Knife Field.

A two-dimensional, cross-sectional, compositional simulator study was performed to develop the water and CO₂ (WAG) portion of the test (Appendix 30). Following a 15 percent PV (pore volume) slug of preflush water, the WAG injection scheme would commence and then be followed by drive water alone.

The optimum CO₂-water injection method was strongly dependent on reservoir properties. The WAG ratio that gave the best mobility control was dependent upon the extent to which water and CO₂ segregated in the reservoir. This segregation was controlled by capillary, gravity, and viscous-force interactions across the minitest interval and layers of stratification. The optimum CO₂ volume to be injected depended on: 1) CO₂ storage or trapping behind the CO₂-water front, 2) the extent to which stratification caused bypassing, and 3) fingering and dispersive mixing at the CO₂-oil front (the simulator did not represent these last two effects).

Work to optimize the WAG ratio and CO₂ slug size involved choosing a base case injection scheme and assigning likely values for all parameters. Each parameter was then varied from the base-case value and the sensitivity of recovery and process performance to it was determined by simulation results. Three different WAG ratios were analyzed. They were: 1) 1:1, 2) 0:1, and 3) 3:1 (reservoir barrels of water/reservoir barrels of CO₂). The following results were observed:

1. Although ultimate recovery was more or less the same for all the CO₂ floods, breakthrough of injected fluids was earliest for the 3:1 WAG ratio and latest for the 1:1 WAG ratio. For CO₂ alone, breakthrough was slightly earlier than for the 1:1 WAG ratio. On this basis, the 1:1 WAG ratio was selected for the minitest. The improvements that a 1:1 WAG ratio flood gave over CO₂ alone were 2.3 percent PV more oil and a small improvement in breakthrough time. This improvement in recovery appeared to be worth the extra effort involved in carrying out a WAG-type flood.
2. Ultimate recoveries after about one (1) hydrocarbon pore volume (HCPV) total fluid injection (800-1,000 days) were high for all the CO₂ flood simulations: a) 76.5 percent original oil in place (OOIP) for the 1:1 WAG ratio, b) 74.2 percent OOIP for CO₂ alone, and c) 77.5 percent OOIP for the 3:1 WAG ratio, compared with 41.2 percent OOIP for a waterflood. Cumulative CO₂:oil ratios from this simulation were all low, about 1 Mscf/bbl. It should be realized that these CO₂ flood predictions in a cross-sectional model did not account for areal sweep and capture efficiency effects, and other effects such as viscous fingering and dispersive mixing, and were optimistic. Also, some oil that was attributed to the CO₂ flood could have been recovered by primary and secondary methods. However, the fact that gravity segregation of CO₂ and water, and gravity override of oil by CO₂ did not seem to be important, even for the assumed $K_v/K_h = 1$, was a positive factor. Bypassing of oil because of permeability stratification appeared to be limited. Overall, vertical sweep efficiency appeared to be good.

Conclusions of simulation studies were:

1. The compositional simulator represented CO₂-Little Knife crude oil behavior and the development of multiple-contact miscibility in slim-tubes.
2. Residual-oil saturation was low above the minimum miscibility pressure and did not depend on CO₂-water ratio.
3. A 1:1 water-CO₂ ratio appeared, on the basis of breakthrough time, to be the best of those investigated. Recovery in the cross-sectional model after one (1) HCPV total fluid injection was 57.2 percent PV or 76.5 percent OOIP. (These numbers include primary and secondary oil and are not corrected for areal sweep and capture efficiencies.)

The following information was used to determine the project injection sequence:

1. Pattern Pore Volume (PV) = 779 M ft³
= 139 M bbl
2. Hydrocarbon Pore Volume (HCPV) = 587 M ft³
= 105 M bbl
3. Injection Rates: Water = 1,150 BPD
CO₂ = 40 tons/day
4. Reservoir Volume Factors: Water = 1.04 R bbl₁/bbl
CO₂ = 74.1 R ft³/ton

FLUID INJECTION

On December 11, 1980, the preflush water injection phase commenced. The injection water was filtered, produced, Mission Canyon Formation water. A total of 29,539 BW (21 percent PV) was injected at the rate of 1,150 B/D. A tracer, isopropanol, was injected with the preflush in a concentration of 0.05 percent by volume (approximately 25 gal/D.). The injected preflush volume was larger than the proposed simulation preflush volume because the anticipated starting date was delayed. As a result, the reservoir pressure in the minitest area was lower, and additional injection was required to repressure to 3,500 psi.

The water and CO₂ (WAG) injection phase was started on January 7, 1981. The 1:1 WAG ratio volume (reservoir barrels water/reservoir barrels of CO₂) was injected in five slugs. Each slug consisted of 5 percent HCPV of CO₂ (400 tons) and 5 percent HCPV of water (5,000 Bbl). A total of 2,094 tons of CO₂ and 20,621 barrels of water were input. Another tracer, n-propanol, was injected with the WAG water in a concentration of 0.05 percent by volume.

WAG injection was completed on March 25, 1981, followed immediately by the drive-water phase. Drive-water injection was maintained at approximately 1,150 B/D until the flood-fronts had passed each observation well. Injection was terminated on September 24, 1981. The fluid injection schedule is located in table 2, with bottom-hole injection pressure shown on figures 7, 11, 13 and 15. The daily injection field data for both water and CO₂ are located in appendix 32.

There were no major problems encountered during the fluid injection phase. However, due to unseasonably warm temperatures in January and February, the CO₂ injection rates were hard to maintain at the 40 ton/day rate. This problem was caused by the liquid CO₂ flashing into a gas near the injection pump suction followed by gas-locking of one or more plungers. In order to alleviate the problem the line insulation was painted silver, the pump was covered, and liquid CO₂ was sprayed directly onto the suction end of the pump.

LOGGING PROGRAM

Because there were no producing wells in the minitest, an extensive effort was made to design an adequate logging and sampling program to obtain as much information as possible²⁶. The primary objectives of the well logging program were the determination of: 1) porosity, 2) original oil saturation, 3) waterflood residual-oil saturation, 4) oil, CO₂, and water saturations at each observation well as a function of time, and 5) timing of CO₂ and water breakthrough.

Open-hole logs from each well were analyzed for original oil saturation and porosity. Overall, the computed log porosity compared favorably with core analysis. Original oil saturations were also computed from the TDT logs recorded during the log-flow-log well tests. Waterflood residual oil saturation was determined during the log-inject-log test run on the injection well.

An in-depth study was made on injection well no. 1 to determine its waterflood residual oil saturation. Three different techniques were used in the analysis. The first technique consisted of calculating the flushed zone oil saturation using the Micro-SFL to determine flushed zone resistivity and porosity from Gulflog (proprietary computer-generated log analyses). The other two techniques used Thermal Decay Time (TDT) data obtained after water injection. One method used these data with a calculated value of sigma matrix. The other method calculated residual-oil saturation independent of sigma matrix. The average of the three techniques was a 44.8 percent, 35.5 percent and 40.9 percent residual-oil saturation for the X, Y, and Z layers (layer designations related to simulation studies), respectively (Table 3).

Oil, water, and CO₂ saturations in the observation wells were computed from TDT logs taken during monitoring procedures. Before monitoring could begin, all of the wells had to have base-run TDT surveys. These TDT surveys provided the capture cross-section and ratio for the formation under conditions which existed prior to drilling the wells. These "original" conditions were necessary because any changes in log response, after the base log, would be interpreted as changes due to the flood process. The final TDT log run during the log-flow-log test was used as the base log for monitoring procedures.

Before water breakthrough, gradiomanometers were run to establish the depth of the oil/water contact in casing (or tubing) in each well. This information was used in determining the bounds for diffusion correction (change in capture cross-section measurement due to migration of neutrons from formation to borehole) of sigma and ratio.

Prior to interpretation, each of the monitor TDT logs was checked for proper calibration. This check was done by crossplotting the monitor run data versus the base data. The data were zoned so that the crossplot did not include the test zone. If the data were found to be miscalibrated, the entire data array was adjusted for offset and gain. The amount of diffusion correction was also determined in this manner. The starting and ending depth for correction was found using the gradiomanometer data.

Initial plans called for logging each of the wells on a monthly basis until significant changes occurred. Because of mechanical problems in observation well no. 1 this was not possible. The first monitor run was made on this well March 9,

1981. Water breakthrough was confirmed from sampling and indicated by the TDT. Because changes had now occurred at one of the wells, monitoring was stepped up to two week periods. This frequency continued for the rest of the project.

A triangulation technique²⁷ was developed for interpretation of the monitor logs (Fig. 79). The technique used open-hole computer log analysis and a base run pulsed neutron log (TDT) to compute triangles whose vertices represented sigma and ratio responses of 100 percent oil, water, and CO₂ saturations for the given porosities. The triangles were computed and stored on a foot by foot basis. Subsequent TDT runs were analyzed by locating the position of the latest sigma/ratio data point within its previously determined triangle and solving graphically for oil, water, and CO₂ saturations.

The only parameters needed for this technique which were not determined previously were ratio water, ratio oil, sigma CO₂ point (response with CO₂ filled porosity), and ratio matrix point. To determine ratio water all that was needed were sigma oil (Σ_{hy}), ratio oil, sigma water (Σ_w), a base run, and a TDT run representing an increased water saturation but no free formation gas or CO₂. The TDT run performed during the log-inject-log on injection well no. 1 was used for the increased water saturation point. Sigma water and sigma oil were previously determined in the analysis of the injection well. Ratio oil was derived by the logging service company. By using the base run data and the injection data the slope of the line between 100 percent oil and 100 percent water was determined. A line could then be constructed having this slope with sigma oil and ratio oil as the end point. Where this line intersected the sigma water point determined ratio water (Fig. 79). Sigma matrix apparent was calculated by solving the volumetric equation using TDT data, sigma oil, sigma water, and computed log-derived porosity and water saturations. Sigma CO₂ point was established by replacing the oil and water in the porosity with CO₂ and solving volumetrically. The final step was to solve for the ratio matrix point. The solution for this point was derived graphically. A line was constructed using the water saturation from the computed log and the base run TDT data. This line intersected sigma matrix apparent at the ratio matrix point. It was assumed that the ratio of the matrix was equal to the ratio of CO₂. Because this was not exactly the case there was a finite error in the system. The error at 10 percent CO₂ saturation was approximately one and a half (1.5) percent pore volume too high. This error decreased to less than one (1) percent at six (6) percent CO₂ saturation. The resulting error in water saturation was less than one (1) percent pore volume when CO₂ saturation was 30 percent pore volume. Because the CO₂ saturations were not large enough to cause more significant errors in the calculations, the system was not changed.

The monitor logging results are presented in tables 4 and 5. Because of the large amount of information involved, only the volumetric averages for the X, Y and Z layers are presented on table 4. Monitor logging of observation well no. 2 indicated a decrease in sigma and ratio on May 5, 1981. This response would normally indicate an increase in oil saturation, assuming the base log was accurate. Because the zone did not change after that date, it was concluded that the base log was not reflecting original conditions in the "W" layer. The base log for the "W" layer was made equal to the May 19, 1981 run. The earlier increase in S_w was attributed to residual mud filtrate. Other than these changes there were no significant indications of saturation changes in the "W" layer in any of the observation wells (Table 6).

Because of mechanical problems in observation well no. 1 it was not possible to log the first monitor TDT until March 9, 1981. At that time the well had already seen injection water and some CO₂. The monitor log analysis indicated water breakthrough but not a significant amount of CO₂. The first significant log indicating CO₂ breakthrough was obtained on June 15, 1981.

The first log indications of water breakthrough in observation well no. 2 occurred on March 23, 1981. The first definite CO₂ indications occurred on May 5, 1981.

Monitor logging on observation well no. 3 showed water breakthrough on May 5, 1981, and the first definite indications of CO₂ on May 20, 1981.

Table 5 is a summarization of the final saturations, as calculated by the monitoring technique, for each of the observation wells. The Y layer ranged from 29.7 percent final oil saturation in observation well no. 1 to 15.2 percent oil saturation in observation well no. 2.

To verify the final monitor logging oil saturations a log-inject-log (L-I-L) process was also performed on observation wells no. 2 and 3. The results from the two techniques agreed very well on observation well no. 2. The monitoring technique results indicated a 15.2 percent oil saturation for the Y layer and the log-inject-log (L-I-L) 15.0 percent. The results from the L-I-L process run on observation well no. 3 indicated an oil saturation of 11.4 percent for the Y layer. This compares with 25.9 percent oil saturation as calculated from the monitoring technique. The initial injection rate for the L-I-L was higher than specified. Excess stripping of oil probably occurred as a result of this high rate.

Additional information about the logging program and triangulation technique as well as tabulated data for each of the well's monitor runs can be found in appendix 33. The monitor TDT and gradiomanometer logs from each observation well can be found in appendices 34, 35 and 36.

FLUID SAMPLING PROGRAM

Obtaining fluid samples from each observation well on a periodic basis was another method of determining the advance of the flood front²⁸. These results could then be compared to logging results. Subsurface fluid samples were taken at monthly intervals through February, 1981, at which time the frequency was increased to every other week to insure that the CO₂ front would not pass the observation wells without being detected. Subsurface samples were obtained along with separator gas samples until water breakthrough occurred. After water breakthrough it was necessary to gas-lift the wells to obtain the separator gas samples. The procedure for collecting separator-gas samples after water breakthrough involved bleeding the wellhead pressure to zero (0) psig on the day prior to sampling to remove the majority of the N₂ remaining from the previous gas-lift operation. On the day of sampling, the wellhead pressure was again reduced and a sample of the gas taken just before starting gas-lift operations. Gas-lift operations were terminated after approximately 10 barrels of fluid had been produced at the separator. The subsurface sampler was then used to collect a water sample. From the analysis performed on these samples, it was possible to determine within several days the time of breakthrough for the preflush water, CO₂, and the WAG water at each observation well.

Table 7 reports the compositional analysis of each subsurface oil sample obtained from observation wells no. 2 and 3. Tables 8 through 13 report the composition on a N₂ and H₂S-free basis of the separator gas samples obtained from each observation well. Some of these samples were contaminated with large concentrations of nitrogen from the gas-lift operation. Therefore, when these are reported on a nitrogen and hydrogen sulfide-free basis, the resulting figures can be somewhat misleading. Analyses were made on the produced waters from each observation well for the tracers that were placed in the preflush and WAG water and these results are given in table 14. Isopropyl alcohol (IPA) was placed in the preflush water and normal propyl alcohol (NPA) was placed in the WAG water. The carbon dioxide ¹³C/¹²C ratio was determined on the solution CO₂ and on the injected CO₂. The isotopic value for the solution CO₂ was determined to be -2.3°/° (parts per thousand) and that of the injected CO₂ near -49°/°. With this large difference, the arrival of the injected CO₂ at each observation well was easily determined. The values listed in table 15 are expressed in the common delta notation.

$$\delta^{13}\text{C} = \frac{(\text{}^{13}\text{C}/\text{}^{12}\text{C})_{\text{sample}} - (\text{}^{13}\text{C}/\text{}^{12}\text{C})_{\text{standard}}}{(\text{}^{13}\text{C}/\text{}^{12}\text{C})_{\text{standard}}} \times 1000$$

The values are reported with respect to the international PDB (Peedee Belemnite) standard in per mil (°/°) or parts per thousand. The values shown in figures 80, 81 and 82 have been calculated on a percentage basis as follows [observed $\delta^{13}\text{C}$ - (-2.3°/°)] divided by [-49°/° - (-2.3°/°)] times 100.

Results of the fluid analysis made on each observation well are shown graphically in figures 80, 81 and 82. The time at which each component responded at each observation well was dependent upon the reservoir characteristics and the distances from the injection well. In general, they all showed the same behavior with respect to each fluid. The IPA placed in the preflush water reached each observation well first, increased to a maximum and then declined. The NPA placed

in the WAG water reached each observation well after CO₂ breakthrough, increased to a maximum concentration and then declined. Due to mechanical problems in observation well no. 1, by the time the first fluid samples were obtained both CO₂ and IPA in the preflush water were present at the wellbore. Carbon dioxide breakthrough occurred simultaneously with the IPA in the preflush water in observation well no. 3 and some six weeks after IPA breakthrough in observation well no. 2 based on the CO₂ ¹³C/¹²C isotope ratio analysis. This CO₂ isotope analysis was a very good method because nitrogen contamination from the lift gas had no effect on the results. The CO₂ content in observation well no. 3 separator gas after breakthrough was not as definitive as in observation wells no. 1 and 2.

Based upon the results obtained from fluid sampling, the following conclusions were made:

- 1) Analysis of the CO₂ isotope ratio proved to be a very successful technique in determining CO₂ breakthrough.
- 2) Arrival times of the preflush and WAG waters at each observation well were successfully determined by using two different alcohol tracers.
- 3) When the observation wells were produced for sampling using nitrogen gas-lift, compositional analysis of the separator gas for CO₂ content did not provide reliable results.

Additional information on the fluid sampling program and procedures can be found in appendix 37.

PRESSURE CORING

Zabolotny Observation Well No. 4

The success of the minitest was evaluated, in part, by drilling a pressure core well, observation well no. 4. (Appendix 38 contains the daily drilling report for observation well no. 4 and also includes daily drilling reports for injection well no. 1 and observation wells no. 1, 2 and 3). The well was drilled through a "swept" portion of the Mission Canyon Formation to determine the effectiveness of the water and CO₂ (WAG) process and confirm TDT log residual-oil saturations (Fig. 3). In order to obtain good core and reservoir information, it was necessary to utilize a coring fluid that would exert a hydrostatic pressure of not more than 200-300 psi greater than formation pressure.

The formation pressure in the Mission Canyon was at a minimum pressure of approximately 3,500 psi at 9,800 feet, which was less than the fresh water (.433 psi/foot) gradient. Since the determination of residual-oil saturation was a primary objective of this test, an oil-based mud was ruled out. The viable alternative was a fluid whose hydrostatic pressure could be significantly reduced by means of gaseous injection. Due to the presence of hydrogen-sulfide gas, the most feasible alternative was to inject an inert gas. Nitrogen was selected for reasons of safety, economy, and availability.

The well was spudded on May 9, 1981, with the core target area being approximately half way between the injection well and observation well no. 2 (Fig. 3). Due to flowlines and other surface equipment, it was not possible to rig-up directly over the target area. Therefore, the rig was located 500 feet to the east and the well was directionally drilled. This surface location was not critical because the well would have to be directionally controlled.

Produced formation water was used as the base for the drilling fluid. That water was then saturated with NaCl and the following additives were used to impart the desired fluid properties: starch, attapulgite (salt-water clay), and lime. This mud was used to drill to 9,793 feet, then the well was logged, and intermediate casing was set. The logs for observation well no. 4 are in Appendix 39. The remaining fluid in the hole was then displaced with the specialized coring fluid.

The coring fluid composition was designed considering the following parameters:

- 1) overbalance pressure of not more than 300 psi over formation pressure,
- 2) minimum drilled solids,
- 3) non-dispersed,
- 4) wide particle-size distribution,
- 5) low "spurt-loss".

Laboratory tests were conducted using fresh water as the base fluid. The lowest attainable mud weight from these tests was 9.1 lb/gal, resulting in a

differential pressure of approximately 1,100 psi. Therefore, gas injection was used as a means of lowering the hydrostatic pressure. The following injection points were considered: 1) a parasite string tied into the surface casing at a specified depth, 2) the mud pump suction, or 3) the stand pipe. The decision was made to inject into the stand pipe. With alternatives one and two there would have been problems with cuttings removal and controlling downhole pressures.

The desired hydrostatic pressure of 3,800 psi was based on maintaining 200 psi greater than the estimated formation pressure (3,500 psi) plus an additional 100 psi for safety. The specialized coring fluid weighed 9.0 lb/gal which resulted in a hydrostatic pressure of 4,586 psi at 9,800 feet. Thus, the coring fluid hydrostatic pressure was 786 psi greater than desired. It was estimated that 460 SCF/min of nitrogen injection would lighten the hydrostatic pressure sufficiently. The calculations for determining this rate are contained in appendix 40. With the use of a manometer, run inside the drill string to just above the bit, the circulating hydrostatic pressures were checked. The nitrogen injection rate was adjusted according to the manometer reading at the surface until the desired hydrostatic pressure was attained. This satisfied the first coring fluid composition parameter (i.e., having an overbalance pressure of not more than 300 psi over formation pressure).

The second criteria for the coring fluid was that it be a low-solids fluid. The first step taken to assure this objective was to flush the surface circulating system (mud pits, pumps, and mud lines) thoroughly before mixing the coring fluid. Also, throughout the coring operation, special attention was given to solids removal to maintain the overall solids content at a minimum.

Based on observed laboratory results shown in tables 16 through 19, the formulation of the coring fluid met the other requirements i.e., non-dispersed, wide particle-size distribution, and low "spurt-loss". These results indicated that a coring fluid with a composition similar to sample no. 1 (Table 16) and sample no. 3 (Table 18) would provide suitable rheological properties and exhibit a low "spurt-loss".

The following composition, used in this project, was selected on the basis of the lab results discussed above.

Coring Fluid Composition

Bentonite	12.5 lb/bbl Modified
Starch	4.0 lb/bbl
Carboxymethyl Cellulose	1.0 lb/bbl
Inert Clay	40.0 lb/bbl
Chelated Zinc Tannate	1.0 lb/bbl

In addition, a radioactive tracer (tritium, a beta source) was added to the coring fluid to check for invasion of coring fluid into the core.

Due to the presence of hydrogen sulfide (H_2S) in the Mission Canyon Formation, special safety measures were necessary. The coring fluid was pretreated with chelated zinc tannate, signs were posted on location, and special training was given to all personnel. Hydrogen sulfide safety equipment was

installed as well as a rotating head, mud-gas separator, degasser, back-pressure valves, and diverter lines.

One problem associated with the nitrified coring fluid was gas-entrainment. The viscosity was such that air and gas could not readily break out of the coring fluid at the surface. Surfactants, which might have eliminated the problem, were not used since core wettability could have been altered. However, the problem was greatly reduced by "pinching back" on the butterfly valve leading to the mud-gas separator. This restriction created enough shear to thin the fluid and allow the gas to be more easily removed. Also, placing the mud-mixing and solids-control equipment discharge lines below the mud level in the pits helped to minimize the problem.

Information about pre-pressure coring, the core tool, and the low-invasion gel used can be found in appendix 40. Fifty-six feet of the Mission Canyon Formation were pressure cored from a depth of 9,803 feet to 9,859 feet (Fig. 83). Total length of core recovered was 45.3 feet. Of the seven pressure cores cut, all maintained pressure except core five. A brief description of each core run follows:

- Run no. 1: Cored 8 feet. Recovered barrel with 3,550 psi. The gauge of the bit was damaged by junk in the hole.
- Run no. 2: Cored 8 feet. Recovered barrel with 3,200 psi.
- Run no. 3: Cored 8 feet. Recovered barrel with 2,000 psi. The low pressure caused by a cut "O" ring on the regulator section.
- Run no. 4: Cored 8 feet. Recovered barrel with 3,100 psi.
- Run no. 5: Cored 8 feet. Recovered barrel with -0- psi. The loss of pressure caused by a piece of core stuck in the ball valve, not allowing the ball to close. About 7-1/2 feet of rock was recovered.
- Run no. 6: Cored 8 feet. Recovered barrel with 3,800 psi.
- Run no. 7: Cored 8 feet. Recovered barrel with 3,000 psi. The low pressure caused by a damaged "O" ring in the regulator section.

The pre-set regulator which activated the high-pressure nitrogen reservoir in the core barrel was set at 3,800 psi. The nitrogen supply chamber was not large enough to sufficiently compensate for thermal contraction of the nitrified coring-fluid between the outer core barrel and inner barrel during retrieval of the core and prior to its being frozen. It was not until the sixth core run that a decision was made to circulate non-nitrified coring fluid to the bit before closing the coring tool. Core six retained full pressure. Failure to maintain full pressure on core seven was due to "O" ring damage in the high-pressure nitrogen reservoir. Appendix 40-A contains drill times, weights, RPM's, mud weights, and other data on each pressure core run.

Oil and water saturations from core analysis of the pressure core in observation well no. 4 are compared to oil and water saturations from core analysis in injection well no. 1 and observation wells no. 1, 2 and 3 (Fig. 84).

Appendix 39-C shows analyses of the seven pressure cores as well as the tracer-fluid analysis. A cylindrical plug was drilled from each frozen core segment selected to test for filtrate invasion. Each plug was drilled concentrically to the axis of the core segment (along its vertical axis). This yielded a drilled "plug" and a remaining portion, the "donut". Of the twelve samples taken from observation well no. 4, five had a higher reported filtrate concentration in the plug than in the donut³⁰. Intuitively this should not be, since the plugs were cut from the center of the donuts. The five samples are listed in table 20. The first item of interest, and only common feature of all, is that they were recovered at pressures lower than the reservoir pressure. The cores were cut with a mud pressure of about 3,800 psi. The lower pressures indicate that some fluid movement occurred as a result of pressure depletion. The second item that yielded meaningful comparisons was using the maximum experimental error to determine the limits of the filtrate concentrations. The error is ± 10 percent of the radioactivity reading. This comparison showed that only two samples, no. 4 and 8, had filtrate concentration differences that were beyond experimental error. The next comparison was between the analyses of the nearest cores to the plug and donut samples. The obvious item in these analyses was the voidage in the cores. Samples no. 4 and 8 had the highest voidage. This high voidage indicated that these samples had the greatest amount of fluid movement. This fluid movement probably related directly to pressure depletion. Radioactive tracers served as good indicators of filtrate invasion. Where filtrate invasion, by pressure depletion, occurred it is doubtful that a high degree of accuracy in pressure core fluid saturations resulted (Appendix 41).

Table 21 gives oil, water, and CO₂ saturations along with permeability and porosity vs. depth for each pressure core³¹. Oil and water saturations were corrected to reservoir conditions using formation volume factors (1.66 for oil, 1.056 for water). CO₂ saturations (actually the amount of CO₂ present irrespective of whether dissolved in oil or water or present as a free-gas phase) were calculated from the mole fraction CO₂ in the gas, the volume of gas evolved, and the core pore volume. The depths given are those estimated to correspond to log depths and not those in appendix 38. The approximate locations of the W, X, Y and Z layers, as designated for the simulation work, are also shown in table 21.

The extent to which oil saturation was changed by flushing and pressure reduction depended on a number of factors. A saturation at or below waterflood residual was not affected by flushing in a balanced pressure system.* Pressure reduction was significant only if it was below the bubble-point pressure and gas was evolved. With no CO₂ added, this pressure was 2,700 psi. At high CO₂ concentrations, the bubble-point pressure was at, or close to, 3,800 psi. Even with some gas evolution, oil saturation reduction was limited to shrinkage as a result of solution gas loss at least at initially low oil saturations. Oil saturations in the less than 10 percent PV range have to be related to the CO₂ miscible displacement process.

*In a study of flushing during coring by Jenks, et al³², it was determined that overbalance pressures of 300 psi or less would minimize stripping of residual oil.

In all cases, the stock tank oil saturations represented an absolute lower limit to the actual saturation. Where compositional changes had not occurred, the volume-factor-corrected oil saturation was a lower limit. Likewise, the CO₂ saturation in-situ could not be less than that contained in the cores.

Core no. 1, pressure 3,550 psig, and
Core no. 2, pressure 3,200 psig *
(W layer - 9,803 to 9,816.7 feet)

These cores were flushed with filtrate but were retained above the bubble-point pressure (2,700 psi). Only trace amounts of CO₂ corresponding to that naturally occurring in the solution gas were present. Oil saturations are probably good estimates of waterflood residuals. It was uncertain, however, whether the oil saturations in-situ were actually that low. Water saturations were most likely high (as indicated by $S_w + S_o > 100$ percent) because of water imbibition in the core barrel as oil shrinkage occurred.

Core no. 3, pressure 2,000 psig
(Bottom of W layer and X layer - 9,819 to 9,824.5 feet*)

This core was flushed with filtrate and was reduced below the original bubble-point pressure. Even though pressure depletion must have occurred, CO₂ saturation averaged 2.3 percent PV, well above that occurring naturally. Oil saturation averaged 17.9 percent PV. Water saturations, again, were most likely high.

The pressure depletion introduced considerable uncertainty. The oil saturation and the presence of CO₂, however, suggested some CO₂-related displacement. Core five which was recovered with no pressure, by comparison, contained much more oil.

Core no. 4, pressure 3,100 psig
(Y layer - 9,827 to 9,832 feet)

Oil saturations in this core were low - 6 percent PV average on a stock tank basis. (The volume factor correction was used in table 16 for consistency, but is probably too high because of stripping of the solution gas by CO₂.) CO₂ saturations were high and indicated free CO₂ present. The loss of pressure from 3,800 psi (original pressure) to 3,100 psi probably resulted in some CO₂ being lost.

Core no. 5, pressure 0 psig
(Z layer - 9,835 to 9,840 feet*)

This core lost all its pressure as well as being substantially flushed by mud filtrate. Despite this, oil saturations were high - 32.7 percent PV. This high oil saturation in the core suggested that this zone was totally unaffected by CO₂ and that oil saturation was no lower than waterflood residual.

* Core depth from drill-pipe measurements. Approximate electrical-log correlation in figure 85.

Core no. 6, pressure 3,800 psig, and
Core no. 7, pressure 3,000 psig
(9,843 - 9,859 feet)

The comments made for cores one and two apply (Fig. 83).

A comparison of oil saturations predicted by the Gulflog with those obtained from the pressure core analysis is shown in figure 85. Agreement was generally good over layers X, Y and Z, or at least consistent with the idea that the core data represented a lower boundary to oil saturation. Agreement was less consistent in the W layer and below the Z layer.

The very low residual oil saturations associated with CO₂ flood multiple-contact miscible displacement were seen only in a four foot zone in core four in the layer Y (9,828 - 9,831 feet). At the top of core four, in the top of layer Y, and in core three and the bottom of the layer W, CO₂ saturation and CO₂ concentration in evolved gas, above ambient levels, together with oil saturations, which appeared to be below waterflood residual oil levels, were present and suggested some CO₂-related displacement. However, pressure was not completely retained in core three, so that oil saturations there were suspect.

The monitor log data from observation well no. 2, at the time the observation well no. 4 pressure core was cut (Fig. 86 and 87), may help in resolving this uncertainty. The log data showed CO₂ present above the very low oil saturation zone to the same extent as was seen in observation well no. 4. Significant oil displacement as a result of this CO₂ seemed to be limited, however, to the Y layer. This may indicate that the CO₂ which penetrated the bottom of the W layer in observation well no. 4 also did not result in important oil displacement.

As a result of the pressure coring operations the following conclusions were realized:

1. Very low residual-oil saturations associated with multiple-contact miscible displacement by CO₂ were seen in a four foot interval in the middle of the Y layer (9,828.0 - 9,832.0 feet).
2. Less efficient displacement (but still better than waterflooding) seems to have occurred in the Y layer above this interval. The presence of CO₂ in the W layer may not be significant in terms of oil recovery.
3. The pressure core analysis and interpretation were a worthwhile part of the Little Knife CO₂ flood minitest in terms of the information gained.

Additional information about the pressure core operation and analysis can be found in appendices 40 and 42.

* Core depth from drill-pipe measurements. Approximate electrical-log correlation in figure 85.

MINITEST SIMULATION

As previously mentioned, two simulation models were used in various dimensional modes during the minitest³³. A three-dimensional black-oil simulator was used to characterize the reservoir, history match production, and compute the amount and rate of water injection needed to maintain pressure in the minitest area. A one-dimensional compositional model was used to match the laboratory slim-tube test performance. By matching the miscibility test data, the one-dimensional mode was utilized to determine a rough estimate of the CO₂ slug design. A two-dimensional, cross-sectional, compositional simulator model was used to further develop and optimize the water/CO₂ injection sequence. The two-dimensional model was then expanded to the three-dimensional mode in order to monitor the performance of the minitest.

The minitest project interval was subdivided into four layers (W, X, Y and Z) for the simulation study (Fig. 88). These intervals were selected based upon the porosity and permeability characteristics. The results of the core and Gulflog analyses are displayed in tabular form in table 22. The properties analyzed included the log depth, thickness, porosity from cores and Gulflogs, horizontal and vertical permeabilities from core analyses, and initial oil saturation and water-flood residual saturation from Gulflog analyses.

Since the test pattern consisted of a single injection well and four observation wells in an inverted four-spot configuration, covering five (5) acres, it was estimated that only a small portion of the total field would be affected by the minitest. Therefore, an area immediately surrounding the minitest and enclosing 640 acres (one square mile) was modeled. Only three producing wells, which were completed in the project interval in this area, were considered to significantly influence the pilot. These three producing wells, Zabolotny 4-3-1A, Zabolotny 1-3-4A and Zabolotny 2-3-3A, were included in the simulation model.

The Gulf compositional simulator³⁴ calculated the distribution of all the individual components of the hydrocarbon system through space and time and also the distribution of these components in the gas and liquid phases. The simulator considered convective miscible transport of each component through the two hydrocarbon phases. The interphase mass transfer of each component between the oil and gas phases was governed by the equilibrium coefficients (K-values) under the assumption of thermodynamic equilibrium. The effects of gravity and capillary forces were included in the three-phase flow equations which were governed by a generalized form of Darcy's law.

The Peng-Robinson equation of state^{35, 36 and 37} was incorporated into Gulf's compositional simulator to predict reservoir fluid properties and phase behavior. A modified Peng-Robinson phase package computer program³⁸ developed at Gulf's Houston Technology Center was used to match the laboratory measured data from the differential liberation study and the CO₂ swelling tests. The optimal parameters for the Peng-Robinson equation of state are given in tables 23 and 24. The fluid composition was grouped into a total of seven pseudo components: CO₂, H₂, C₁ and N₂, C₂, C₄*, C₁₀* and C₁₄*. Nitrogen was included in methane. Propane, butanes, and pentanes were combined as C₄*. Hexane and heptanes, plus were lumped together and then divided into C₁₀* and C₁₄*, according to Lin³⁸. The hydrocarbon phase properties were computed as functions of pressure, temperature, and composition using the Peng-Robinson equation of state. A two-dimensional K-value, as a

function of pressure and CO_2 concentration, was read-in as input data and was generated externally by the Peng-Robinson equation of state. Additional model input parameters associated with water properties and rock compressibility are presented in tables 25 and 26. The generated values are shown in figures 38⁹ through 95. The phase viscosities were evaluated by the Thodos correlation³⁹. Excellent agreement between the laboratory and calculated values was obtained. The deviation between the measured and the calculated stock tank oil density was about five (5) percent. This caused a deviation between the measured and calculated differential formation volume factor (B_o) of four (4) percent at saturation pressure. The average absolute deviation between the measured and calculated oil viscosity for a 50:50 CO_2 -oil mixture (near the critical region) was about 10 percent.

Capillary pressure data were available on 12 core samples from observation well no. 1. These data were averaged for each layer and are shown in figure 96. The curves of water-oil relative permeability versus water saturation for each layer are presented in figures 97 through 100. These relative permeability curves were based on the laboratory measured values. The end points in the curves were adjusted based upon the field observed initial oil saturations and waterflood residual-oil saturations. Further adjustments were made to match water saturation profiles observed at the three observation wells. Gas-oil (drainage) relative permeability data for a nitrogen and mineral oil system measured on a restored core from observation well no. 3 were used to estimate CO_2 -oil (imbibition) relative permeability curves. The residual-gas saturation (imbibition curve) to the waterflood was estimated to be 15 percent. Three phase oil relative permeability was calculated using Stone's correlation⁴⁰. Additional information about the relative permeability investigation work can be found in appendices 31 and 42.

The simulator employed the IMPES⁴¹ (Implicit Pressure Explicit Saturation) type numerical procedure that resulted in an implicit pressure equation and three explicit saturation equations. The set of simultaneous pressure equations was solved by a direct method that used an alternating diagonal ordering scheme. The saturation equations were solved explicitly.

The coordinate system used for this study is illustrated in figure 101. The X-direction was chosen along the line connecting injection well no. 1 and observation well no. 1. This direction was along the average fracture strike direction (Fig. 52). The relative well locations for the production and minitest wells are given in table 27.

A rectangular grid consisting of $11 \times 11 \times 2$ was prepared to represent one quadrant of the minitest area. Zone D (layers X, Y and Z) was considered as one layer. This grid system was used in the preliminary simulation study to match the bottom-hole pressures at injection well no. 1 and the observation wells. Water and CO_2 breakthrough times at the three observation wells were also considered in this preliminary history match. This $11 \times 11 \times 2$ grid system was then extended to an $11 \times 11 \times 4$ grid system (Fig. 102) to study the stratification effects on the fluid saturation distributions. The four-cell vertical dimension of the grid structure was necessary to depict the four layers previously discussed. A rectangular grid consisting of $16 \times 15 \times 4$ (Fig. 103) was used to simulate the entire CO_2 minitest area. This grid system included injection well no. 1, four observation wells, and

three Zabolotny production wells. Finally, an 11x11x6 grid system was used for the sensitivity study.

In the preliminary simulation study using the grid systems of 11x11x2 and 11x11x4, a separate geological model was prepared for each observation-injection well pair (quadrants I, II and III in figure 101). Table 28 shows porosity, permeability, initial oil saturation, waterflood residual-oil saturation, and thickness for each layer.

Final simulation runs were made using a 16x15x4 grid system, that included all eight wells. Average geological properties for each layer in this model were used. Porosity, S_{oi} , S_{orw} , and the thicknesses for layers X, Y and Z were based on detailed information available from the logs and core analysis (Table 22). However, the thickness of layer W and the horizontal and vertical permeabilities were varied by matching the four-well pulse test responses at the three observation wells. The comparisons between the observed and model predicted values for the four-well pulse tests are shown in figures 104, 105 and 106. During the matching process, it was necessary to increase the thickness of layer W. The calculated permeabilities were almost 2.5 times that of the measured values from the whole core analysis. These higher average permeabilities were interpreted to be the results of the effect of short noncontinuous fractures dispersed somewhat uniformly across the minitest area. The porosity-permeability correlation and the core measured permeabilities are shown in figure 107. The permeability-porosity correlation modified as a result of pulse test matching was used in the study. The vertical permeabilities between layers were found to be small compared with the horizontal permeabilities. The X-direction (northeast-southwest) permeabilities were increased by a factor of 1.25 over the Y-direction (northwest-southeast) values. This alteration was made to satisfy the fracture orientation study on the core from the injection well.

The pressure performance matches are shown in figures 108 through 111. Excellent matches were obtained between the field recorded bottom-hole pressures and computed (model) pressures in the observation wells. No significant differences were observed among the three grid systems (11x11x2, 11x11x4, 16x15x4) for the bottom-hole pressure calculations at all the minitest wells. Field data showed that the bottom-hole pressures at the injection well increased to 4,800 psia during the water preinjection phase. Then bottom-hole pressures decreased to 4,000 psia during CO_2 and 3,700 psia during shut-in. A skin factor of 12 was required to match field data in the preflush phase. The maximum deviation between the observed and computed bottom-hole pressure at the injection well was about 300 psia during either the shut-in or CO_2 injection periods. In the drive water injection phase, the bottom-hole pressure was about 4,600 psia. The skin factor was reduced from 12 to 8 during the drive water injection phase. This improvement may have been due to the leaching effect on the carbonates during CO_2 injection.

Excellent match between the observed and model predicted pressures at observation well no. 1 was obtained throughout the entire history. The predicted bottom-hole pressures were approximately 50 psia lower than the observed values before May 20, 1981, at observation wells no. 2 and 3. The maximum deviation between the observed and computed pressures was only 75 psia at observation wells no. 2 and 3.

The triangulation technique^{17, 18} to interpret TDT logging data evaluated water, CO₂-free oil, and CO₂ saturations. These saturation values were computed at various points in time and compared with the model calculated values.

The water saturation history matches at the observation wells during the course of the minitest are shown in figures 112 through 117. Comparison between the simulation results and field observed data showed good agreement. The model predicted water saturation profiles for each layer are compared with the field logging data in figures 112 through 114. The lines represent the simulation results using a 16x15x4 grid system. The discrete points represent the observed field data based on pulsed-neutron logs. The initial and final water saturations calculated from pulsed neutron logs at observation well no. 1 were lower than the corresponding calculated values for observation wells no. 2 and 3. The simulation results were based on the average input values for all three observation wells (Table 28). The field observed water saturations for layer Y at observation well no. 1 on May 18 and June 2, 1981, were low. In matching these data, the permeability-porosity correlation was adjusted slightly and the vertical permeabilities between layers were reduced substantially.

The water breakthrough times for zone D (layer X+Y+Z) were in excellent agreement with the logging data (Figs. 115, 116 and 117). Based on the water tracer analysis (Table 14), the water breakthrough at observation well no. 1 occurred before March 9, 1981. And the water breakthrough at observation wells no. 2 and 3 occurred on March 23, 1981 and May 5, 1981, respectively. These data were consistent with data from pulsed-neutron logs.

Most of the injected CO₂ dissolved in the reservoir fluids and traveled to the observation wells. Part² of the injection CO₂ was trapped by water in the CO₂-swept zone in the vicinity of the injection well. The solubility of CO₂ in the water phase was not considered in the model because of the model limitation. It was estimated that 72 SCF of CO₂ would dissolve in one barrel of water under the reservoir conditions.

Figures 118, 119 and 120 show the profiles of CO₂ content at the observation wells from separator gas analysis (Tables 8 through² 13), CO₂ isotope analysis (Table 15), and logging data. Figure 118 shows CO₂ breakthrough on or about March 12, 1981, at observation well no. 1 from isotope analysis, separator gas analysis, and logging data. Figure 119 shows CO₂ breakthrough on or about May 6, 1981, at observation well no. 2 from separator gas analysis, CO₂ isotope analysis, and logging data. From figure 120, both logging and CO₂ isotope analysis indicated that CO₂ breakthrough did occur on or about May 6, 1981. However, there was no indication of CO₂ breakthrough until July 15, 1981, at observation well no. 3 from separator gas analysis. The CO₂ isotope analysis was more reliable than the separator gas analysis because nitrogen contamination from the lift gas had little effect on the results.

The CO₂ saturation history matches for the individual layers X, Y, Z, and zone D at the observation wells during the course of the minitest are shown in figures 121, 122 and 123. The comparison between the simulation results and field observed data indicated good agreement. The solid lines represent the simulation results using a 16x15x4 grid system. The discrete points represent the observed data based on pulsed-neutron logs. It was noted that no appreciable amount of CO₂ was detected in layer Z at any of the observation wells. However, some CO₂ did

migrate to layer X at observation wells no. 1 and 3 (but not in observation well no. 2). This CO₂ migration indicated that some gravitational segregation may have occurred in the reservoir.

Figure 124 shows the swelling factor of oil-CO₂ mixtures versus CO₂ concentration at 245°F for the Little Knife crude oil. These data were used in computing the oil saturation on a CO₂-free basis.

The oil saturation history matches at the observation wells during the course of the minitest are shown in figures 125 through 130. The discrete points represent the field observed values based on TDT logs. The lines represent the simulation results using the 16x15x4 grid system. The model predicted oil saturation profiles for each layer are compared with the field logging data in figures 125, 126 and 127. The comparison between the simulation results and the logging data for oil saturations in zone D (layer X+Y+Z) at the three observation wells are shown in figures 128, 129 and 130. As seen from these figures, satisfactory history matches are achieved for the three observation wells.

The comparison of model predicted oil saturations at observation well no. 4 with that obtained from pressure-core analysis and Gulflog analysis is shown in figures 131 and 132. The grid location of observation well no. 4 in the 16x15x4 system was (5,10). The well was spudded on May 5, 1981. Open-hole logs were run on July 15, 1981, for correlation purposes, and an intermediate casing string was set. Pressure-cores were taken from the project interval on July 17, 1981. Open-hole logs were then run over the pressure-core interval on July 20, 1981. The Gulflog was computed by combining the two open-hole log suites.

In figures 131 and 132, solid lines represent the observed data and dashed lines represent simulation results using the 16x15x4 grid system. Oil saturation profiles for observation well no. 4 obtained from Gulflog analysis were the CO₂-free oil saturations at reservoir conditions, while the oil saturation profiles obtained from pressure-core analysis were the oil saturations measured at stock tank conditions. The model-predicted oil saturations were in satisfactory agreement with the observed values from both Gulflog and pressure-core analysis for layer Y. However, the model-predicted oil saturations were somewhat low for layer X and high for layer Z compared with the Gulflog oil saturations. (These were consistent with the phenomena observed at observation well no. 2.) The results indicated that the actual vertical permeability between layers X and Y should be lower than three (3) md in quadrant II of the minitest area (Fig. 101).

Figures 133, 134 and 135 show the model-predicted fluid saturations for layer Y at the end of CO₂ injection (March 25, 1981). Figures 136, 137 and 138 show the model-predicted fluid saturations for layer Y on July 17, 1981. Figure 139 shows the calculated CO₂-free oil saturations on July 17, 1981. The radius of the CO₂-swept zone, at zero or a very low value of residual oil saturation, in the minitest area was estimated to be 110 feet.

Simulation results showed that the percentage of oil-in-place (on December 11, 1980) displaced for the straight waterflood in the minitest area was 37 percent (on a STB basis) from the entire project interval. The CO₂ flood with 1 to 1 WAG ratio in the minitest area was 50 percent (on a STB basis) from the entire project interval. The simulation results are given in table 29.

Figure 140 shows the simulated oil recovery (on a STB basis) as a percent of oil-in-place at the beginning of the minitest (December 11, 1980) for the CO₂ WAG process and the straight waterflood by "producing" all three observation wells. The simulated fluid production in the three observation wells was maintained such that the average reservoir pressure in the minitest area was identical to the observed pressure history in the actual minitest operation. Figure 140 shows that the waterflood and CO₂ flood recoveries were equal to 35 percent and 44 percent of oil-in-place, respectively.

The minitest was started on December 11, 1980, at an average pressure of 3,350 psia; whereas, the average original reservoir pressure in the minitest area was about 4,400 psia. Based upon the natural depletion from this original pressure to 3,350 psia, about six (6) percent of OOIP was recovered from the reservoir. This estimate was based upon an independent simulation study of the natural depletion (fluid expansion) mechanism.

Thus, if the oil recovery is based upon the OOIP, the following recoveries would be obtained:

$$\begin{aligned} \text{Primary} + \text{Waterflood} &= 6 \text{ percent} + 0.94 \times 35 \text{ percent} = 38.9 \text{ percent} \\ \text{Primary} + \text{CO}_2 \text{ enhanced waterflood} &= 6 \text{ percent} + 0.94 \times 44 \text{ percent} = 47.4 \\ &\text{percent} \end{aligned}$$

(where, natural depletion recovery = 6 percent, remaining OIP on 12/11/81 = 94 percent of OOIP, waterflood recovery = 35 percent, and CO₂ flood recovery = 44 percent).

An areal grid system was prepared to represent one quadrant of the minitest area including observation wells no. 2 and 4. This grid system was identical to the one used before except it had six rather than four layers. Layer Y was divided into three layers Y1, Y2 and Y3. The input data for the reservoir rock properties are given in table 30.

Results of this simulation run indicated (Figs. 141 through 145) that computed CO₂ saturations were slightly less in the middle-Y zone than the observed log values, and slightly more in the upper-Y zone than the observed log values. However, the composite match between the observed and computed CO₂ saturations for layer Y was essentially the same for the six and four layer models.

Figures 146 and 147 show comparisons of model-predicted CO₂-free oil saturations with the saturations obtained from the logging and pressure-core data for observation well no. 4.

SWEEP EFFICIENCY

The sweep efficiency in the minitest area was quantified in both the areal and vertical modes. This quantification was based on the simulation of minitest performance.

Areal sweep efficiency, layer-by-layer basis, is defined as:

$$\frac{\text{Pore volume in layer swept by CO}_2}{\text{Total pore volume in layer within minitest pattern}}$$

Sweep efficiency in the vertical mode is defined as:

$$\frac{\text{Pore volume in vertical cross section swept by CO}_2}{\text{Total pore volume in vertical cross section within minitest pattern}}$$

The carbon dioxide content of the reservoir fluid was approximately one-to-two (1-2) percent prior to the injection of extraneous carbon dioxide. The presence of carbon dioxide above the pre-injection saturation in a given grid block in the minitest simulation model was used to denote that the grid block had been swept by carbon dioxide.

Two levels of carbon dioxide saturation in the reservoir fluid were used to calculate sweep efficiency ... three (3) percent and 10 percent. These values of carbon dioxide saturation were calculated after 217 days of injection, on August 17, 1981, and after 1.33 HCPV of total fluid injection. The resulting sweep efficiencies are as listed in table 31.

The areal sweep was 100 percent of the minitest pattern. The vertical sweep efficiency was approximately 52 percent. Thus, the pattern sweep efficiency for carbon dioxide approached 52 percent at the end of the test.

COMMERCIALIZATION OF THE CO₂ MISCIBLE DISPLACEMENT PROCESS

The reservoir model developed for the minitest area was extended to 160-acre spacing. A 15x15x4 rectangular grid was prepared to represent one quadrant of a five-spot pattern. This grid system included only one injection well and one production well. Layer W was not perforated in the production or the injection well.

The initial pressure distribution was determined on the basis of an initial reservoir pressure of 4,390 psi at a datum plane of 7,200 feet subsea. The original oil-in-place (OOIP) at the beginning of the production (1-1-78) was calculated to be 2,928 MSTB for a unit well in the 160-acre five spot pattern. The average oil production from Zabolotny Wells 1-3-4A, 2-3-3A, and 4-3-1A was assigned to the production well in the model. The current operation of natural depletion was continued until the average reservoir pressure declined to 2,500 psi as of 1-1-83. Next, water was injected at the rate of 1,200 B/D from 1-1-83 to 3-1-84 to raise the average reservoir pressure to 3,500 psi. A straight waterflood or a 1:1 CO₂ WAG process was then implemented at a constant reservoir pressure of 3,500 psi by balancing fluid withdrawal. For the 1:1 CO₂ WAG process, alternate slugs of five (5) percent HCPV (based on Zone D) CO₂ and water were injected. A constant pressure waterflood continued after a total of 25 percent HCPV CO₂ was injected.

Simulation results showed that 40 percent and 48 percent of OOIP could be recovered for the straight waterflood and 1:1 CO₂ WAG process, respectively. This gave 8 percent incremental oil recovery by the CO₂ WAG process over the straight waterflood. The ratio of CO₂ requirement to the incremental oil production was estimated to be 5 MSCF/STB. This CO₂ requirement was corrected by a factor of 1.1 to account for CO₂ solubility in water.

RESULTS OF SIMULATION STUDIES

Based upon the results of this study, the following conclusions were made:

1. A satisfactory history match has been achieved. The computed bottom-hole pressures and fluid saturation changes at the observation wells were in good agreement with the observed values.
2. Amount of oil displaced (on a STB basis) as a percent of oil-in-place at the beginning of the minitest (December 11, 1980) for the straight waterflood process was 37 percent from the entire project interval.
3. Amount of oil displaced (on a STB basis) as a percent of oil-in-place at the beginning of the minitest (December 11, 1980) for a CO₂ flood with 1:1 WAG ratio in the minitest area was 50 percent from the entire project interval.
4. Only a trace of CO₂ migrated to the less permeable top layer (layer W). Ninety-five (95) percent of the CO₂ stayed in layers X and Y.
5. The Peng-Robinson equation of state accurately predicted physical properties of the mixtures of Little Knife crude oil and carbon dioxide.
6. Tabulated K-values (equilibrium ratios) generated from the Peng-Robinson equation of state were found to be adequate to predict the phase behavior of the CO₂ flood process.
7. Gulf's compositional simulator successfully simulated the CO₂ MCM (multiple-contact-miscible) process within engineering accuracy.

Additional information about the simulation study can be found in appendix 43. Appendix 44 contains a report detailing the calculations of fluid properties and miscibility conditions for miscible-displacement processes using the Peng-Robinson equation-of-state program.

OBSERVATION WELL SATURATION DATA ANALYSIS

Changes in oil, water, and gas saturations determined from monitor logs taken in the observation wells during the Little Knife CO₂ project were analyzed for CO₂-displacement-mechanism characteristics⁴². Three distinct mechanisms important in defining the total amount of oil displaced from the project area were identified: 1) waterflooding, 2) waterflooding accompanied by CO₂ swelling of oil where CO₂ was transported in solution, and 3) simultaneous CO₂-water displacement where a vapor phase was present. Displacement efficiency was highest for (3) where multiple-contact miscibility could be developed, lowest for (1) and intermediate for (2). Vertical sweep efficiency was highest for (1) essentially complete over the X, Y and Z layers. A lower vertical sweep was seen for zones in which (2) occurred, and lower still where (3) occurred.

The sequence and general characteristics of the displacement process were qualitatively the same in each well. Water invasion generally occurred first and was limited primarily to high porosity X, Y and Z layers although it was fairly complete over those layers. Invasion by fluids containing, by engineering estimates, dissolved CO₂* followed and was ultimately over somewhat less of the vertical interval than for water. Vertical sweep efficiency by free gas, when it arrived, was significantly less than that of water and dissolved gas. On the average for the three observation wells, vertical sweep by CO₂ in any form was about half that of water, and vertical sweep by free CO₂ was about half that of CO₂ in any form.

Final gas saturations (Figs. 148, 149 and 150) were more or less the highest that occurred in the wells. Gas saturation hysteresis was not seen despite the large volume of drive water injected.

Where water displacement occurred in the absence of significant gas, oil saturation was reduced usually to no less than about 40 percent PV. When significant gas (no less than 5-10 percent PV) was present together with high water saturation, lower oil saturations, in the 20-30 percent PV range, were obtained. Very low oil saturations in the zero to 20 percent PV range were reached only when free gas was present. These trends are most clearly seen in figures 151 through 159.

A low oil saturation, free-gas zone, once formed, did not seem to expand rapidly in the vertical direction with time. A comparison of observation well no. 2 and observation well no. 4 data showed that observation well no. 4 pressure-core saturation data, within the significant uncertainty of the pressure-core data, matched observation well no. 2 saturation data at the time the pressure core was taken, particularly in the thickness of the very low oil saturation zone. This match occurred despite the fact that observation well no. 4 was closer to the injection well and would have seen CO₂ earlier.

CO₂ was not miscible on first contact with Little Knife crude oil at pressures that existed in the pilot area. Laboratory tests showed that multiple-contact miscibility could be developed at these pressures and could

*Tracer data, although somewhat uncertain because of the use of nitrogen in gas lifting, strongly suggested that the gas saturation was in all cases CO₂.

result in very low residual-oil saturations. This mechanism, however, required a mobile free-CO₂ saturation. The correspondence of very low oil saturation zones with the presence of free gas in those zones was consistent with this mechanism. The fact that very low oil saturations, as low as a few percent pore volume, were obtainable in the presence of a high water saturation was also consistent with laboratory results. The fact that oil saturations higher than this are present together with free gas suggests that displacement was not yet complete when the project was terminated.

Where no free-gas saturation existed, mechanisms for reduction of oil saturation below waterflood residual were: 1) displacement of oil by CO₂-swollen oil followed by water displacement, and/or 2) waterflooding to residual² oil followed by contacting with CO₂-saturated water resulting in swelling and partial mobilization of that oil. In either case, the lowest achievable residual-oil saturation was related to the CO₂-swelling factor and is discussed in appendix 45-B. If a waterflood residual-oil saturation of 40 percent PV is assumed, then the minimum residual-oil saturation from the above two mechanisms would range from 27 percent PV at 3,700 psi to 30 percent PV at 3,500 psi. These values are consistent with oil saturation data in appendix 45-A where gas saturation was less than that needed to form a free-gas saturation.

Reasons for incomplete vertical sweep by free CO₂ could have been that: 1) permeability trends caused channeling, 2) insufficient CO₂ was available at the observation wells to form free CO₂ over the entire interval, and/or 3) free-CO₂ swept interval represented an instability (a finger). Permeability variation did not seem to have been completely responsible. If it were, there should also have been an effect on vertical sweep by water. Insufficient CO₂ did not seem to have been responsible; the same type of vertical sweep seemed to have occurred in observation well no. 4 (where more CO₂ would presumably be available) as in observation well no. 2.

Instability, possibly augmented by some permeability variation, appeared to be the most likely explanation. Although instabilities are generally considered to be damped by dispersive mixing in miscible systems, the effect of dispersion in a multiple-contact-miscible system will only be to equalize CO₂ partial pressure (more properly fugacity). It will not affect a saturated-vapor finger in saturated liquid.

CO₂ transport and consequent oil displacement in this project was very different from that seen in linear laboratory systems. Even after 146 percent PV drive-water injection, CO₂ saturation at the observation wells was, for the most part, still increasing or at least was not decreasing, while oil saturation in some places was still decreasing. This behavior may indicate that there was still a net flow of CO₂ at the observation wells at the time of the last monitor logs.

With incomplete vertical sweep, for whatever reason, oil will be bypassed. Large quantities of CO₂ can accumulate in solution in this oil, primarily, and also in water as a result of convective and dispersive mixing and will move only at a rate related to the flow of these fluids. Appendix 45-C shows that transverse dispersion may be important over the time and vertical distances involved in this project.

An important benefit of the alternating slugs of water injected with CO₂, in addition to any mobility control effect, may have been to reduce the capacity of these bypassed fluids to retain CO₂. Because of the much lower CO₂ solubility in water than in oil at reservoir conditions, waterflooded zones above and below CO₂-swept zones would retain less CO₂ than if those zones had not been waterflooded.²

Departures from ideal miscible flood behavior seen in this project did not indicate that a CO₂ flood at Little Knife would respond any less favorably than other successful carbonate reservoir CO₂ floods. Incremental recoveries over waterflooding for CO₂ floods have been reported⁴³ as ranging from 3 percent PV to 12 percent PV with most in the 7 percent PV to 10 percent PV range. Nonidealities such as seen here would be necessary to explain recoveries of this magnitude, considering the very high displacement efficiency associated with multiple-contact-miscible CO₂ flooding in laboratory systems, and, in fact, may be a natural consequence of CO₂ flooding in real reservoirs.

Based on the results of laboratory testing and analysis of the monitor logs the following conclusions were made:

1. Three distinct displacement mechanisms appeared to be operative in the Little Knife CO₂ project: 1) waterflooding, 2) waterflooding accompanied by CO₂ swelling of oil where CO₂ was transported in solution, and 3) simultaneous CO₂-water displacement where a vapor phase was present. All are important in determining the total amount of oil displaced from the project area.
2. Displacement efficiency was highest where water and gaseous CO₂ displacement occurred; oil saturations in the zero to 20 percent PV range were reached. Displacement by CO₂ in solution was less efficient, giving 20-30 percent PV² oil saturations. Waterflooding alone was least efficient, giving oil saturations which were mostly in the 40 percent PV range. The very low gaseous CO₂-water residual-oil saturations were in agreement with laboratory tests which showed that multiple-contact miscibility could be achieved at reservoir conditions and that high water saturation would not interfere with miscibility development.
3. Vertical sweep efficiency was highest for water displacement, less for displacement by CO₂ in solution, and lowest for vapor phase CO₂ displacement.

Additional graphs and other information can be found in appendix 45.

CORROSION STUDY

As reported earlier in the well completion section of this report, a corrosion study was conducted as an aid in the selection of materials and the design of well completions for future, effective large scale operations⁴⁴. Potential corrosion problems were first examined in the laboratory and then later in the Little Knife Field.

For the laboratory investigation, the corrosive environment during CO₂ injection in the Little Knife Minitest was assumed to be a saturated salt brine solution containing about 7,000 ppm potassium, 19,000 ppm calcium, 2,800 ppm magnesium, 136 ppm sulfate, 300 ppm bicarbonate, and 10 ppm iron in the presence of 10-60 volume percent CO₂, 5-10 percent H₂S, and the remainder methane. This environmental description was based on the water analysis and physical properties of typical reservoir fluids obtained from Little Knife wells (Tables 32 and 33).

Autoclave tests (Tables 34 and 35) designed to simulate representative field environments were performed on various materials to evaluate their potential use in a CO₂ flood. The materials evaluated included the following: 17-4PH, L-80 casing, Incoloy 825, Hastelloy C-276, Inconel 625, Cast 410 stainless steel, K-Monel and 316 stainless steel. The test results showed that the high nickel-chromium-molybdenum metals, such as Inconel 625, Incoloy 825 and Hastelloy C-276, had the lowest corrosion rates. Although somewhat inferior to the more exotic alloys, 316 stainless, K-Monel and 17-4 PH gave moderate corrosion resistance to CO₂-H₂S-water environments. All the materials tested performed significantly better than carbon steel (L-80) and 410 stainless steel.

Following termination of the CO₂ minitest, surface and downhole tubulars and equipment involved in the operation were visually inspected (Tables 36 and 37) by field personnel for evidence of corrosion. This inspection indicated that all the equipment appeared to be in good condition.

A tubing inspection for corrosion in all four 2-7/8 inch tubing strings was completed by service company personnel (Appendix 46). Results of the inspection indicate that the coatings (TK-2 and TK-7) were chipped or cracked in the box and pin end areas of numerous joints; otherwise, the integrity of the coatings over the remainder of the pipe appeared to be satisfactory (Tables 38 and 39). Defects in coatings were attributed to wireline and logging tool work performed through the tubing during the pilot test. As expected, corrosion was evident in areas where the coating was chipped from the tubing wall (Appendix 46).

Several two and four-inch surface coupon racks were placed at various locations in the injection and production lines of the observation and offset field production wells. A total of twenty-two racks containing metal and coated coupons were evaluated for corrosion resistance. The results of these tests (Tables 39 through 43) showed that corrosion rates were generally low for all materials tested. For example, corrosion for C-75 in various surface locations ranged from only 0.008 to 0.9 mils per year, while no corrosion was detected on 316 stainless steel.

Metal and plastic-coated corrosion coupons were also evaluated in six flow-through type downhole racks in minitest observation and offset production wells. The downhole rack in the CO₂ injector was not recovered because of well problems.

These test results (Tables 39 through 42) indicated very low downhole corrosion rates, i.e., 0.1-0.7 mils per year for C-75 and less than 0.07 mils per year for 316 stainless. Of the coated coupons, TK-7 performed best in the more severe downhole production well environments.

In addition to downhole racks, several downhole corrosion nipples (subs) from observation wells no. 2 and 3 were analyzed for corrosion by visual inspection, pit-depth measurements, and photomicrograph analysis of the nickel plating integrity and microstructure of the stainless steels. Corrosion of these nipples was found to vary from zero to moderate on 316 stainless steel and C-75, respectively. Results of the visual inspection of the tubing subs by Gulf's Houston Technology Center personnel are shown in table 44. For comparison, photographs of the samples are shown in appendix 46. Moderate corrosion was evident on the C-75 and L-80 nipples as indicated by pit-depth measurements performed by an independent laboratory (Table 45). The photomicrograph analysis of the nickel plating showed that the integrity of the nickel plating on the 316 stainless steel and N-80 was satisfactory. No inclusion or deformation of the plating was found on any of the subs. The photomicrograph also revealed no corrosive attack on unplated 316 stainless steel. Table 46 gives results of corrosion studies of minitest wellhead equipment.

Overall performance of the materials selected and used in the Little Knife CO₂ project was good. This performance was evident from field inspection of equipment and the low corrosion rates determined by coupon analysis. Because of low-volume production in the minitest observation wells and the low water cuts (<30 percent) and low CO₂ production (<1 percent) in the offset wells, the field test results were not totally conclusive for this particular project. Based on past field experience and laboratory testing, significant corrosion of carbon steel in CO₂-oil-water mixtures does not occur until the water cut approaches about 50 percent. Apparently, under such conditions, the oil phase provides sufficient protection to the metallic surface to inhibit corrosion at the lower water fractions.

Of all plastic coatings tested, TK-7 performed best in production wells where H₂S was present. According to these tests, TK-7 gave better corrosion protection than TK-2 in water-wet, high temperature, H₂S environment. This finding also has been confirmed by the coating manufacturer. The failure of TK-7 coating in the observation well no. 2 was positively identified from the spectrographic analysis of the ash content in the recovered debris and was attributed primarily to mechanical operations in the well. Probably because of insufficient H₂S concentrations, no visual evidence of TK-2 failure in the injection well has been detected.

The only other evidence of failure to date was the recovery of several pieces of teflon tubing-connection rings from several of the observation wells. Upon examination of the tubing string, it was apparent that the problem was depth related, i.e., poorer condition of rings at greater tubing depths. This problem may be a function of temperature on the teflon ring material.

Corrosion rates in the observation wells probably would have been much greater than actually measured if the wells had been continuously produced, thus, providing a more severe and, possibly, more representative corrosive environment as a result of higher water and CO₂ fractions. Since downhole environments are

likely to differ appreciably, results of this study should be used cautiously in predicting corrosion and selecting materials for other CO₂ floods. The corrosion potential for any given CO₂ prospect should always be determined separately. It should also be pointed out that all of the corrosion testing was done under "un-stressed" conditions.

Based upon the data and laboratory results presently available, the following can be concluded from the Little Knife CO₂ Minitest:

1. Materials recommended and used performed adequately in the low water (<30 percent), low CO₂ (<1 percent), and high H₂S (>5 percent) minitest environment.
2. Of the coated coupons, TK-7 appeared to provide the best protection in the presence of H₂S and under downhole conditions. Coated coupons in surface production facilities all appeared to perform well in the mild environment present.
3. Corrosion rates for various materials obtained from the minitest should not be generalized to be applicable to any other CO₂ project. The rate of corrosion probably would increase in a continually produced field environment.
4. All coupons and nipples were in an unstressed condition. If these materials were in actual service their corrosion rates might change.

Additional information can be found in appendix 47.

CONCLUSIONS

The Little Knife CO₂ minitest confirmed, by field testing, the results of laboratory CO₂ miscible displacement tests. The minitest indicated that the CO₂ miscible displacement process has technical potential for commercialization in a dolomitized carbonate reservoir that has not been extensively waterflooded and that has an indicated high remaining oil saturation.

The minitest was carried out without major difficulties. CO₂ and water were injected at the planned rates, and pressure was maintained, in the five-acre project area, above the 3,400 psi minimum miscibility pressure.

Many techniques were successfully used to characterize the reservoir and the fluids as well as to monitor the test performance. A logging method that utilized pulsed neutrons to measure capture cross-sections and the ratio of near to far detector count rates monitored fluid saturations to the required precision. Also, bottom-hole pressure, fluid samples, tracers, carbon isotope analyses, pulse tests, pressure cores, laboratory tests, simulation runs, and a detailed geological study all contributed to the test design and interpretation.

Materials used in the minitest wells performed satisfactorily. However, corrosion may have differed from measured rates had the wells been continuously produced.

Both the logs and pressure core results showed zones of very low oil saturations (less than 5 percent) in regions swept by both CO₂ and water, confirming the development of multiple contact miscibility and the high displacement efficiencies observed in the laboratory.

A numerical compositional simulation model provided a satisfactory history match of the pressures, saturations, and fluid compositions observed throughout the test, effectively combining the fluid property data, reservoir description, and process mechanisms.

No unexpected anisotropies were encountered. Areal sweep was 100 percent of minitest pattern. Vertical sweep by CO₂ was incomplete because of stratification and the possible occurrence of viscous fingers. The vertical sweep efficiency was approximately 52 percent. Pattern sweep efficiency for carbon dioxide approached 52 percent.

The displacement efficiency of the CO₂ miscible process, as indicated by the simulation study, for the five-acre minitest area was 50 percent of the oil-in-place at the start of the project, compared with an efficiency of 37 percent for a waterflood. Thus, only 3.1 Mscf of CO₂ were required per incremental barrel of displaced oil. The absence of producing wells and the fact that only one zone within the Mission Canyon Formation was flooded favorably influence these figures.

ACKNOWLEDGEMENTS

Thanks are given to the various members of Gulf Oil Corporation for their contributions and assistance in preparing this report.

REFERENCES

1. White, T. M. and Lindsay, R. F.: "Enhanced Oil Recovery by CO₂ Miscible Displacement in the Little Knife Field, Billings County, North Dakota," DOE 5th Sym. Enhanced Oil & Gas Recovery & Improved Drilling Tec. (1979) V. 2, N-5/1-19.
2. *Svor, T. R. and Price, J. M.: "Results of Water Injection from Cased-Hole Log Analysis in the Zabolotny Injection No. 1 Well," Gulf Science and Technology Tech. Memorandum No. 445STL084 (August 1980).
3. *Kingelin, G. F., Cleland, R. B. and Barrett, D. L.: "Little Knife CO₂ Minitest Project, Multiwell Pulse Test Report," Gulf Science and Technology Tech. Memorandum No. 444TL207 (May 1980).
4. *Hickey, M. C., Hurd, T. A., Kingelin, G. F. and Larsen, W. K.: "Reservoir and Formation Characterization - Little Knife CO₂ Minitest Project," Gulf Science and Technology Tech. Memorandum No. 445TM093 (March 1981).
5. Lindsay, R. F.: "Anatomy of a Dolomitized Carbonate Reservoir, the Mission Canyon Formation at Little Knife Field, North Dakota," Amer. Assoc. Petrol. Geol. Bull. (1982) V.66, N.5, 594.
6. Wilson, J. L.: "Carbonate Facies in Geologic History," Springer-Verlag (1975) 471.
7. Irwin, M. L.: "General Theory of Epeiric Clear Water Sedimentation," Amer. Assoc. Petrol. Geol. Bull. (1965), V.49, N.4, 445-459.
8. Maiklem, W. R., Bebout, D. G. and Glaister, R. P.: "Classification of Anhydrite - A Practical Approach," Can. Petrol. Geol. Bull. (1969) V. 17, N. 2, 194-233.
9. Shinn, E. A., Halley, R. B., Hudson, J. H. and Lidz, B. H.: "Limestone Compaction: An Enigma," Geology (1977) V.5, 21-24.
10. Murray, R. C.: "Origin of Porosity in Carbonate Rocks," Jour. Sed. Petrol. (1960) V.30, N.1, 59-84.
11. Asquith, G. B.: "Subsurface Carbonate Depositional Models: A Concise Review," Petrol. Pub. Co. (1979) 121.
12. Kastner, M.: "New Insights into Origins of Dolomite," Amer. Assoc. Petrol. Geol. Short Course Notes, Dolomite and Dolomitization (1982).
13. Kastner, M. and Baker, P. A.: "A New Insight into the Origin of Sedimentary Dolomite," 1982 Yearbook of Science Tech., McGraw-Hill.
14. Baker, P. A. and Kastner, M.: "Constraints on the Formation of Sedimentary Dolomite," Science (1981) V.213, 214-216.

15. Lindsay, R. F. and Kendall, C. G. St. C.: "Depositional Facies, Diagenesis and Reservoir Character of the Mission Canyon Formation (Mississippian) of the Williston Basin at Little Knife Field, North Dakota," Soc. Econ. Paleont. Mineral. Core Workshop No. 1 (1980) 79-104.
16. Lindsay, R. F. and Kendall, C. G. St. C.: "Depositional Facies, Diagenesis and Reservoir Character of the Mission Canyon Formation (Mississippian) of the Williston Basin at Little Knife Field, North Dakota," Carbonate Petroleum Reservoirs-Casebook Examples (In Press).
17. Bathurst, R. G. C.: "Carbonate Sediments and their Diagenesis," Elsevier, Amsterdam (1975) 650.
18. Thomas, G. E.: "Lineament-Block Tectonics: Williston-Blood Creek Basin," Amer. Assoc. Petrol. Geol. Bull. (1974) V. 58, N. 7 1305-1322.
19. *Hodgson, R. A.: "Little Knife Fracture Study Preliminary Report," Gulf Science and Technology Tech. Memorandum No. 4224DC80 (July 1978).
20. *Bigelow, E. L.: "Fracture Detection: Core vs. Log Comparison, Little Knife CO₂ Project," Gulf Science and Technology Tech. Memorandum No. 4453KR03-27 (May 1980).
21. Lindsay, R. F.: "Pore and Throat Systems of the Mission Canyon Formation at Little Knife Field, North Dakota, U.S.A. - A Preliminary S.E.M. View," Scanning Electron Microscopy in Geology (In Press).
22. Wardlaw, N. C.: "Pore Geometry of Carbonate Rocks as Revealed by Pore Casts and Capillary Pressure," Amer. Assoc. Petrol. Geol. Bull. (1976) V. 60, N. 2, 245-257.
23. Wardlaw, N. C. and Taylor, R. P.: "Mercury Capillary Pressure Curves and the Interpretation of Pore Structure and Capillary Behavior in Reservoir Rocks," Can. Petrol. Geol. Bull. (1976) V. 24, N. 2, 225-262.
24. Pettijohn, F. J.: "Sedimentary Rocks," Harper & Row (1957) 718.
25. *Razor, R. W., Haulenbeek, R. B., Avenshire, R. A. and Thakur, G. C.: "Little Knife CO₂ Minitest Water Injection Simulation," Gulf Science and Technology Company Report No. 445RL029 (July 1980).
26. *Svor, T. R.: "Logging," Houston Technology Center Tech. Memorandum No. 445TN148 (June 1982).
27. Svor, T. R. and Globe, M. P.: "A Three-Phase Quantitative Monitoring Method for CO₂ Floods," SPE/DOE 1982 Symposium on Enhanced Oil Recovery, Tulsa, Oklahoma (April 1982) paper 10684.
28. *DeVaney, W. E.: "Fluid Sampling," Houston Technology Center Tech. Memorandum No. 445TN146 (June 1982).
29. *England, A.: "CO₂ Mini-Test Pressure-Core Well," Houston Technology Center Tech. Memorandum No. 446-TN-022 (June 1982).

30. Nettle, R. L.: "Zabolotny Observation No. 4 Plug and Donut Analysis," Memorandum (May, 1982).
31. *Ehrlich, R.: "Analysis of Observation Well No. 4 Pressure Core Data - Little Knife CO₂ Project," Gulf Research and Development Company Tech. Memorandum No. 441TN388 (June 1982).
32. Jenks, L. H., Huppler, J. D., Morrow, N. R. and Salathial, R. A.: "Fluid Flow within a Porous Medium Near a Diamond Core Bit," Jour. Can. Petrol. Tech. (Oct.-Dec., 1968) 172-180.
33. *Lin, C. J., Patel, Y. R. and Broussard, E. S.: "Little Knife Field CO₂ Minitest Compositional Simulation - Billings County, North Dakota," Houston Technology Center Company Report No. 445RN063 (June 1982).
34. *Chaudhari, N. M.: "Compositional Simulator Users' Manual," Gulf Research and Development Company Production Research Department Report No. 441RM192 (June 1981).
35. Peng, D. Y. and Robinson, D. B.: "A New Two-Constant Equation of State," I&EC Fund., 15 (1976) 59.
36. Robinson, D. B. and Peng, D. Y.: "The Characterization of the Heptanes and Heavier Fractions," Research Report 28, GPA, Tulsa, Okla., 1978.
37. *Lee, S. T.: "Application of the Peng-Robinson Equation of State to Determine Reservoir Fluid Properties and Predict Equilibrium Phase Behavior," GR&DC Production Research Department Report No. 441RL186 (January 1980).
38. Lin, C. J.: "Phase Behavior Package Computer Program Using the Peng-Robinson Equation of State," Private Communication.
39. Jossi, JA., Stiel, L. I. and Thodos, G.: "The Viscosity of Pure Substances in the Dense Gaseous and Liquid Phases," A.I.Ch.E.J. (1962), V. 8, 59.
40. Stone, H. L.: "Estimation of Three-Phase Relative Permeability and Residual Oil Data," Jour. Can. Petrol. Tech. (October-December, 1973) 53-61.
41. Kazemi, H., Vestal, C. R., and Shank, G. D.: "An Efficient Multi-Component Numerical Simulator," Soc. Petrol. Eng. Jour. (October 1978), V. 12, N. 5, 355-368.
42. *Ehrlich, R.: "Analysis of Observation Well Saturation Data Little Knife CO₂ Project," Gulf Research and Development Company Tech. Memorandum No. 441TN387 (June 1982).
43. Stalkup, F. I.: "Carbon Dioxide Flooding: Past, Present and Outlook for the Future," Jour. Petrol. Tech. (August 1978) 1102-1112.
44. *Morris, R. A. and Larkin, S.D.: "Corrosion Study for Little Knife CO₂ Minitest," Houston Technology Center Tech. Memorandum No. 445TN147 (June 1982).

45. Proctor, R. M. and Macauley, G.: "Mississippian of Western Canada and Williston Basin," Amer. Assoc. Petrol. Geol. Bull. (1968) V. 52, N. 10, 1956-1968.
46. Wittstrom, M. D. Jr. and Hagemeyer, M. E.: "A Review of Little Knife Field Development, North Dakota," Williston Basin Symposium, Montana Geol. Soc. (1978) 361-368.
47. Wittstrom, M. D. Jr. and Hagemeyer, M. E.: "A Review of Little Knife Field Development," Oil & Gas Jour. (1979) V. 77, N. 6, 86-92.
48. Carlson, C. G. and Anderson, S. B.: "Sedimentary and Tectonic History North Dakota Part of Williston Basin," Amer. Assoc. Petrol. Geol. Bull (1965) V. 49, N. 11, 1833-1846.
49. Habicht, J. K. A.: "Paleoclimate, Paleomagnetism and Continental Drift," Amer. Assoc. Petrol. Geol. Studies in Geol. (1979) N.9, 31.
50. Nettle, R. L., Lindsay, R. F. and Desch, J. B.: "Enhanced Oil Recovery by CO₂ Miscible Displacement in the Little Knife Field, Billings County, North Dakota," DOE/BETC/IC Annual Report-Enhanced Oil Recovery (1980) V. 3, G-4/1-15.

*These references are available on open file at the Bartlesville Energy Technology Center, Bartlesville, Oklahoma.

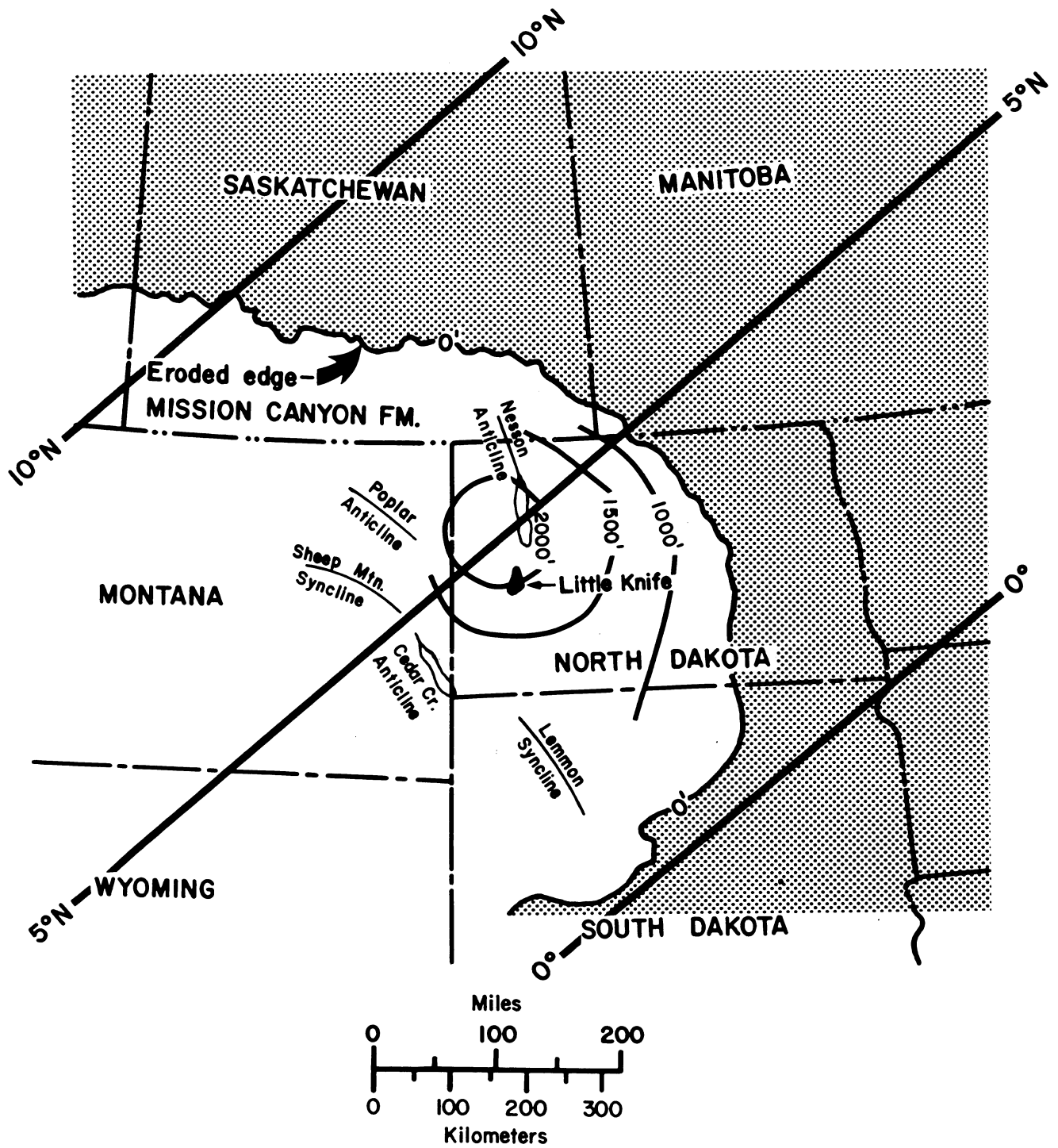


Fig. 1-Index map of Williston Basin, including: a) eroded edge of Mission Canyon Formation (Proctor and Macauley⁴⁵), b) major surface and subsurface structural features (Wittstrom and Hagemeyer^{46, 47}), c) isopach thickness of Madison Group (Carlson and Anderson⁴⁸), and d) the generalized paleolatitude during the Carboniferous (Habicht⁴⁹).

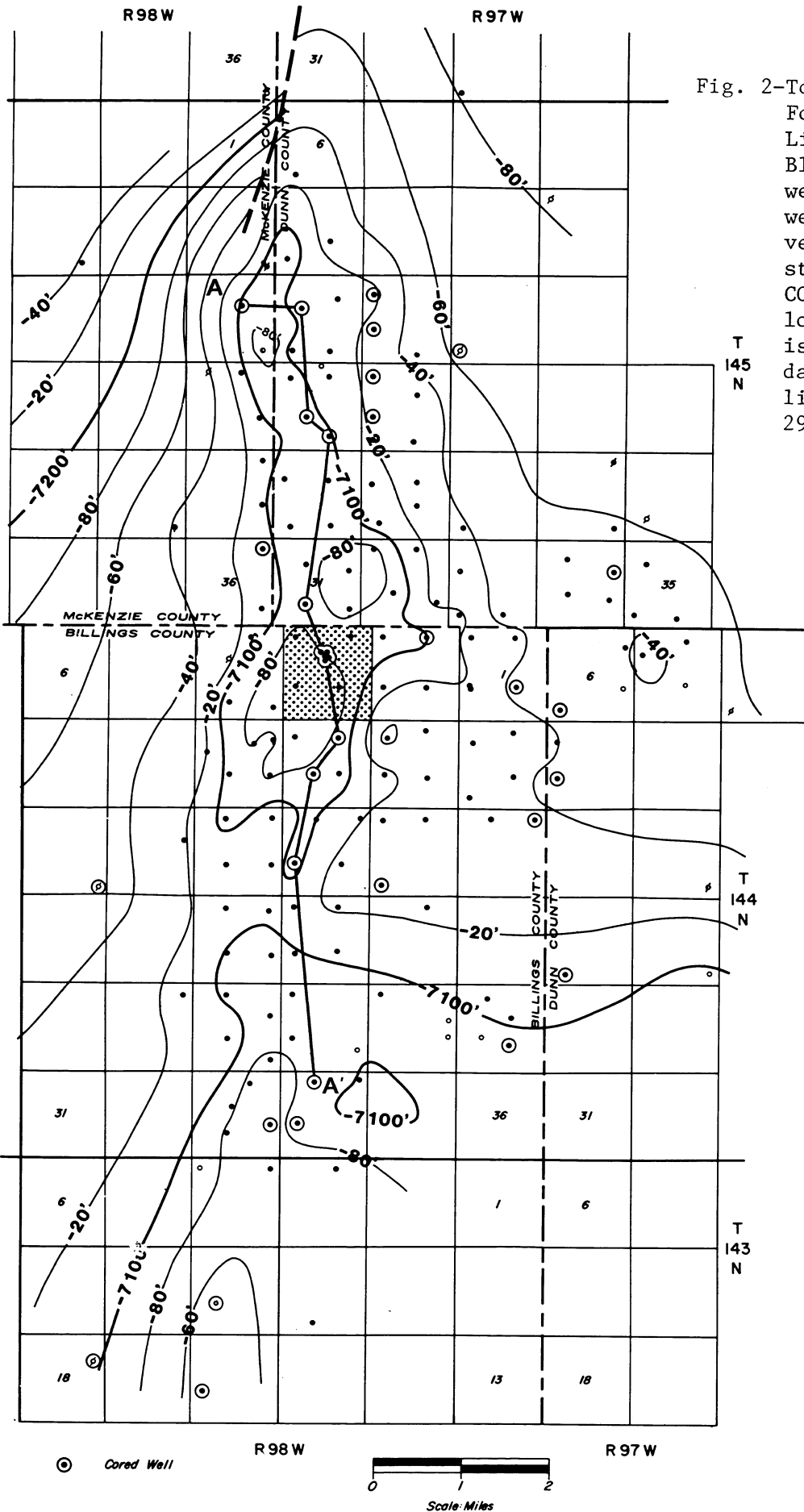


Fig. 2-Top of Mission Canyon Formation structure map, Little Knife Field. Black dots represent well locations. Circled wells are cored. Inverted four spot within stippled section is the CO₂ minitest project location. Structure map is contoured on a subsea datum. Cross section line A-A' is for Figure 29.

● Cored Well



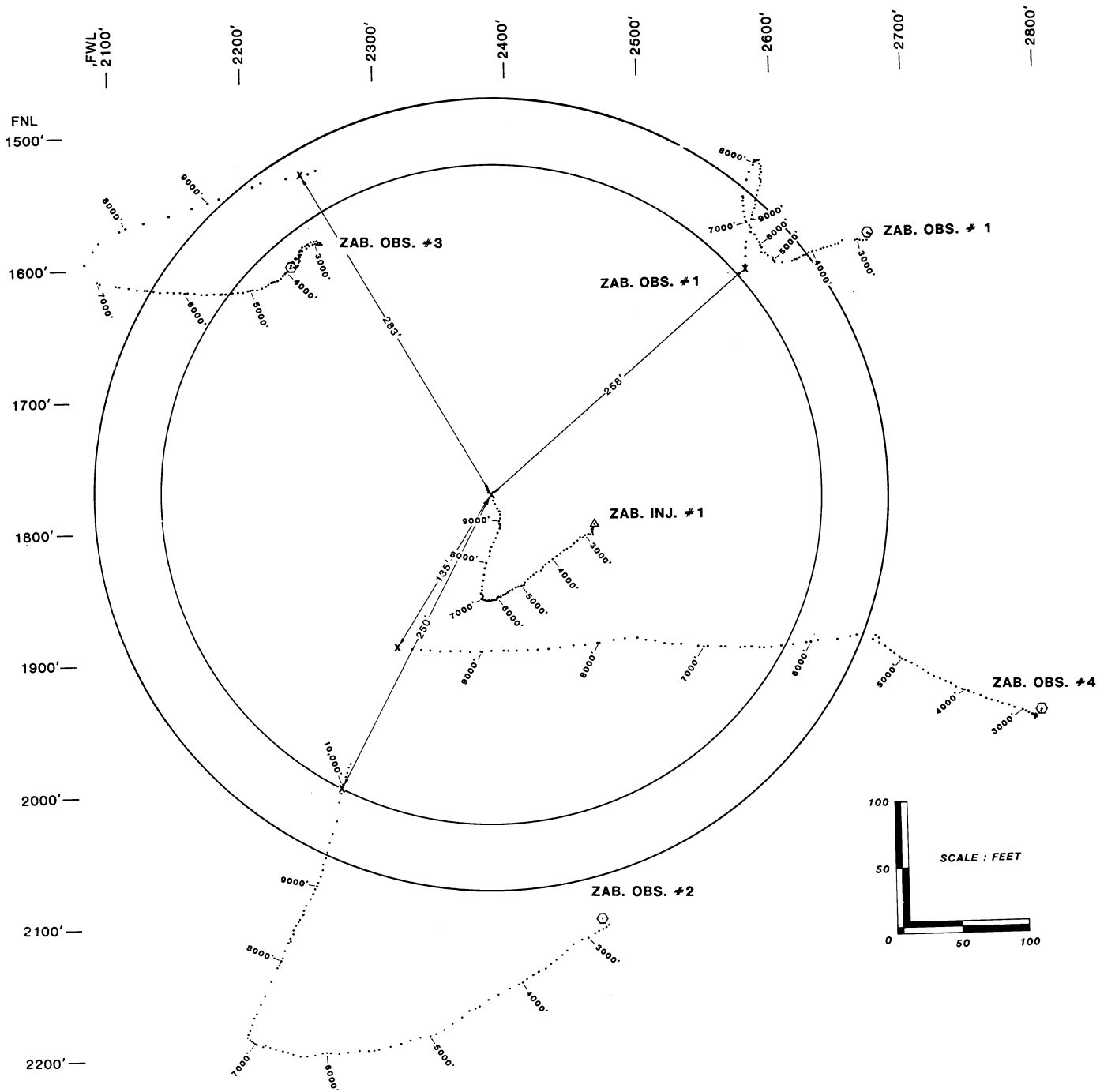


Fig. 3-Little Knife CO₂ minitest pattern, an inverted four spot, in Sec. 3, T144N, R98W, Billings County, North Dakota. The outer circle is 600 feet in diameter, inner circle is 500 feet in diameter. Center of the circle is the reservoir location of the central injection wellbore. Surface and reservoir locations of each wellbore, as well as the direction each well drilled, is calculated and plotted from gyroscopic multi-shot surveys run in each well. Depth marks are noted from 3,000 feet to TD at 500-foot intervals.

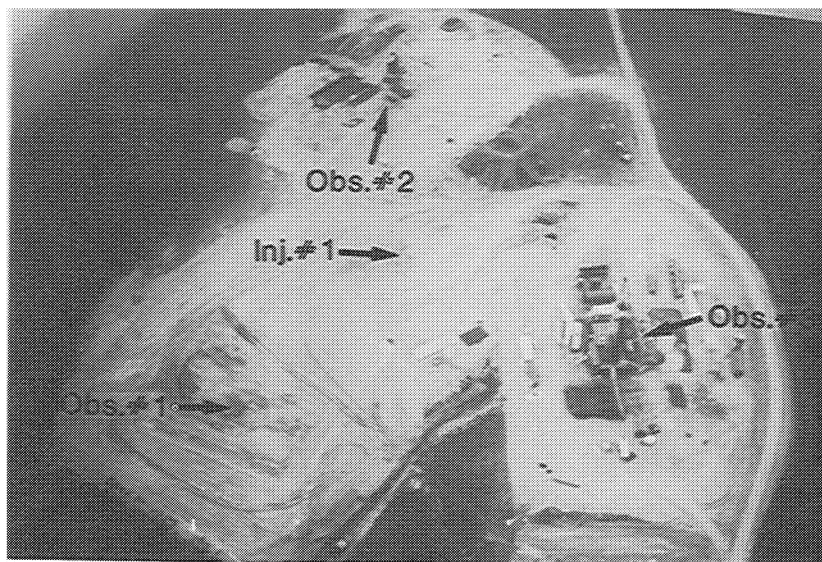
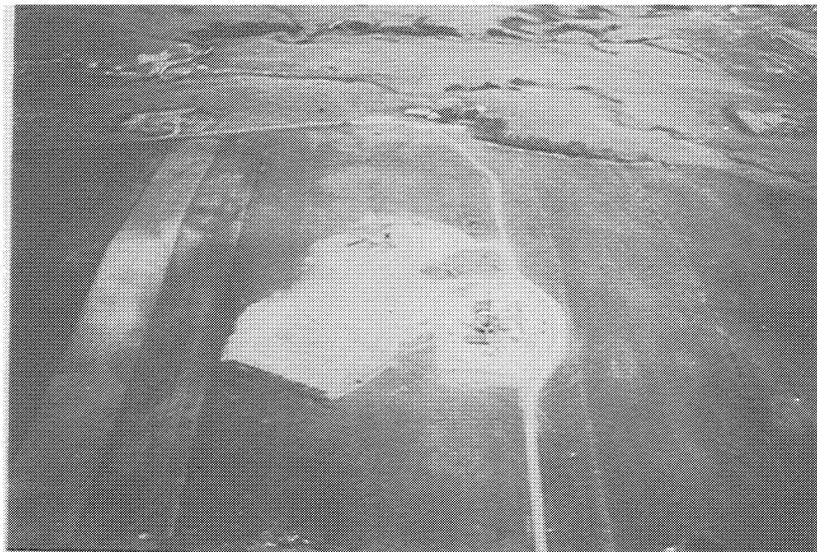


Fig. 4-Little Knife CO₂ minitest location. View in both photos is directly south. Upper photo illustrates the low-lying countryside, under cultivation, surrounding the minitest location. Bottom photo is a close-up view of the minitest location, with each of the four wells labeled. Observator well no. 3 is in the process of having open hole logs run, after reaching TD.

ZABOLOTNY INJECTION #1 TUBING SETTING

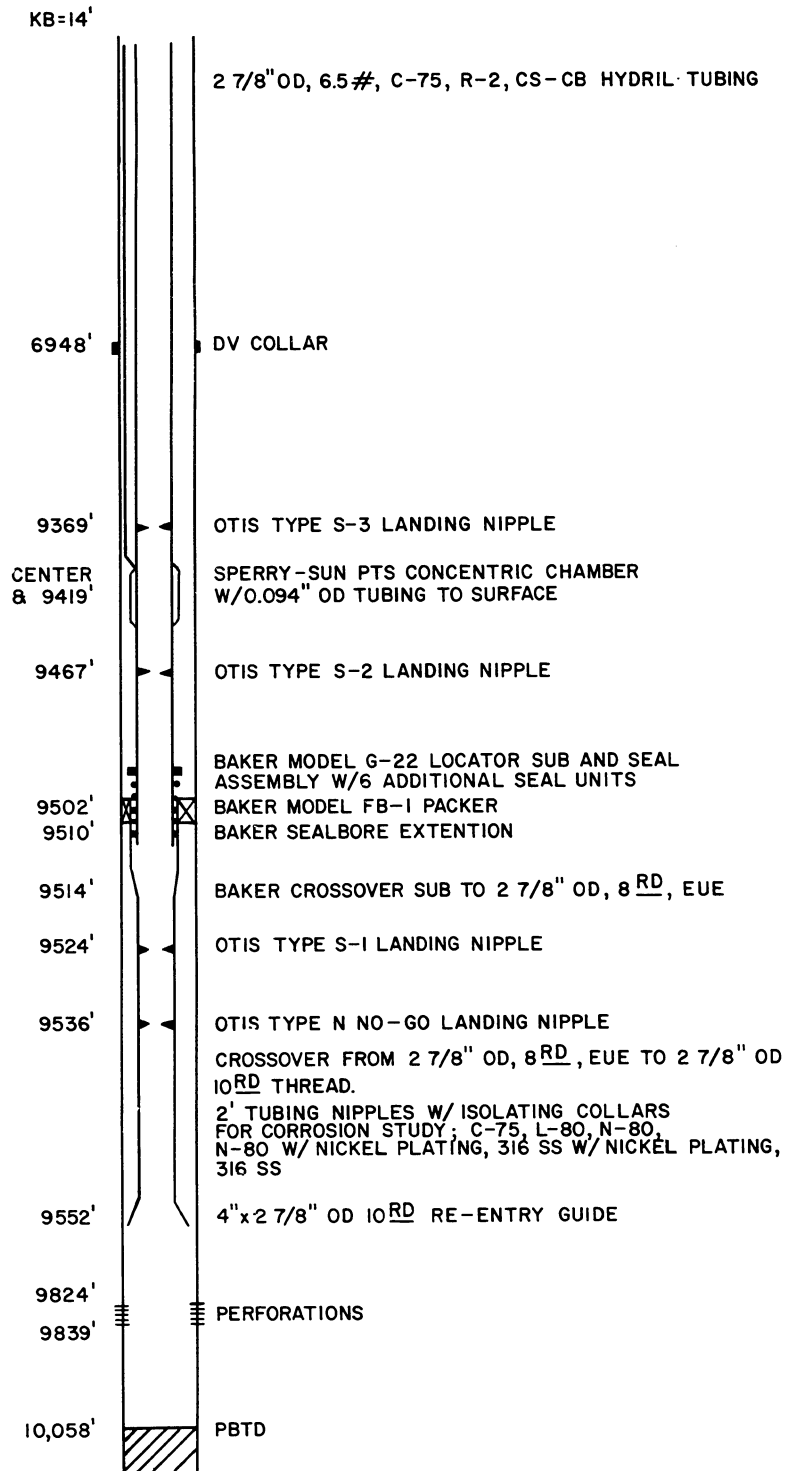


Fig. 5-Casing and tubing settings in injection well no. 1. The casing is 5-1/2" OD, L-80, R-III, 8rd, LT&C. The weight below the DV collar is 23.0#/ft. and the weight above is 17.0#/ft. The tubing is 2-7/8" OD, 6.5#/ft., C-75, R-2, CS-CB, Hydril, coated internally with TK-2.

ZABOLOTNY INJECTION # 1

TUBING SETTING

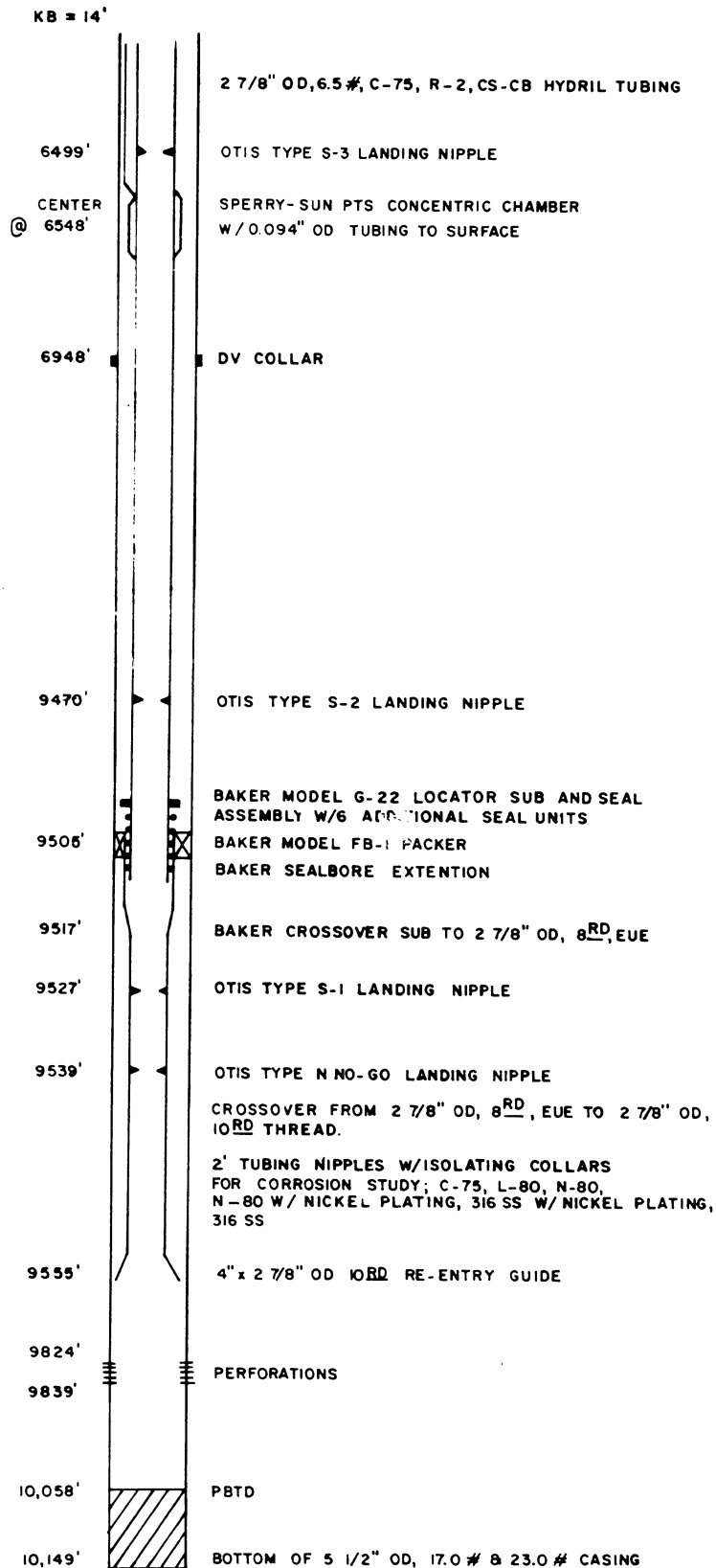


Fig. 6-Modified tubing setting to avoid "tight" spots in injection well no. 1.

Zabolotny Injection #1 - Pressure History

BOTTOM - HOLE PRESSURE @ -7200' (psi)

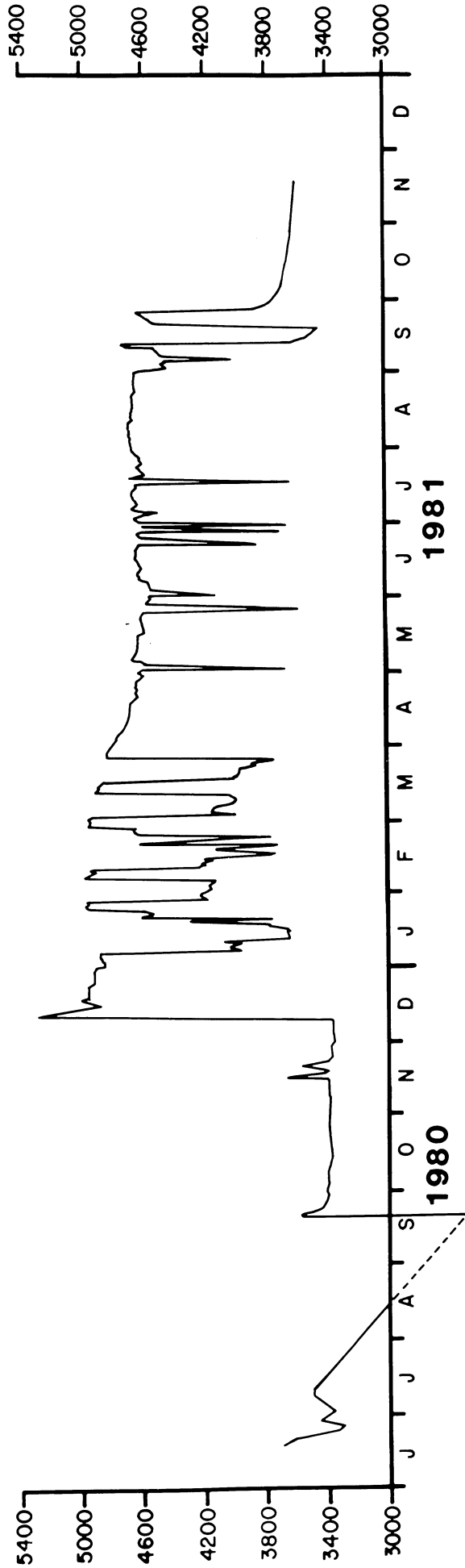


Fig. 7-Pressure history curve for injection well no. 1. All recorded pressures are gradient corrected to a common datum of -7,200 feet.

WELLHEAD SCHEMATIC INJECTION WELL

BOTTOM HEAD CONNECTION TO BE $2\frac{7}{8}$ " HYDRIL CS-CB
THREADED PIN.

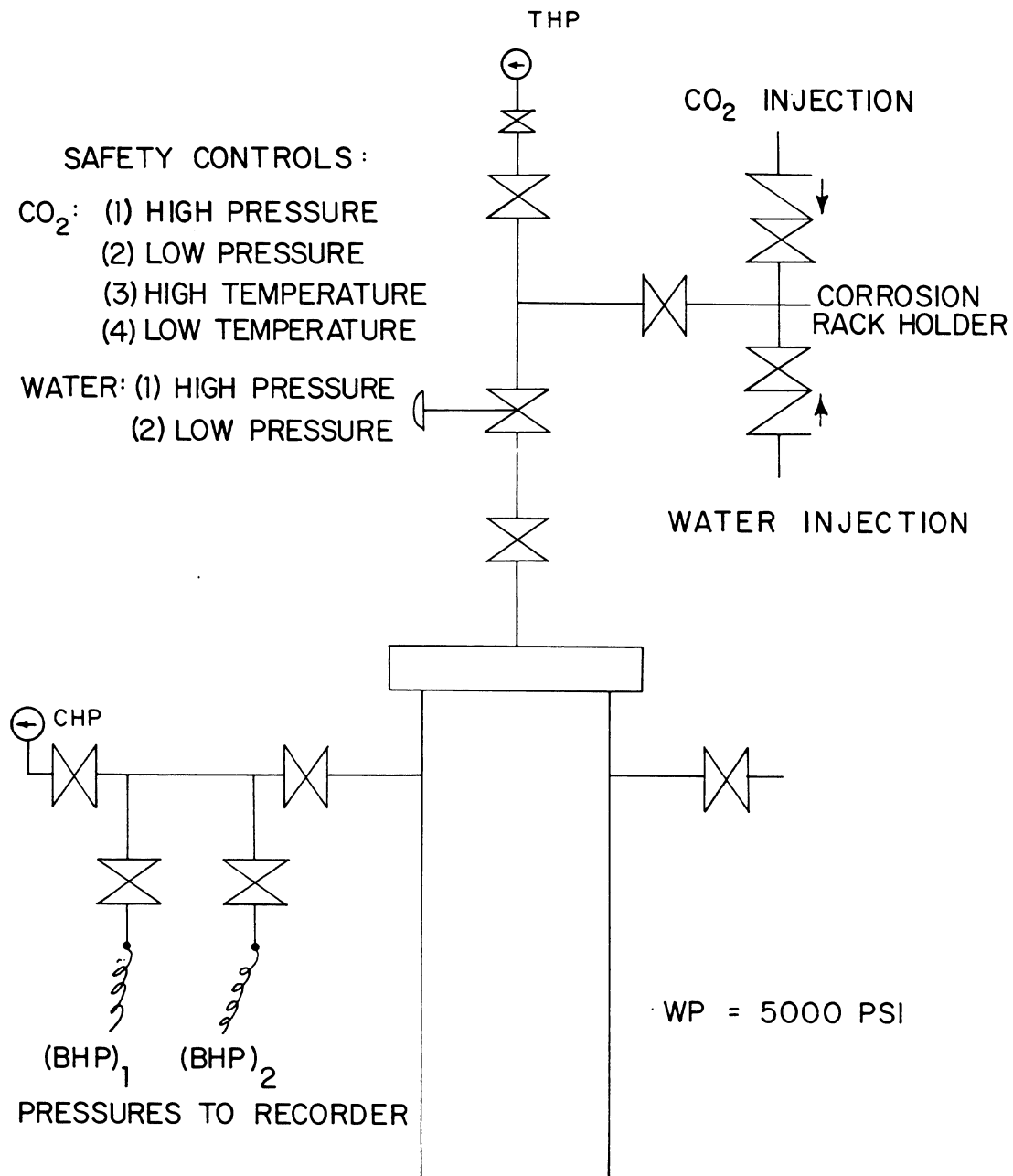


Fig. 8-Wellhead schematic of injection well no. 1. The wellhead casing fittings are coated with D-trim, which is H₂S corrosion resistant, and has an Inconel-clad bore, NACE rated for H₂S atmospheres.

WELLHEAD SCHEMATIC OBSERVATION WELL

BOTTOM HEAD CONNECTION TO BE 2 $\frac{7}{8}$ " HYDRIL CS-CB
THREADED PIN.

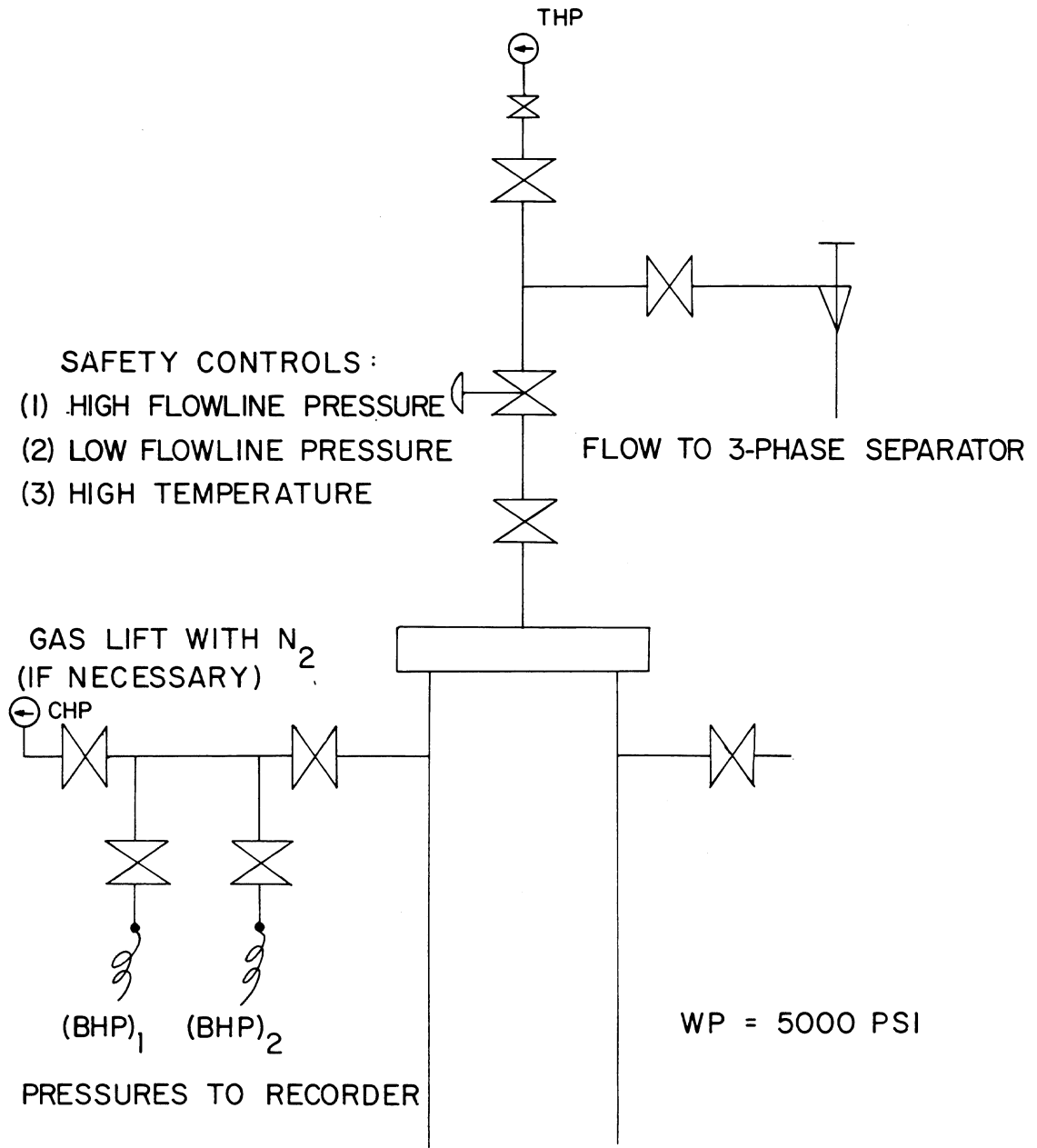


Fig. 9-Wellhead schematic of the observations wells. Each wellhead contains the same metallurgy as injection well no. 1 wellhead with the only difference between them being the valve arrangement.

ZABOLOTNY OBSERVATION #1

TUBING SETTING

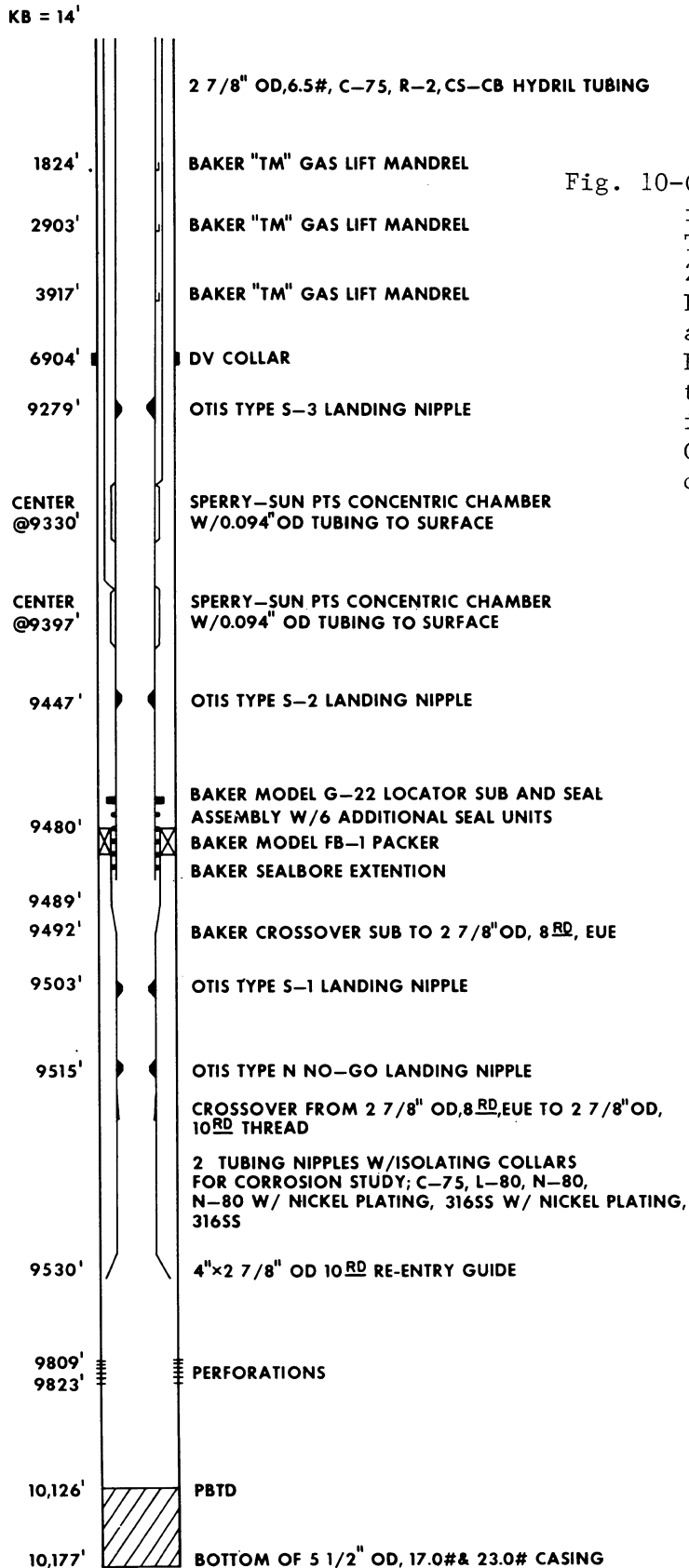


Fig. 10-Casing and tubing settings in observation well no. 1. The casing is 5-1/2" OD, 23#/ft., N-80, R-III, 8rd, LT&C below the DV collar and 5-1/2" OD, 17#/ft., L-80, R-III, LT&C above the DV collar. The tubing is 2-7/8" OD, 6.5#/ft., C-75, R-2, CS-CB, Hydril, coated internally with TK-7.

Zabolotny Observation #1 - Pressure History

BOTTOM - HOLE PRESSURE @ -7200' (psi)

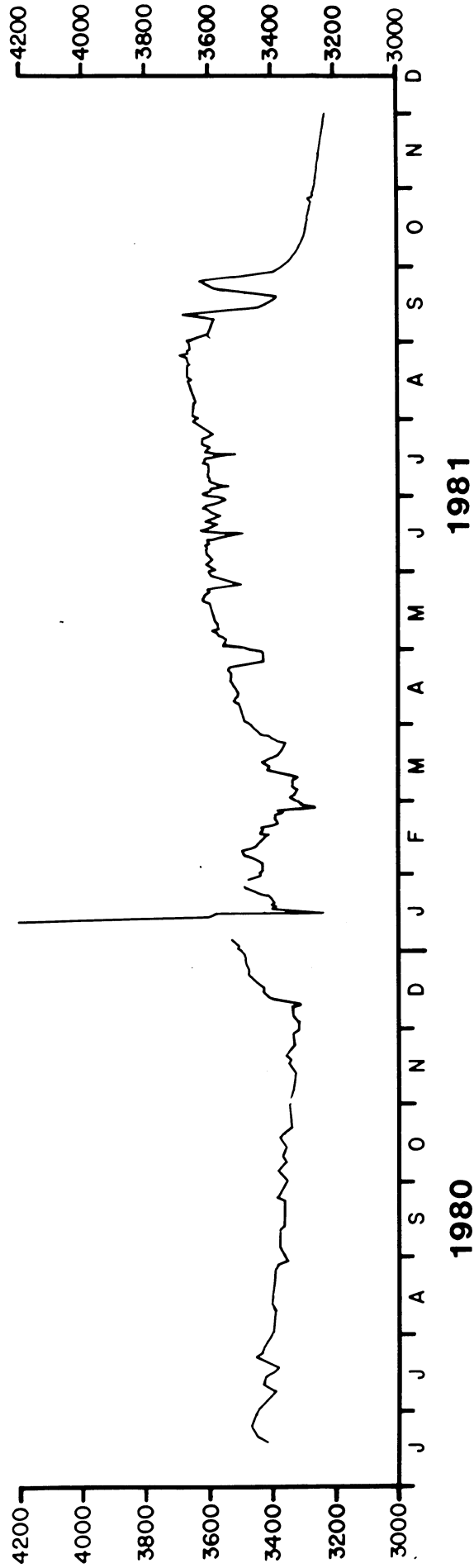


Fig. 11-Pressure history curve for observation well no. 1. All recorded pressures are gradient corrected to a common datum of -7,200 feet.

ZABOLOTNY OBSERVATION #2

TUBING SETTING

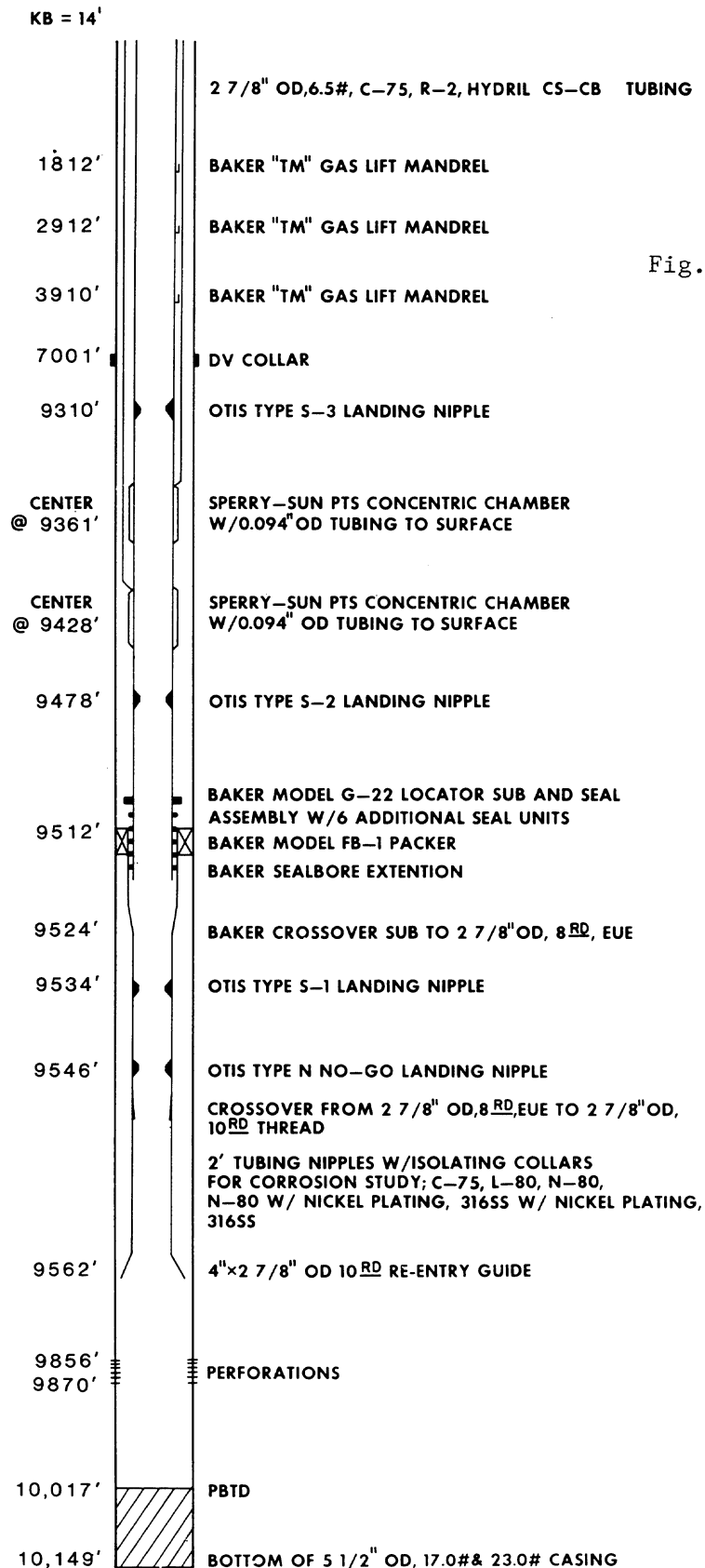


Fig. 12-Casing and tubing settings in observation well no. 2. The casing is 5-1/2" OD, 23#/ft., N-80, R-III, 8rd, LT&C below the DV collar and 5-1/2" OD, 17#/ft., L-80, R-III, LT&C above the DV collar. The tubing is 2-7/8" OD, 6.5#/ft., C-75, R-2, CS-CB, Hydril, coated internally with TK-7.

Zabolotny Observation #2 - Pressure History

BOTTOM - HOLE PRESSURE @ -7200' (psi)

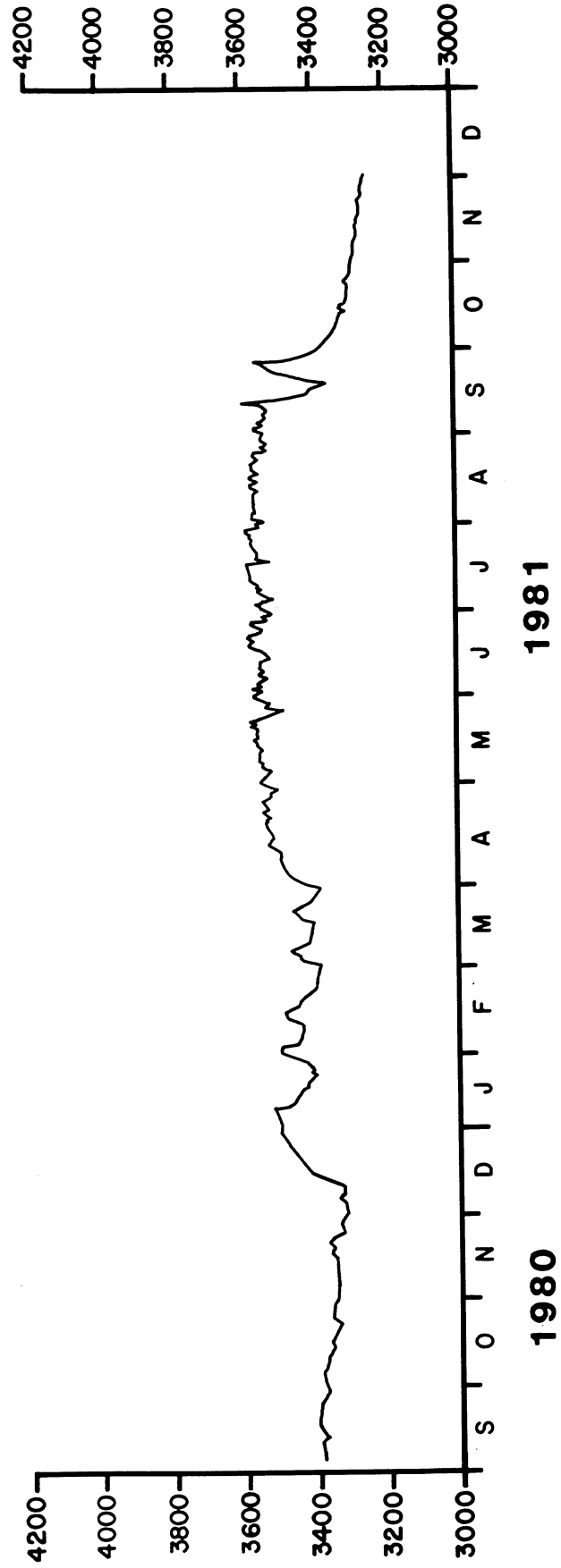


Fig. 13-Pressure history curve for observation well no. 2. All recorded pressures are gradient corrected to a common datum of -7,200 feet.

ZABOLOTNY OBSERVATION #3 TUBING SETTING

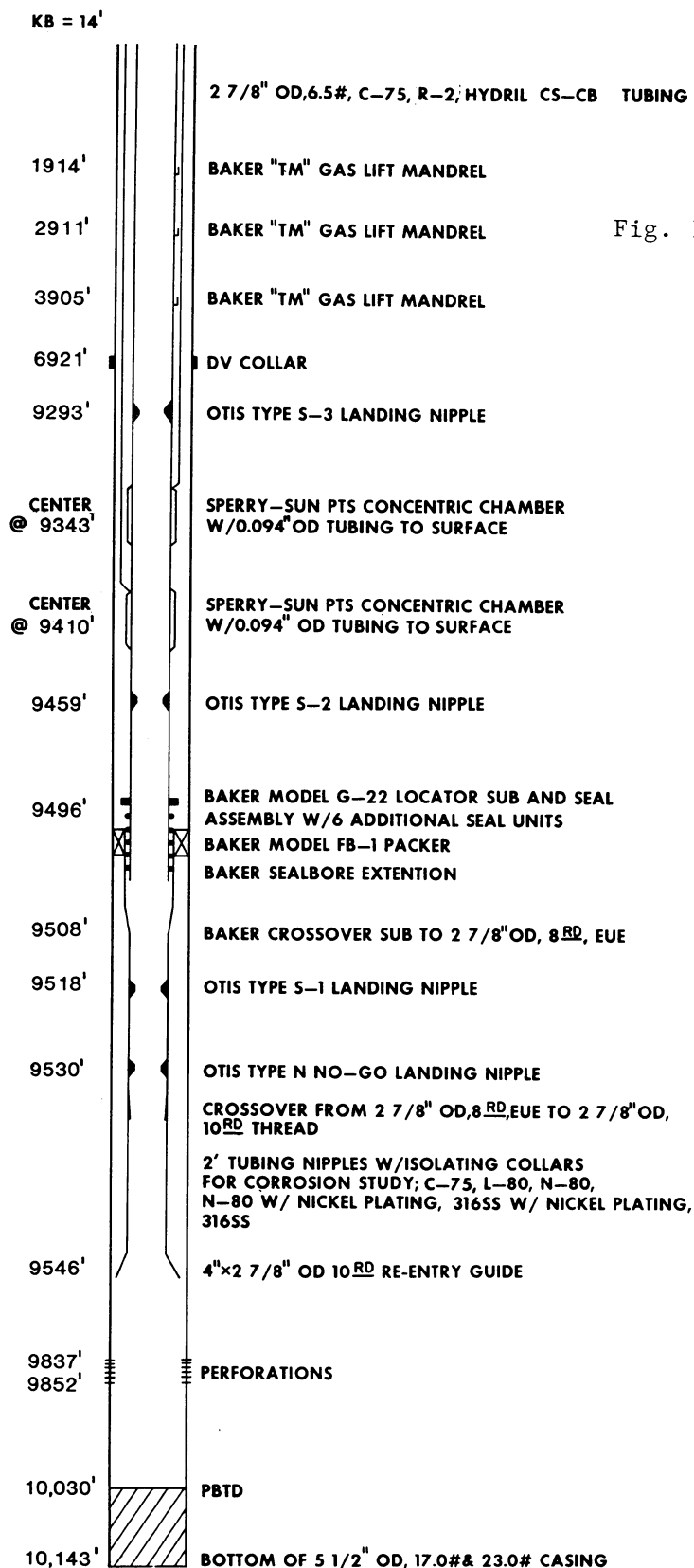


Fig. 14-Casing and tubing settings in observation well no. 3. The casing is 5-1/2" OD, 23#/ft., N-80, R-III, 8rd, LT&C below the collar and 5-1/2" OD, 17#/ft., L-80, R-III, LT&C above the DV collar. The tubing is 2-7/8" OD, 6.5#/ft., C-75, R-2, CS-CB, Hydril, coated internally with TK-7.

Zabolotny Observation #3 - Pressure History

BOTTOM - HOLE PRESSURE @ -7200' (psi)

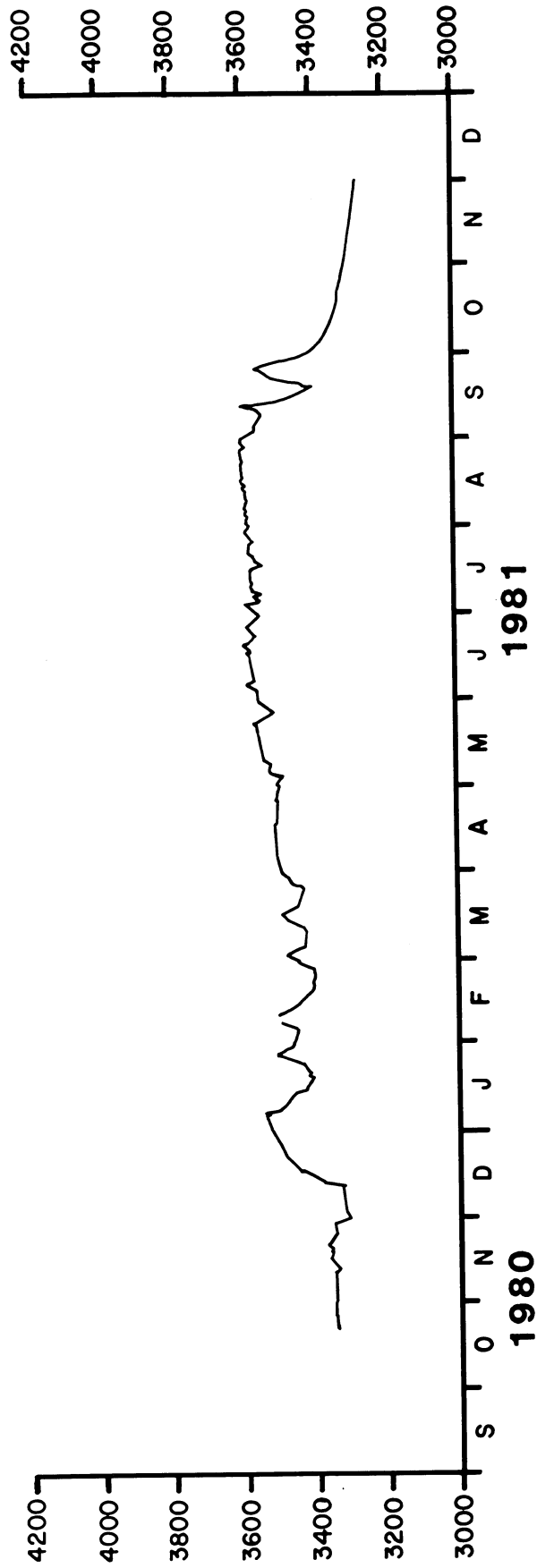


Fig. 15-Pressure history curve for observation well no. 3. All recorded pressures are gradient corrected to a common datum of -7,200 feet.

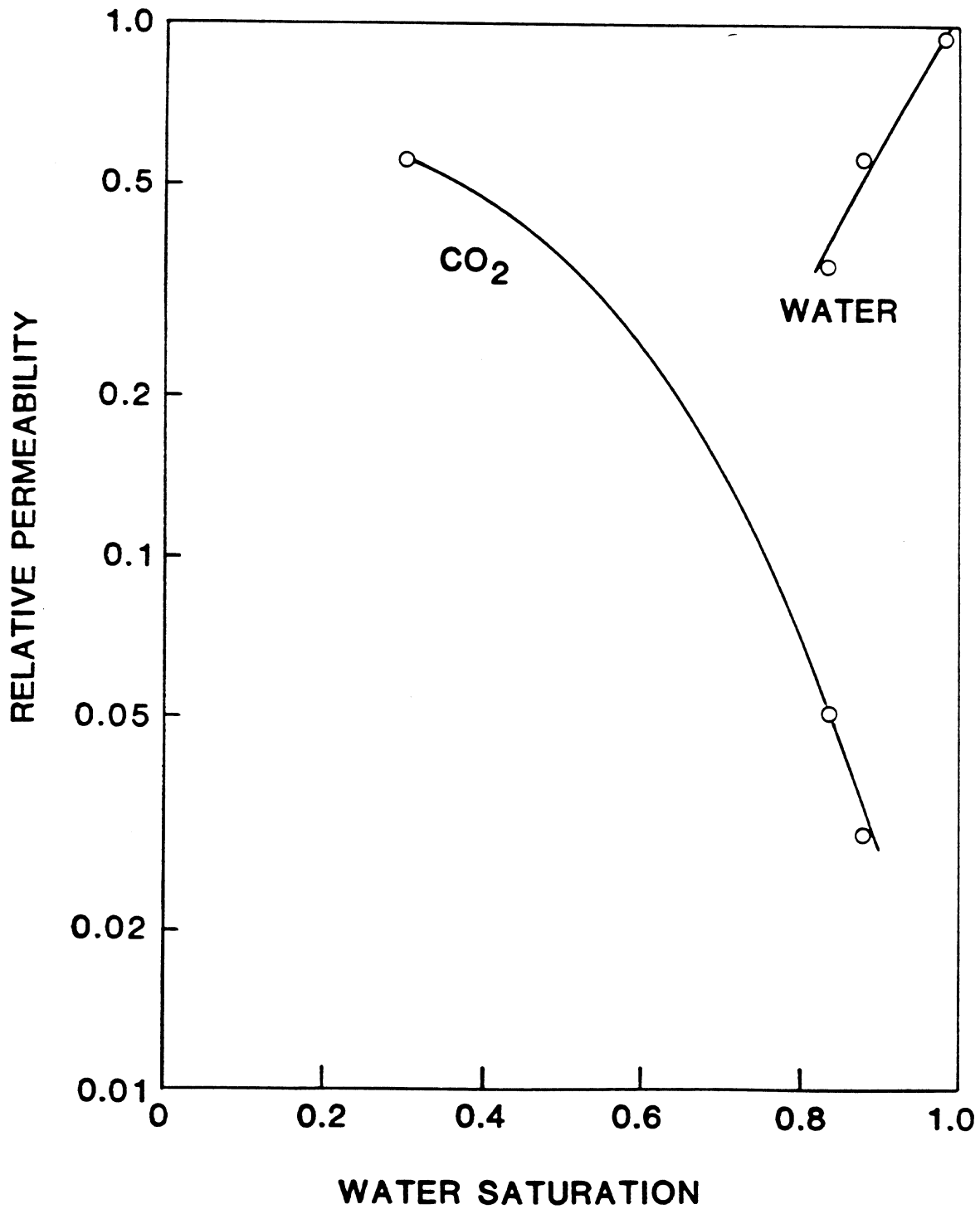


Fig. 16-CO₂-water relative permeabilities. Injection well no. 1, 9,814-9,815 feet, 3,500 psi and 245°F. Extracted core, no oil present, and not corrected for effect of CO₂ solubility in water.

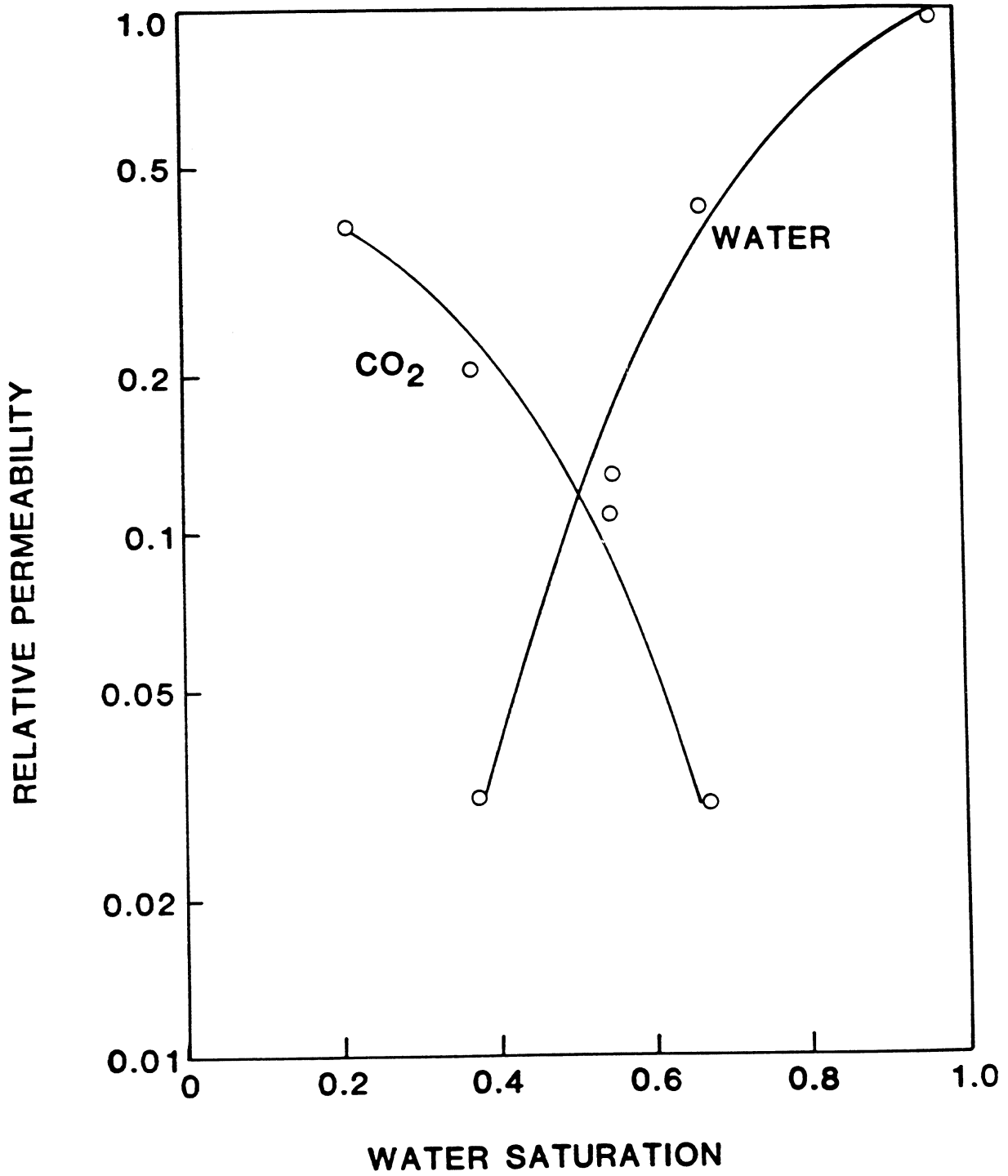


Fig. 17-CO₂-water relative permeabilities. Injection well no. 1, 9,823-9,824 feet, 3,500 psi and 245°F. Native state after CO₂ flood and not corrected for effect of CO₂ solubility in water.

ZABOLOTNY OBSERVATION WELL NO. 1

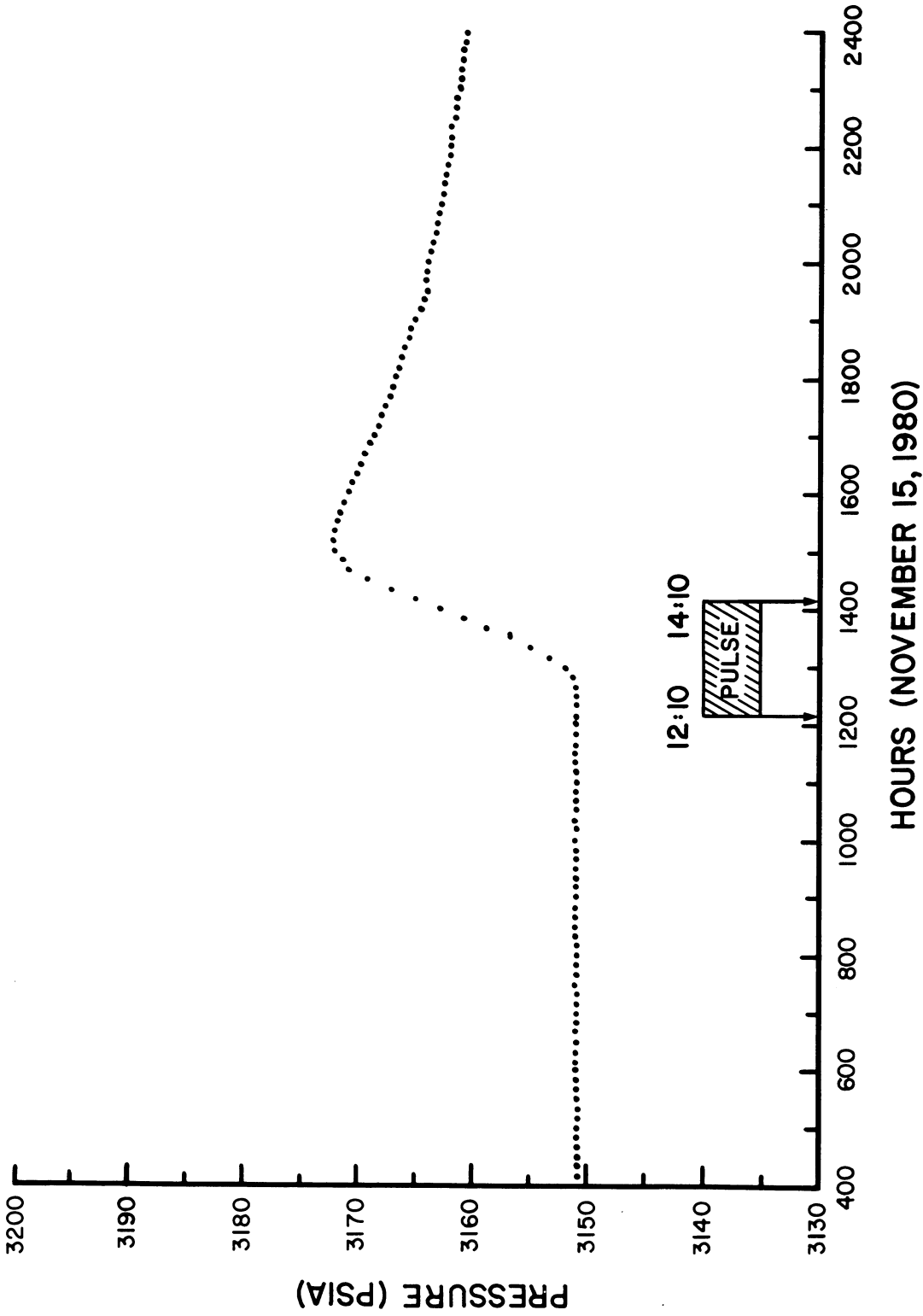


Fig. 18-Four well multi-well pulse test response recorded at observation well no. 1. Pressure (psia) at the surface recorded from the bottom PTS chamber (not helium corrected).

ZABOLOTNY OBSERVATION WELL NO. 2

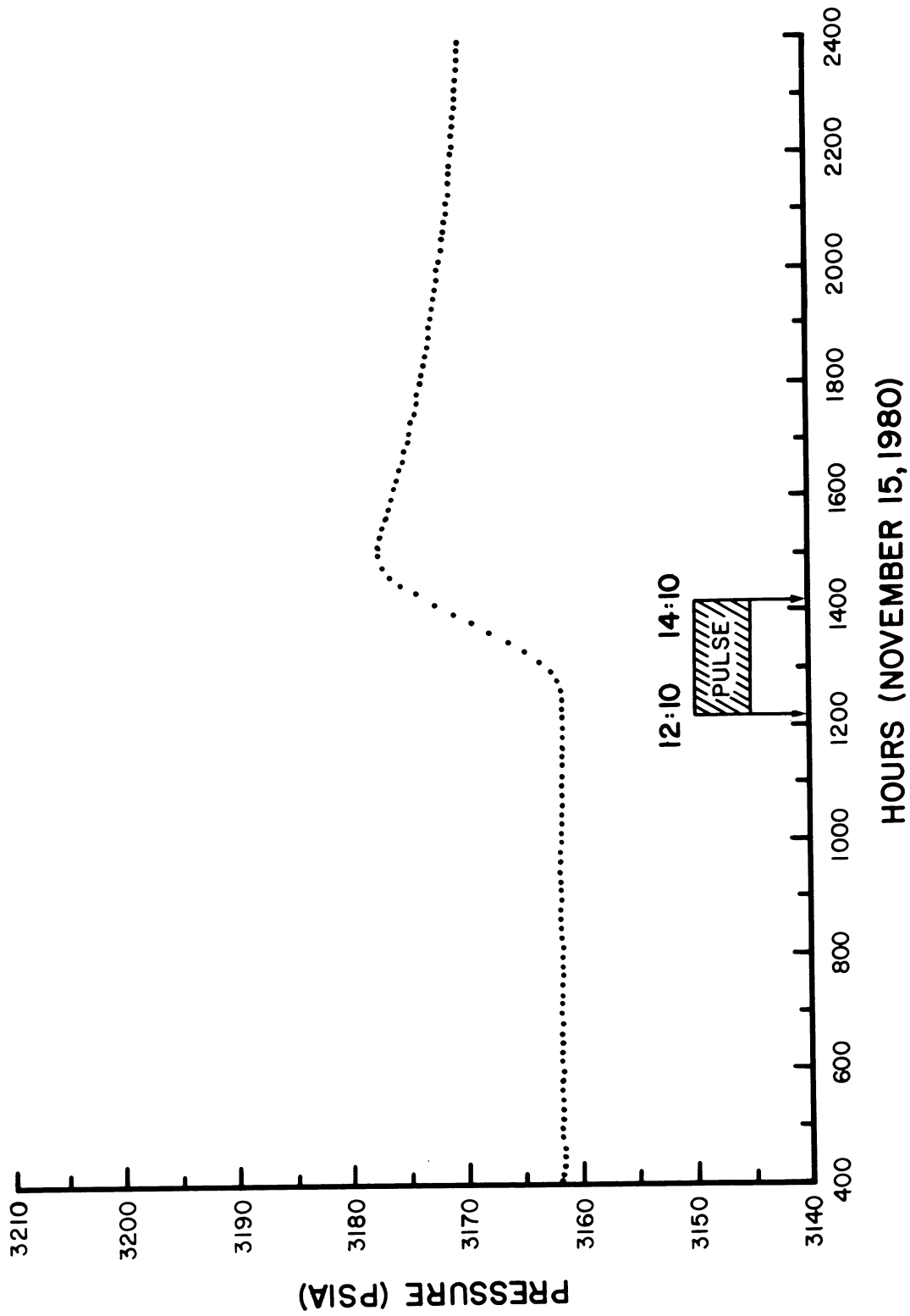


Fig. 19-Four well multi-well pulse test response recorded at observation well no. 2. Pressure (psia) at the surface recorded from the bottom PTS chamber (not helium corrected).

ZABOLOTNY OBSERVATION WELL NO. 3

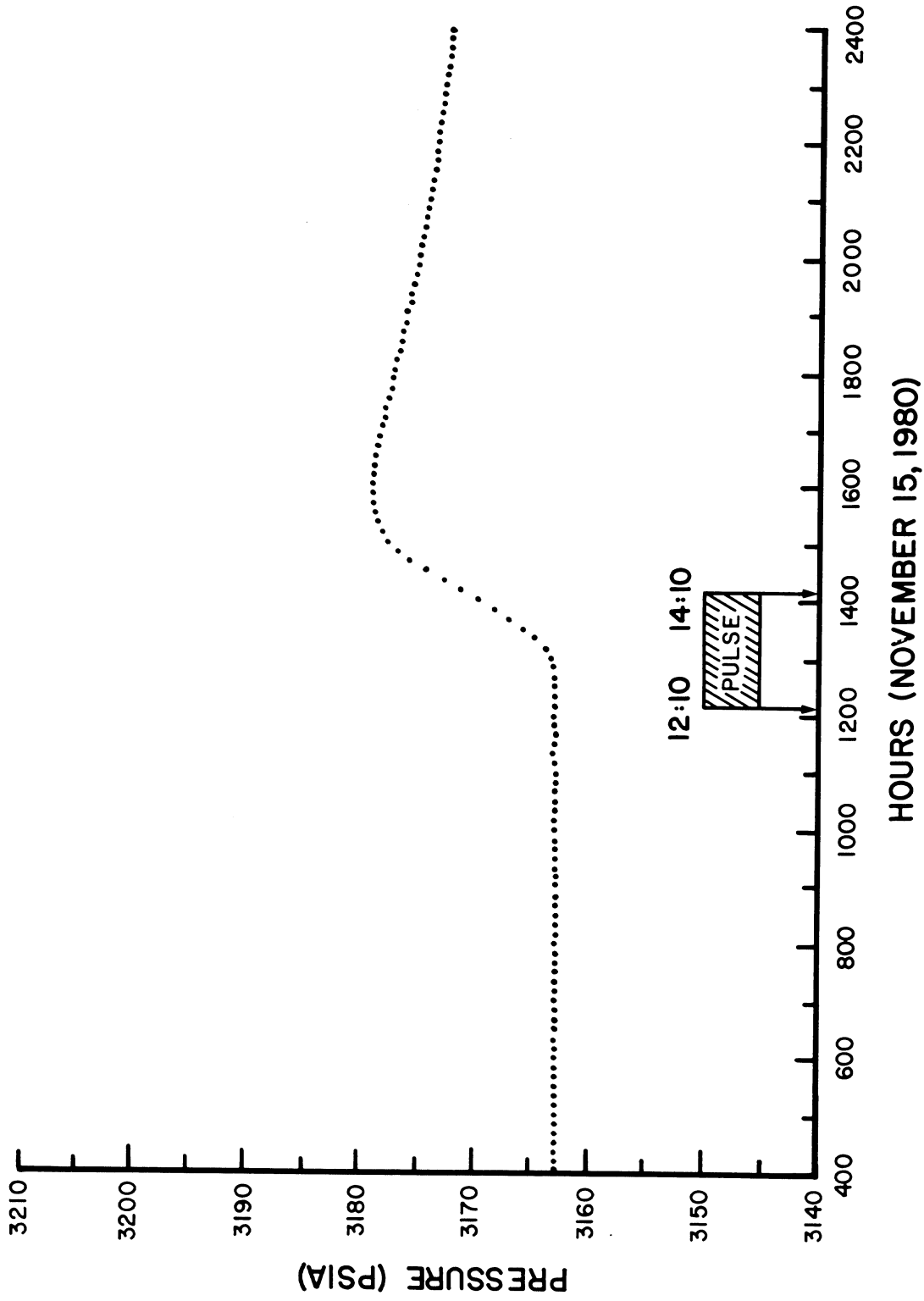


Fig. 20-Four well multi-well pulse test response recorded at observation well no. 3. Pressure (psia) at the surface recorded from the bottom PTS chamber (not helium corrected).

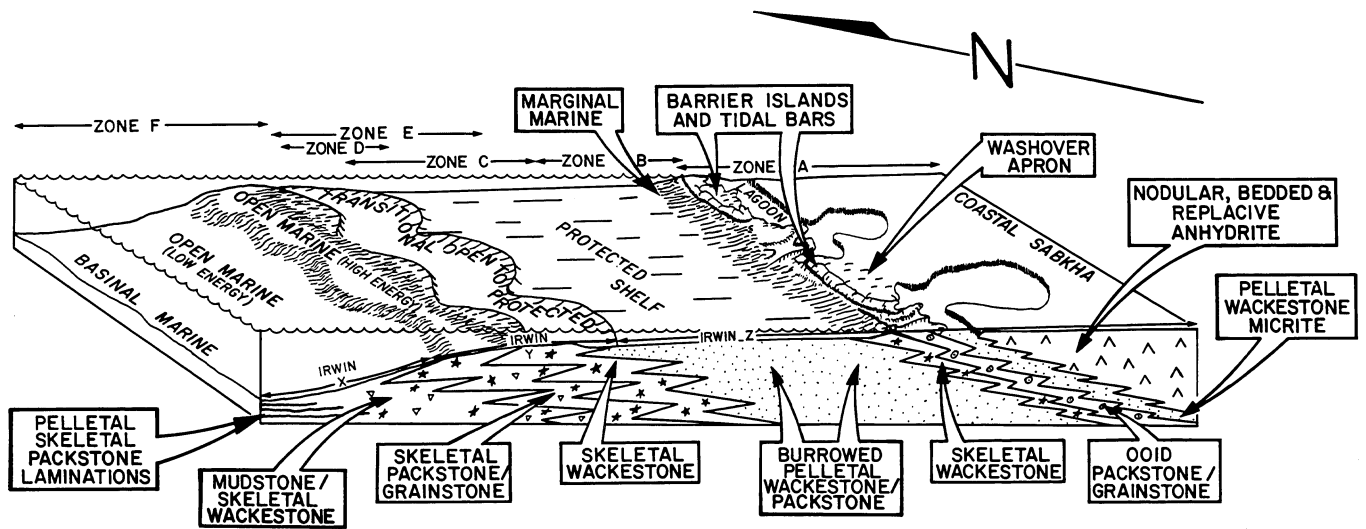


Fig. 21-Idealized depositional setting of Mission Canyon Formation at Little Knife Field. Informal log zonations A-F (top) and Irwin's epeiric sea energy zones X, Y and Z (base) illustrate respective positions both occupied in the depositional system.

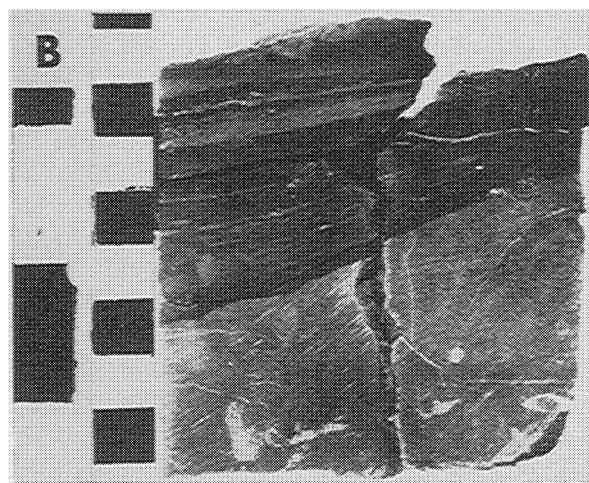
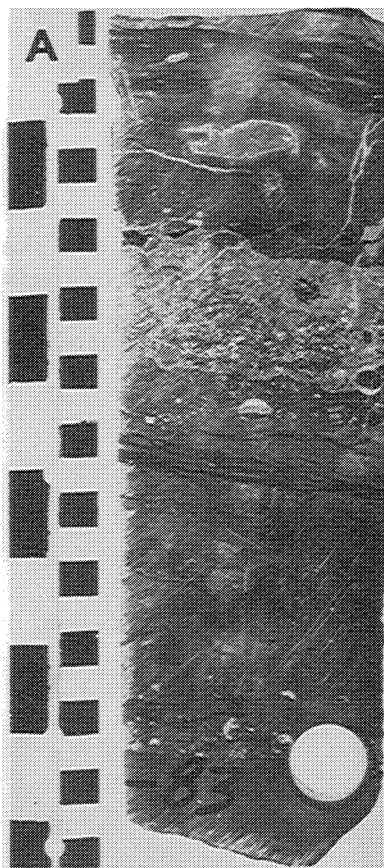


Fig. 22-Basinal marine facies of the Mission Canyon, representing "deeper water," below wave base, deposition: A) note thin beds containing graded bedding, B) note irregular topography or a compactional feature. Dark laminations are pelletal, lighter laminations are skeletal. Scale in inches and centimeters.

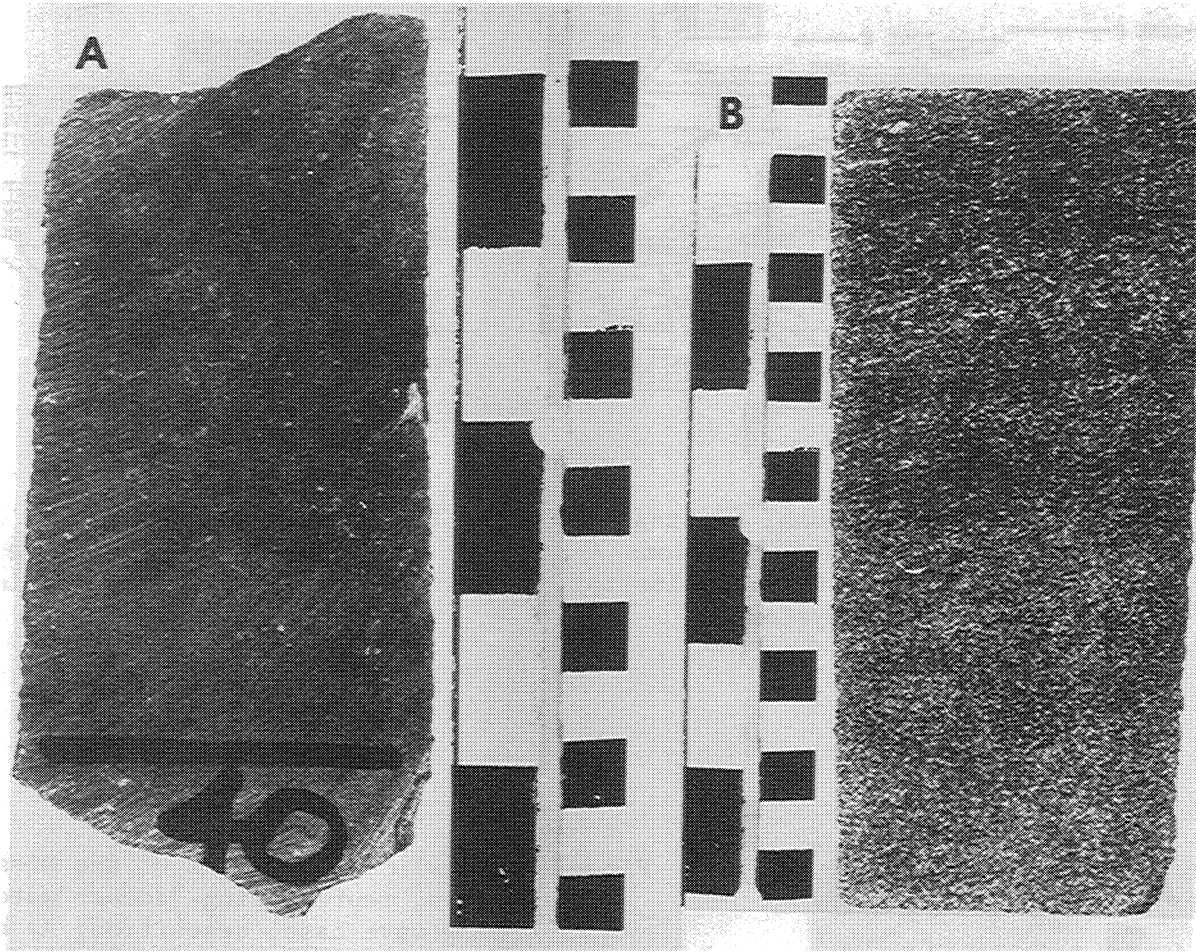


Fig. 23-Open marine facies of the Mission Canyon: A) a mud rich skeletal wackestone deposited below wave base, B) skeletal packstone/grainstone deposited in wave base. Several repetitions of both these beds form major carbonate cycles of mudstone/skeletal wackestone grading up into skeletal packstone/grainstone. Scale in inches and centimeters.

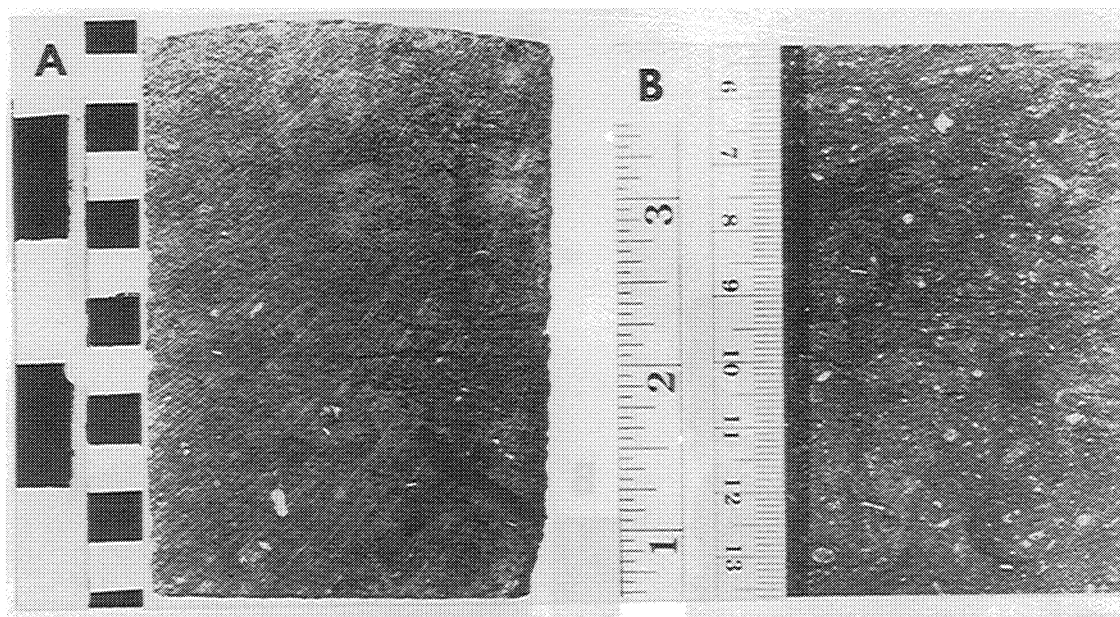


Fig. 24-Transitional open to restricted marine facies of the Mission Canyon: A) injection well no. 1, 9834 feet (2996 m), a burrowed originally mudstone now microcrystal dolostone with some anhydrite replaced burrows, B) originally burrowed skeletal wackestone now fine grained, porous, sucrosic, calcareous dolostone. Subtle repetitions of these beds represent minor carbonate cycles of mudstone grading up into skeletal wackestone. Scale in inches and centimeters.

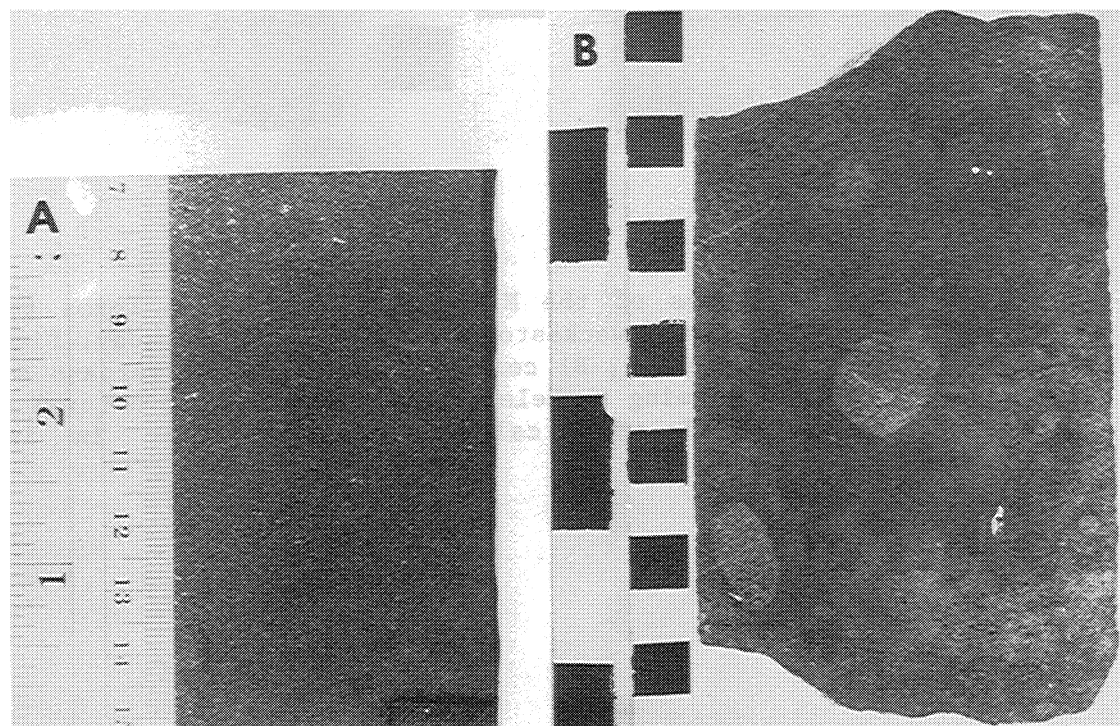


Fig. 25-Restricted marine facies of the Mission Canyon: A) originally completely burrowed, pelletal wackestone/packstone, now calcareous dolostone, B) originally burrowed lime mud now dolostone. Some burrow traces are slightly apparent. Lighter spots are from HCl acid. Scale in inches and centimeters.

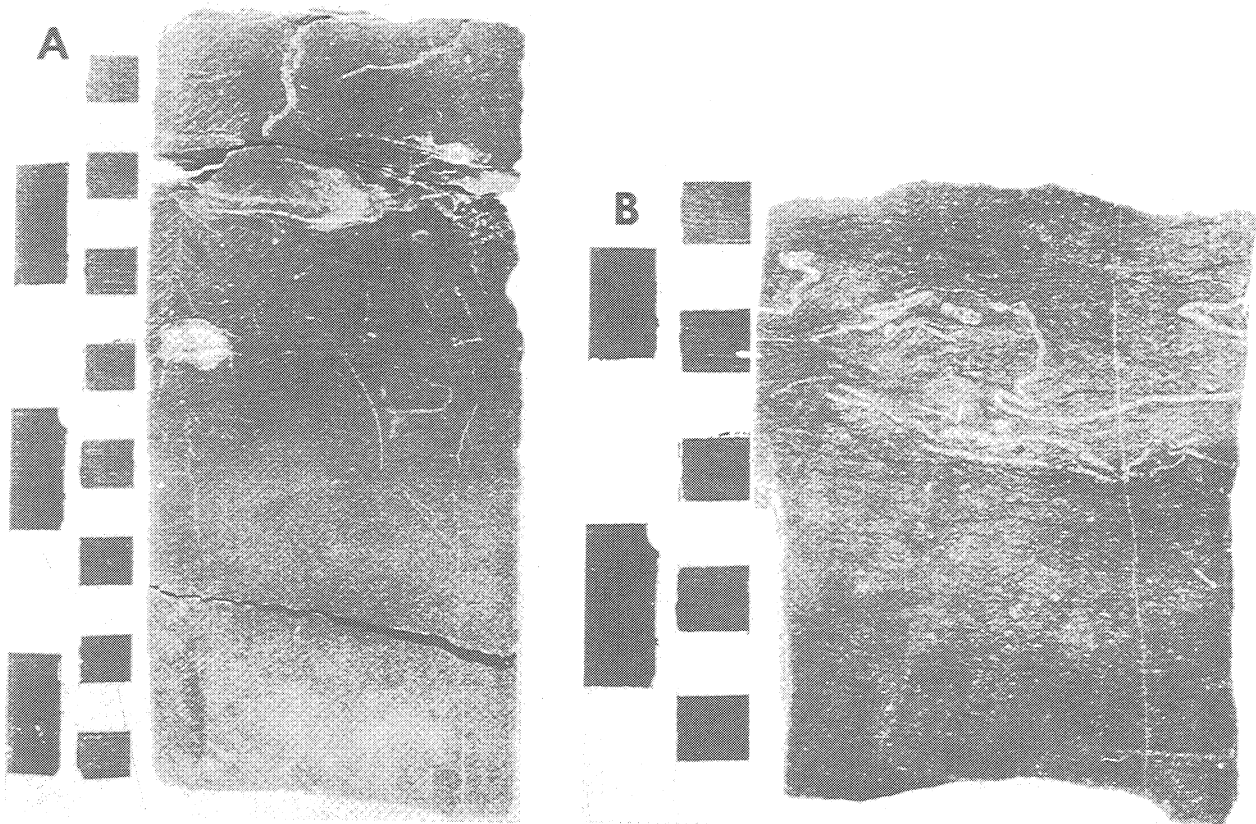


Fig. 26-Marginal marine facies of the Mission Canyon, which forms thin narrow offshore beds of skeletal wackestone: A) composed of muddy, fine skeletal detritus and rugose corals, B) composed of delicate bryozoans and smaller skeletal fragments forming a skeletal wackestone. Note natural en echelon fracture, now filled with calcite cement. Scale in inches and centimeters.

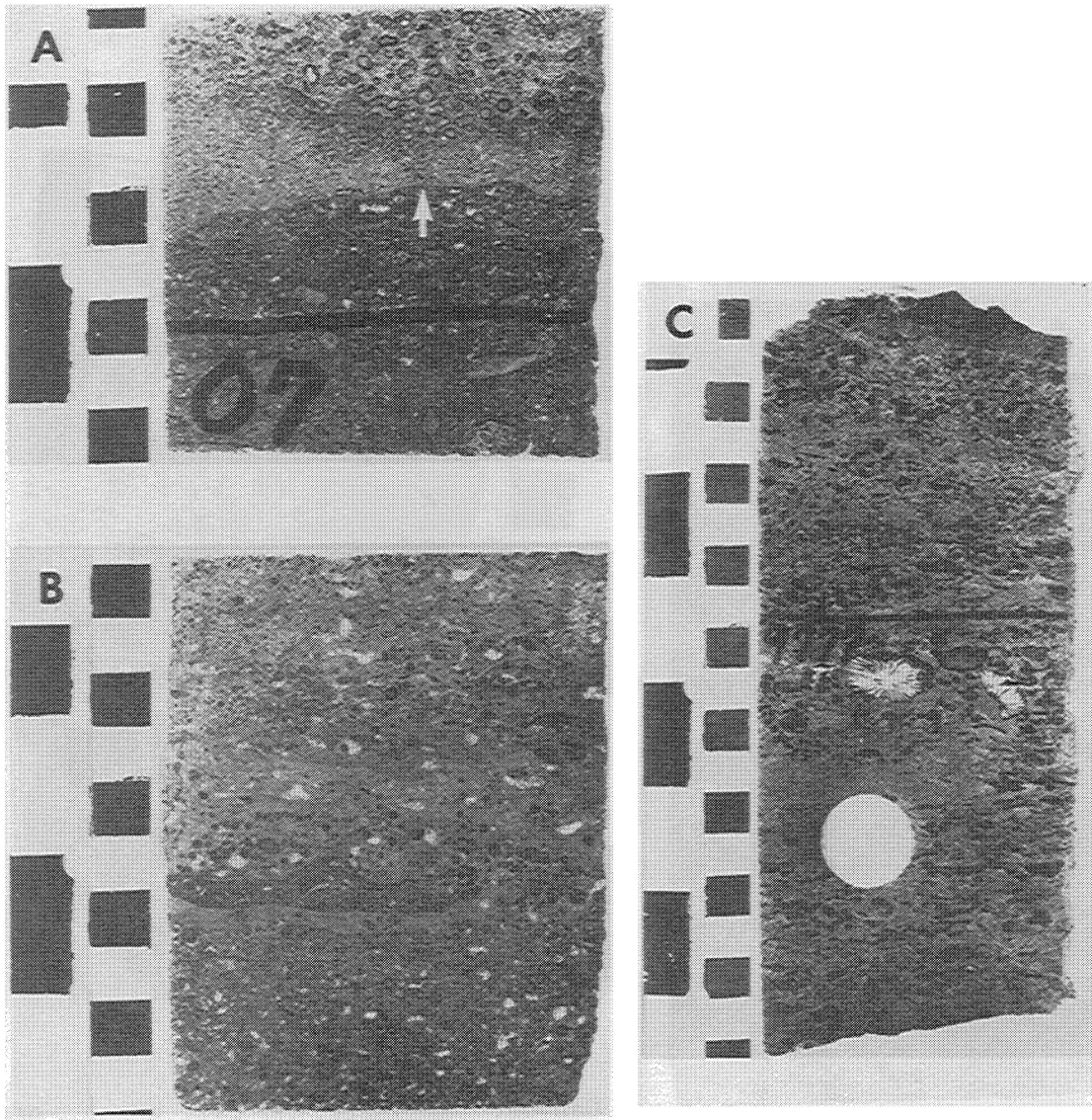


Fig. 27-Intertidal buildup facies of the Mission Canyon, composed of ooid-pisolite-oncolite, skeletal, intraclastic wackestone/grainstones: A) arrow points to thin crust formed during subaerial exposure, B) illustrates packstone/grainstones at base of core separated by a flat lying stylolite from mud and particle layers in upper two-thirds of the core, C) composed of rip-up intraclasts of mud and rugose corals, deposited back onto a washover apron. Scale in inches and centimeters.

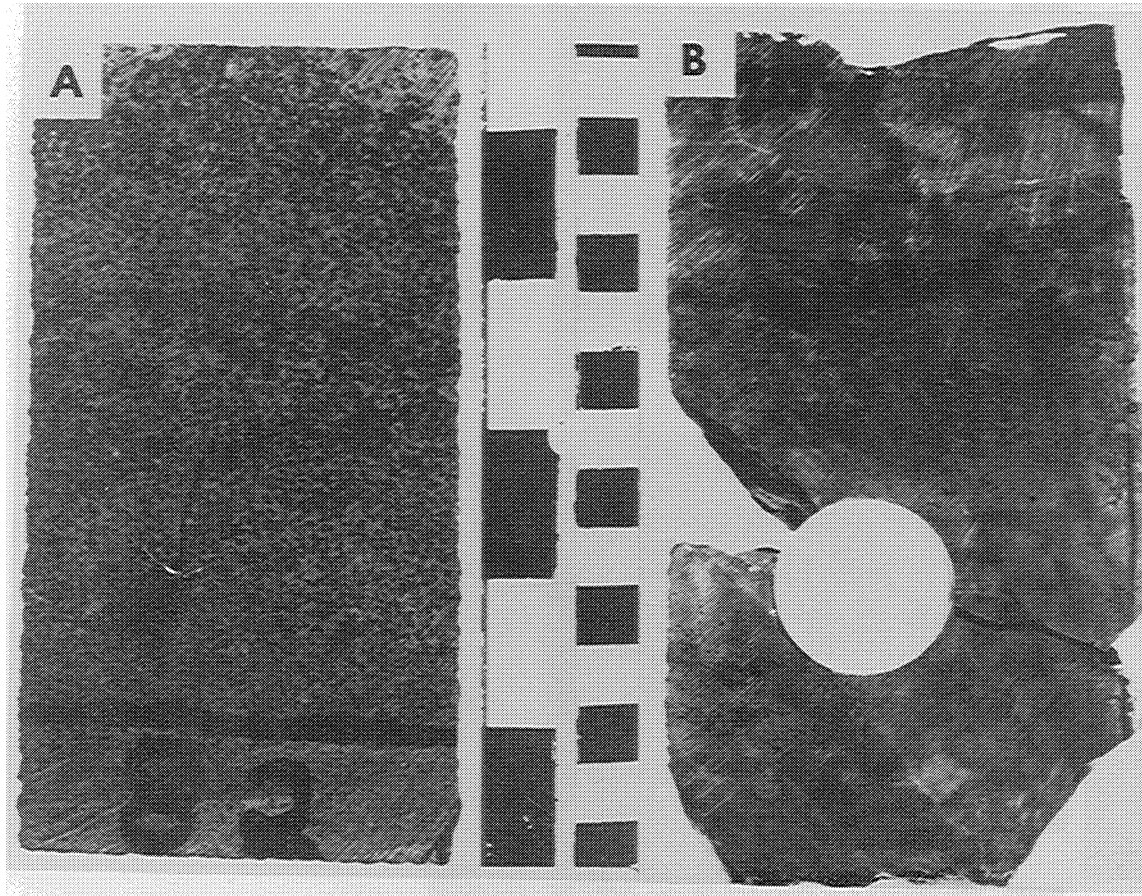


Fig. 28-Lagoon facies of the Mission Canyon: A) injection well no. 1, 9682 feet (2950 m), originally limestone mud where anhydrite porphyroblasts grew in the mud, B) originally burrowed mud which is completely replaced by anhydrite. Scale in inches and centimeters.



Fig. 29-Tidal flat/supratidal sabkha facies of the Mission Canyon: A) carbonate mud and small clasts, replaced by anhydrite, may have been lagoonal muds grading into the sabkha, B) displays possible remnants of a gypsum mush generated in the sabkha, C) large nodular mosaic anhydrite bounded above and below by algal laminations, produced by possible storm flooding of the sabkha or slight invasion of the sabkha by the lagoon, D) storm washover laminations replaced by anhydrite, E) nodular mosaic anhydrite developed upon the sabkha, F) algal laminations replaced by anhydrite, G) arrow points to original gypsum crystals which grew on lagoon floor. Scale in inches and centimeters.

ZABOLOTNY INJECTION #1

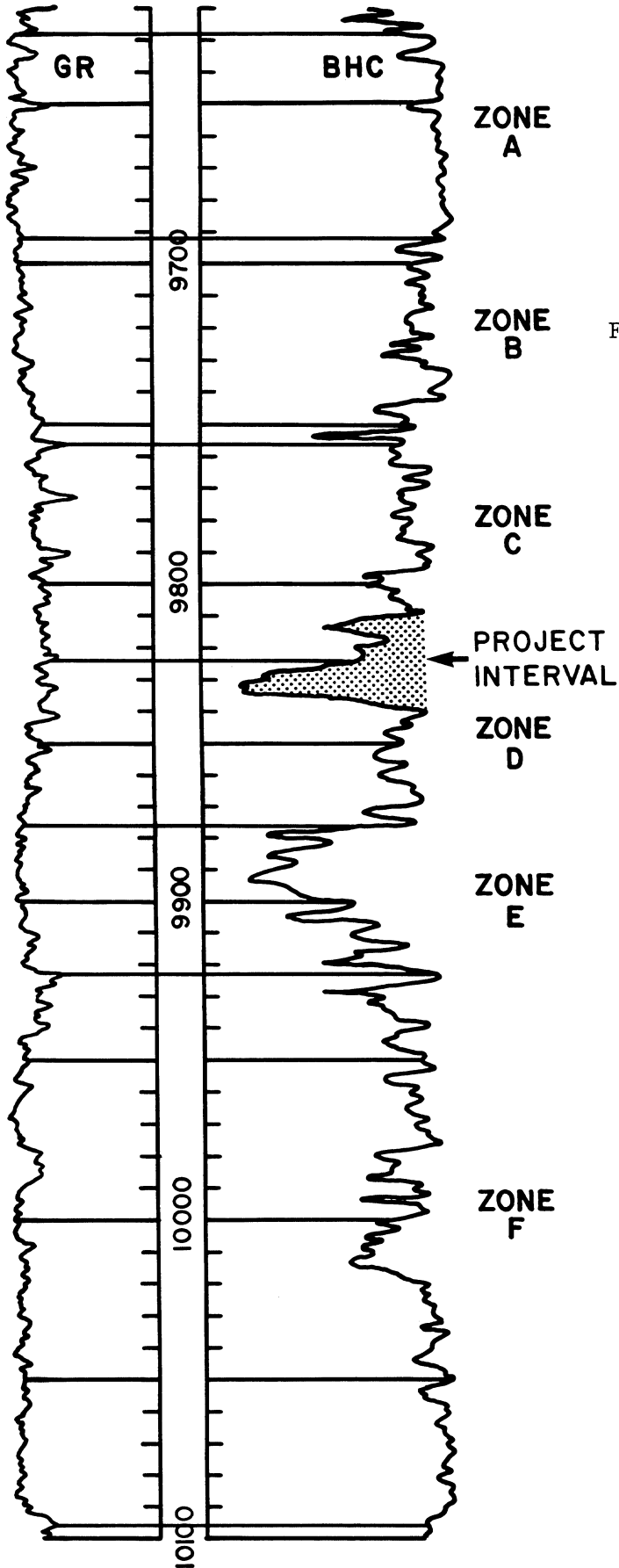


Fig. 30-Injection well no. 1 sonic log (BHC), central well within the CO₂ minitest. The complete Mission Canyon Formation is displayed, including information log zonations A-F. The project interval is shaded, in the base of zone C and top of zone D.

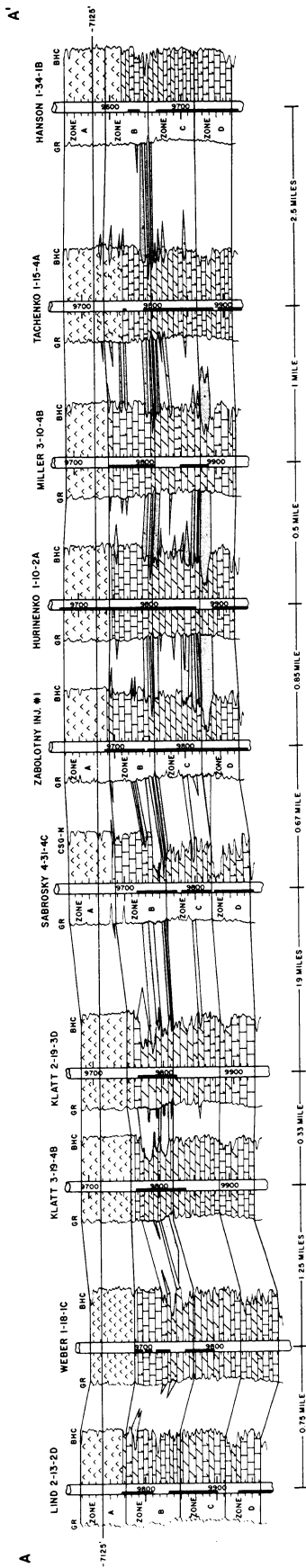


Fig. 31-North-south structural fence diagram A-A' of zones A, B, C and D of Mission Canyon Formation through cored wells in Little Knife Field. Black vertical bars represent cored intervals in each well. Shaded areas are porous hydrocarbon-bearing beds. Lithologies from core and log calculations illustrate rock types and their lateral and vertical relationship. Note thickening of anhydrite beds to the south (A') in zone A and uppermost portions of zone B. Also note changes in zone B and D porosity from porous beds of dolomite, northward, into dense beds of limestone to the south. Progradation is to the northwest, which is outward and toward the viewers left on approximately a 45° angle from the fence diagram. Position of the CO₂ minitest is in the center of the fence diagram, injection well no. 1.

ZABOLOTNY 4-3-1A

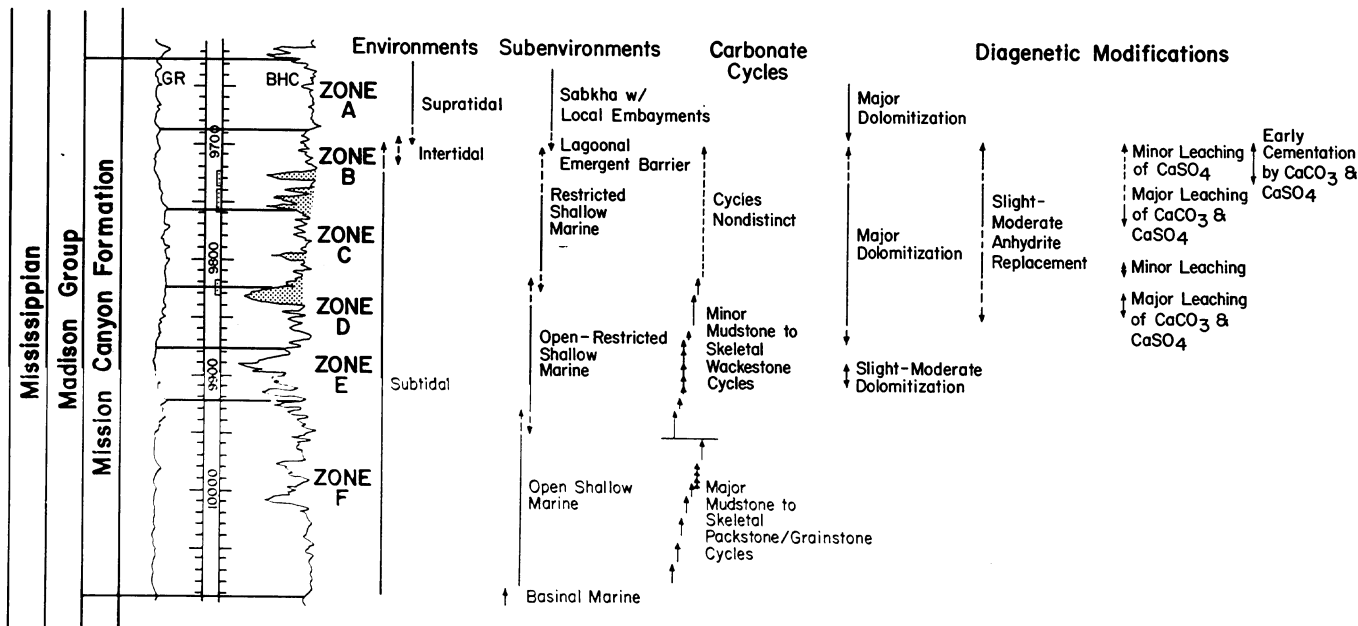


Fig. 32-Type log of Mission Canyon Formation at Little Knife Field, approximately 0.25 miles northwest from the minitest location. Informal log zonations A-F, for field correlation, are illustrated. Depositional environments, carbonate cycles and diagenetic modifications are from a composite section of several cores. Stipple area indicates where hydrocarbon bearing beds are located in this well.

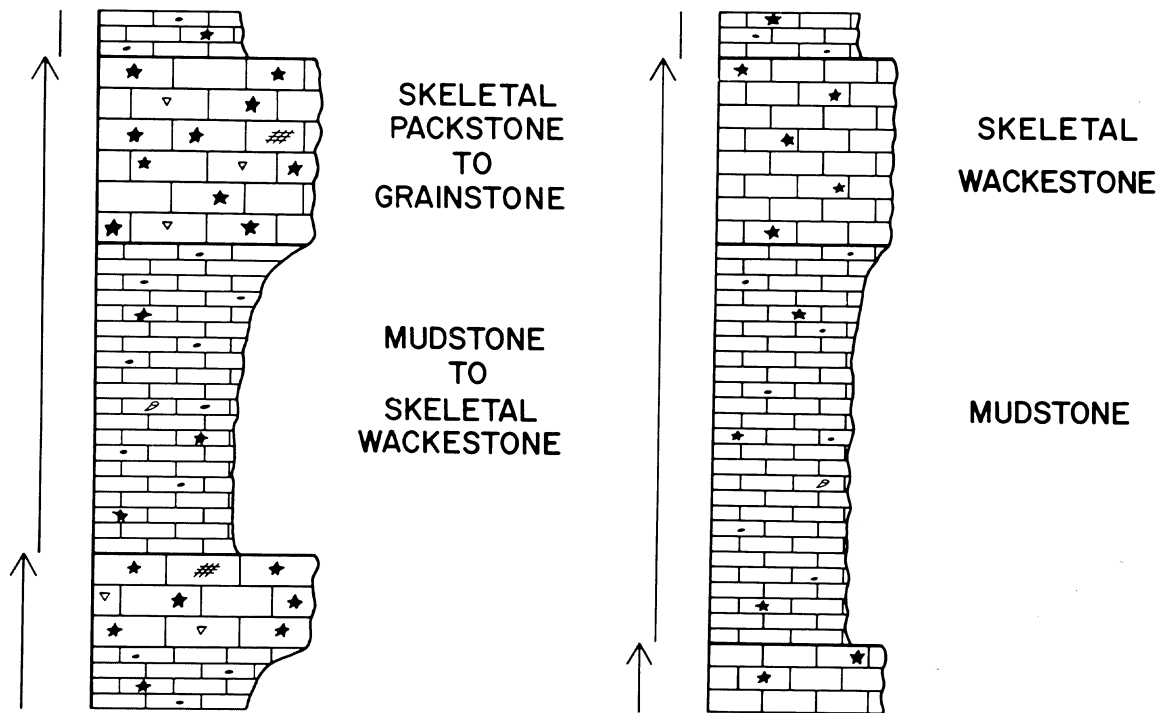


Fig. 33-Carbonate cycles of the Mission Canyon Formation at Little Knife Field. (Left) Example of major carbonate cycles of the open marine facies, with mudstone/skeletal wackestones grading up into skeletal packstone/grainstone capping beds. (Right) Example of minor carbonate cycles of the transitional open to restricted marine facies, with mudstones grading up into skeletal wackestone beds. Both of these cycles are repeated several times in lower two-thirds of the subtidal setting.

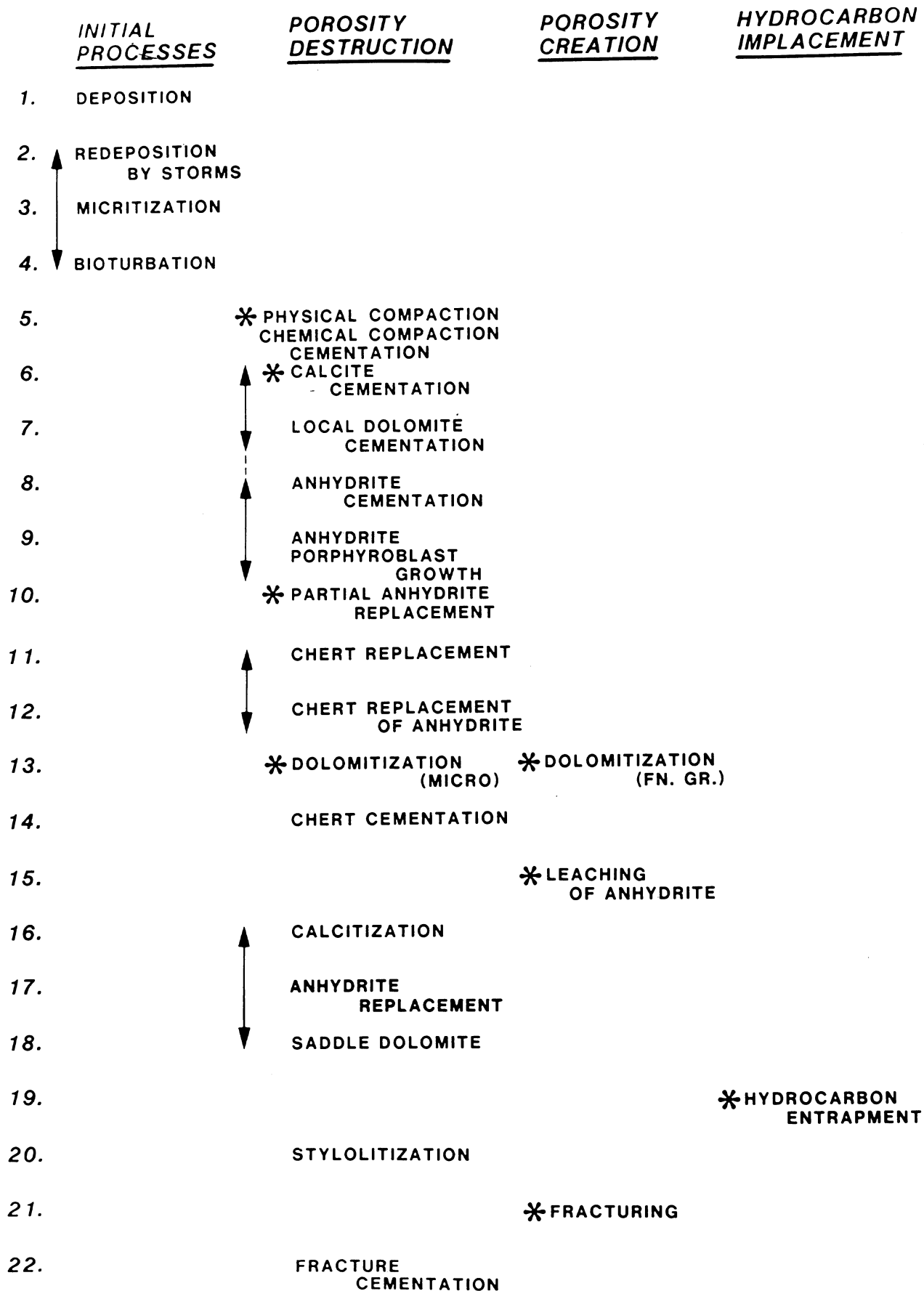


Fig. 34-Events which formed and modified the Mission Canyon Formation at Little Knife Field. Essentially a paragenetic sequence, these events are divided into: 1) initial processes, 2) porosity destruction, 3) porosity creation, and 4) hydrocarbon emplacement.

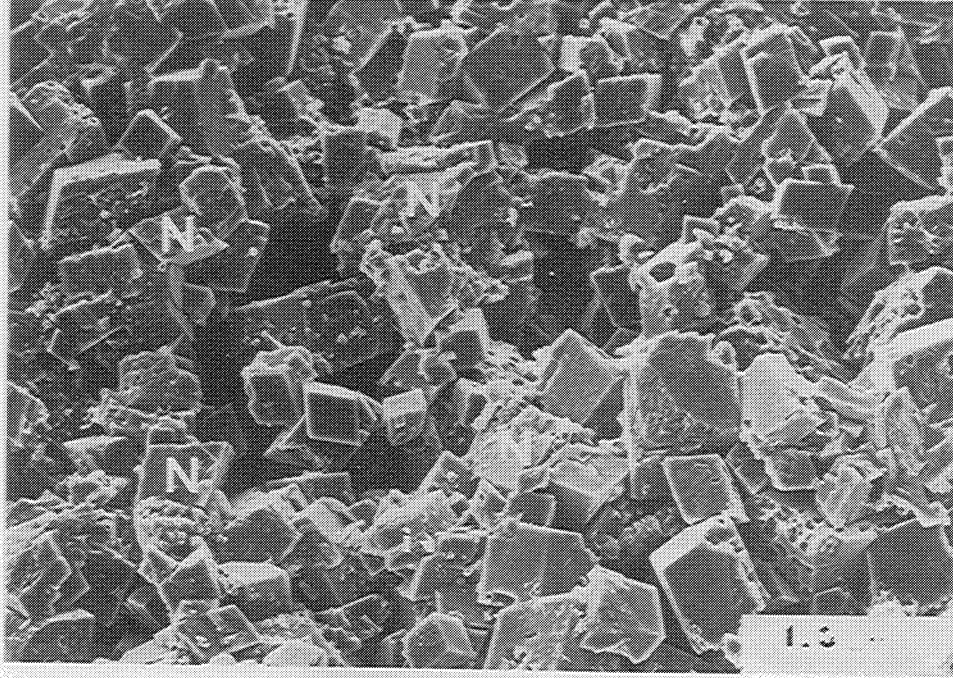


Fig. 35-This sample of dolostone was originally a pellet, now a ghost, which was leached as a source of carbonate during dolomitization. It now forms a moldic pore and is surrounded by a spherically continuous necklace of dolomite crystals (N). The original matrix is dolomitized and forms fine grained dolostone containing intercrystal porosity composed of polyhedral, tetrahedral and interboundary-sheet pores. This sample was etched for fifteen seconds in a ten percent HCl acid to remove small calcite crystals. Scale is 100 micrometers.

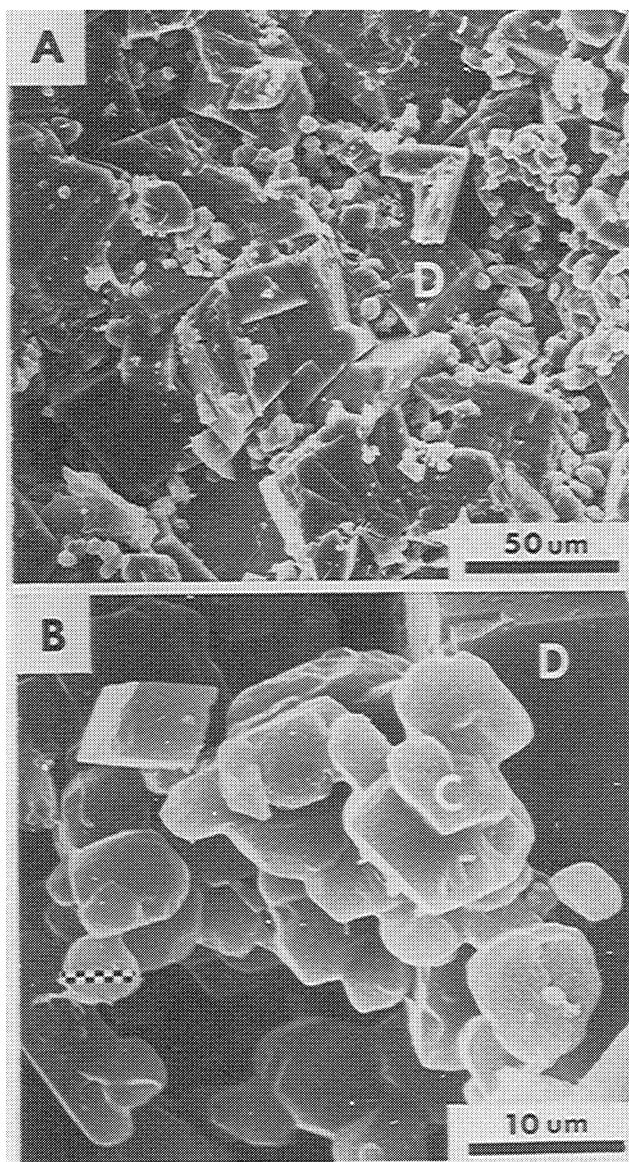


Fig. 36- Calcite crystals sitting upon and partially etched into dolomite crystals. A) Broad view across several dolomite crystals (D) with calcite crystals tending to congregate or be more dispersed. Scale is 50 micrometers. B) Close-up of upper righthand corner of A. Here individual calcite crystals, forming platelets, are coalescing together. Scale is 10 micrometers, smaller scale on left is 6 micrometers.

TRANSITIONAL OPEN TO RESTRICTED MARINE

RESTRICTED MARINE

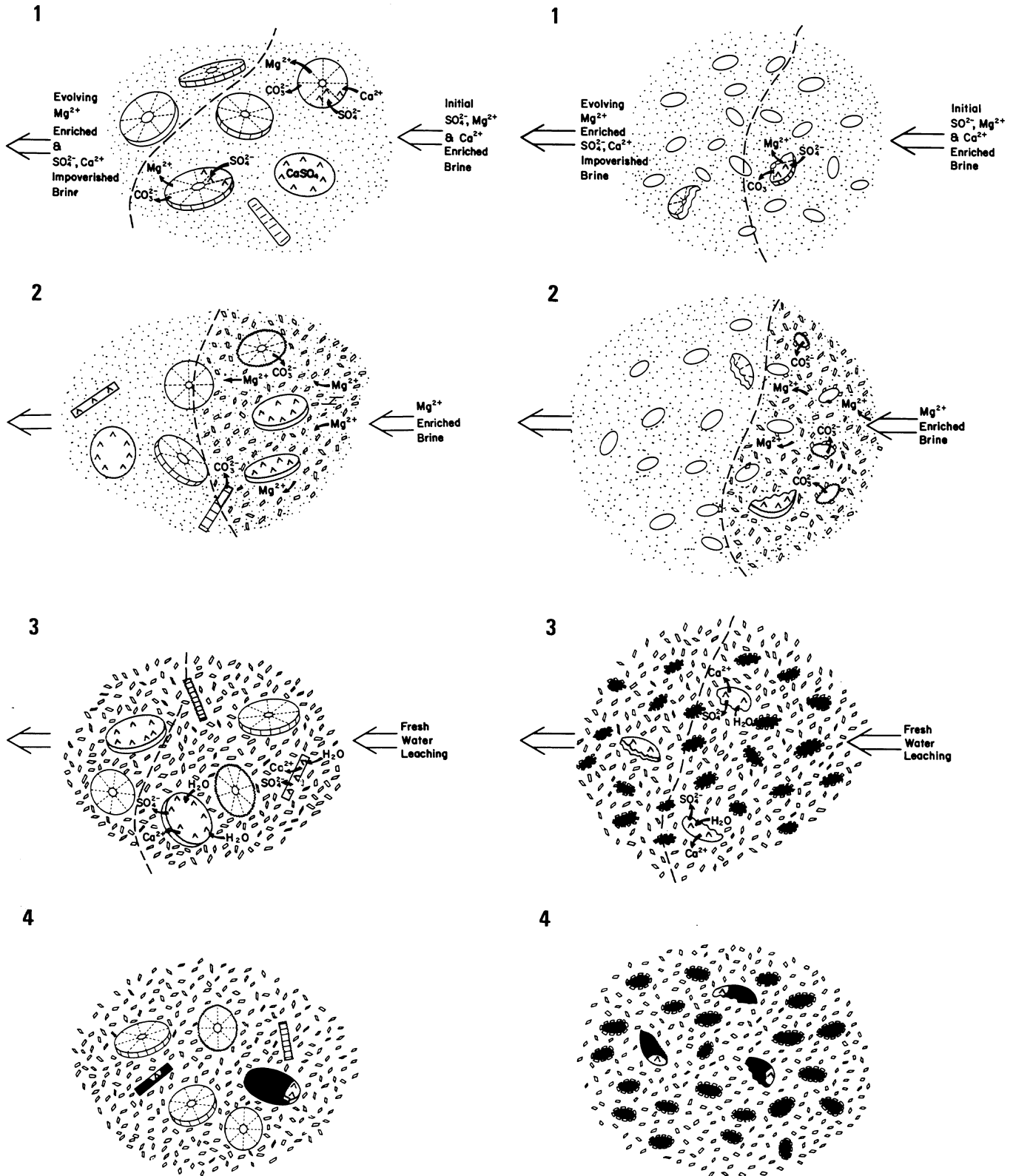


Fig. 37-Simplified sequence of major events which are responsible for producing porous dolostones in the Mission Canyon Formation at Little Knife Field. These events affected both the restricted marine facies and the transitional open to restricted marine facies similarly.

Fig. 38-Stratigraphic fence diagram of zones C and D through
 minitest wells. Shaded central portion of the fence
 diagram is the project interval. North is to the left.
 The central wells, injection well no. 1, sonic log is
 illustrated on left to compare the location of the
 project interval beds to the complete Mission Canyon
 Formation. Black vertical bars in the center of each
 log represent the cored interval.

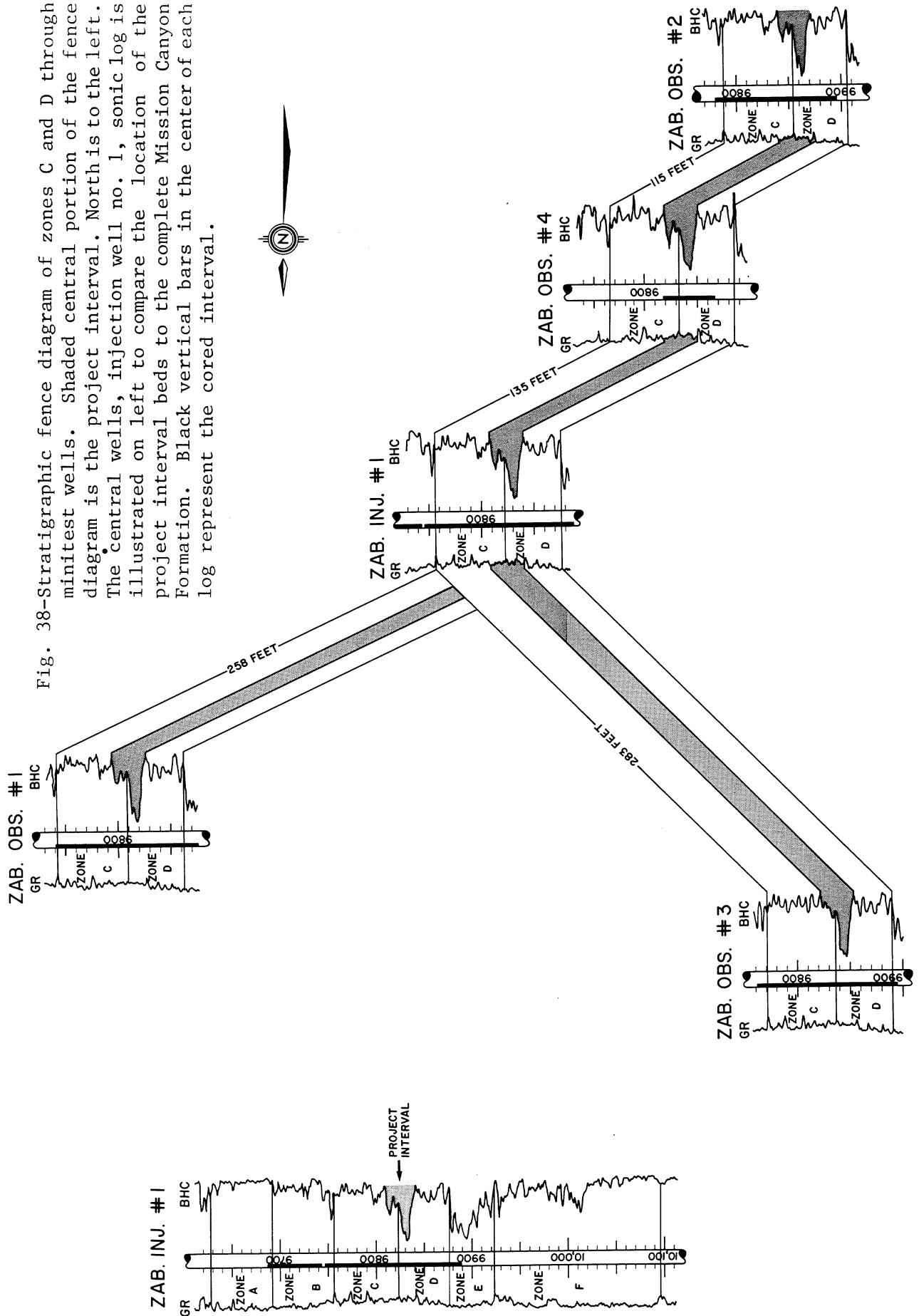




Fig. 39—Close-up view of an average sample of rock from the Little Knife CO₂ minitest. This rock is a partially dolomitized skeletal wackestone. The light particles scattered through the sample are skeletal fragments of crinoid columnals floating in the originally muddy matrix. Discontinuous horizontal and oblique laminations are the outlines of compacted burrows. The original muddy matrix has been dolomitized creating approximately 20 percent porosity in this sample. Dusty appearance of the sample is caused by reflection of light off of dolomite crystal faces. Scale is in inches and centimeters.

Fig. 40-Injection well no. 1. Photomicrographs are from core taken in the CO₂ minitest project interval. Upper photomicrograph (X-nicols and 1/4 plate) is from 9829'11", 25X magnification, of a core sample of rock containing 18.4 percent porosity and 13 md permeability. It consists of a partially dolomitized (D) originally muddy matrix surrounding broken skeletal fragments (C) composed of crinoid columnals. Largest visible pores are moldic pores (M) set within the finely crystalline matrix. Scale is 500 micrometers. Lower photomicrograph (X-nicols and 1/4 plate is from 9827'5", 25X magnification, of a core sample of rock containing 23.5 percent porosity and 88.7 md permeability. It is again a partially dolomitized skeletal wackestone with the muddy matrix, surrounding skeletal fragments (C), now dolomitized. Moldic pores (M), formed by solutioning of anhydrite replaced portions of skeletal fragments (A), are obvious and occasionally tend to form slight solution channels (arrow). Scale is 500 micrometers.

Fig. 41-Observation well no. 1. Photomicrographs are from cores taken in the CO₂ minitest interval. Upper photomicrograph (X-nicols and 1/4 plate) is from 9808'4", 25X magnification, of a core sample of rock containing 20.5 percent porosity and 8.6 md permeability. It is partially dolomitized (PD) skeletal wackestone, containing a dolomitized muddy matrix with skeletal fragments (C), crinoid columnals, floating in the original muddy matrix. Some skeletal fragments have been invaded (I) by dolomite crystals seeking a source of carbonate during dolomitization. Scale is 500 micrometers. Lower photomicrograph (X-nicols and 1/4 plate) is from 9815'3", 25X magnification, of a core sample of rock containing 24 percent porosity and 24 md permeability. Again, the sample has been partially dolomitized (D) throughout the originally muddy portions, with crinoid fragments (C) left floating in the muddy matrix. The dolomitized portions form a fine grained fabric. Moldic pores (M) and incipient solution channels, through the crinoid fragment (arrow), are areas where anhydrite has been leached away. Scale is 500 micrometers.

Fig. 42-Observation well no. 2. Photomicrographs are from cores taken in the CO₂ minitest project interval. Upper photomicrograph (X-nicols and 1/4 plate) is from 9851'4", 25X magnification, of a core sample of rock containing 20.9 percent porosity and 15 md permeability. This portion of the sample is well dolomitized (D) with skeletal ghosts, originally fragments of crinoids forming a skeletal wackestone, now forming moldic pores (M) after being replaced by anhydrite and later leached away. The dolomite maintains a fine grained saccharoidal fabric. Scale is 500 micrometers. Lower photomicrograph (X-nicols and 1/4 plate) is from 9859'5", 25X magnification, of a core sample of rock containing 27 percent porosity and high amounts of permeability. This sample is well dolomitized (D) with many ghosts (G), oval shapes, scattered throughout the field of view. Some elongate moldic pores (M) are present, with the much smaller intercrystal pores not visible on this scale of magnification. Note that the dolomite crystals are gradational in size, in this field of view, between a fine grained and medium grained fabric. Scale is 500 micrometers.

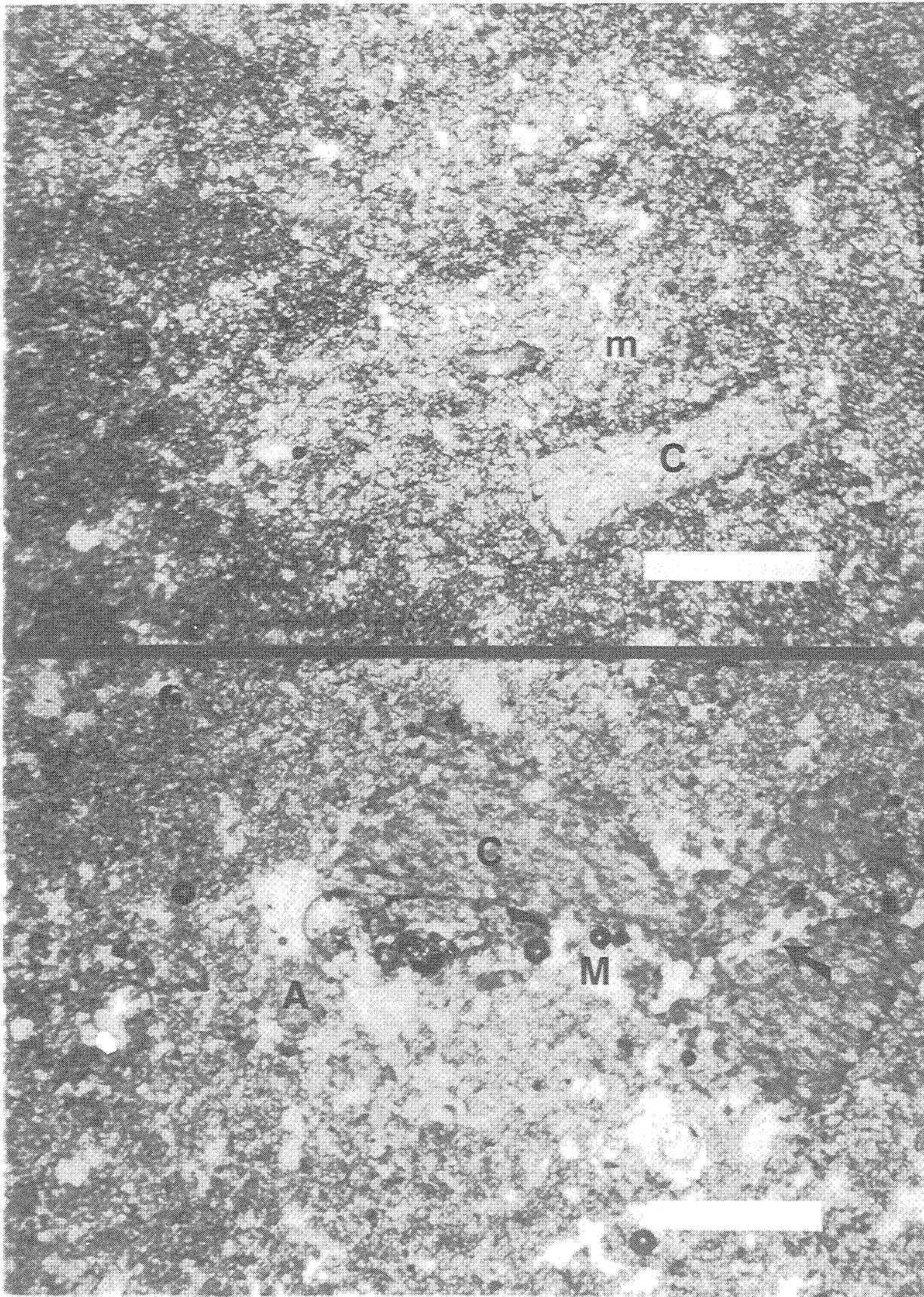


Figure 40

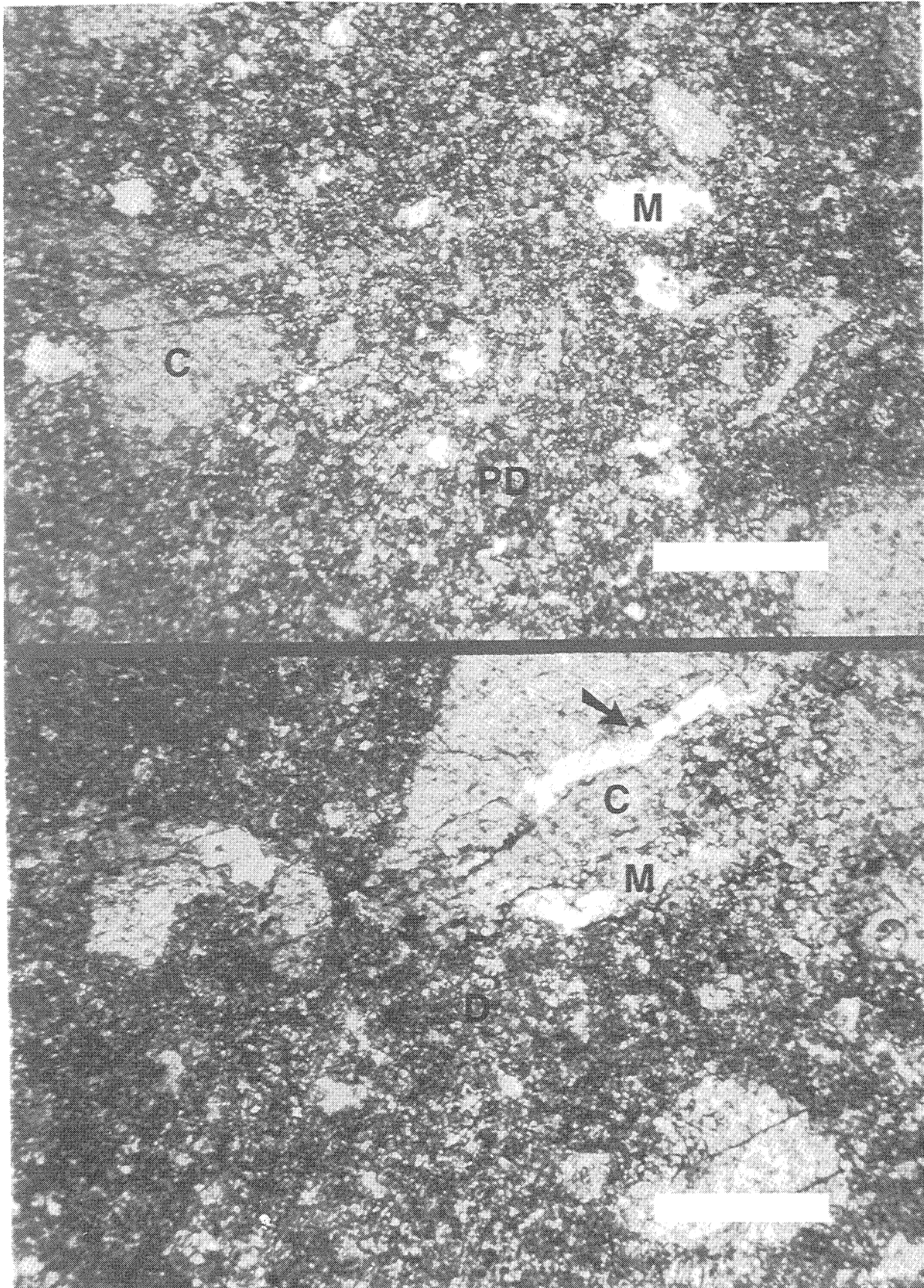
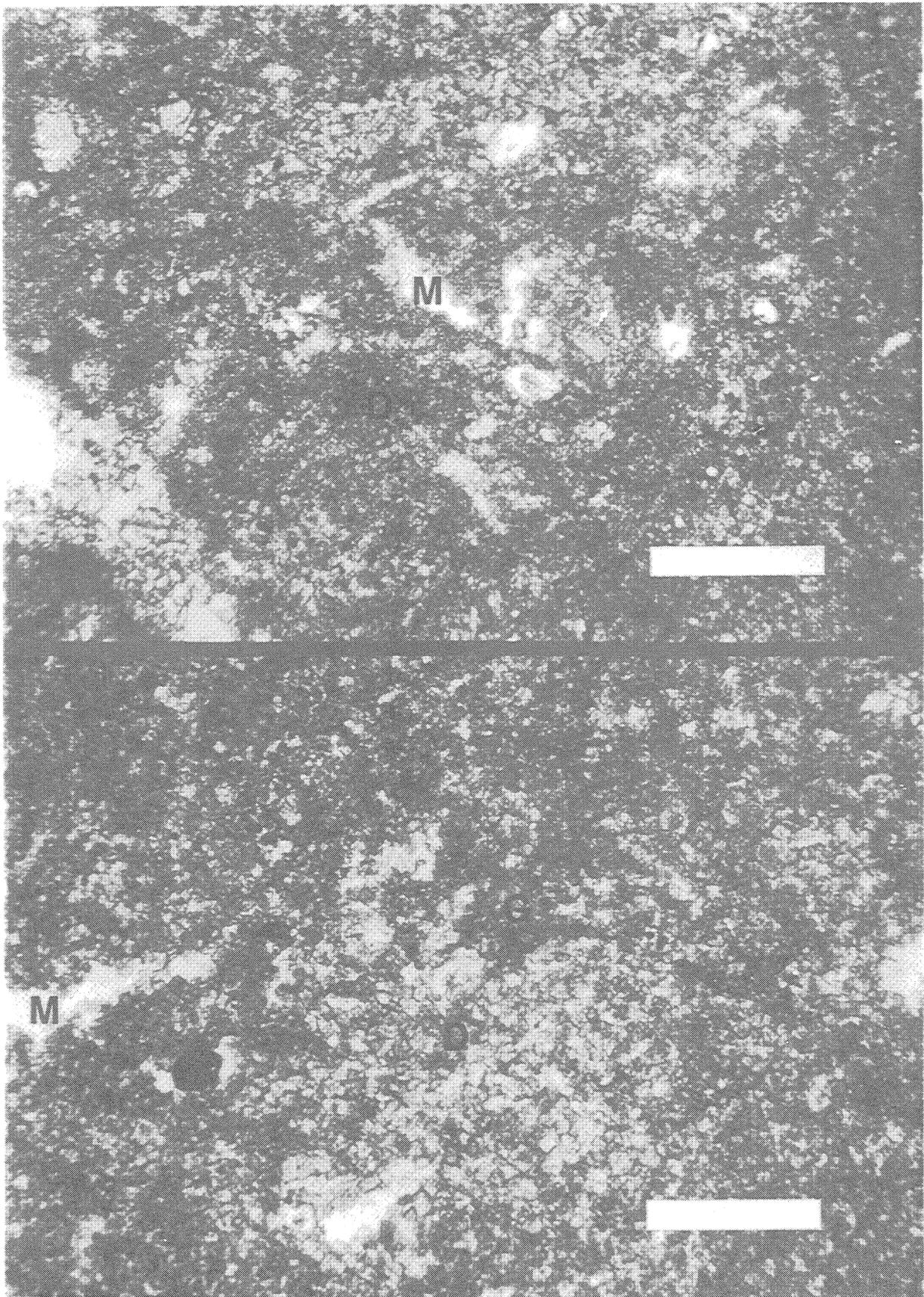


Figure 41



UP

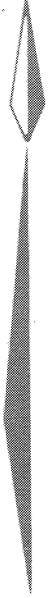


Figure 42

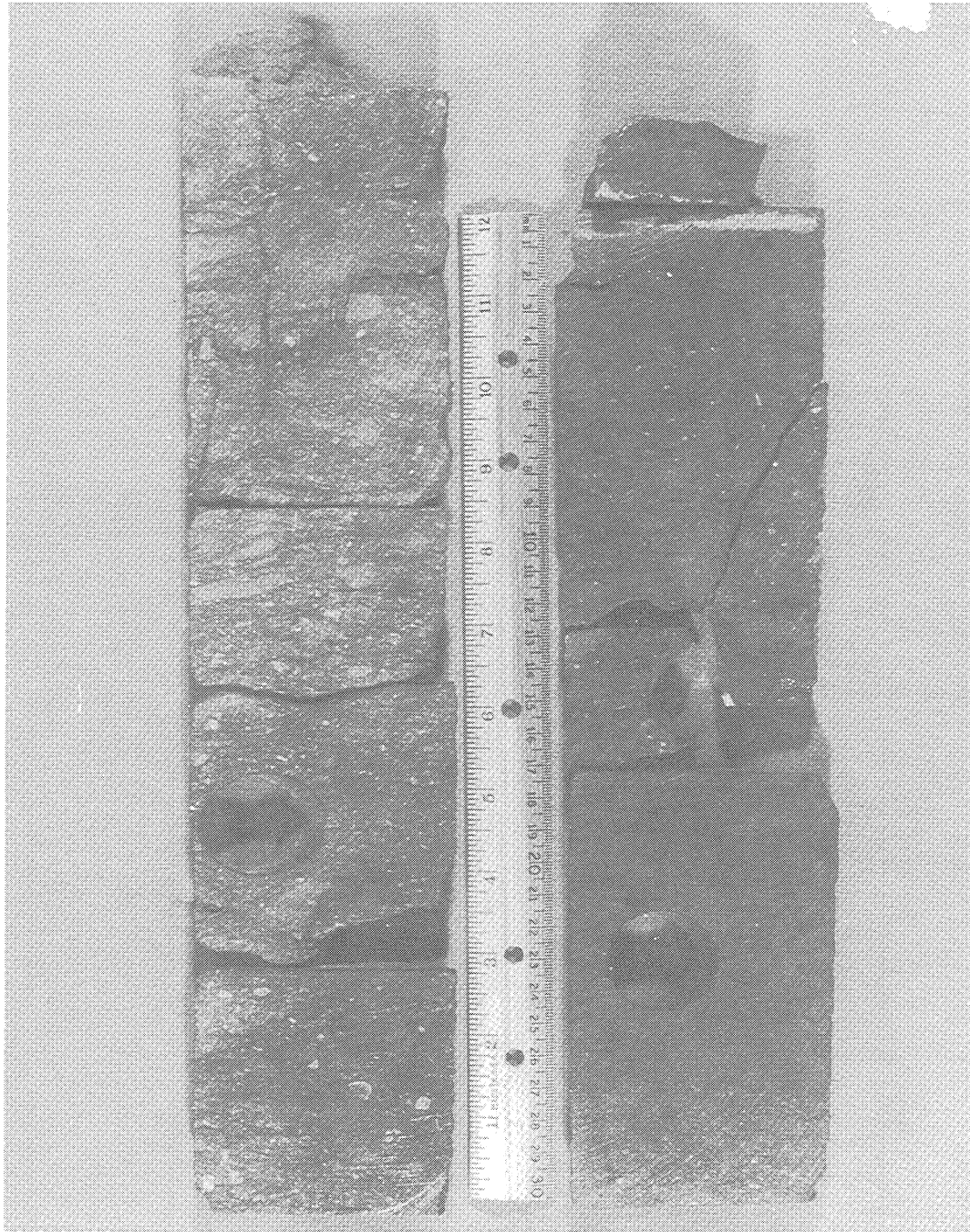
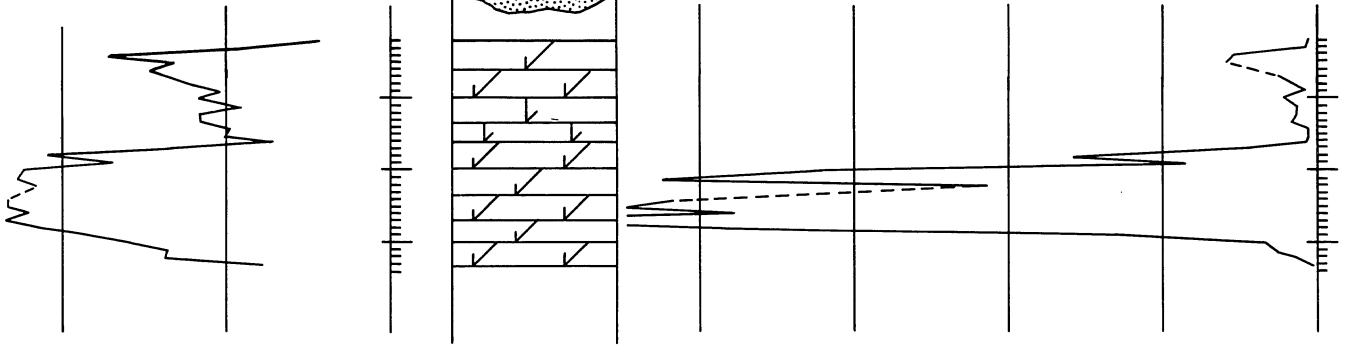
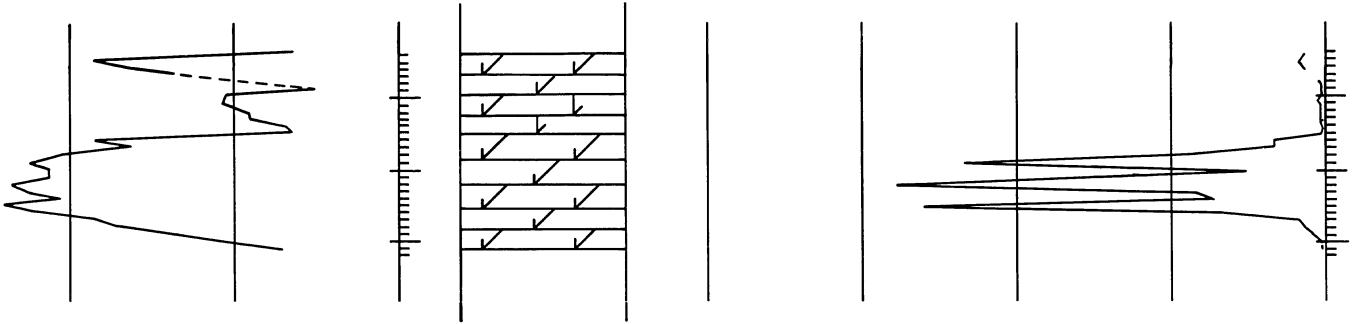


Fig. 43-Core slabs from injection well no. 1, at 9817-19 feet. Crinkly line at upper left is a stylolite created by pressure solutioning. Calcium carbonate from pressure solutioning (stylolitization) has moved out laterally a few inches to reduce porosity down to 7.0 percent and create a marker on sonic logs in the section. This feature forms the top of zone D throughout the CO₂ minitest area. Note the vertical fracture which cuts across the stylolite. Porosity away from the stylolite and down section increases from 7.0 percent at the stylolite to 13.3 percent, one foot below, and 20.9 percent, two feet below it. Scale is in inches and centimeters.

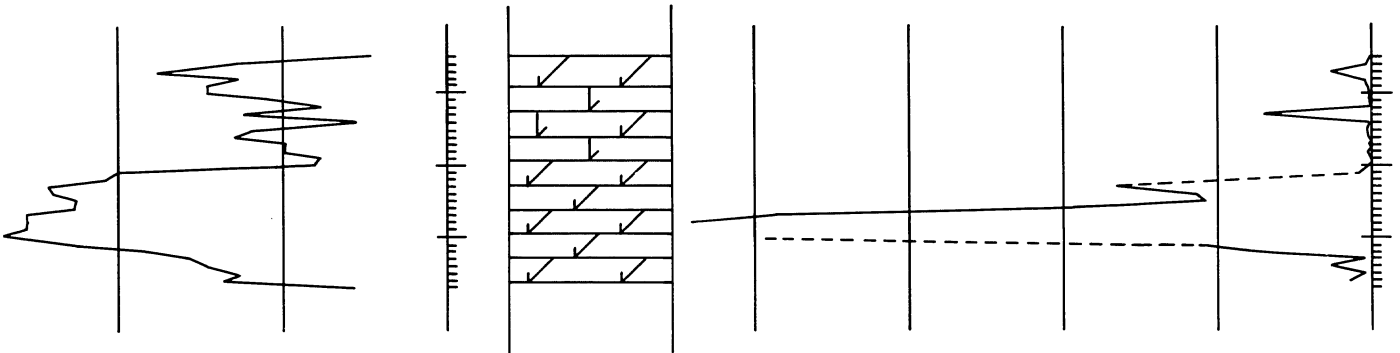
Zabolotny Injection #1



Zabolotny Observation #1



Zabolotny Observation #2



Zabolotny Observation #3

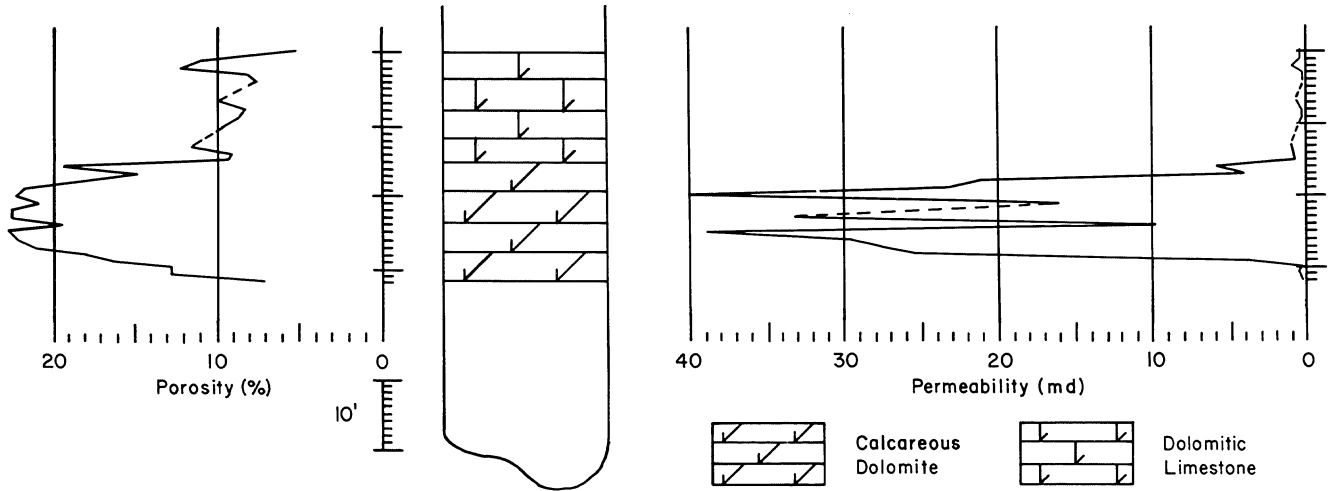


Fig. 44-Whole core porosity (percent) and permeability (millidarcy's) compared to lithology in each Little Knife CO₂ minitest well.

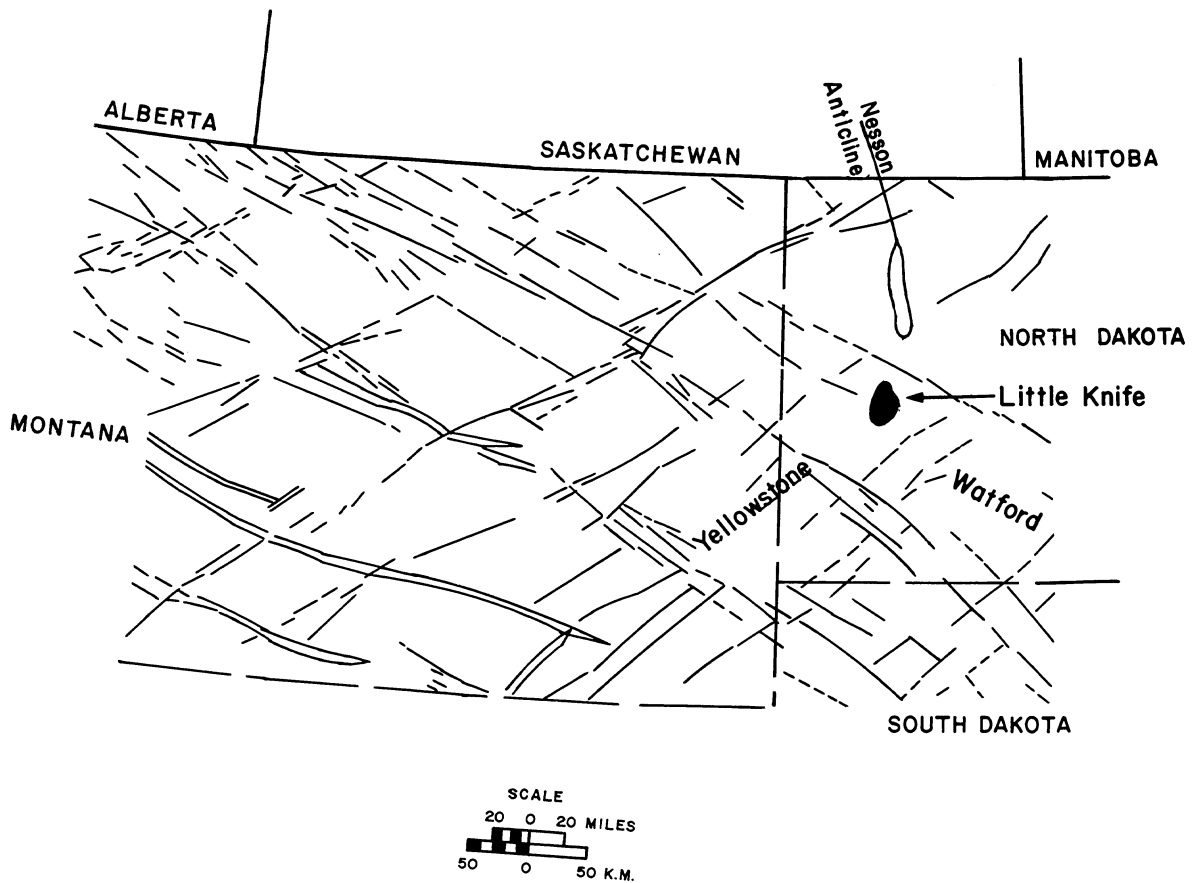


Fig. 45-Surface lineaments mapped through portions of Montana, western North Dakota and northwesternmost South Dakota. Little Knife Field is located within the intersection of the northeast trending Yellowstone Block and northwest trending Watford Block. Location of Nesson Anticline, to the north, is compared to Little Knife Field. Scale is in miles and kilometers. Modified after Thomas¹⁸.



Fig. 46-Surface lineaments from Landsat photographs (thick lines) and aerial photographs (thin lines) in central and northern portions of Little Knife Field. Dashed line shows the field outline. Asterisk marks the position of the Little Knife CO₂ minitest. Modified after Hodgson¹⁹

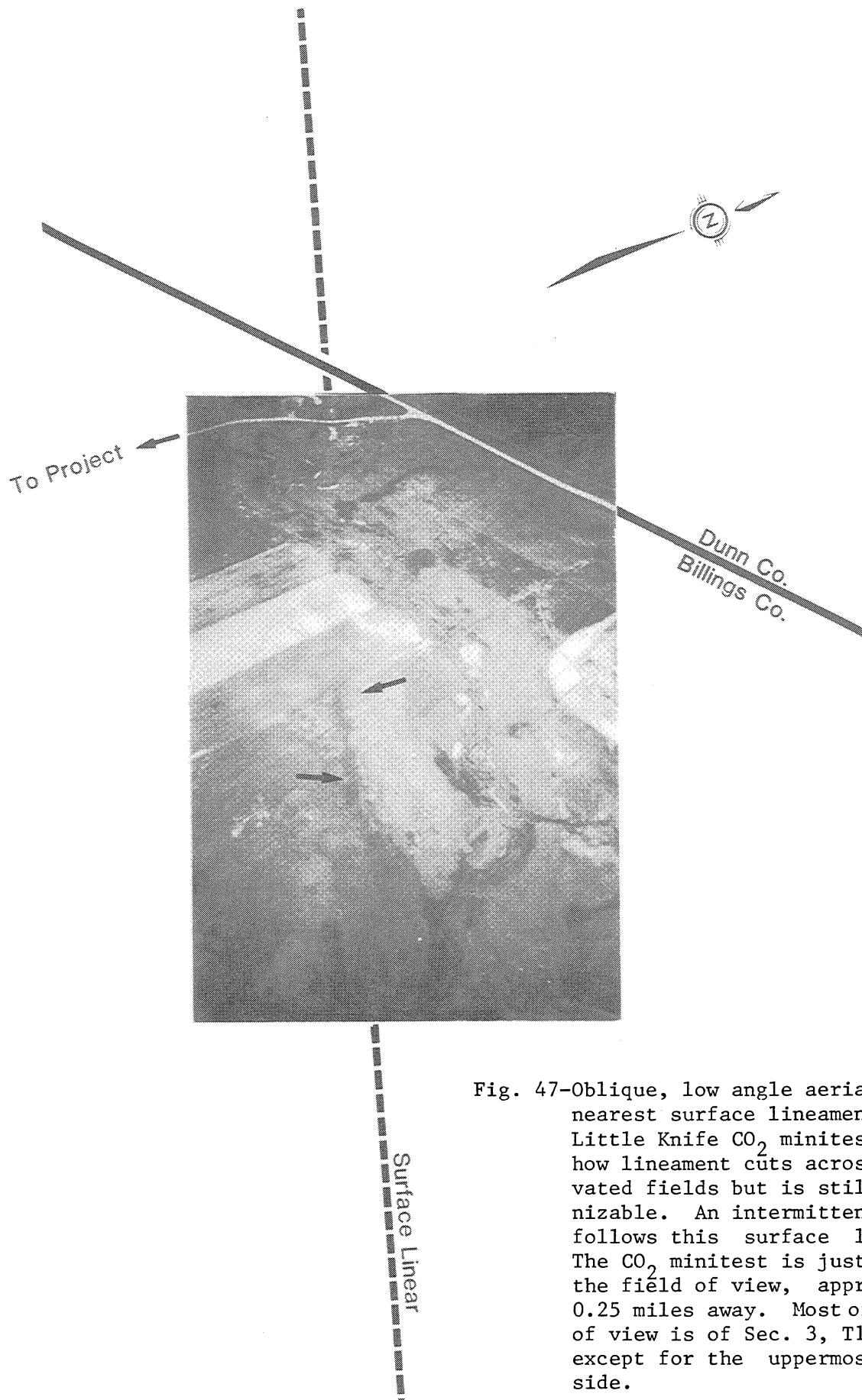


Fig. 47-Oblique, low angle aerial view of nearest surface lineament to the Little Knife CO₂ minitest. Note how lineament cuts across cultivated fields but is still recognizable. An intermittent stream follows this surface lineament. The CO₂ minitest is just left of the field of view, approximately 0.25 miles away. Most of the field of view is of Sec. 3, T144N, R98W, except for the uppermost right side.

Surface Outcrop At Minitest Location

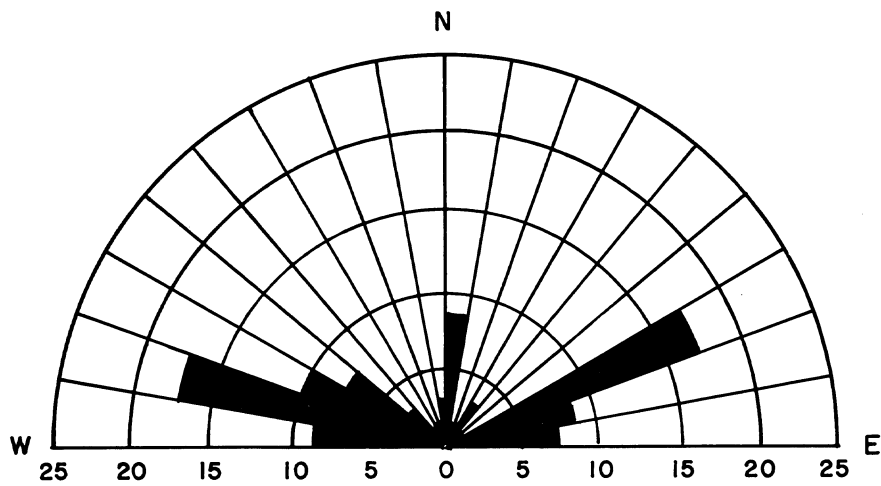


Fig. 48-Surface outcrop fractures measured next to observation well no. 3. Results of 69 apparent strike directions are plotted in 10 degree increments. Numbers along the bottom of the illustration are in percent.

Zabolotny Observation No. 3

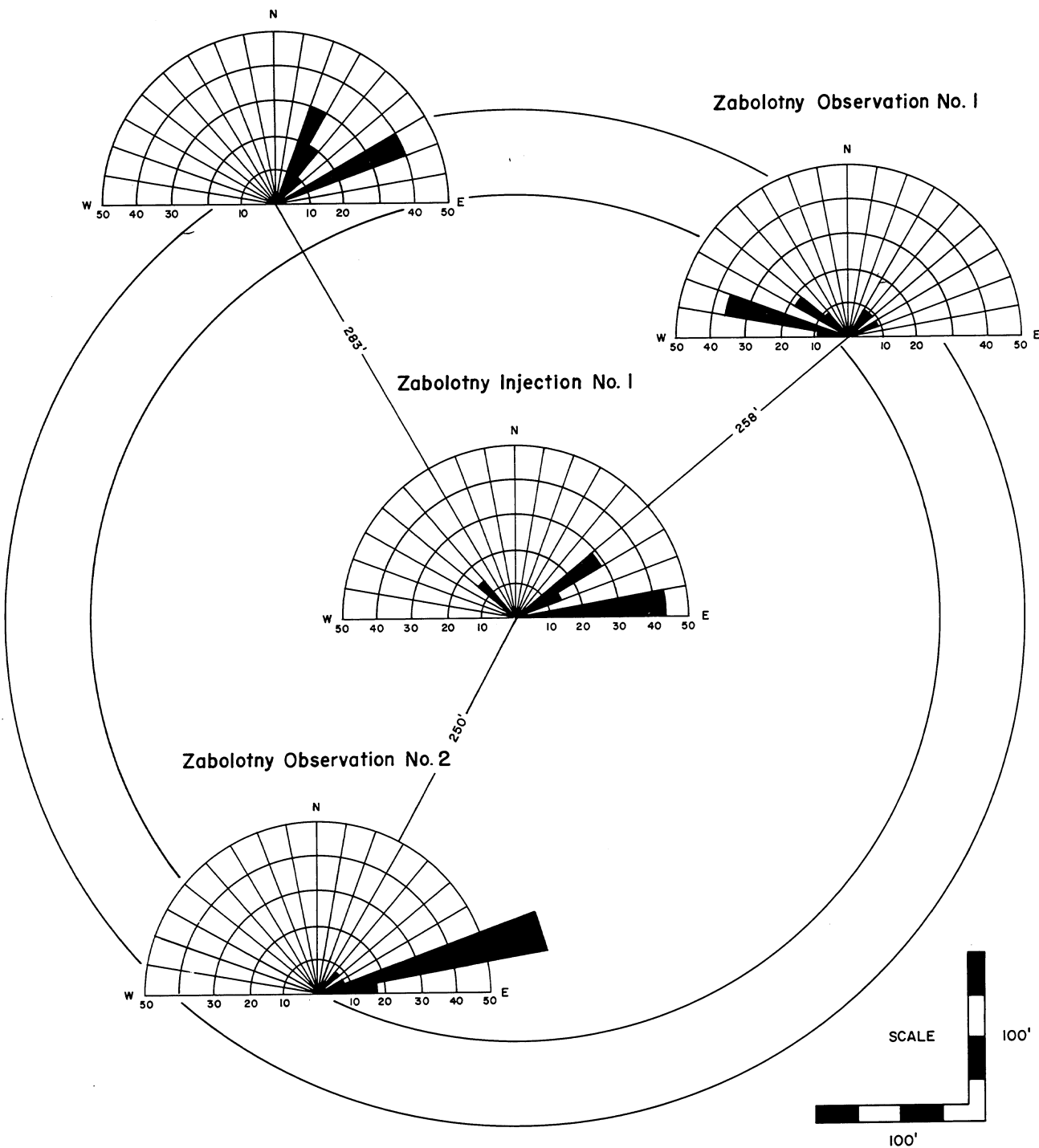


Fig. 49—Fractures measured from oriented cores in Little Knife CO₂ minitest beds. Sets of fractures are grouped in 10 degree increments and displayed as percentages. Exact reservoir bottom-hole well locations are illustrated and their distance of separation within the CO₂ minitest. The outer circle is 600 feet in diameter and the inner circle is 500 feet in diameter.

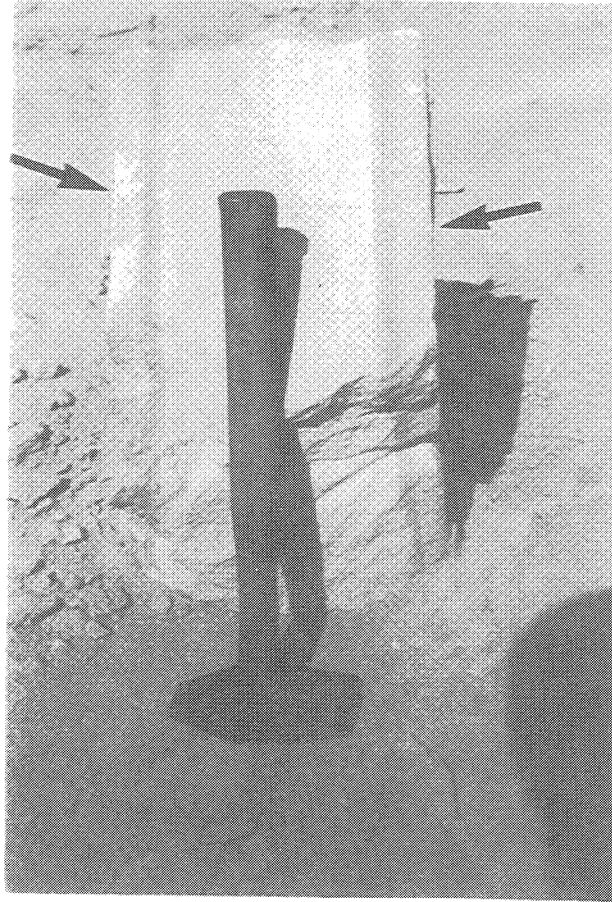


Fig. 50-Blocks of Sentinel Butte Formation, broken-up by bulldozing equipment along fractures, illustrating surface fracture (joint) separation. Separation is between 1-6 feet. Note how iron rich solutions migrating along the fracture (joint) have slightly invaded the sandstone to give it a banded appearance.

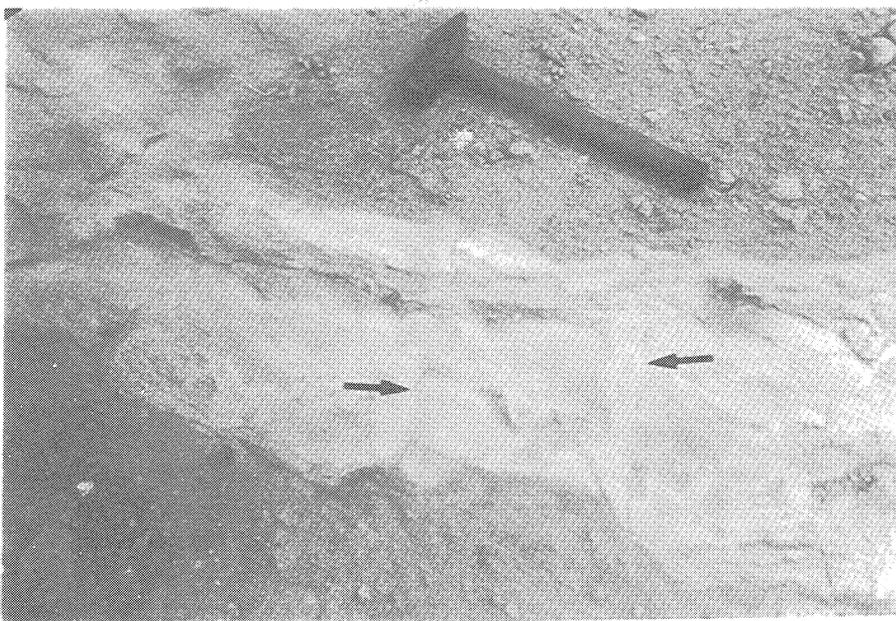


Fig. 51-Outcroppings of Sentinel Butte Formation, next to observation well no. 3, where surface fracture strike directions were measured. The rock type is a lithic sandstone. Upper photograph illustrates cleared areas, next to the drilling site, where some of the fracture strike directions were obtained. Other such locations surrounding the drilling site were also cleaned off and fracture strikes measured. Lower photograph is a closeup of fractures (arrows) and their separation, and is the same area cleaned off in the upper photograph (arrow). Hammer is 18 inches in length. North is to the left.

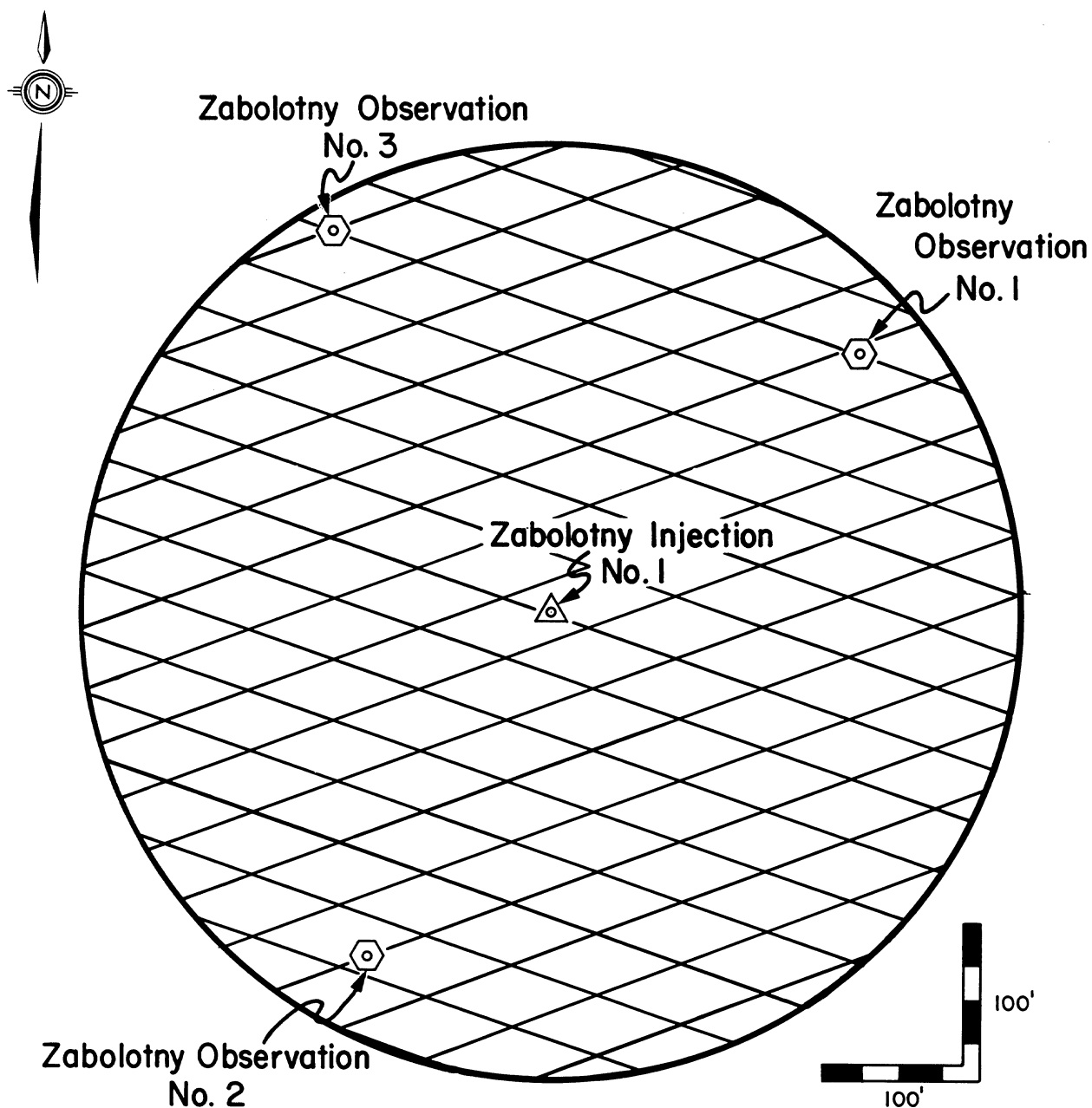


Fig. 52-Generalized illustration representing the average trends of fractures, not individual fractures, through the CO₂ minitest area. All fractures were found to be small, vertical, hairline, en echelon planes which are interpreted to have short lateral lengths. Average strike of these fractures is northwesterly, N. 67 W., and northeasterly, N. 69 E. Calculated permeabilities from multiwell pulse testing reveal no major contribution by fractures, but calculate twice the average matrix permeability and are uniformly distributed across the minitest area. This in situ permeability estimate would signal that fractures may be dispersed in a somewhat uniform manner within the minitest area but that individual fractures are small and terminate abruptly.

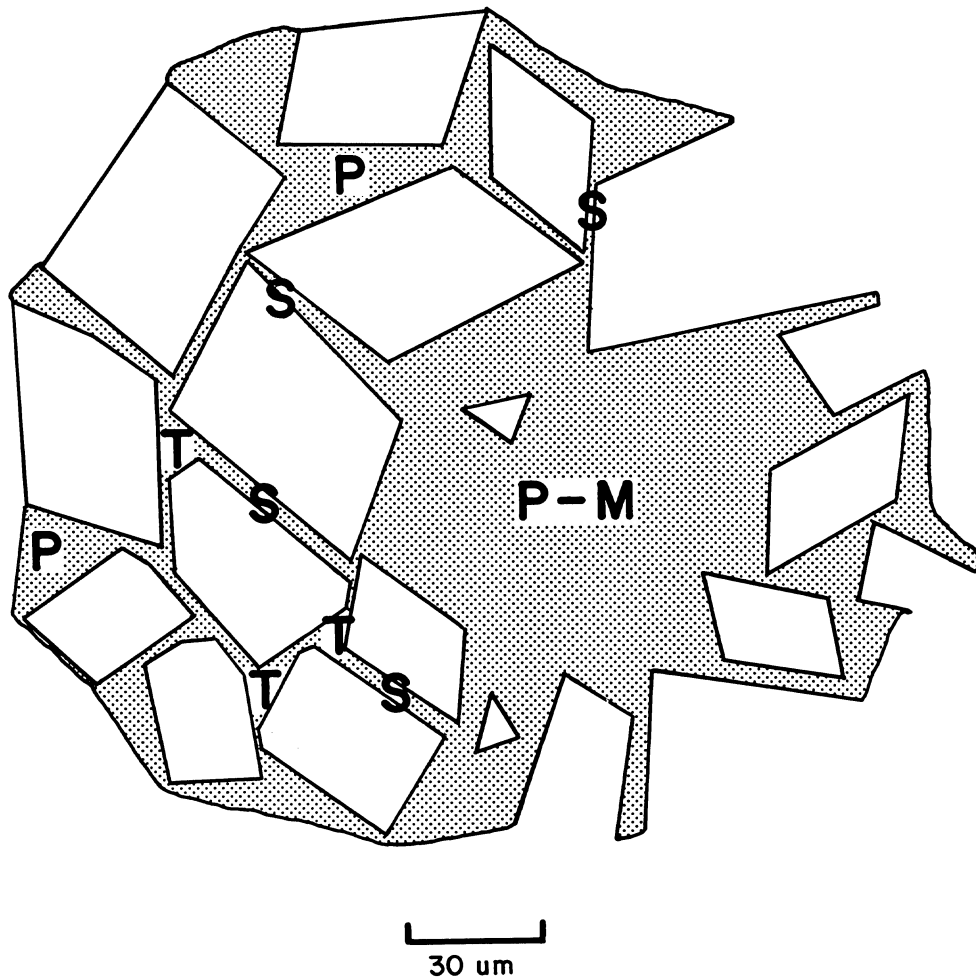


Fig. 53-Generalized illustration (cartoon) of the various pore types and throats in porous portions of the Mission Canyon. Stippled area is pore space surrounding dolomite crystals. A small moldic pore is transitioning, in size, to a large intercrystal polyhedral pore (M-P). Polyhedral pores (P) are the largest intercrystal pores and form a complex polyhedron shape between three or more dolomite crystals, in two-dimensional view. Tetrahedral pores (T) are intermediate sized intercrystal pores, formed where three dolomite crystals begin to impinge together forming a triangular shape in two-dimensional view. Interboundary-sheet pores (S) are the smallest intercrystal pores and form between closely spaced dolomite crystals. Scale is 30 micrometers.

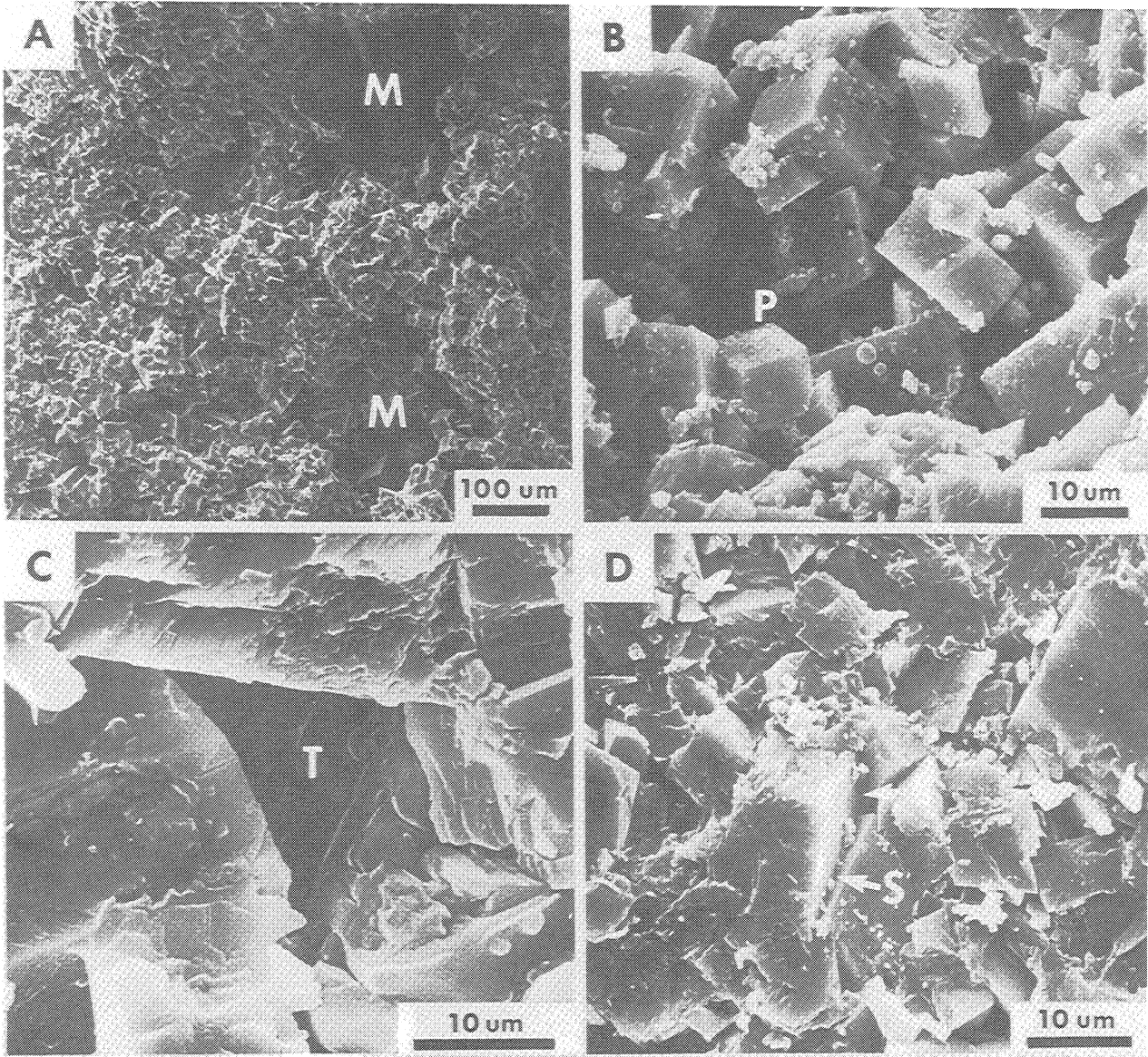


Fig. 54—Scanning electron micrographs of all four pore types in the Mission Canyon Formation at Little Knife Field. A) Two large moldic pores (M) are surrounded by dolomite intercrystal pores. Scale is 100 micrometers, 100X. B) A polyhedral pore (P), illustrating a complex polyhedron shape. Scale is 10 micrometers, 1200X. C) A tetrahedral pore (T) surrounded by three dolomite crystal facies that have partially grown together reducing pore space to a small triangular, tetrahedron shape. Scale is 10 micrometers, 1900X. D) Arrows point to where interboundary-sheet pores (S) are located between dolomite crystals. Scale is 10 micrometers, 1500X.

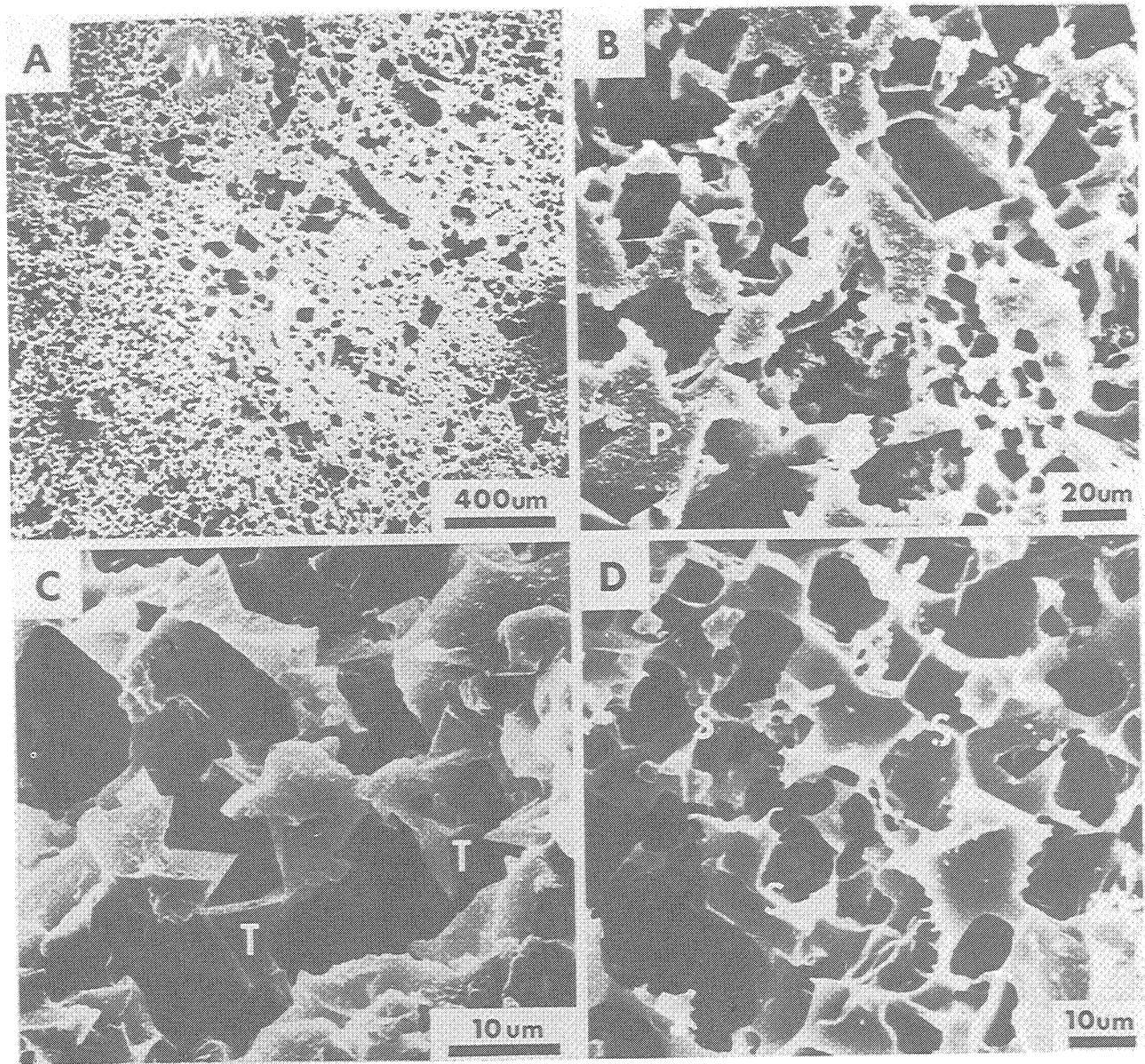


Fig. 55-Scanning electron micrographs of relief pore casts of the various pore types in the Mission Canyon Formation at Little Knife Field. These casts were produced by impregnating the host rock with acid resistant resin and then completely dissolving the sample in diluted HCl acid, which left the pore and throat system standing in relief. A) A moldic pore (M) is surrounded by smaller dolomite intercrystal pores. Note sample was a skeletal wackestone, all large black spaces are where crinoid and brachiopod fragments floated in a dolomitized matrix. Scale is 400 micrometers. B) Polyhedral pores (P) form most of the pore space in this sample. They form many sided complex polyhedrons. Scale is 20 micrometers. C) Injection well no. 1, 9829 feet (2995 m), tetrahedral pores (T) are surrounded by more common polyhedral pores. Scale is 10 micrometers. D) Interboundary-sheet pores form the entire pore system in this particular portion of the sample. Scale is 10 micrometers.

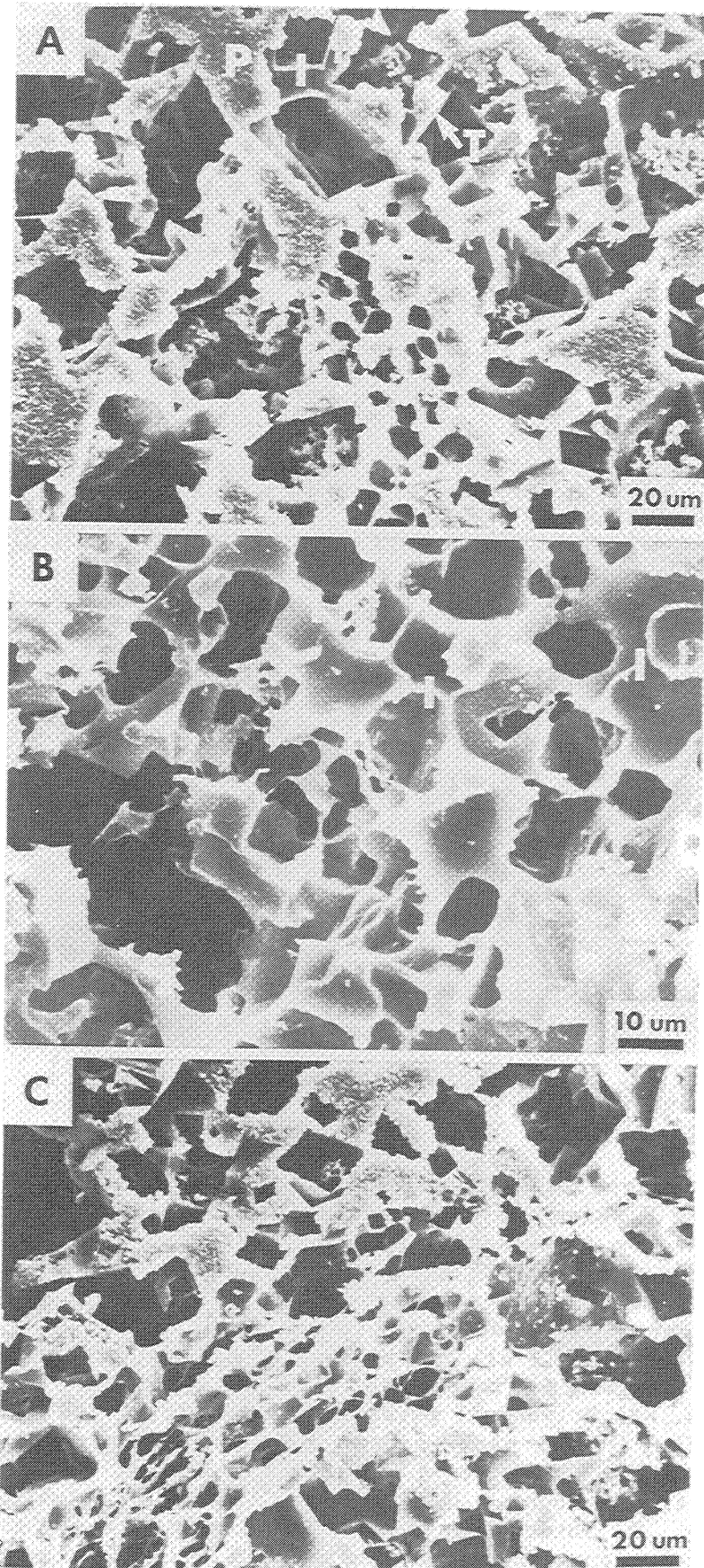


Figure 56

Fig. 56-Scanning electron micrographs (SEM) of relief pore casts of porous bed of Mission Canyon Formation at Little Knife Field. These casts were produced by impregnating the host rock with acid resistant resin and then completely dissolving the sample in diluted HCl acid, which left the pore and throat system standing in relief. The uppermost SEM photo illustrates large polyhedral pores (P) giving way to smaller tetrahedral (T) and interboundary-sheet (I) pores. Both large and narrow throats connect the individual pores. Scale is 20 micrometers. The middle SEM photo demonstrates how the narrow interboundary-sheet pores (I) actively affect permeability although the relative amount of pore space between dolomite crystals is highly reduced. Scale is 10 micrometers. The bottom SEM photo illustrates how dolomite crystal growth can change laterally from crystal spacings associated with large pores and pore throats and grow much closer together to leave only very narrow pore/throats. This relief cast illustrates tortuosity to fluid flow in a dolomitized carbonate reservoir. Scale is 20 micrometers.

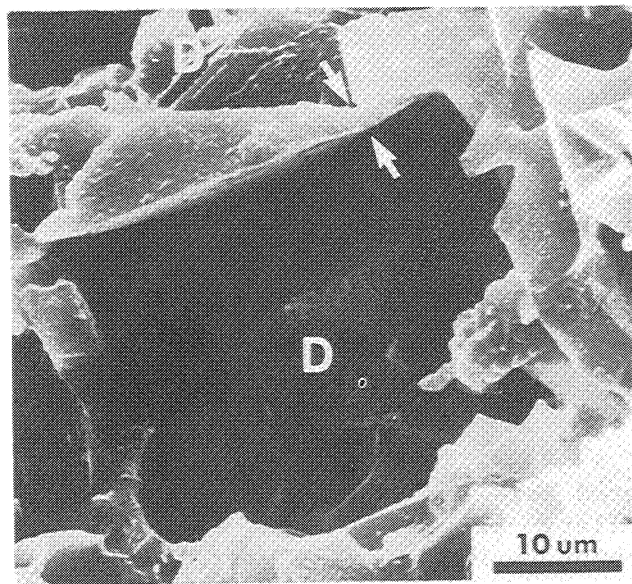


Fig. 57-Injection well no. 1, 9829 feet (2995 m), scanning electron micrograph of a relief pore cast where two dolomite crystals (D) began to grow toward each other at an intermediate angle, reducing pore size, and began to form a triangular shaped tetrahedral pore to the left of the arrows.

ZABOLOTNY INJECTION #1

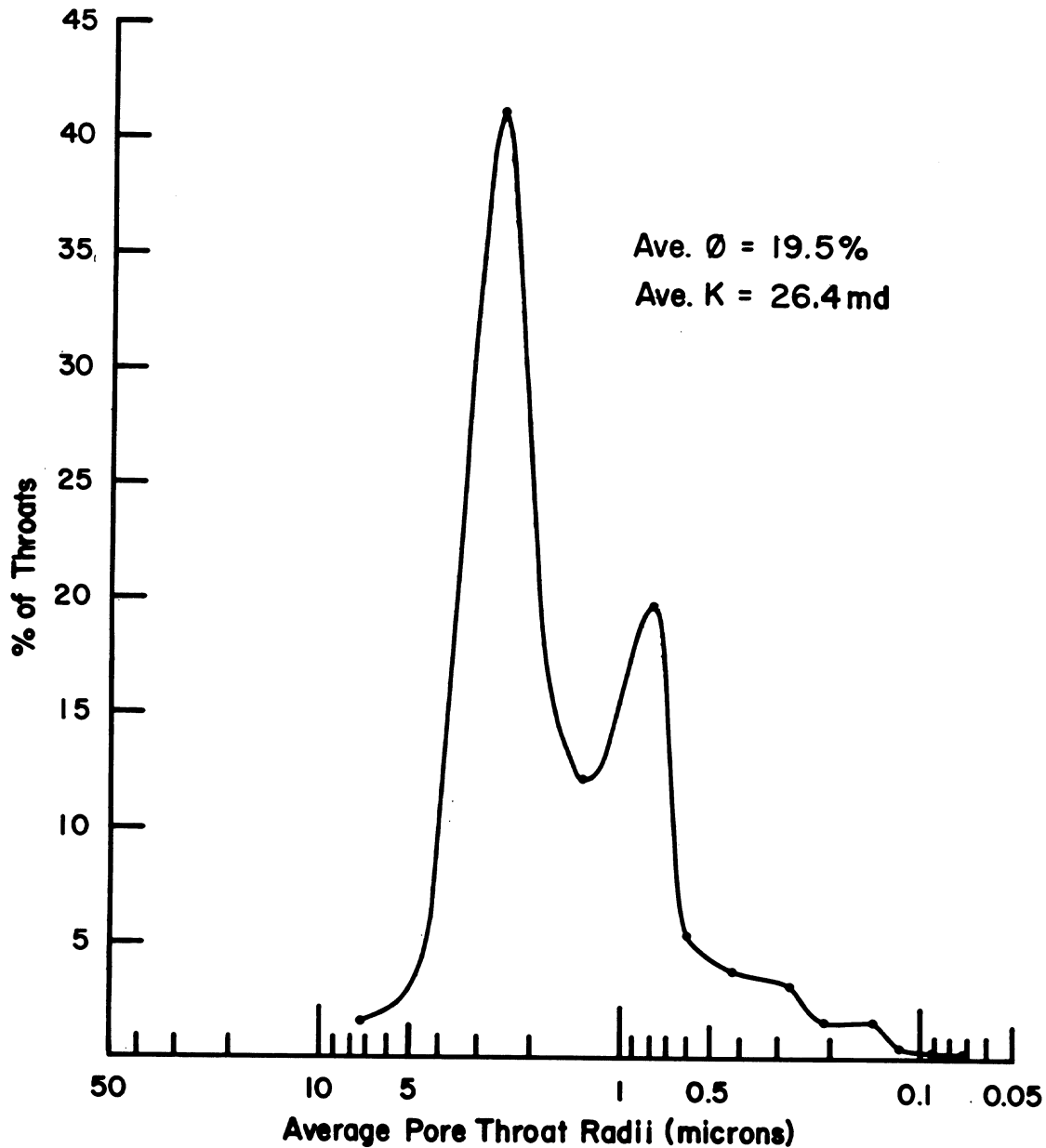


Fig. 58—Average calculated pore throat radii and percent of throats, from mercury injection capillary pressure tests, from core samples across the perforated interval in injection well no. 1. This is a generalized curve produced by averaging several samples together until the average porosity (19.6 percent) and permeability (26.4 md) from whole core analysis matched. In this way average pore throat radii in microns, and their relative abundance, in a percentage, can be plotted. Note two general peaks of abundant throat sizes exist from samples with porosities of 19.5 percent in this well. These calculated throat radii are from the lower half of the CO₂ project interval where highest amounts of porosity and permeability are present (uppermost zone D).

ZABOLOTNY OBSERVATION #1

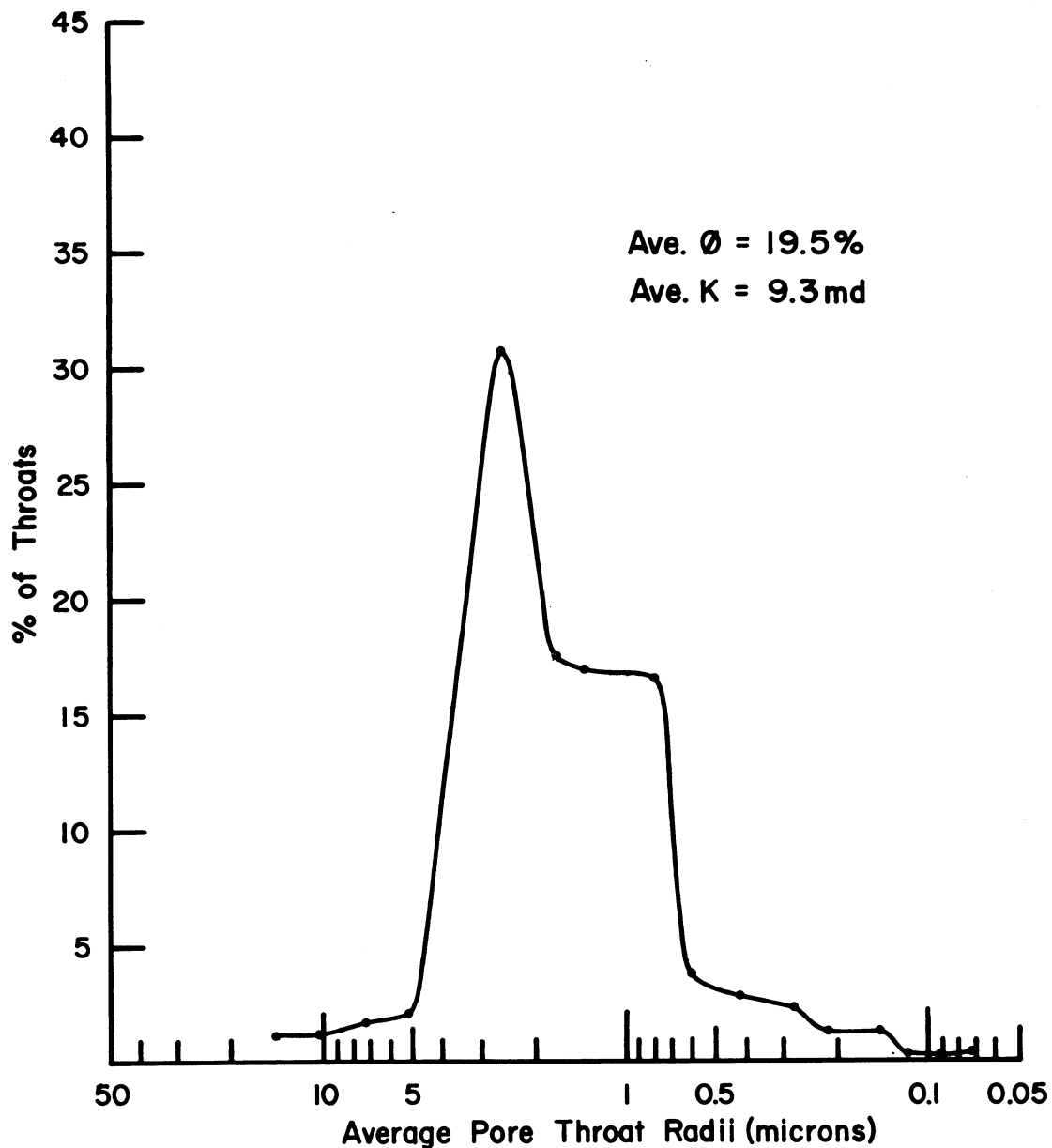


Fig. 59-Average calculated pore throat radii and percent of throats, from mercury injection capillary pressure tests, from core samples across the perforated interval in injection well no. 1. This is a generalized curve produced by averaging several samples together until the average porosity (19.5 percent) and permeability (9.3 md) from whole core analysis matched. In this way average pore throat radii in microns, and their relative abundance, in a percentage, can be plotted. Note how the two general peaks that were present in injection well no. 1 have merged into a single irregular shaped curve with a lower percentage of largest pore throats. These calculated throat radii are from the lower half of the CO₂ project interval where highest amounts of porosity and permeability are present (uppermost zone D).

ZABOLOTNY OBSERVATION #2

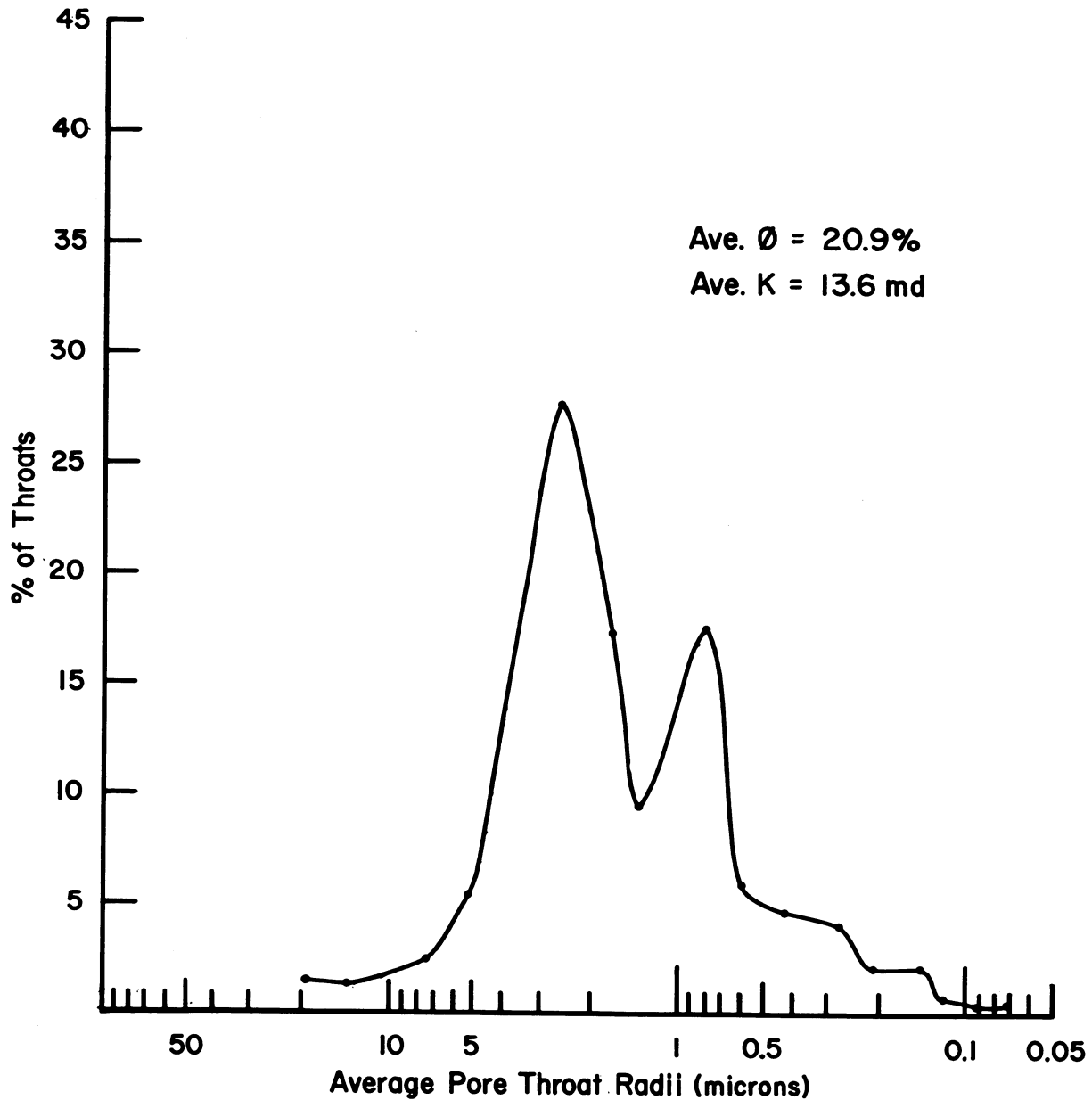


Fig. 60—Average calculated pore throat radii and percent of throats, from mercury injection capillary pressure tests, from core samples across the perforated interval in injection well no. 2. This is a generalized curve produced by averaging several samples together until the average porosity (20.9 percent) and permeability (13.6 md) from whole core analysis matched. In this way average pore throat radii in microns, and their relative abundance, in a percentage, can be plotted. Note that in this well the two general peaks of abundant throat radii sizes are present, as in injection well no. 1, but that the percentage of larger throat radii is lowered. This lowered percentage of throats is slightly compensated for by a slight increase in larger pore throat radii, increasing the width of the curve slightly. These calculated throat radii are from the lower half of the CO₂ minitest project interval where highest amounts of porosity and permeability are present (uppermost zone D).

ZABOLOTNY OBSERVATION #3

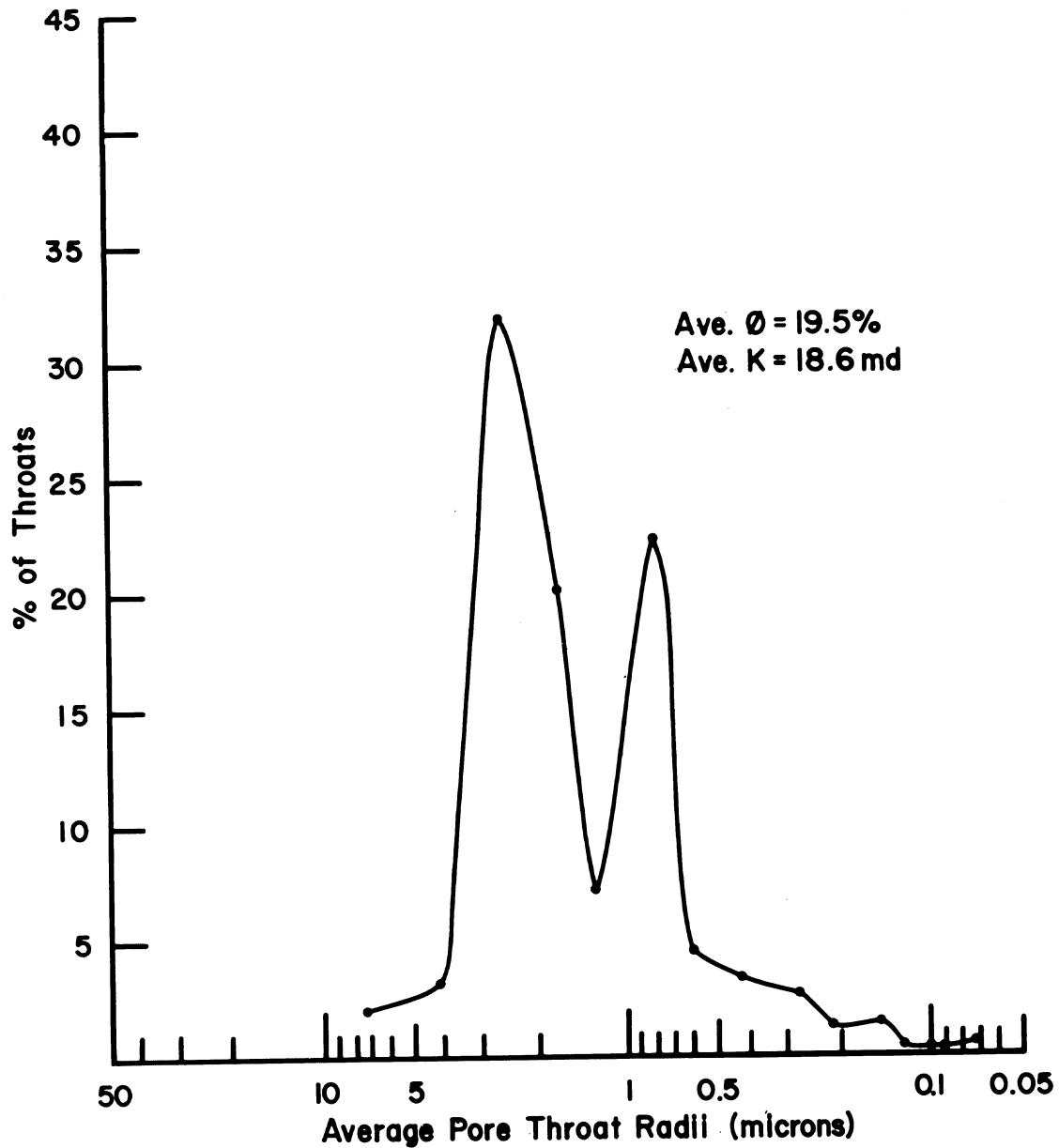


Fig. 61-Average calculated pore throat radii and percent of throats, from mercury injection capillary pressure tests, from core samples across the perforated interval in injection well no. 3. This is a generalized curve produced by averaging several samples together until the average porosity (19.5 percent) and permeability (18.6 md) from whole core analysis matched. Note in this well the two general peaks of abundant throat radii sizes are similar to those in injection well no. 1 and observation well no. 2. These calculated throat radii are from the lower half of the CO₂ minitest project interval where highest amounts of porosity and permeability are present (uppermost zone D).

ZABOLOTNY INJECTION #1

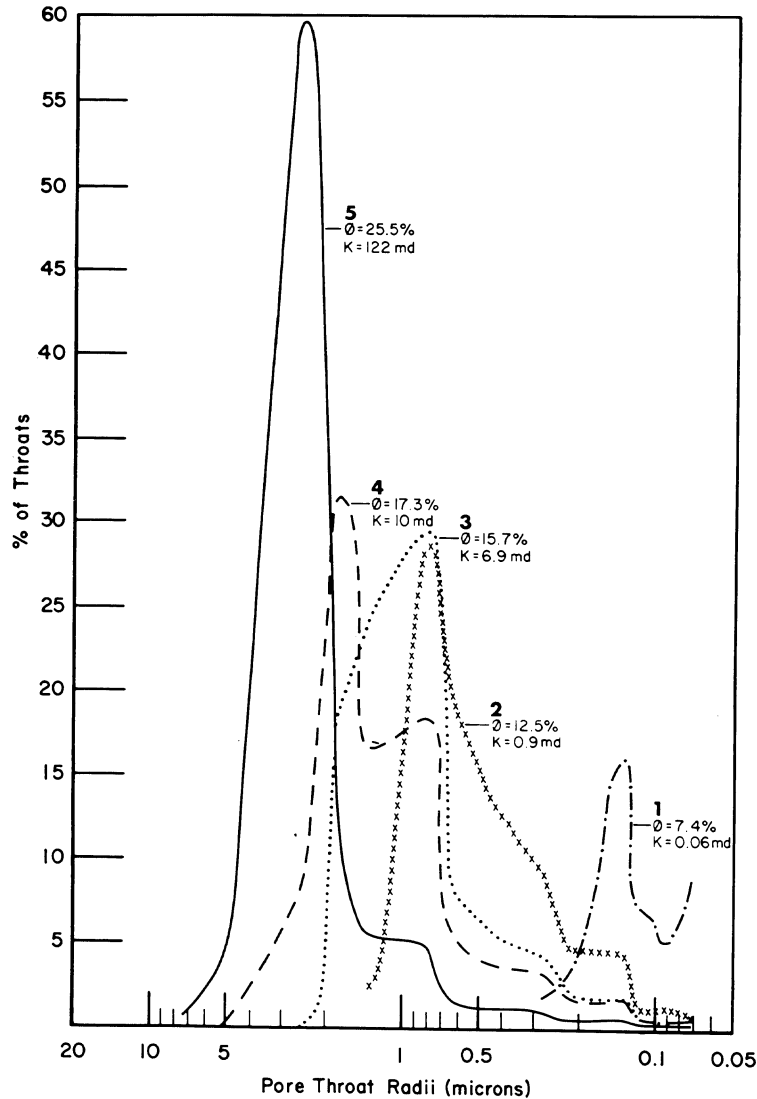


Fig. 62-Representative individual samples of pore throat radii, in micrometers, and percent of throats, calculated from mercury injection capillary pressure curves, in injection well no. 1. Five characteristic pore throat radii vs. porosity and permeability relationships have been isolated into groups. The five pore throat radii curves illustrated are representative of these five groups: 1) The first group is from samples with the smallest pore throat radii measured, averaging 0.21 micrometers, with lowest amount of porosity and permeability, average porosity 6.2 percent and permeability 0.16 md. These samples are from nonhydrocarbon-bearing beds. 2) The second group is from samples with slightly larger pore throat radii, averaging 0.6 micrometers, with lowest amounts of producible porosity, average porosity 10.7 percent and average permeability 0.8 md. 3) The third group is from samples with more abundant pore throat radii, averaging 0.8 micrometers, with fair amounts of porosity and permeability, average porosity 13.6 percent and average permeability 3.5 md. 4) The fourth group is from samples which contain two distinct sizes of average pore throat radii, at 0.8 and 1.8-2.5 micrometers respectively, and good amounts of porosity and permeability, average porosity 19.6 percent and average permeability 22.3 md. 5) The fifth and final group is from samples with abundant, large pore throat radii, at 2.5 micrometers, and highest amount of porosity and permeability, average porosity 24.1 percent and average permeability 85.4 md.

ZABOLOTNY OBSERVATION #1

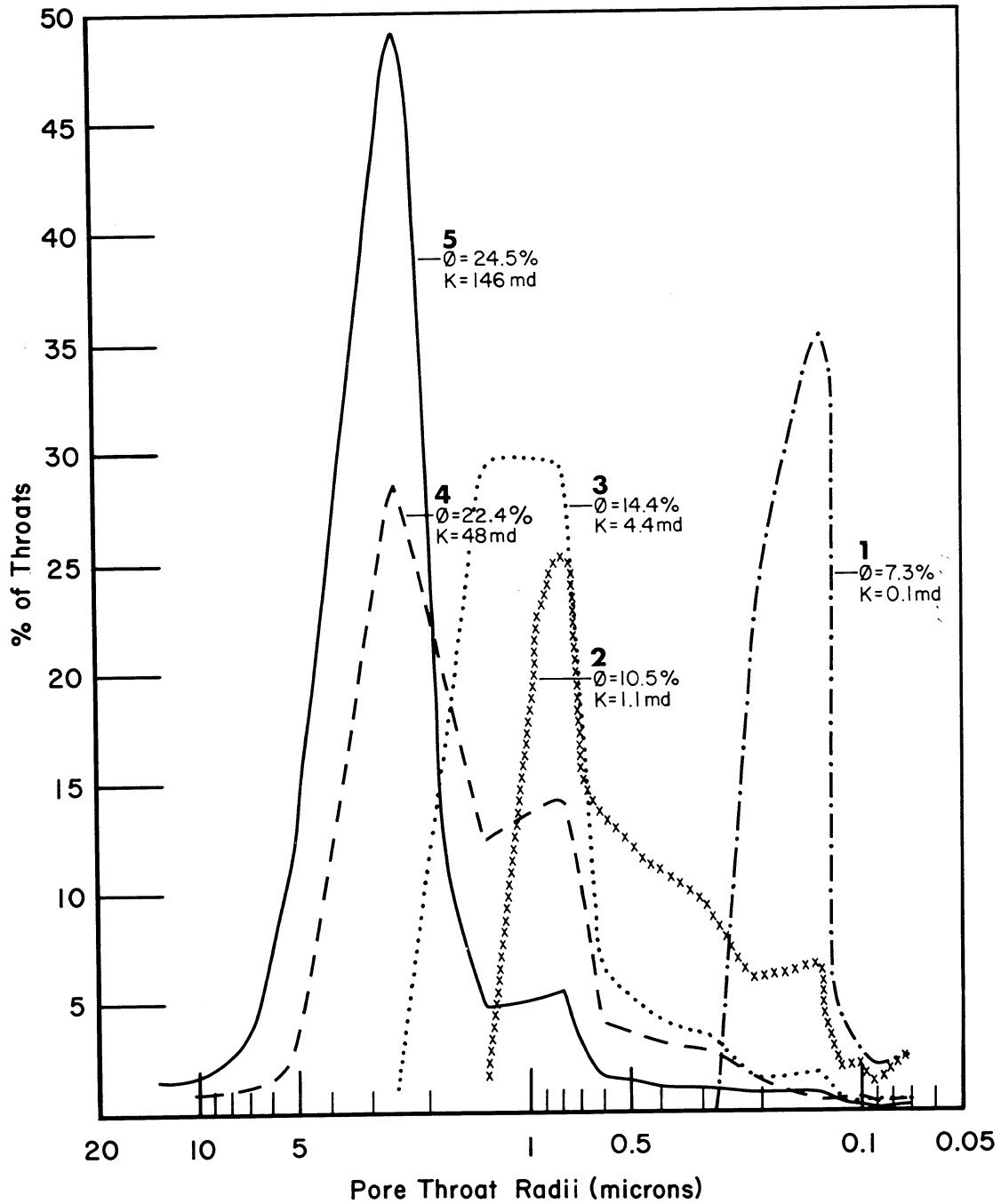


Fig. 63-Representative individual samples of pore throat radii, in micrometers, and percent of throats, calculated from mercury injection capillary pressure curves, in observation well no. 1. Five characteristic pore throat radii vs. porosity and permeability relationships as described in Figure 62, have been isolated into groups.

ZABOLOTNY OBSERVATION #2

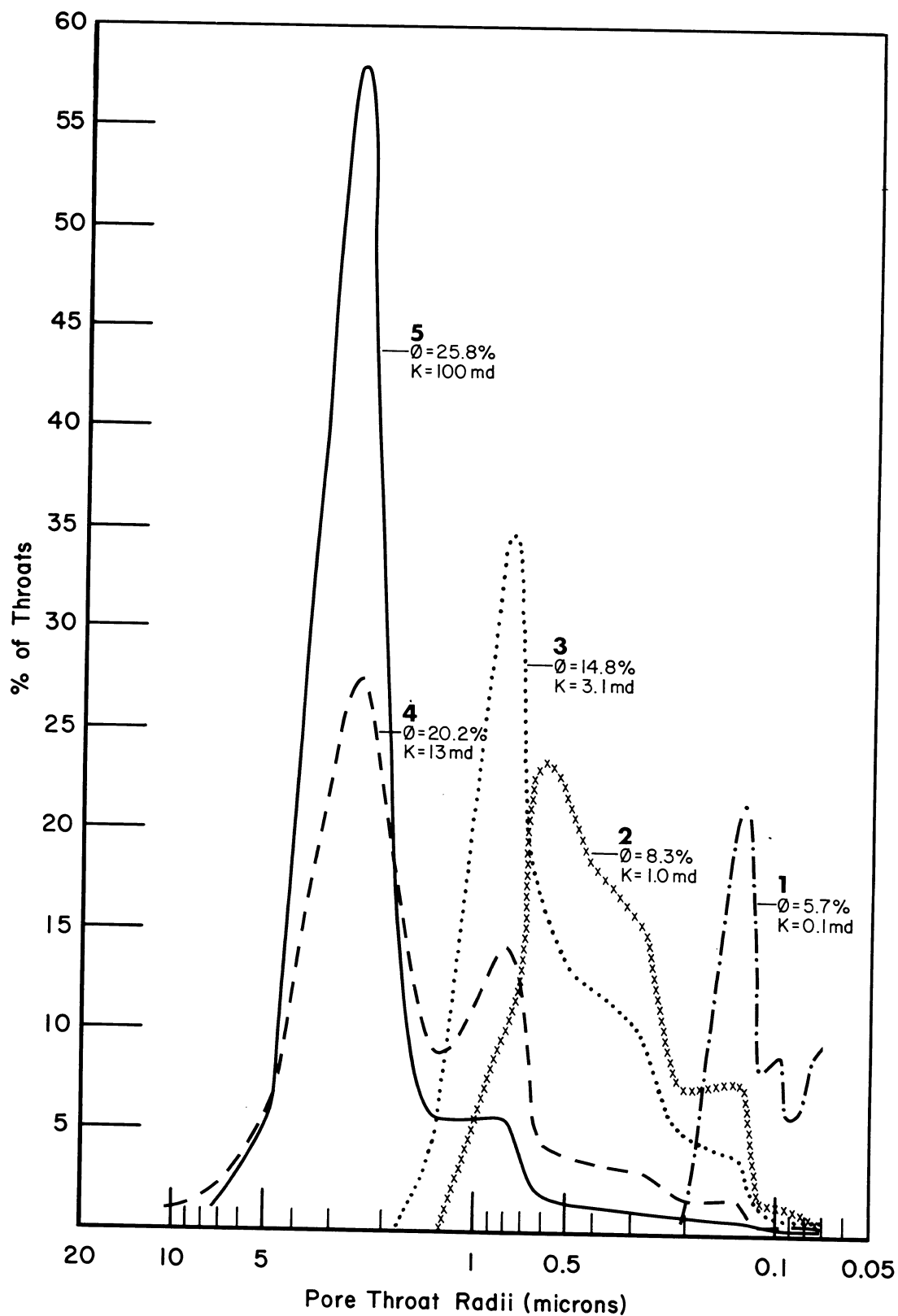


Fig. 64—Representative individual samples of pore throat radii, in micrometers, and percent of throats, calculated from mercury injection capillary pressure curves, in observation well no. 2. Again, five characteristic pore throat radii vs. porosity and permeability relationships, as described in Figure 62, have been isolated into groups.

ZABOLOTNY OBSERVATION # 3

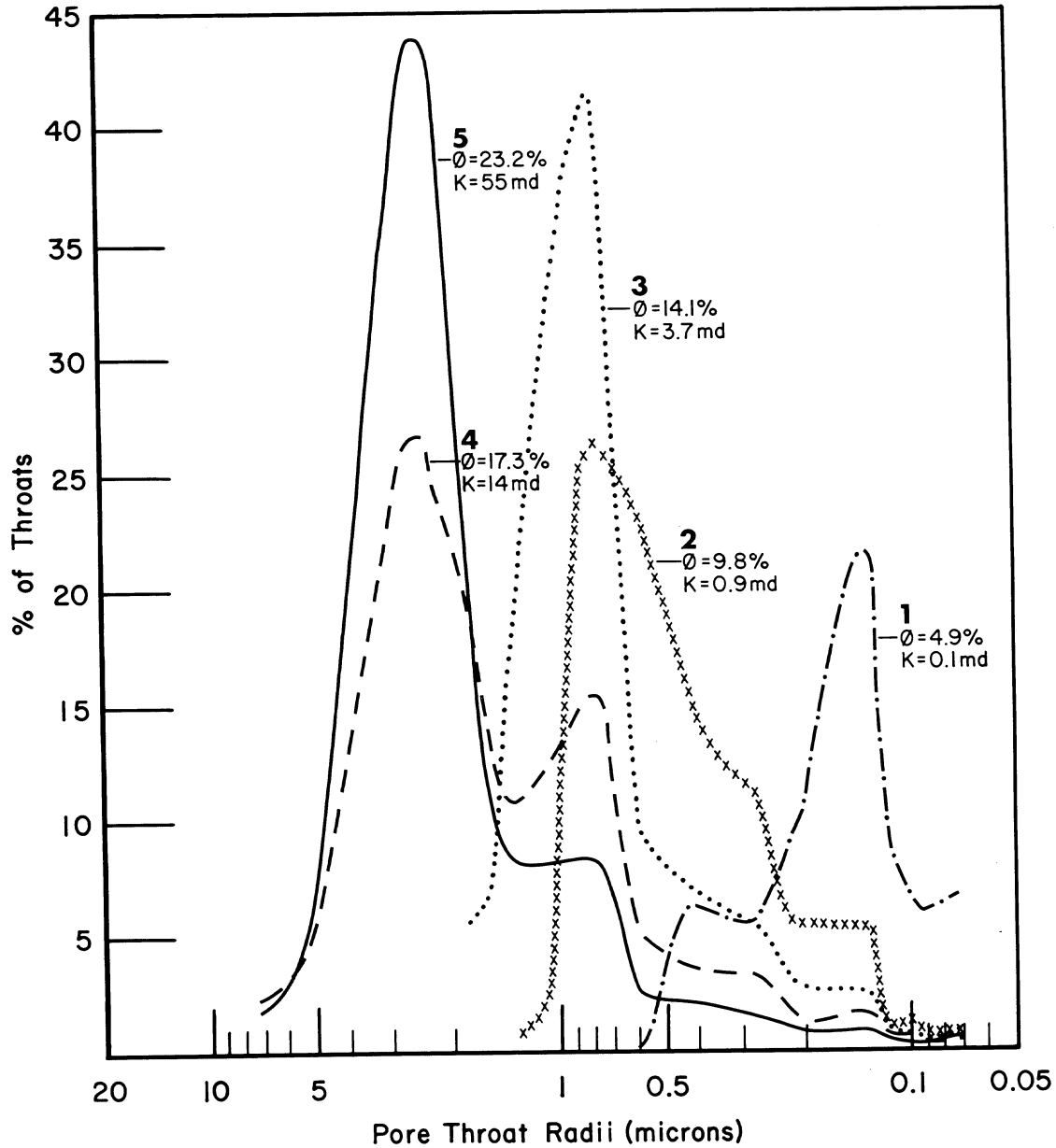


Fig. 65-Representative individual samples of pore throat radii, in micrometers, and percent of throats, calculated from mercury injection capillary pressure curves, in observation well no. 3. The same five characteristic pore throat radii vs. porosity and permeability relationships, described in Figure 62, have been isolated into groups, as in the preceding wells.

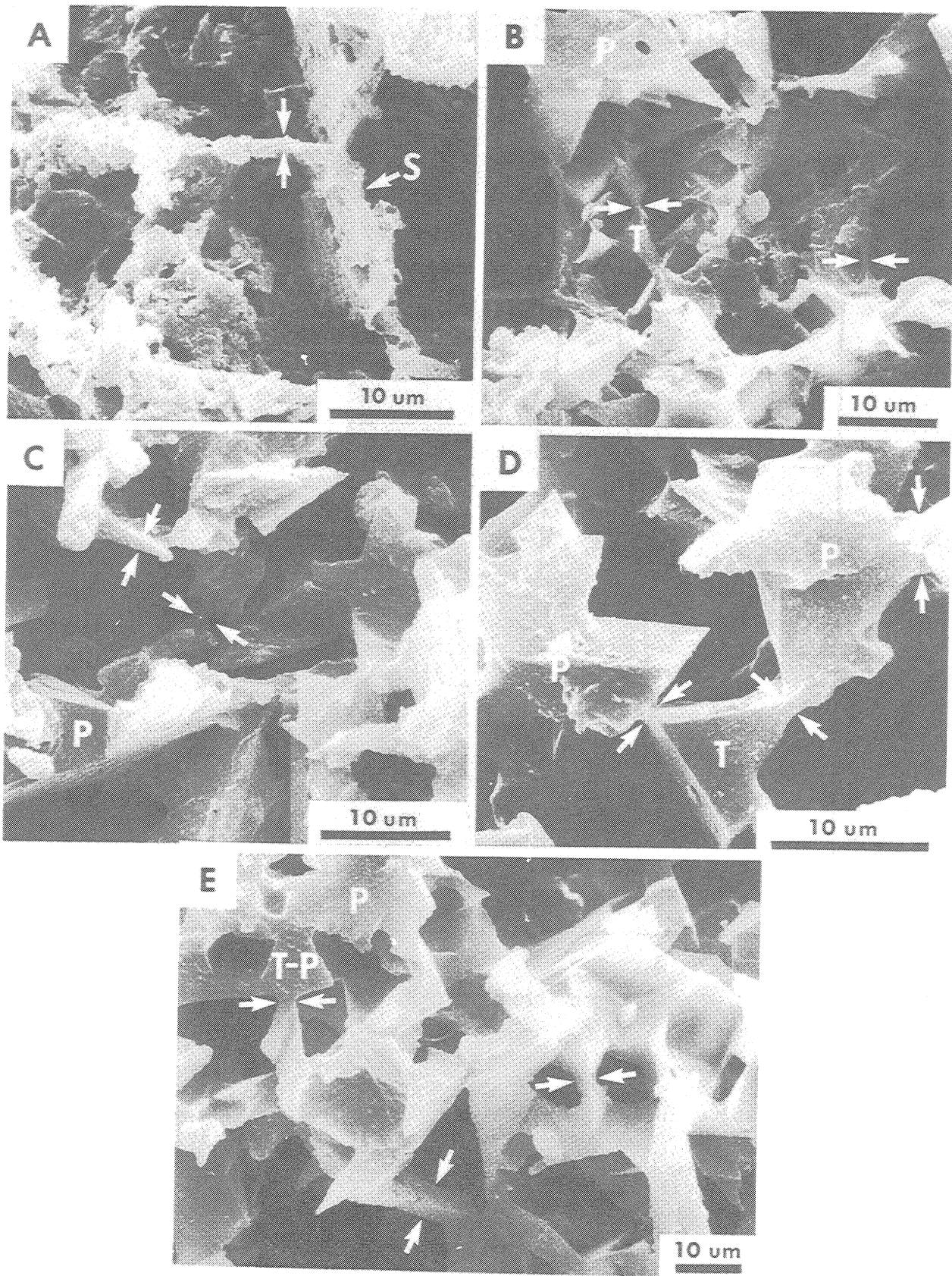


Figure 66

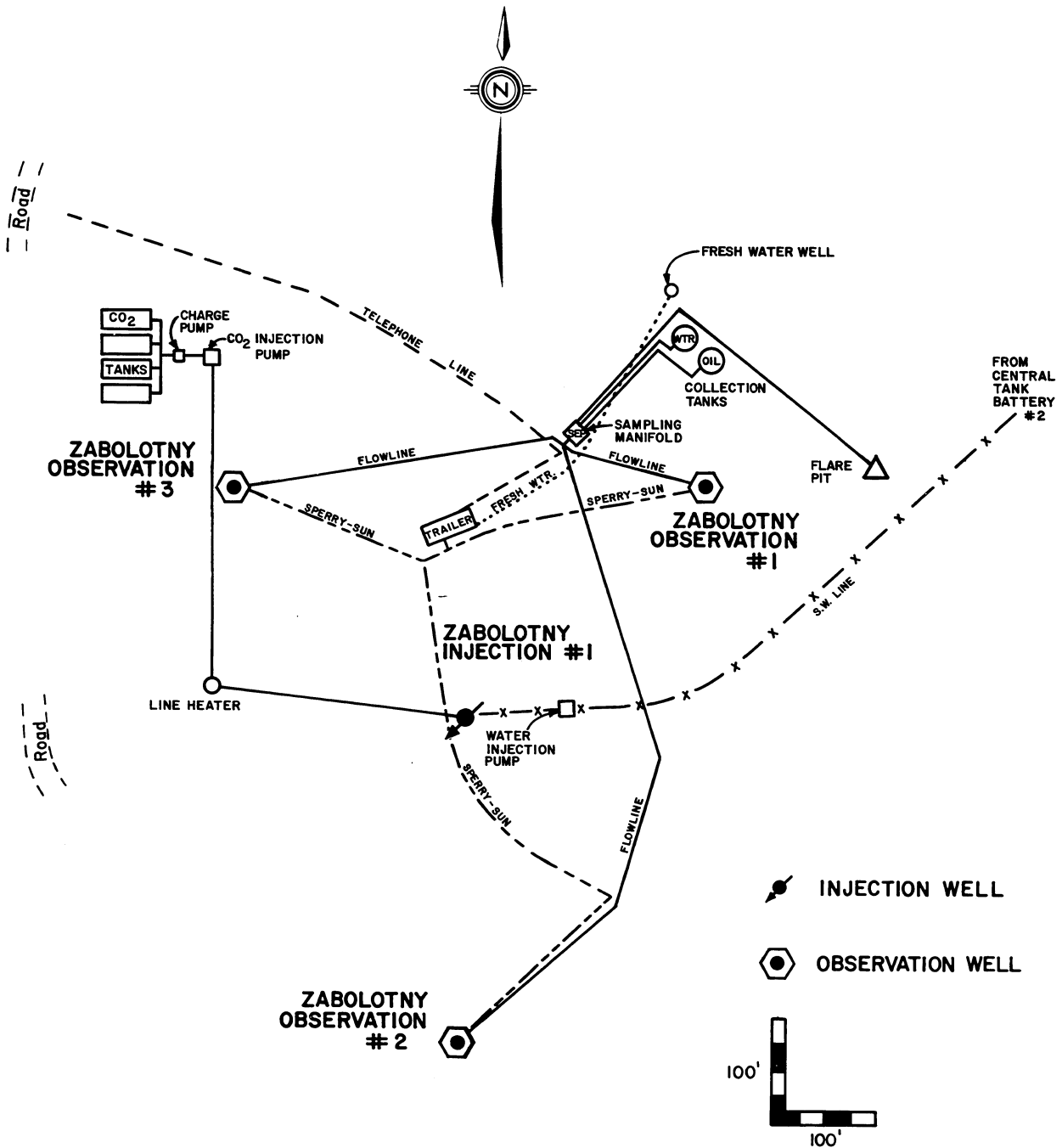


Fig. 68—Layout of surface equipment of the Little Knife CO₂ minitest site. Modified after Nettle, Lindsay and Desch⁵⁰.

CARBON DIOXIDE INJECTION SYSTEM

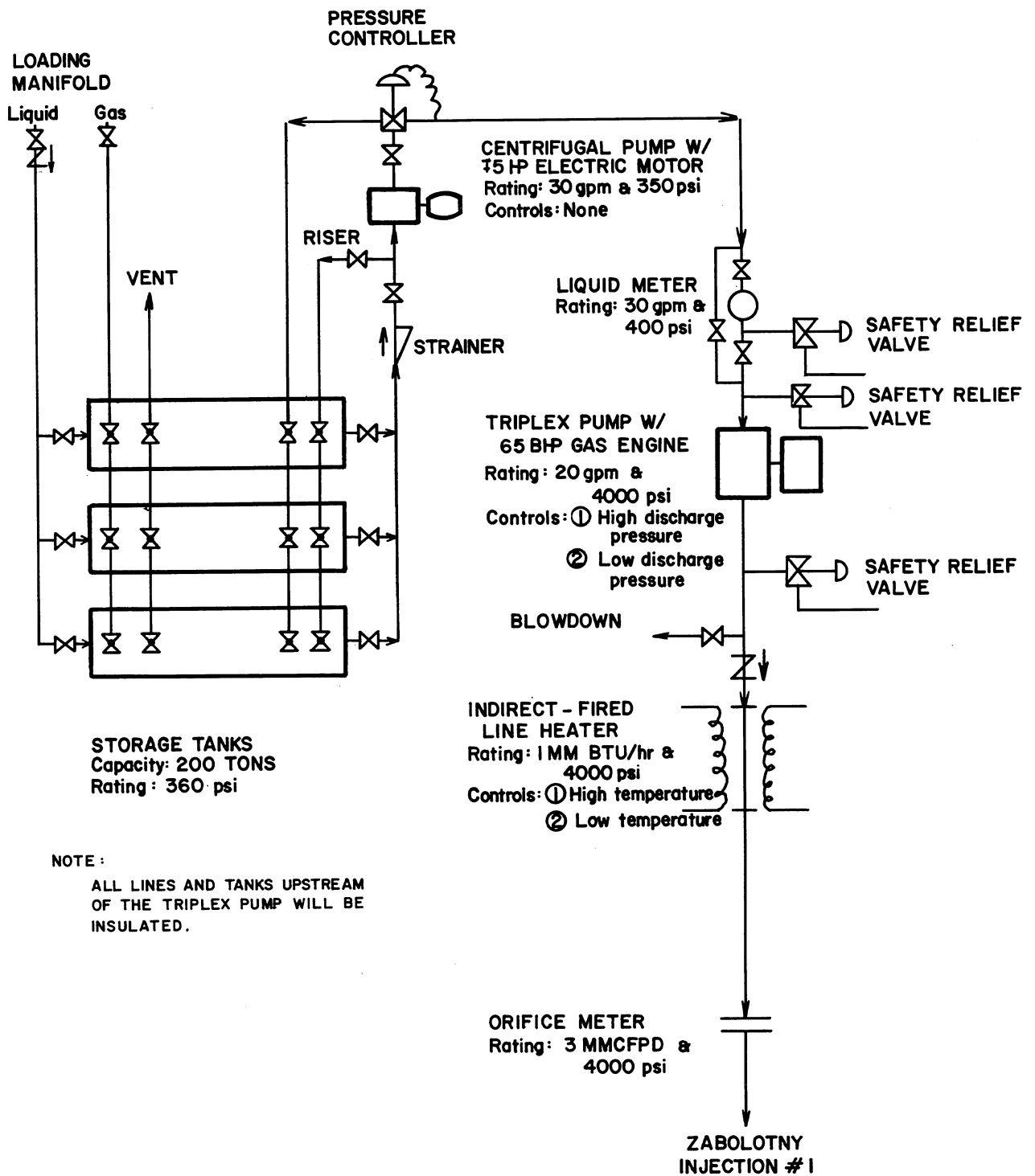


Fig. 69-Carbon dioxide injection system for the Little Knife CO₂ minitest. It consists of storage, metering, pumping and vaporizing sections.

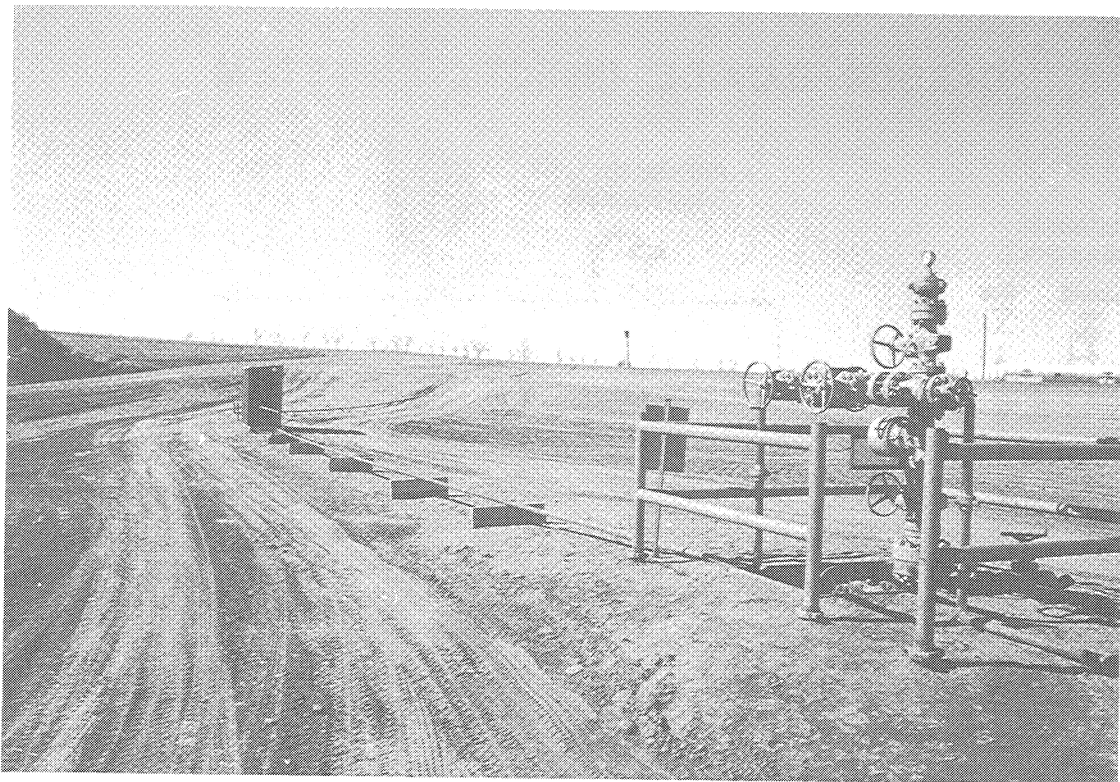


Fig. 70-Injection well no. 1 with CO₂ injection line, gas meter shed, line heater and CO₂ storage tanks in the background.



Fig. 71-Fifty (50) ton capacity liquid CO₂ truck used to haul and store CO₂.

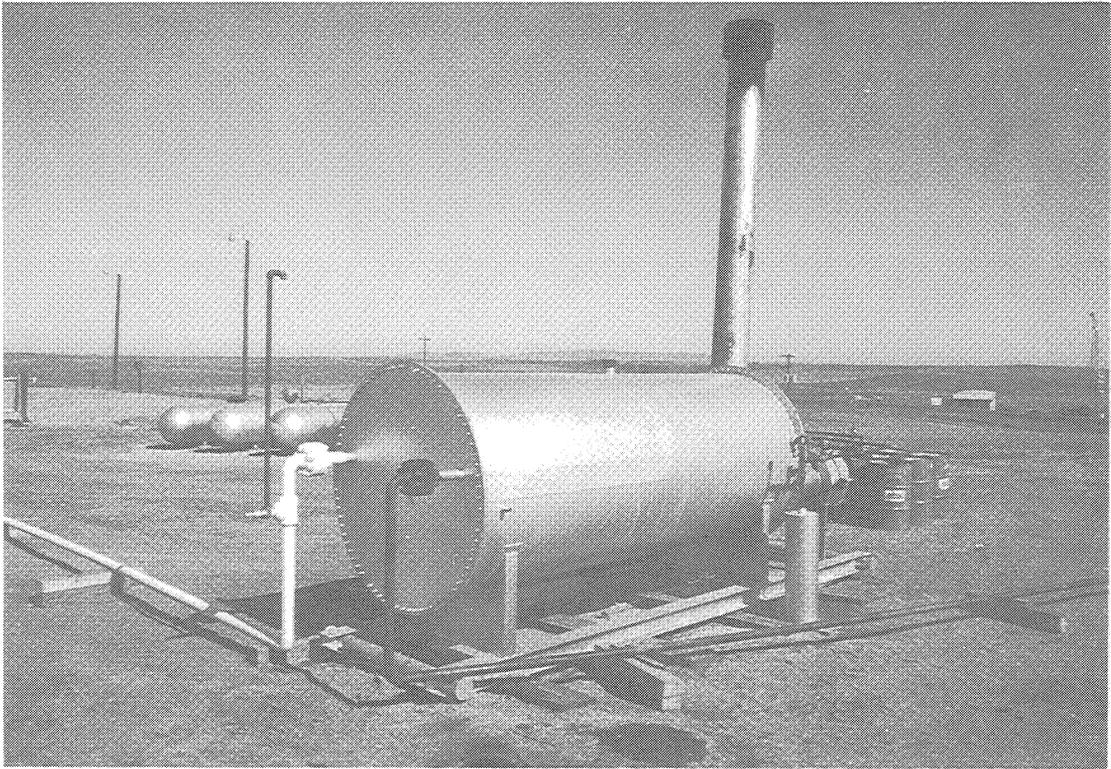


Fig. 72-Glycol indirect line heater which is downstream of the CO₂ injection pump. Propane fuel tanks are in the background.

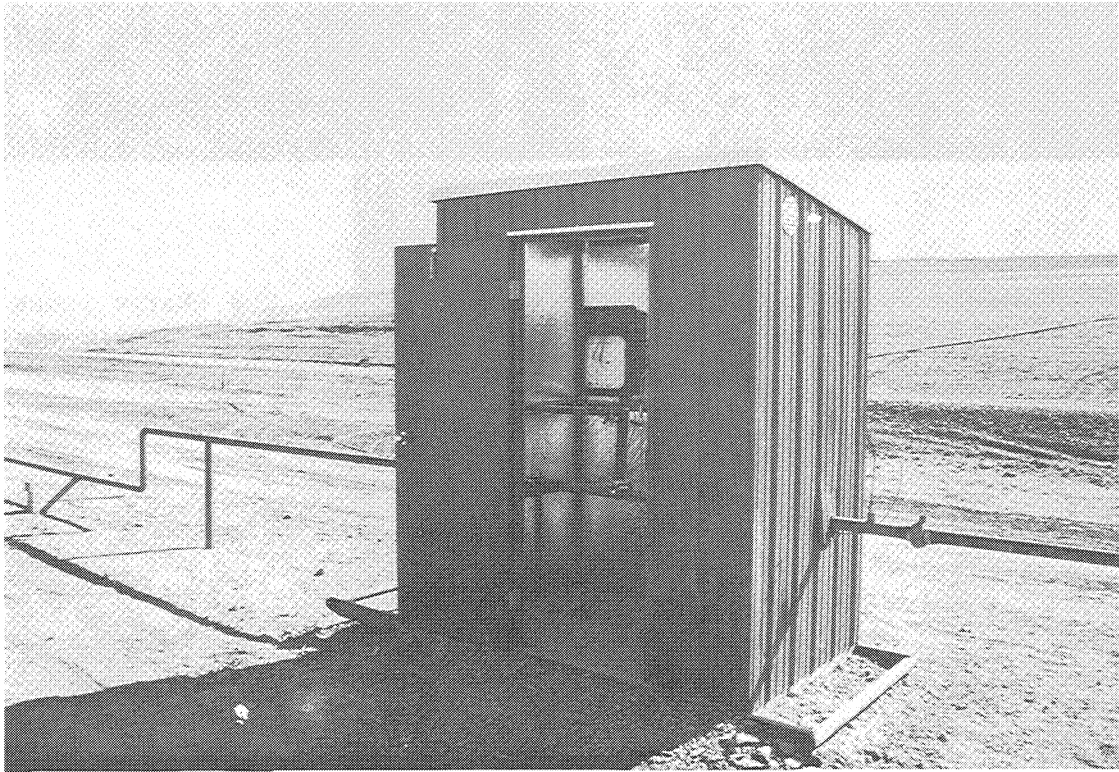


Fig. 73-CO₂ gas meter shed downstream of the line heater at Little Knife CO₂ minitest site.



Fig. 74-Manifold system at back of CO₂ storage tanks. The charge pumps for the CO₂ injection pump are located on the ground, in the middle of the four tanks.

WATER INJECTION SYSTEM

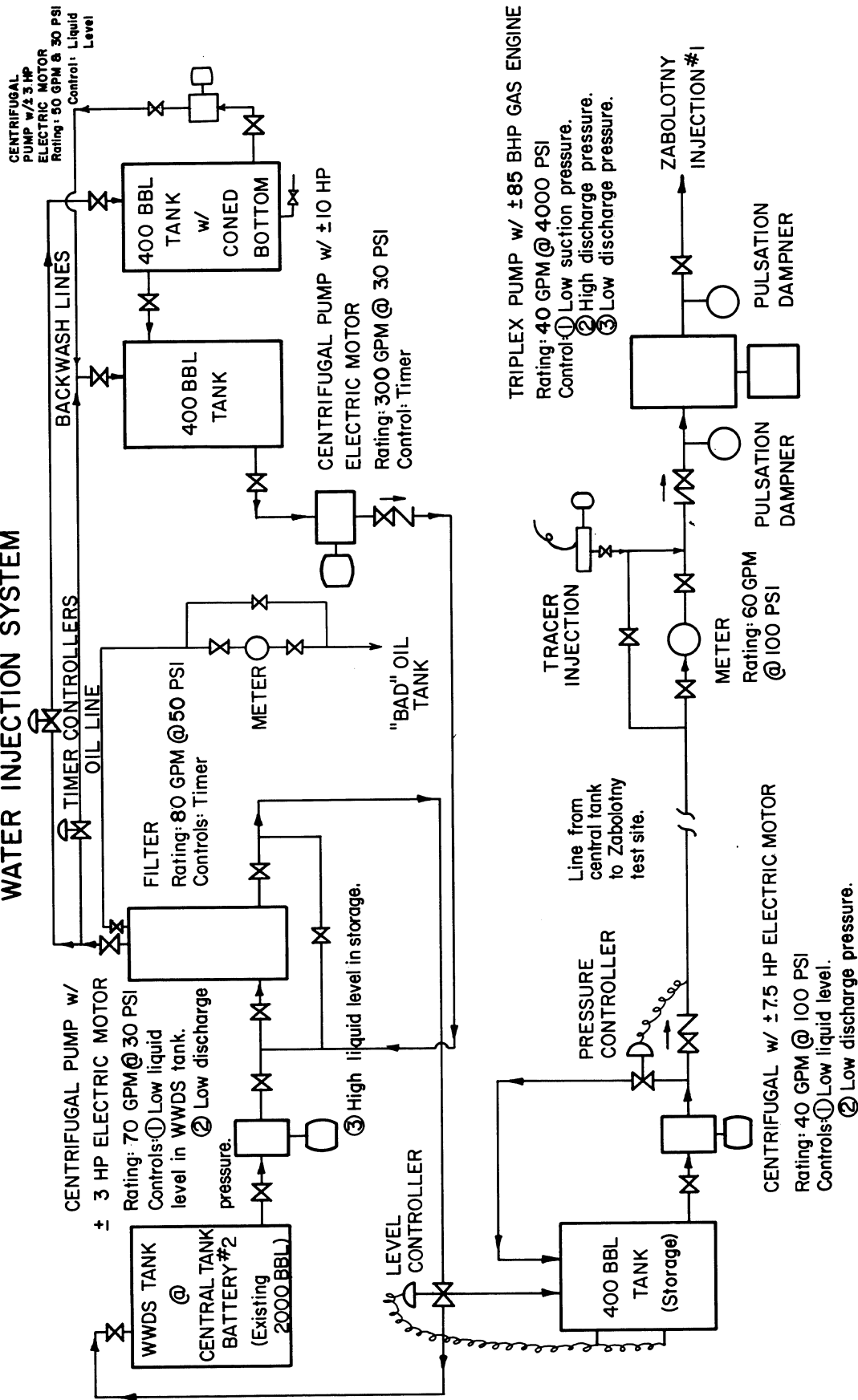


Fig. 75-Water injection system for the Little Knife CO₂ minitest. It consisted of two segments. One segment is the filtering system. The second segment is the injection pump.

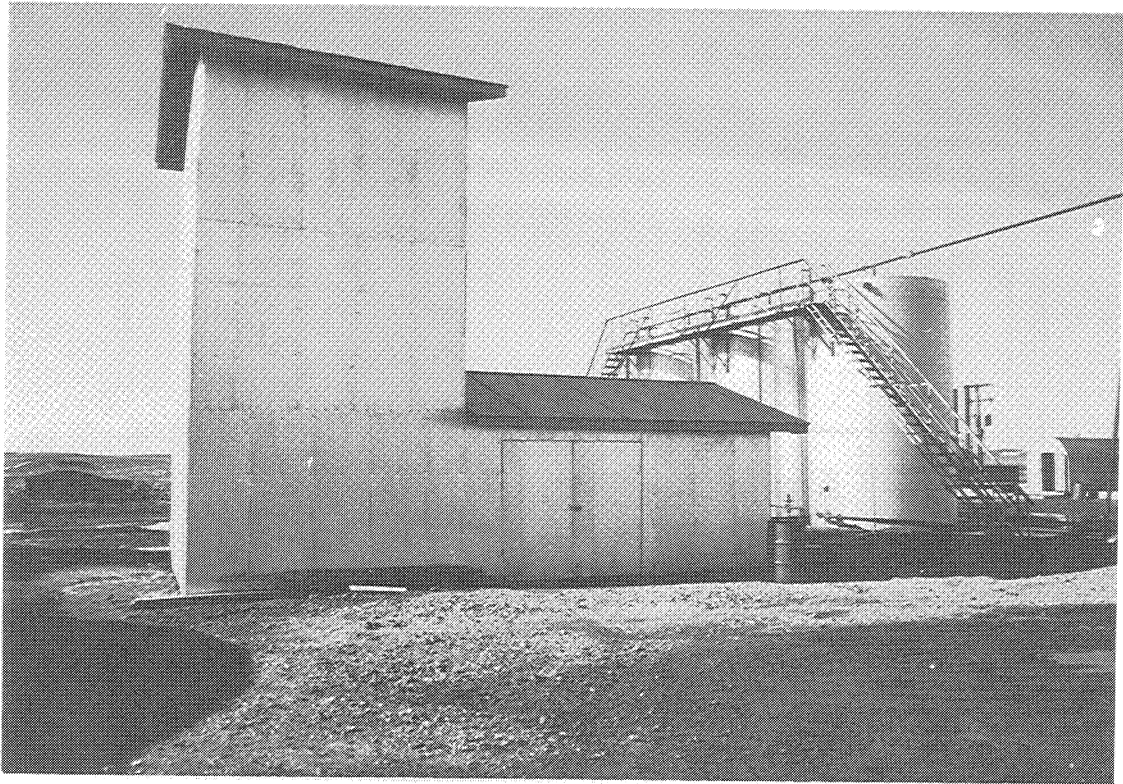


Fig. 76-Salt water filter building with filtered salt water, flush and sludge tanks.

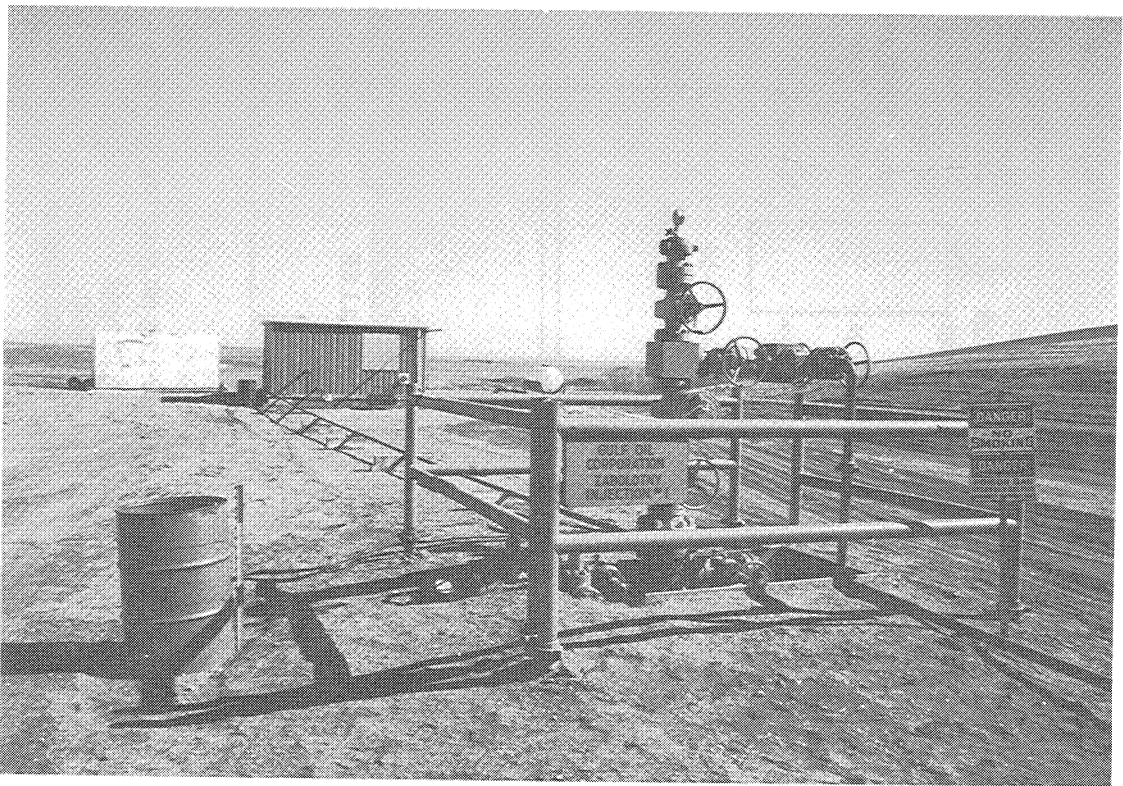


Fig. 77-Injection well no. 1 with salt water injection line, salt water injection pump building and alcohol tracer storage tank in the background.

FLUID SAMPLING SYSTEM

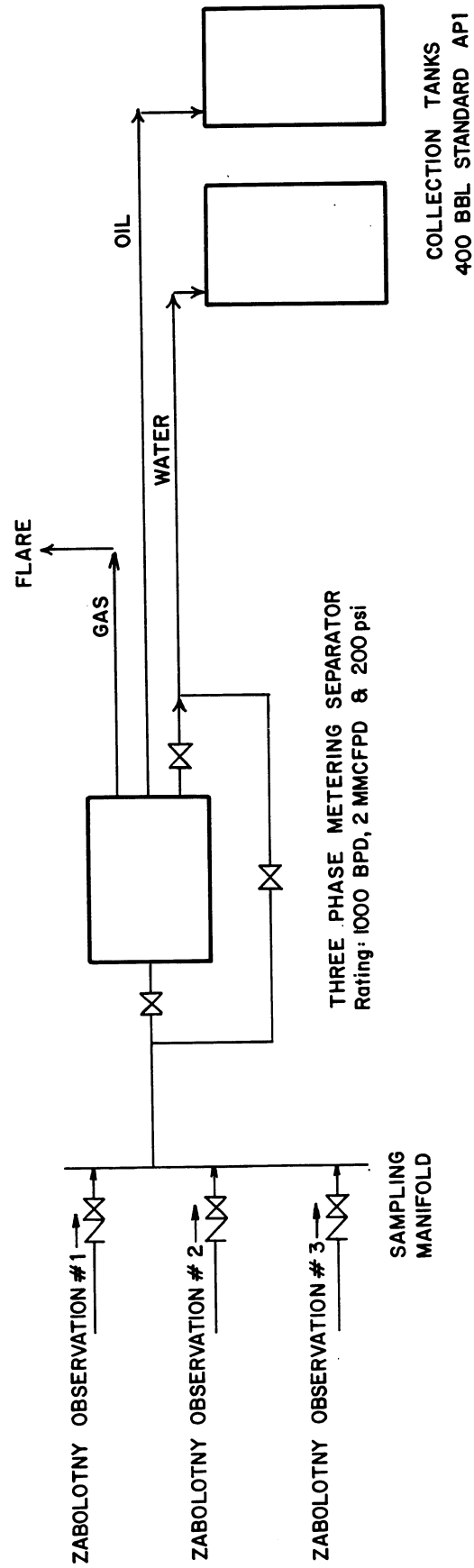


Fig. 78-Fluid sampling system for the Little Knife CO₂ minitest. It consisted of a three-phase metering separator. It was equipped with standard instrumentation, along with level controls for both oil and water and meters for gas, oil and water.

LITTLE KNIFE CO₂ MINITEST

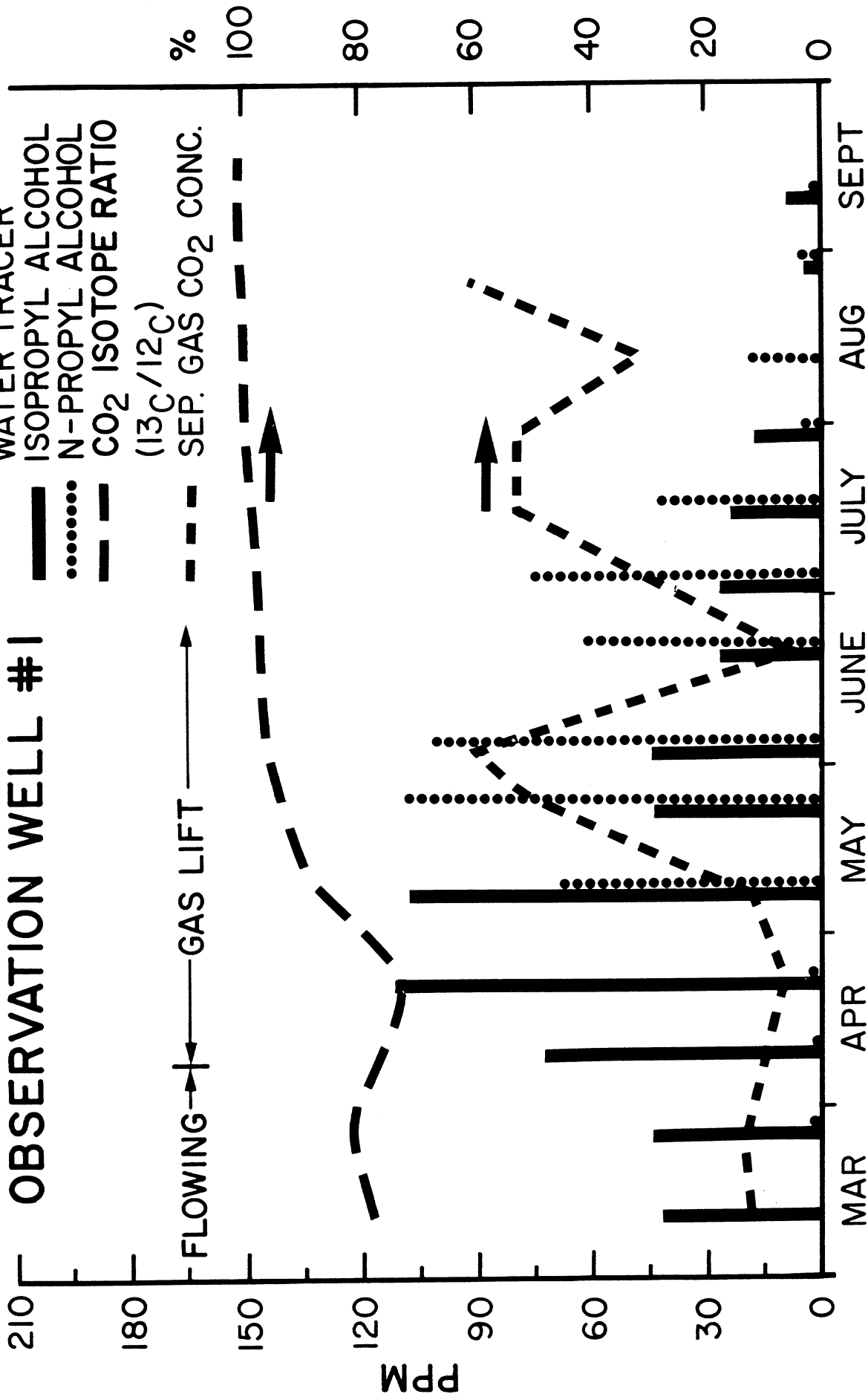


Fig. 80-Isopropyl and n-propyl alcohol tracer, CO₂ ratio and separator gas CO₂ concentration fluid analysis results from observation well no. 1.

LITTLE KNIFE CO₂ MINITEST

OBSERVATION WELL #2

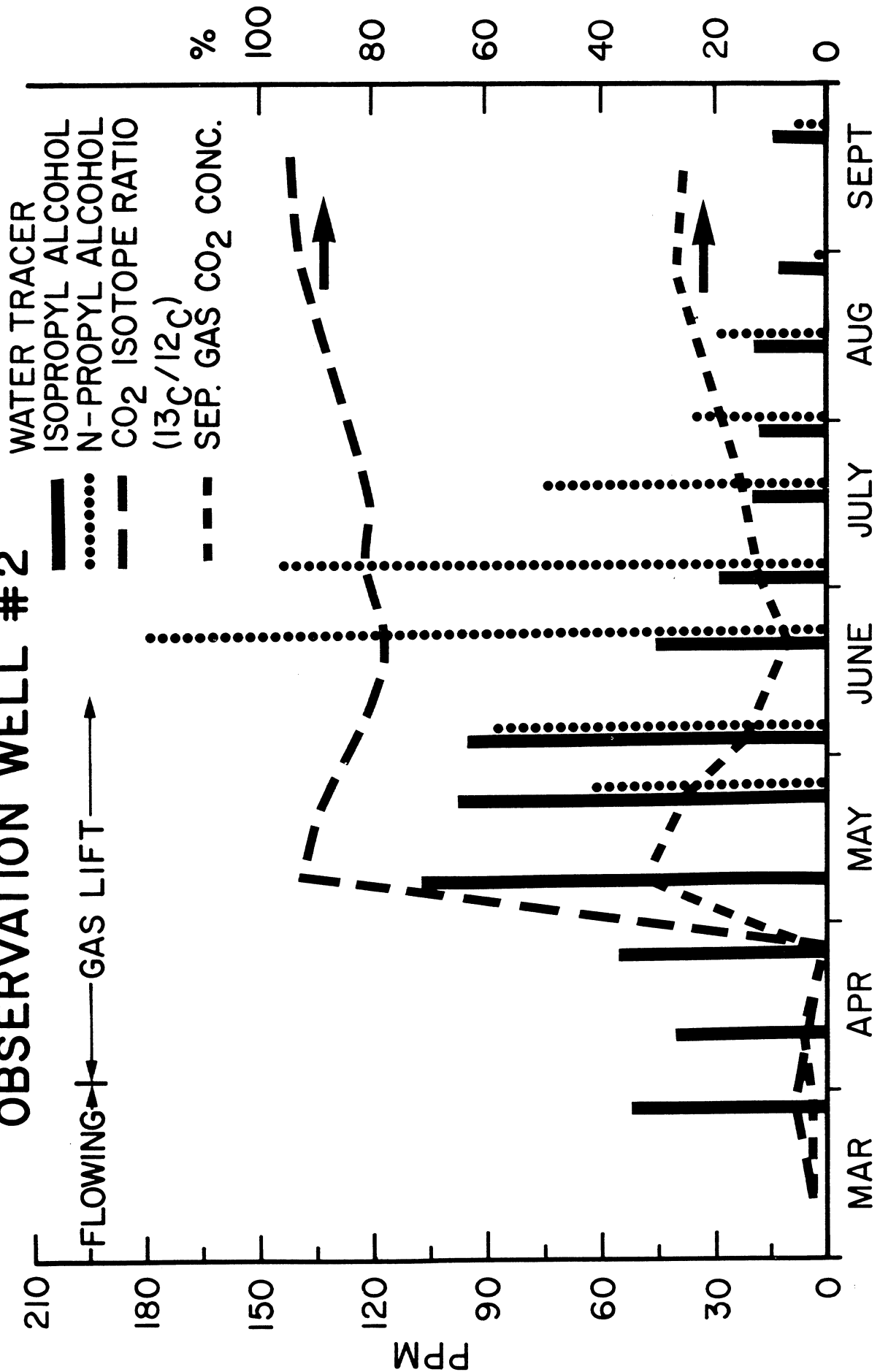


Fig. 81-Isopropyl and n-propyl alcohol tracer, CO₂ ratio and separator gas CO₂ concentration fluid analysis results from observation well no. 2.

LITTLE KNIFE CO₂ MINITEST

OBSERVATION WELL #3

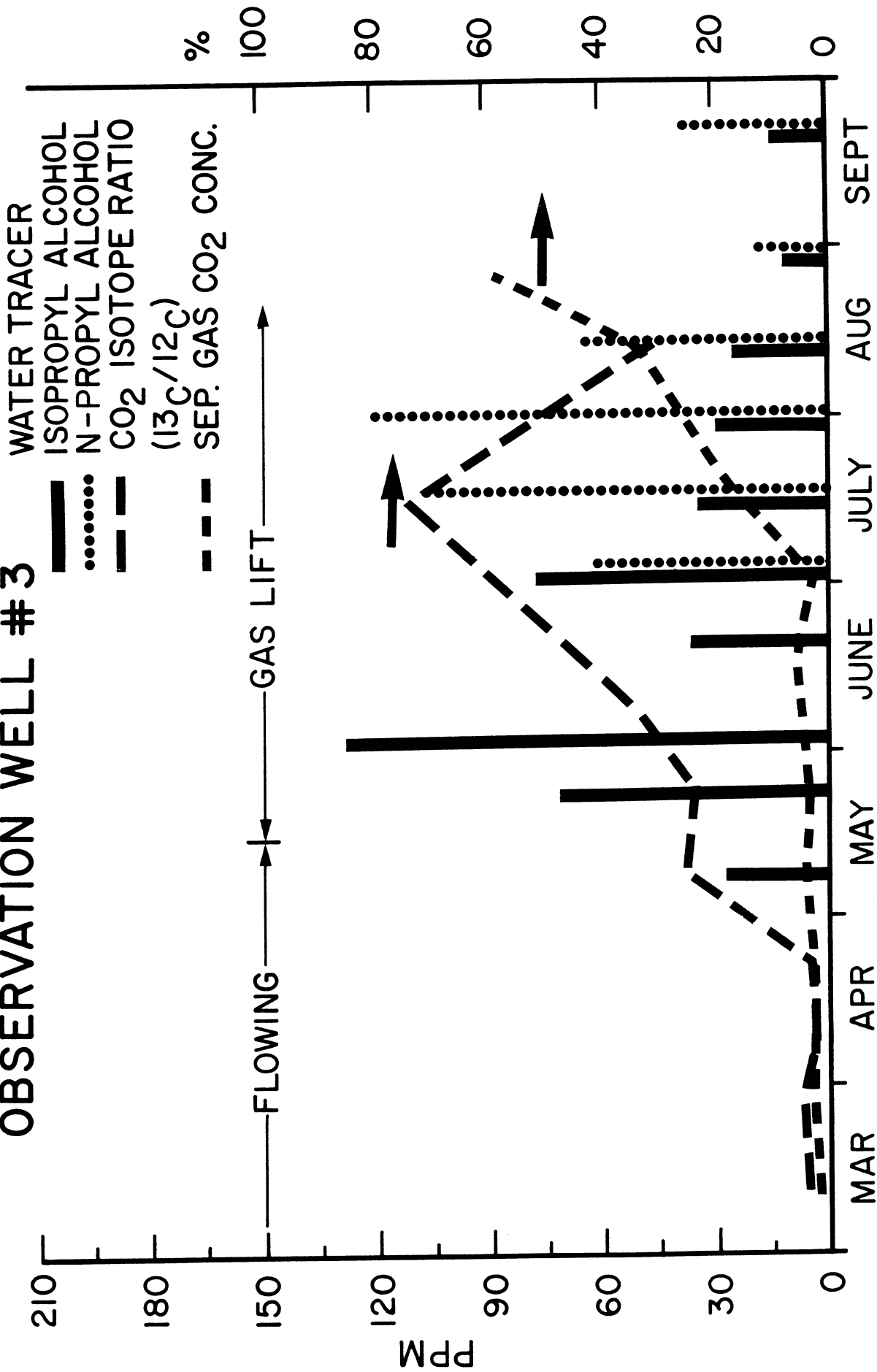


Fig. 82-Isopropyl and n-propyl alcohol tracer, CO₂ ratio and separator gas CO₂ concentration fluid analysis results from observation well no. 3.

**WATER AND OIL SATURATION CORE ANALYSIS
LITTLE KNIFE CO₂ MINITEST**

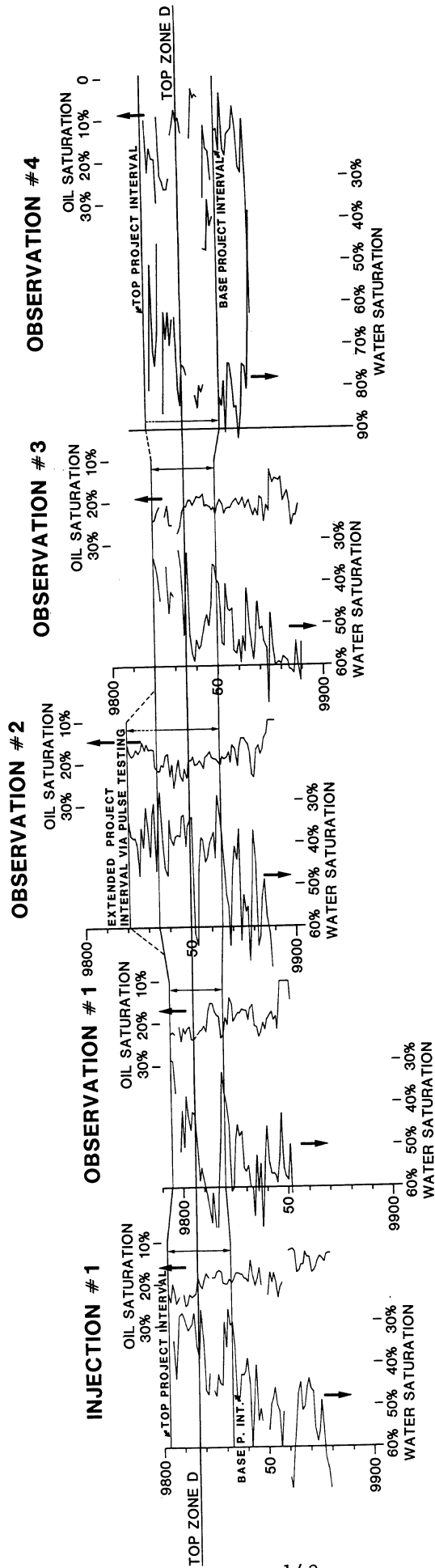


Fig. 84-Oil and water saturations from core analysis in injection well no. 1 and observation wells no. 1, 2, 3 and 4.

- LITTLE KNIFE CO₂ PROJECT --
 COMPARISON OF GULFLOG AND PRESSURE CORE
 OIL SATURATIONS IN ZABOLOTNY OBSERVATION #4
 (CORE DEPTHS ADJUSTED TO LOG DEPTHS) (See Figure 83)

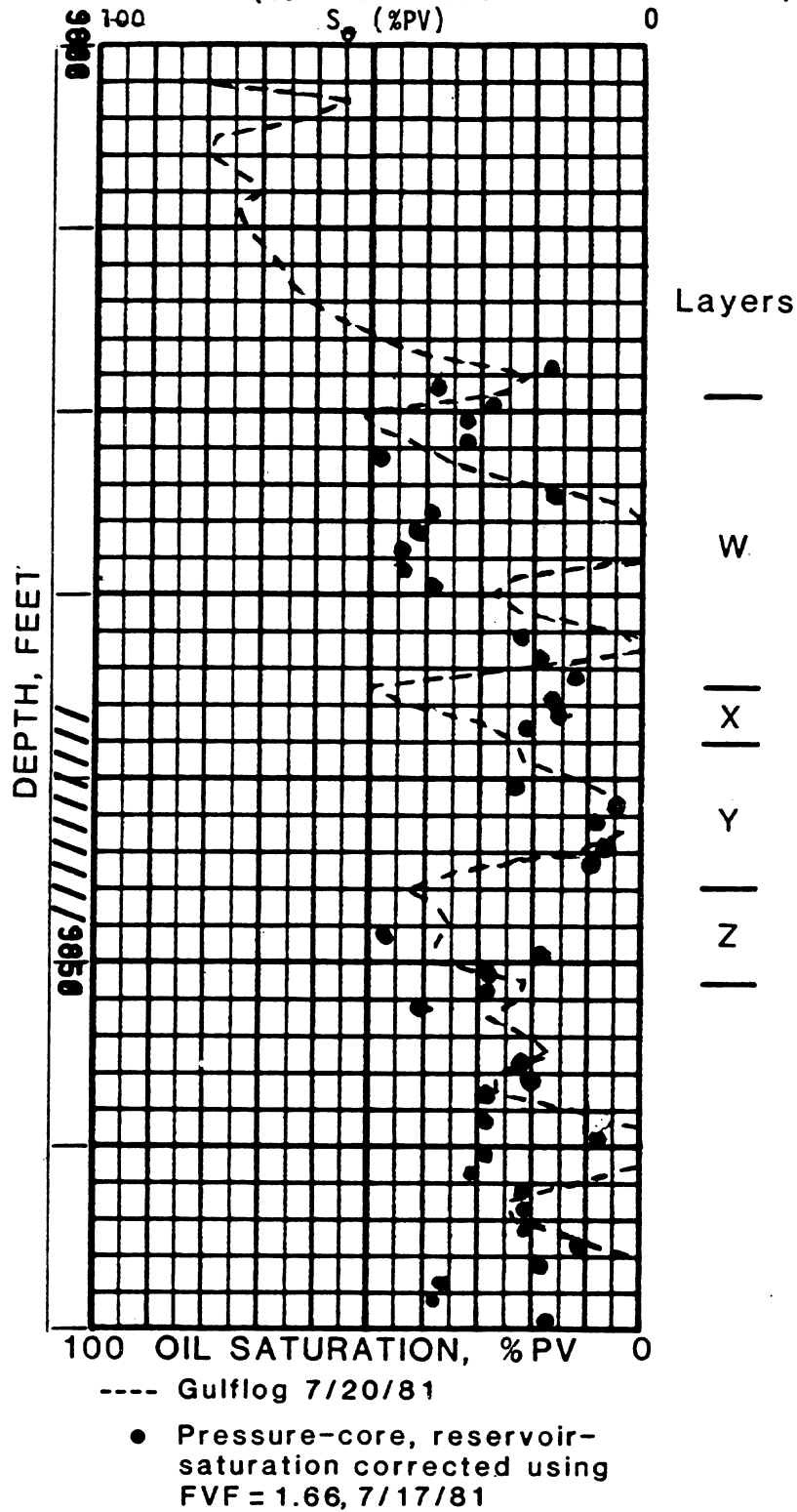


Fig. 85-Comparison of Gulflog vs. pressure-core oil saturations in observation well no. 4 with core depths adjusted to log depths.

Zabolotny Observation - 2 6/30/81

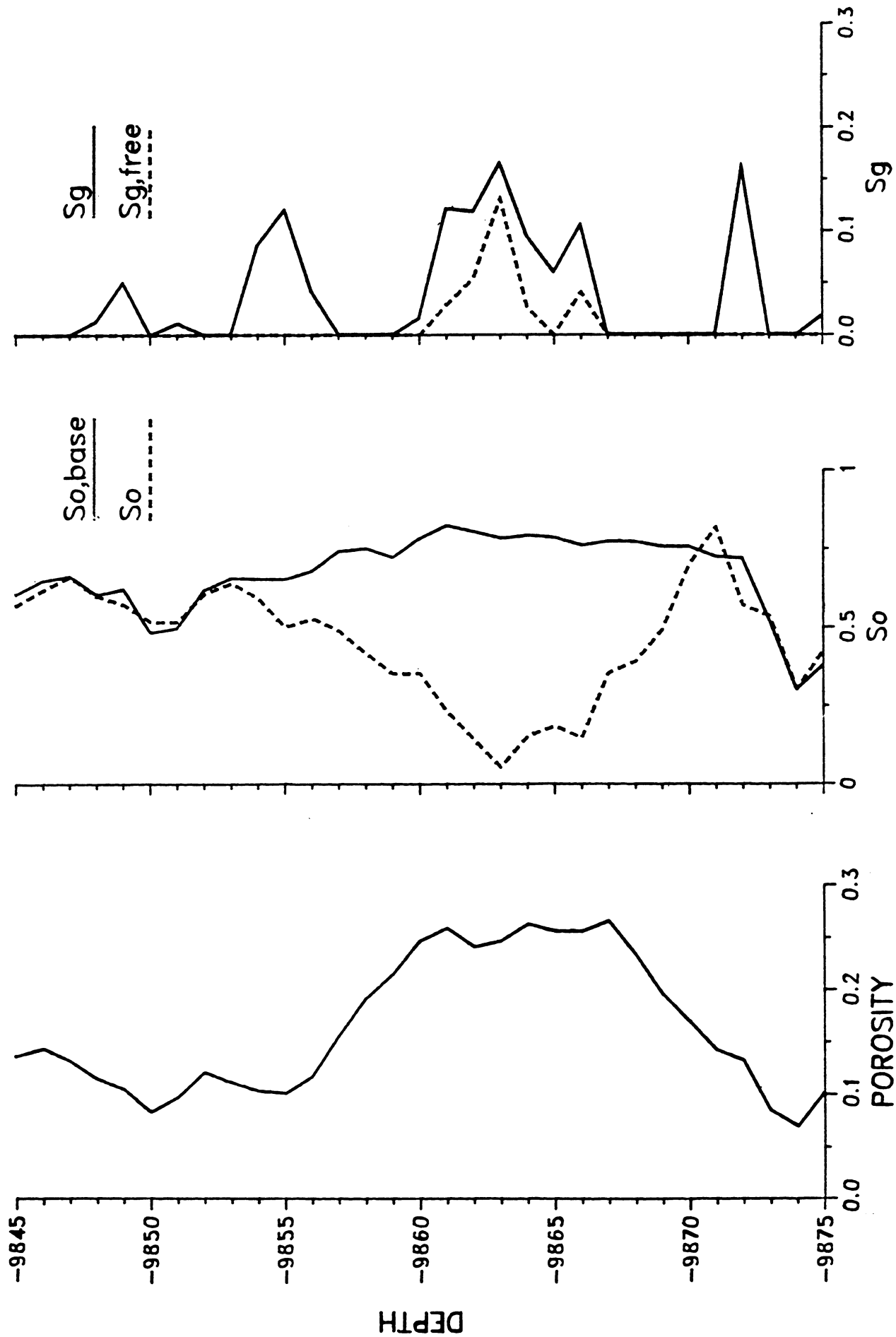


Fig. 86-Monitor-log data: porosity, oil saturation and gas saturation at observation well no. 2 on June 30, 1982.

Zabolotny Observation - 2 7/14/81

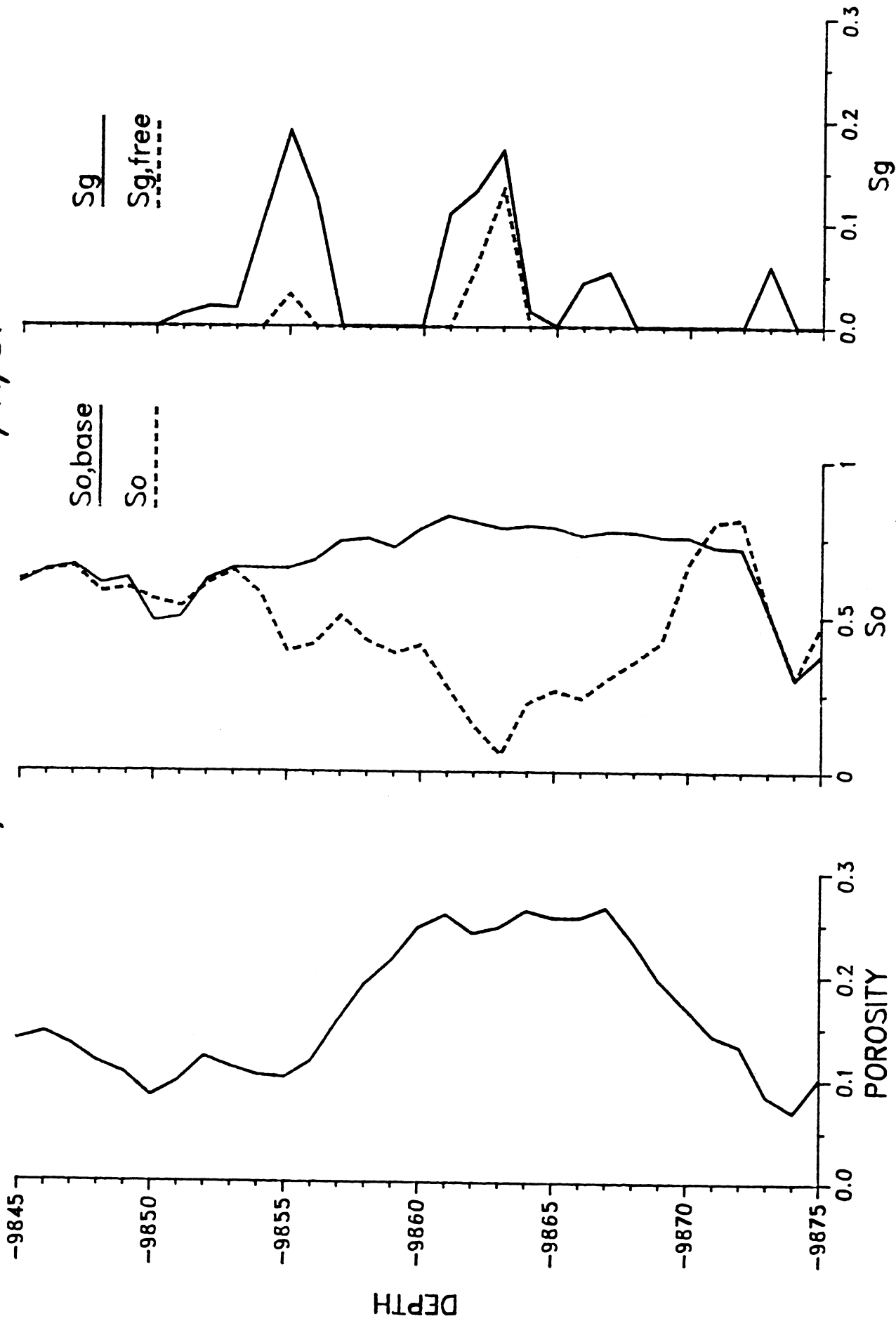


Fig. 87-Monitor-log data: porosity, oil saturation and gas saturation at observation well no. 2 on July 14, 1981.

RESERVOIR CROSS SECTION GRID BASED ON WHOLE CORE POROSITY ANALYSIS

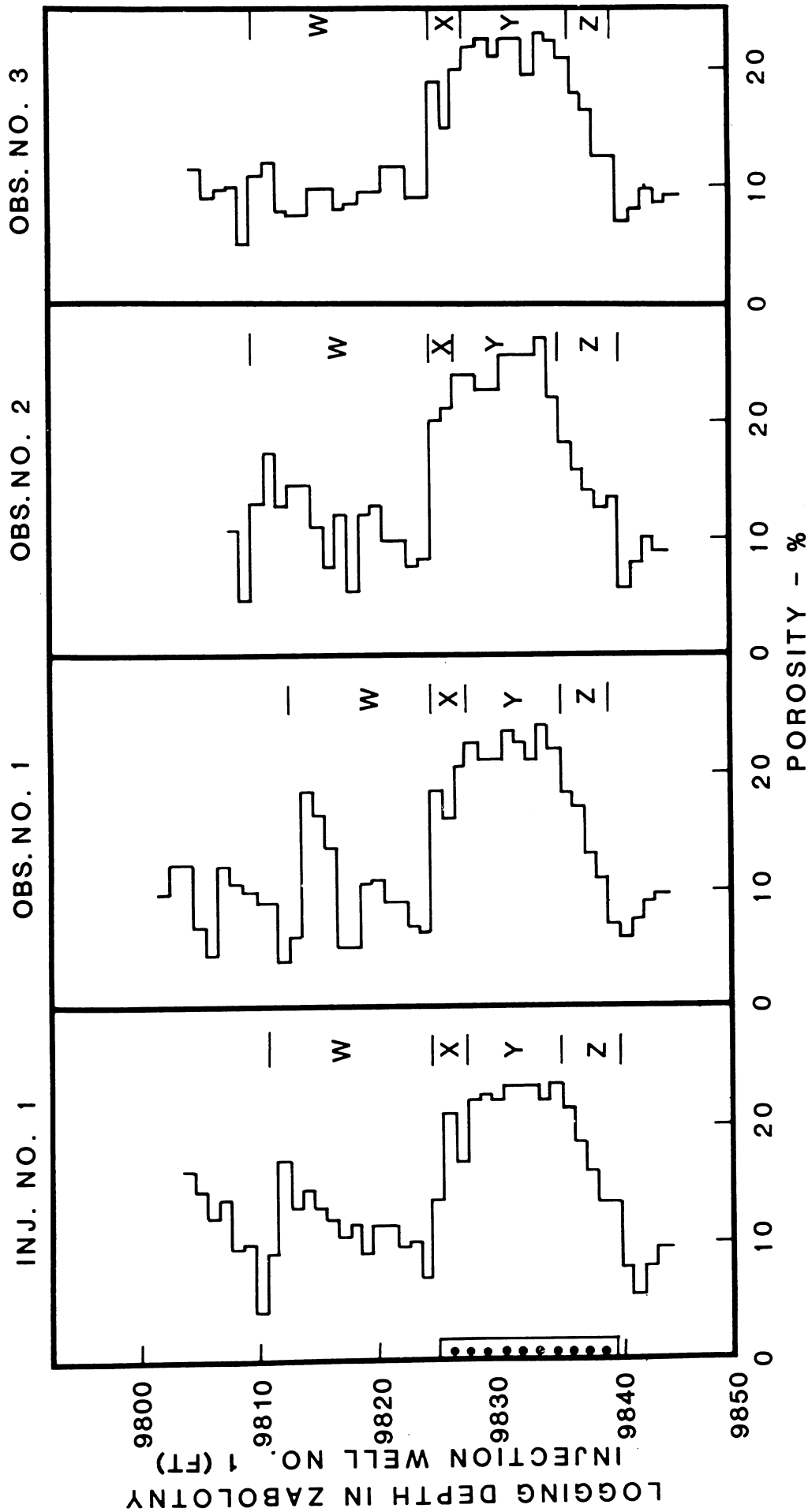


Fig. 88-Reservoir cross-sectional grid based on whole core porosity analysis for layers W, X, Y and Z in injection well no. 1 and observation wells no. 1, 2 and 3.

LITTLE KNIFE ZABOLOTNY 1-3-4A
 OIL DIFFERENTIAL FVF AND
 SOLUTION GAS OIL RATIO AT 245°F

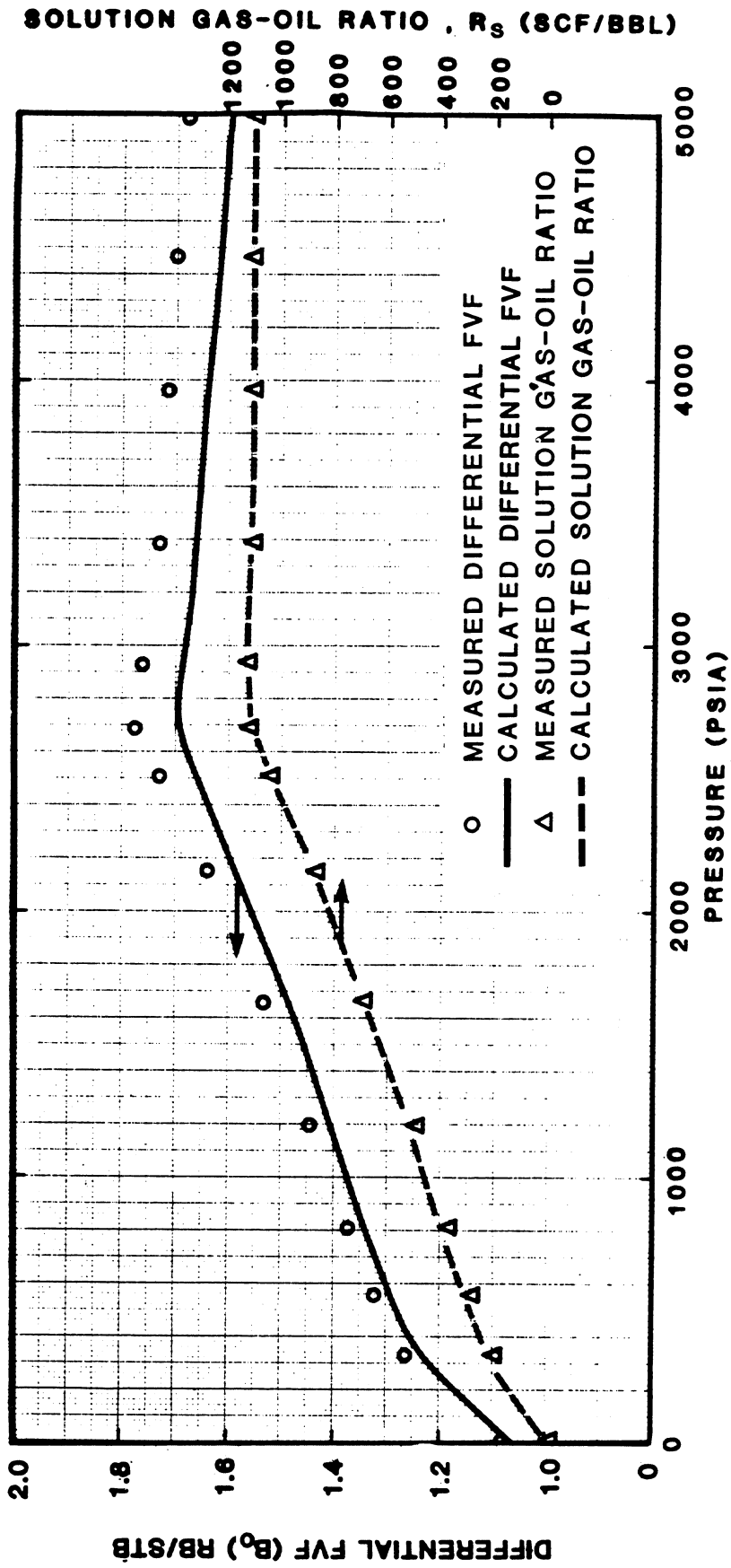


Fig. 89-Oil differential formation volume factor and solution gas oil ratio, both measured and calculated, at various pressures and 245°F, from Zabolotny 1-3-4A.

LITTLE KNIFE ZABOLOTNY 1-3-4A
OIL DENSITY AND VISCOSITY AT 245° F

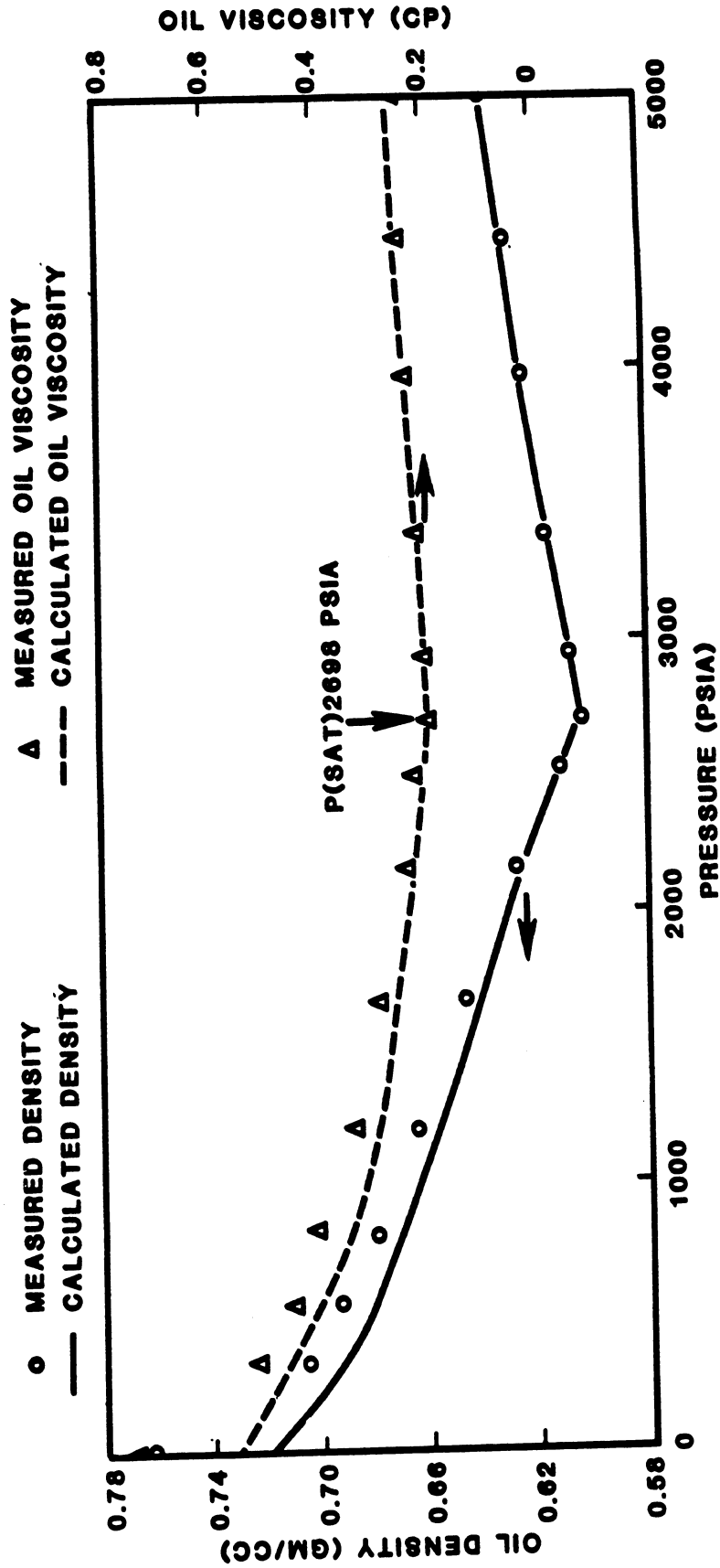
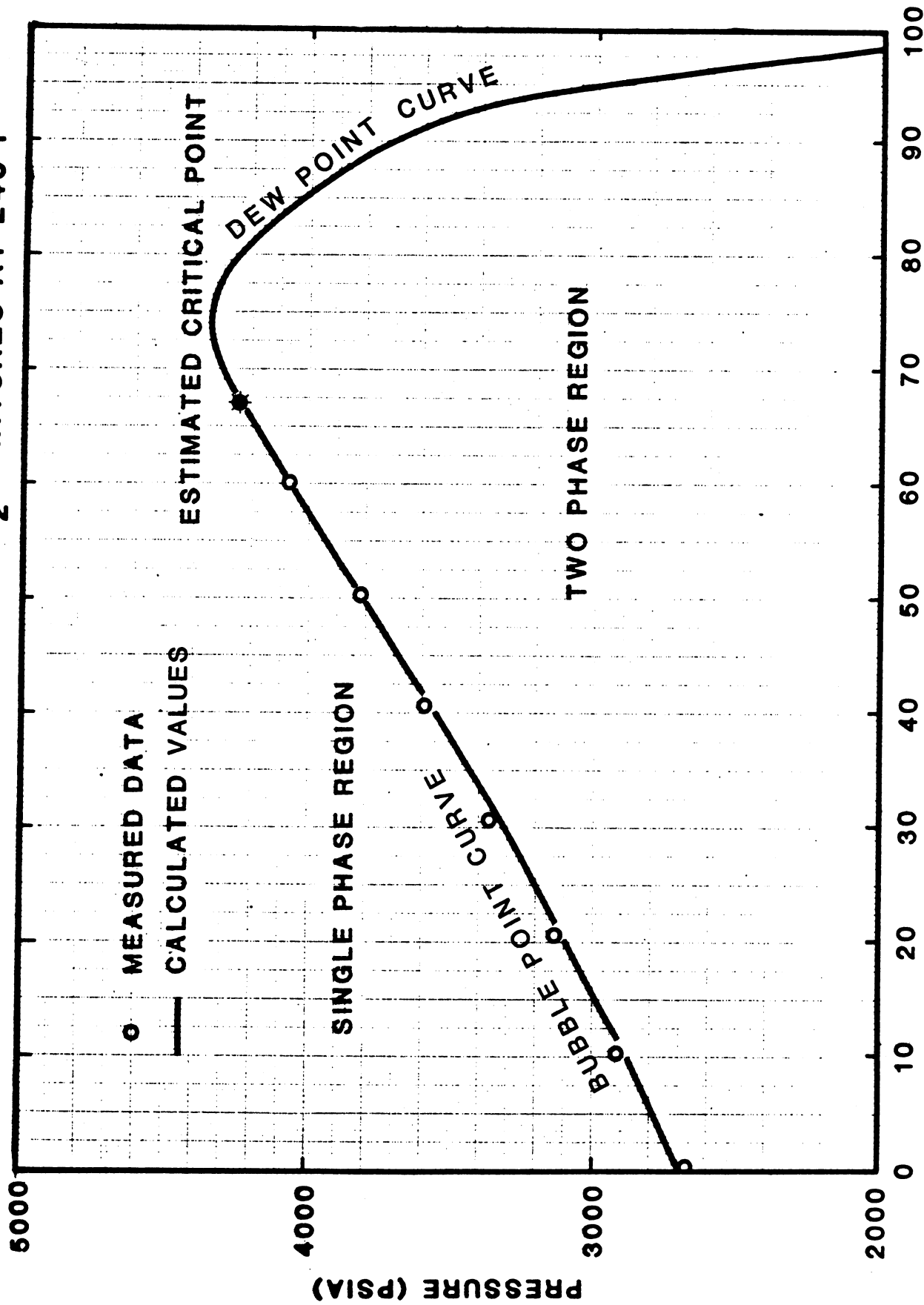


Fig. 90-Oil density and viscosity, both measured and calculated, at various pressures and 245°F, from Zabolotny 1-3-4A.

LITTLE KNIFE ZABOLOTNY 1-3-4A
 PHASE BOUNDARY FOR OIL-CO₂ MIXTURES AT 245°F



MOLE PERCENT CO₂ ADDED TO RESERVOIR OIL

Fig. 91-Phase boundary for oil-CO₂ mixtures at 245°F, at various pressures and mole percent CO₂ added to reservoir oil, from Zabolotny 1-3-4A.

LITTLE KNIFE ZABOLOTNY 1-3-4A
 PRESSURE VOLUME RELATIONSHIP AT 245°F
 FOR OIL-CO₂ MIXTURES

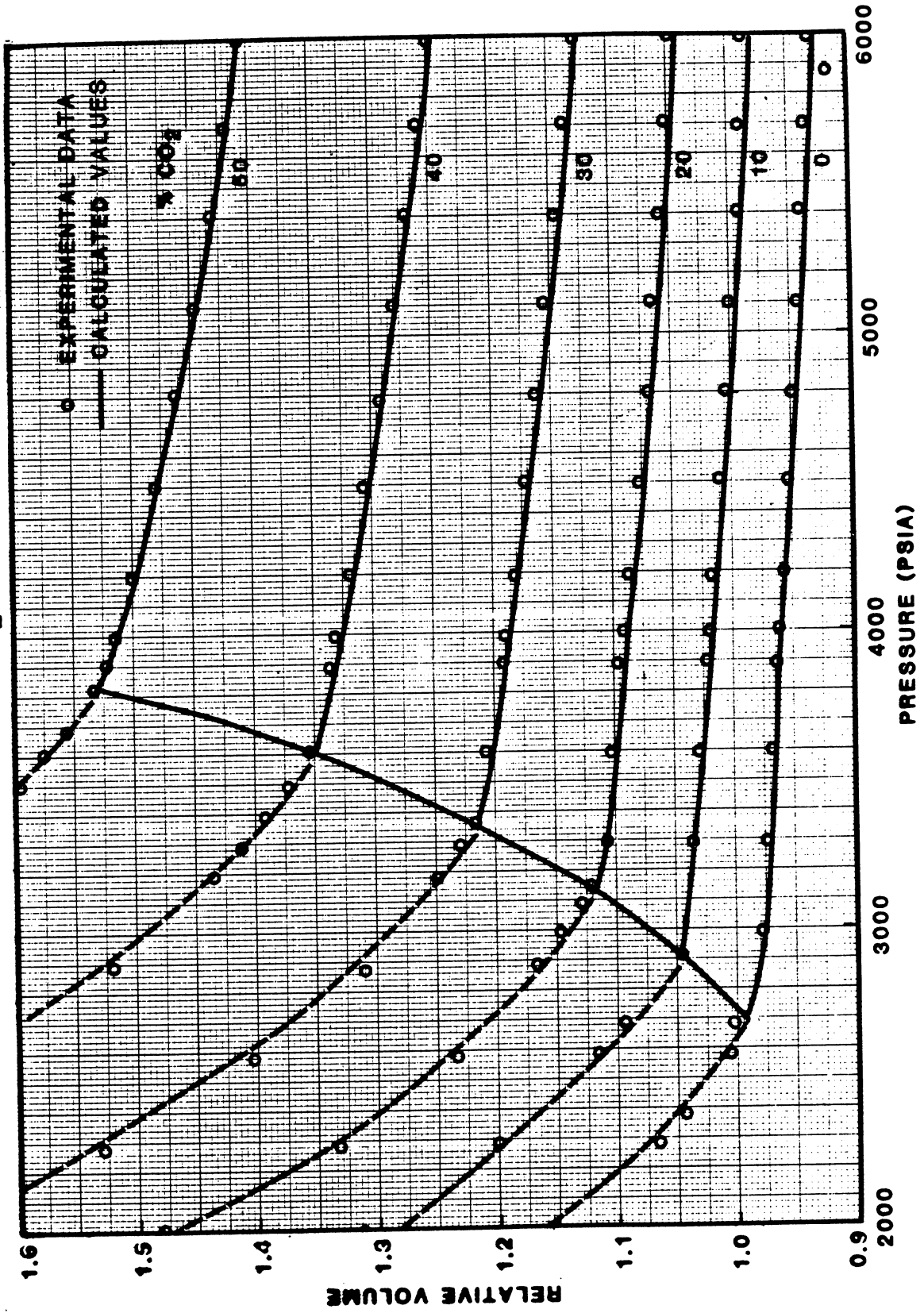


Fig. 92-Pressure volume relationship for relative volumes of oil-CO₂ mixtures, at various pressures and 245°F, Zabolotny 1-3-4A.

LITTLE KNIFE ZABOLOTNY 1-3-4A
VISCOSITY OF OIL-CO₂ MIXTURES AT 245°F (RECOMBINED SAMPLE)

MOLE % CO₂ ADDED

0	30	50
●	▲	x

MEASURED CALCULATED

— - - - - - ······

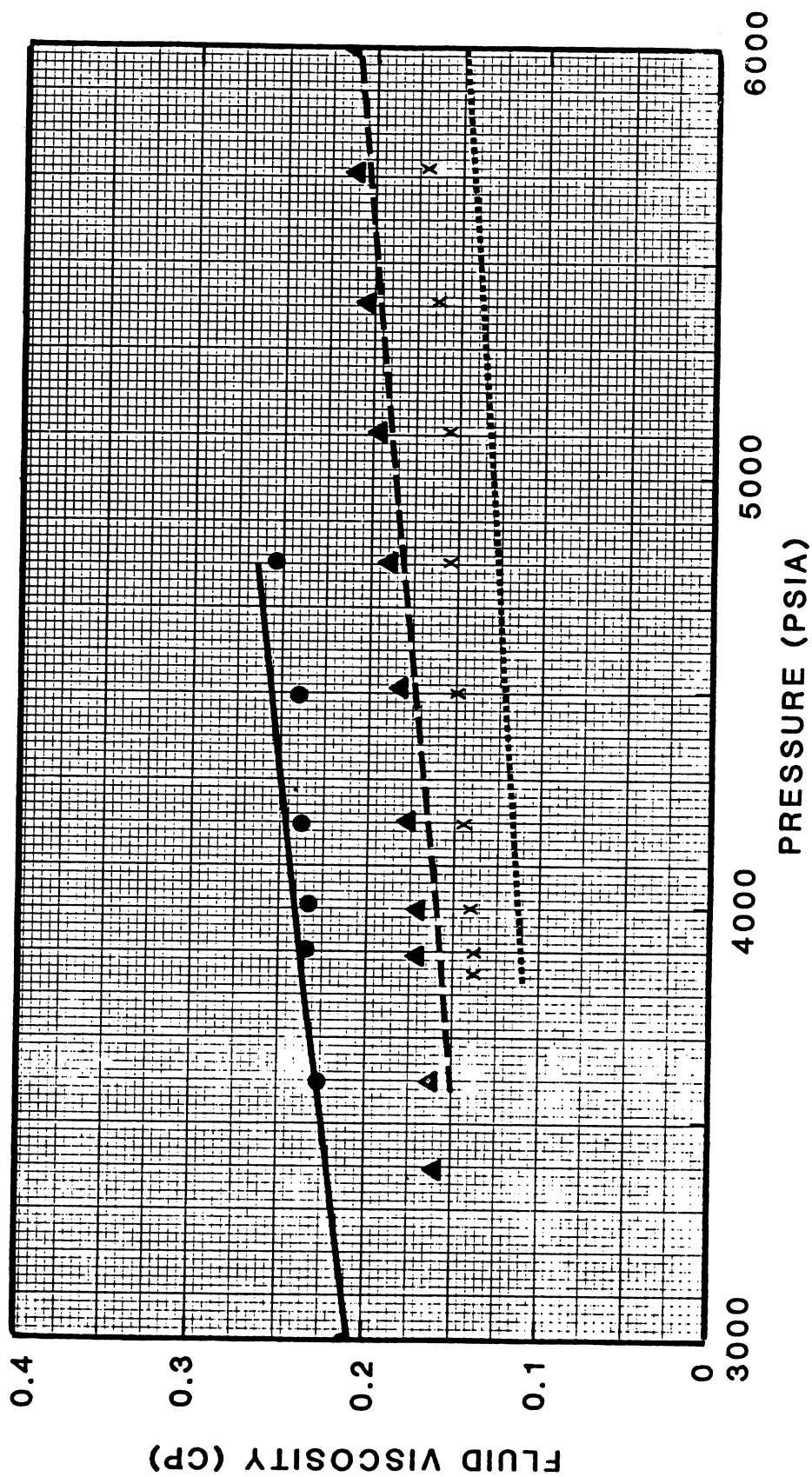


Fig. 93-Viscosity of oil-CO₂ mixtures, both measured and calculated, at various pressures and 245°F, Zabolotny 1-3-4A.

LITTLE KNIFE ZABOLOTNY 1-3-4A
DENSITY OF OIL - CO₂ MIXTURES AT 245° F

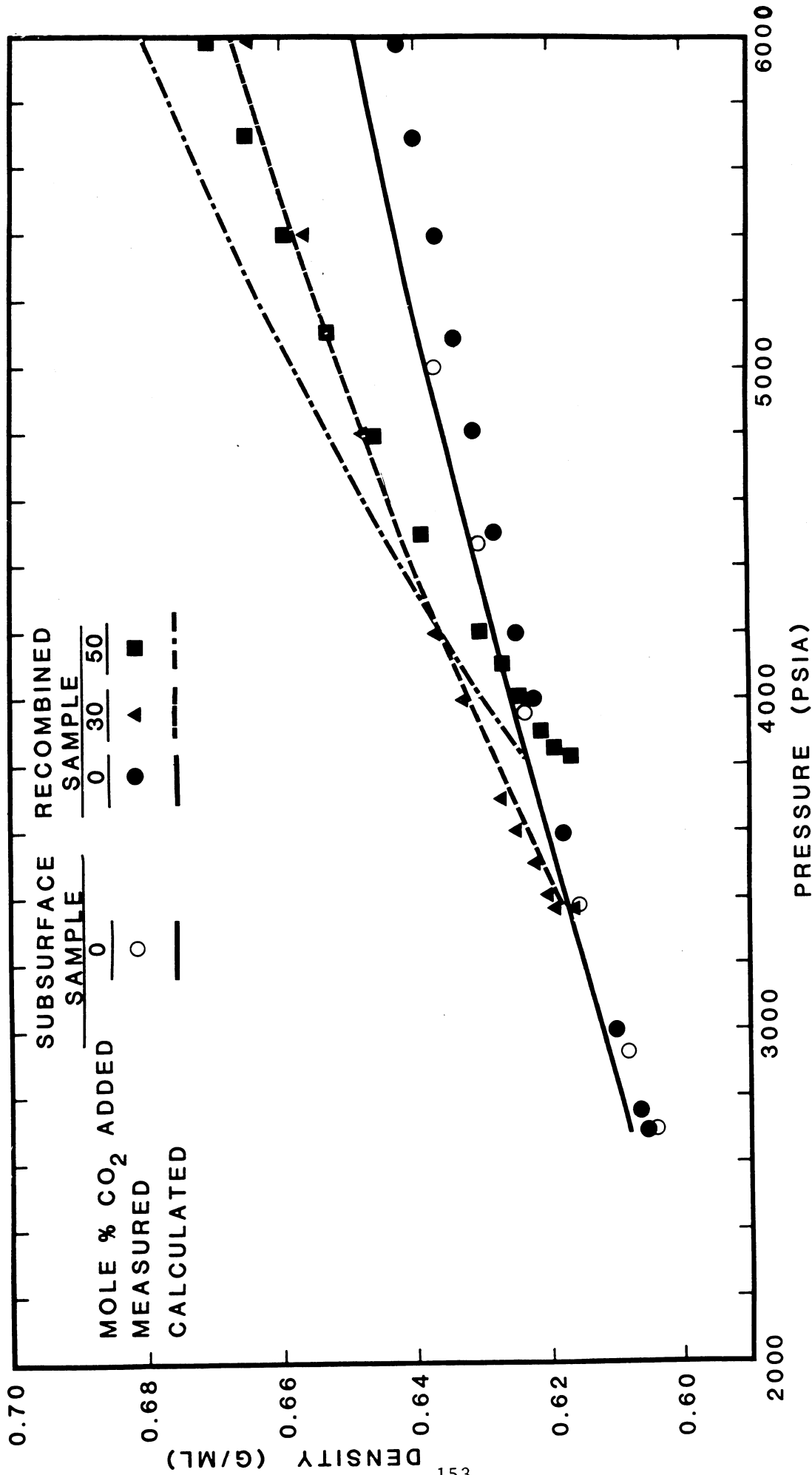


Fig. 94-Density of oil-CO₂ mixtures, both measured and calculated, at various pressures and 245°F, Zabolotny 1-3-4A.

LITTLE KNIFE ZABOLOTNY 1-3-4A
 COEFFICIENTS OF COMPRESSIBILITY OF RESERVOIR OIL WITH CO₂ ADDED AT 245°F

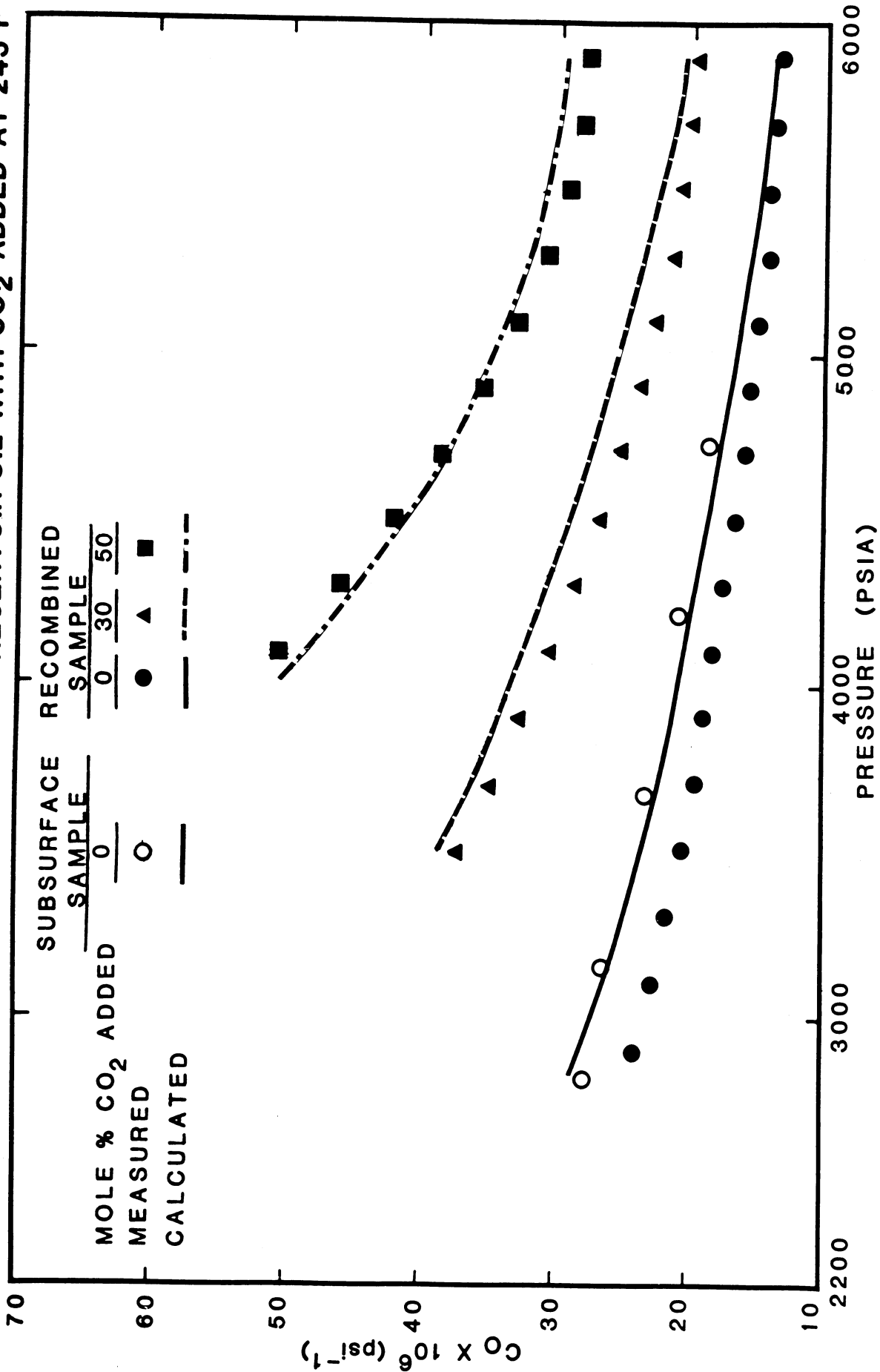


Fig. 95-Coefficients of compressibility of reservoir oil with CO₂ added, both measured and calculated, for subsurface and recombinant samples at various pressures and 245°F; Zabolotny 1-3-4A.

DERIVED OIL-WATER CAPILLARY PRESSURE DATA

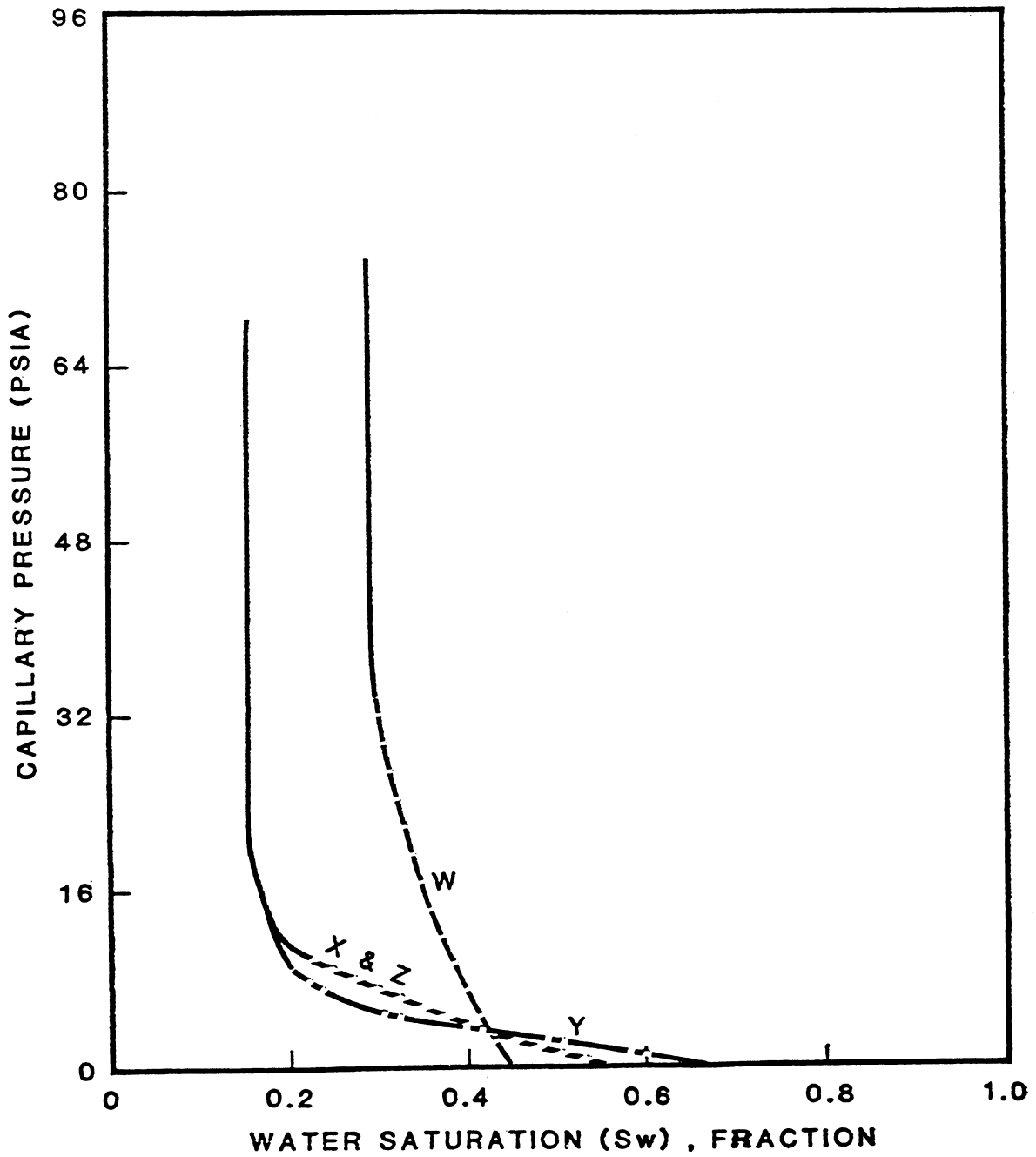


Fig. 96-Derived oil-water capillary pressure data, layers W, X, Y and Z.

RELATIVE PERMEABILITY DATA FOR LAYER W

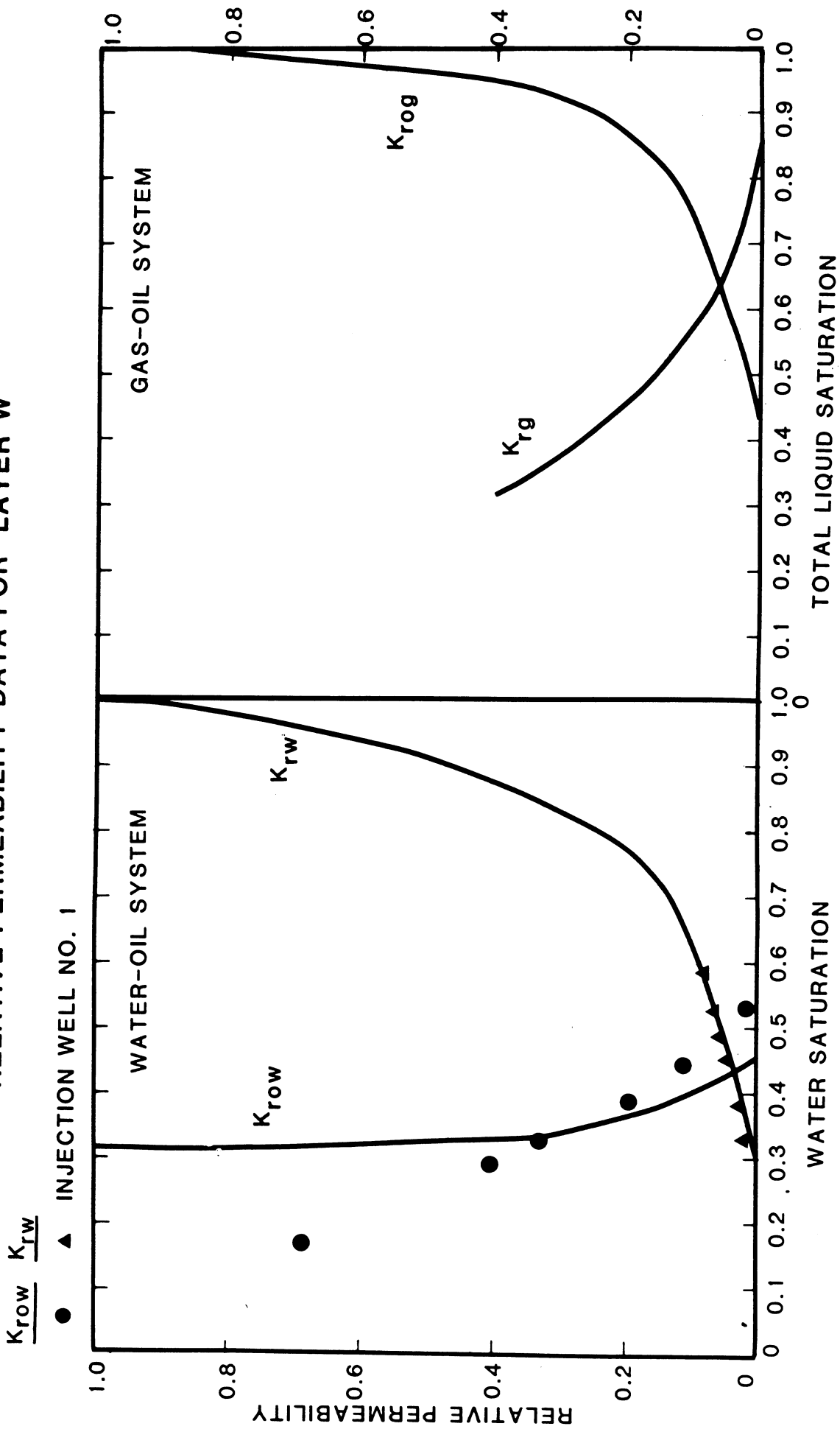


Fig. 97-Relative permeability data for layer W, injection well no. 1.

RELATIVE PERMEABILITY DATA FOR LAYER X

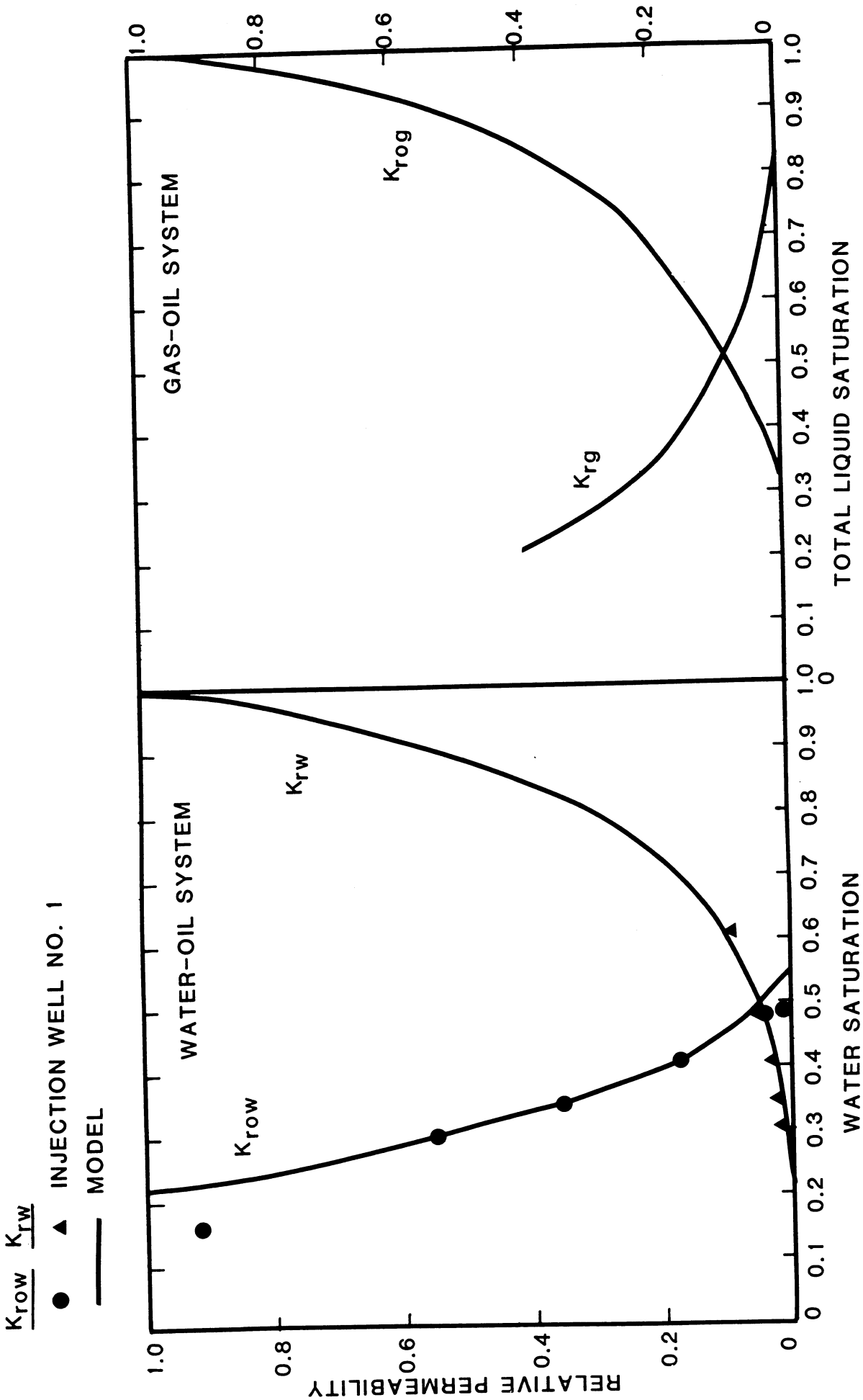


Fig. 98-Relative permeability data for layer X, injection well no. 1.

RELATIVE PERMEABILITY DATA FOR LAYER Y

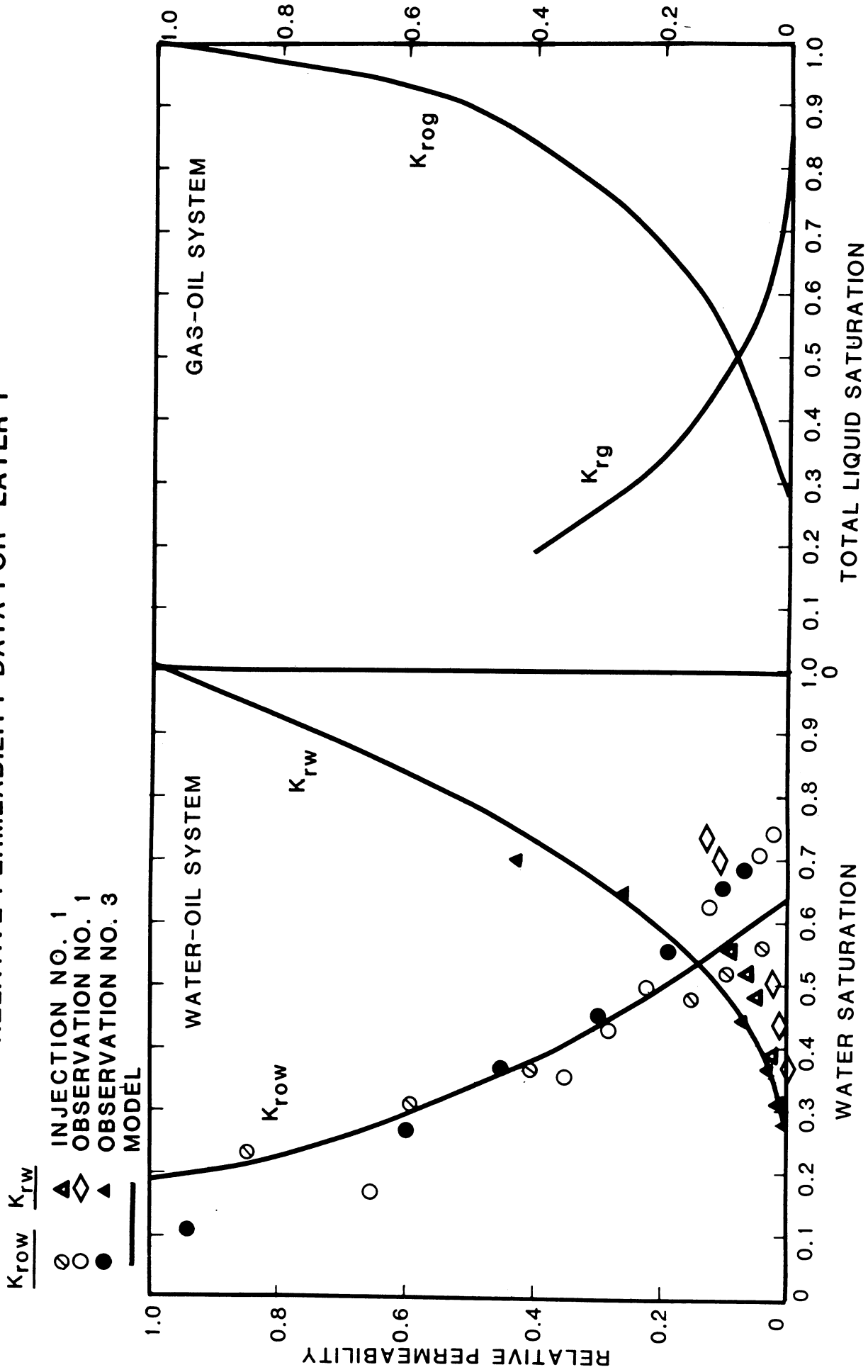


Fig. 99-Relative permeability data for layer Y, injection well no. 1 and observation wells no. 1 and 3.

RELATIVE PERMEABILITY DATA FOR LAYER Z

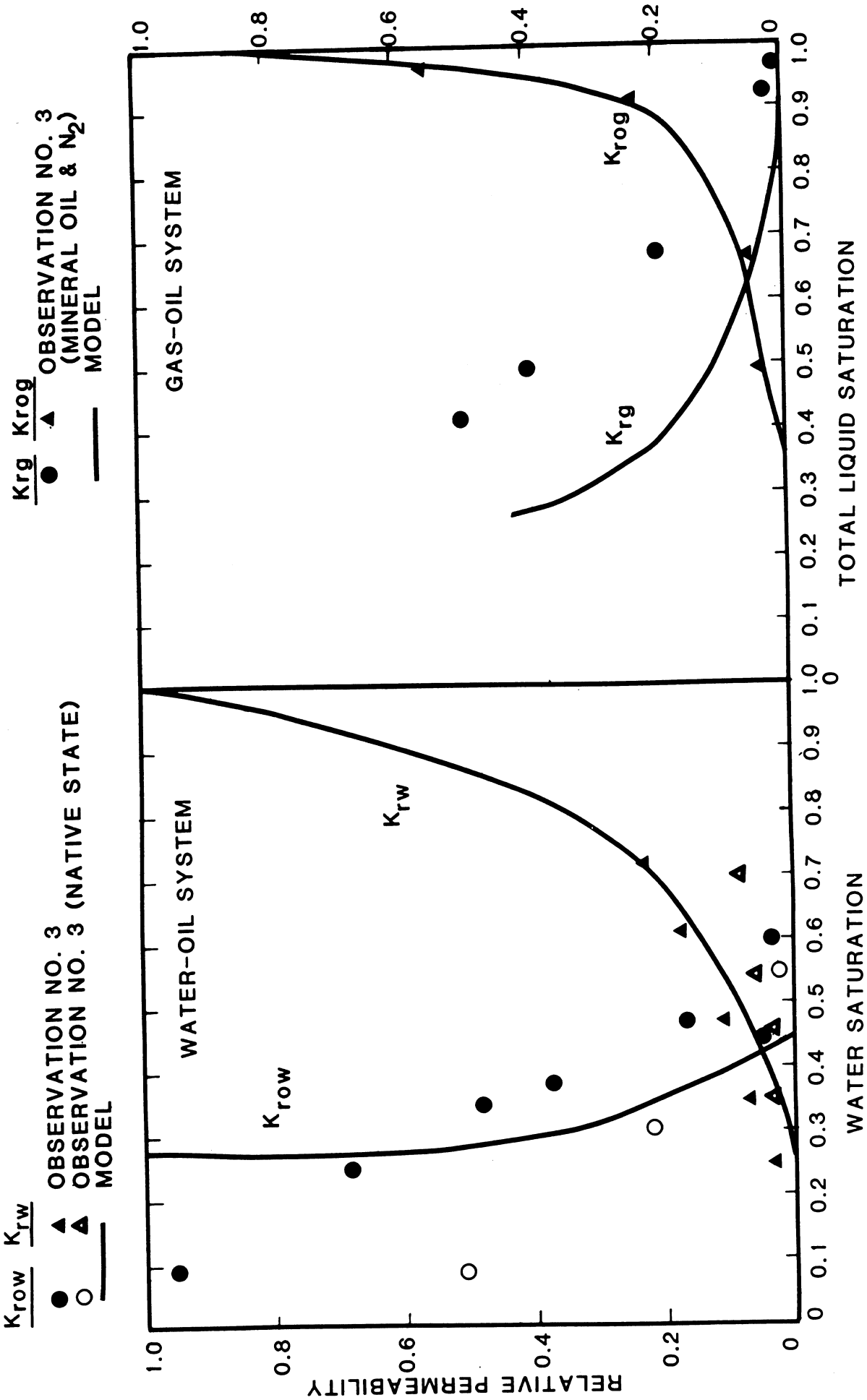


Fig. 100-Relative permeability data for layer Z, observation well no. 3.

COORDINATE SYSTEM FOR THE COMPOSITIONAL SIMULATION

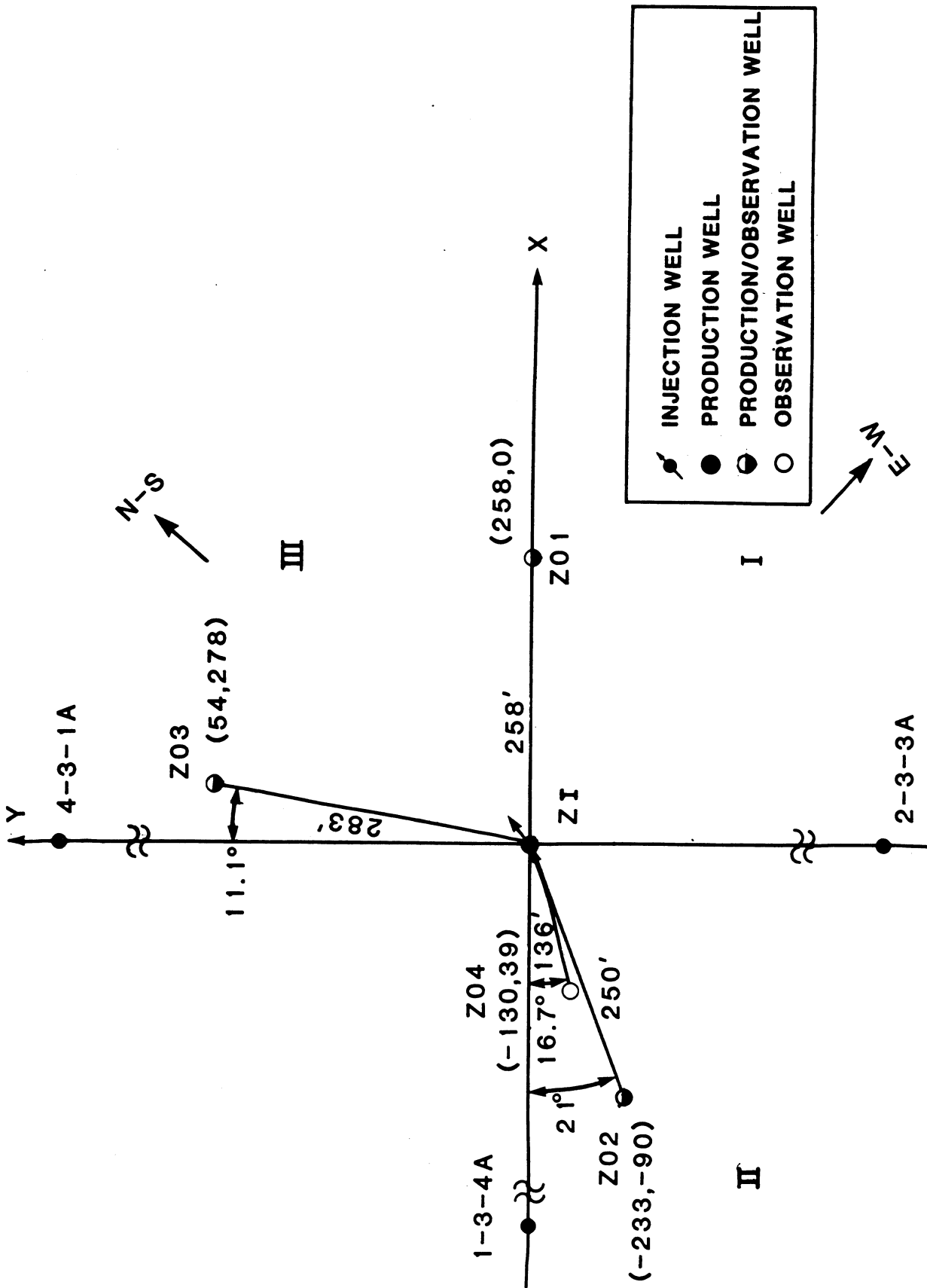


Fig. 101-Coordinate system for the compositional simulation, north is as indicated by arrow in quadrant III.

11 X 11 X 4 GRID SYSTEM



INJECTION WELL



PRODUCTION/OBSERVATION WELL



OBSERVATION WELL

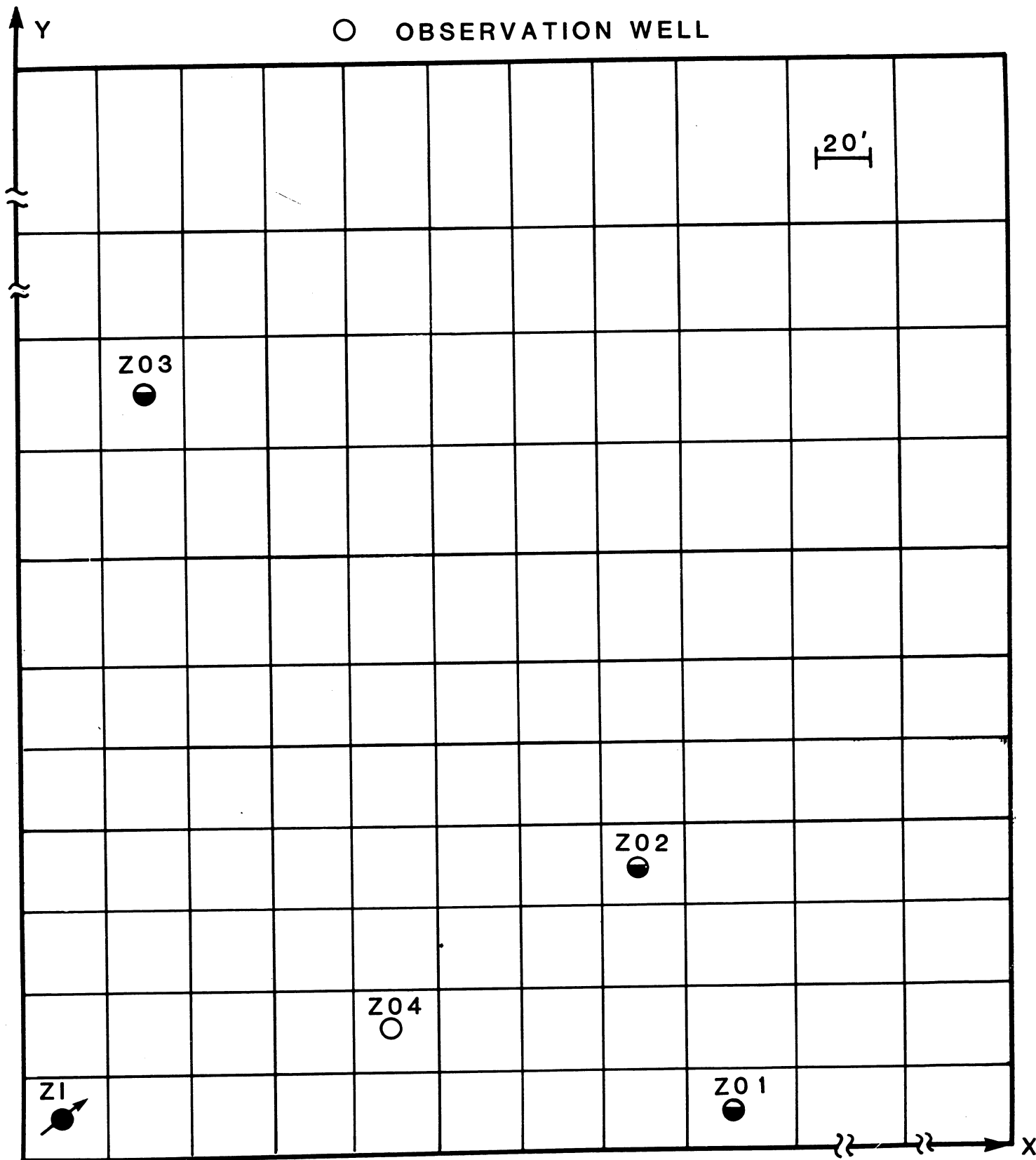


Fig. 102-Grid for the 11x11x4 simulation model.

16 X 15 X 4 GRID SYSTEM

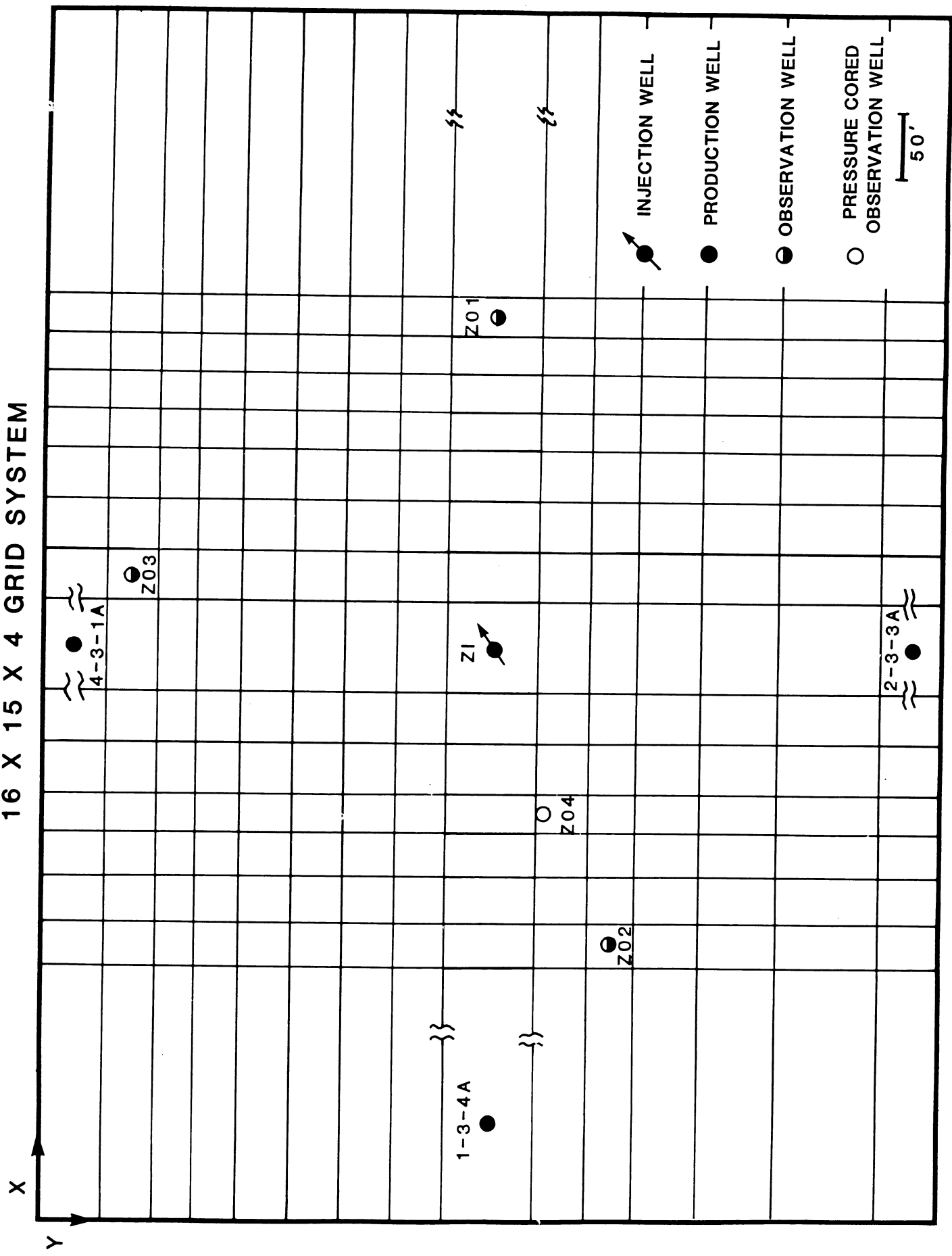


Fig. 103-Grid for the 16x15x4 simulation model.

FOUR-WELL PULSE TEST RESPONSE AT OBSERVATION NO. 1

NOVEMBER 15, 1980

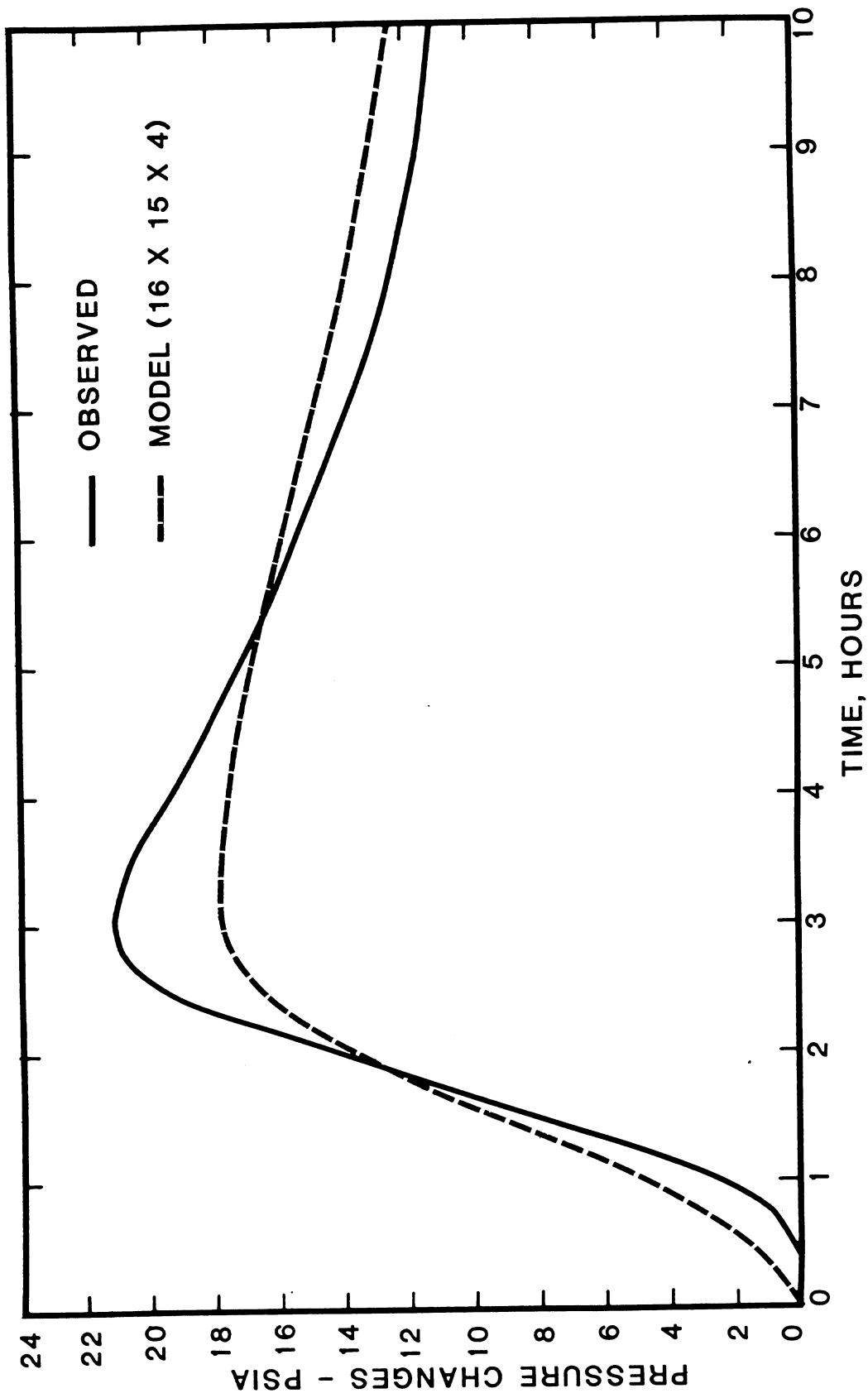


Fig. 104-Simulator match of the four-well multi-well pulse test response, solid line is observed data and dashed line is the simulation model match, at observation well no. 1, November 15, 1980.

FOUR-WELL PULSE TEST RESPONSE AT OBSERVATION NO. 2
NOVEMBER 15, 1980

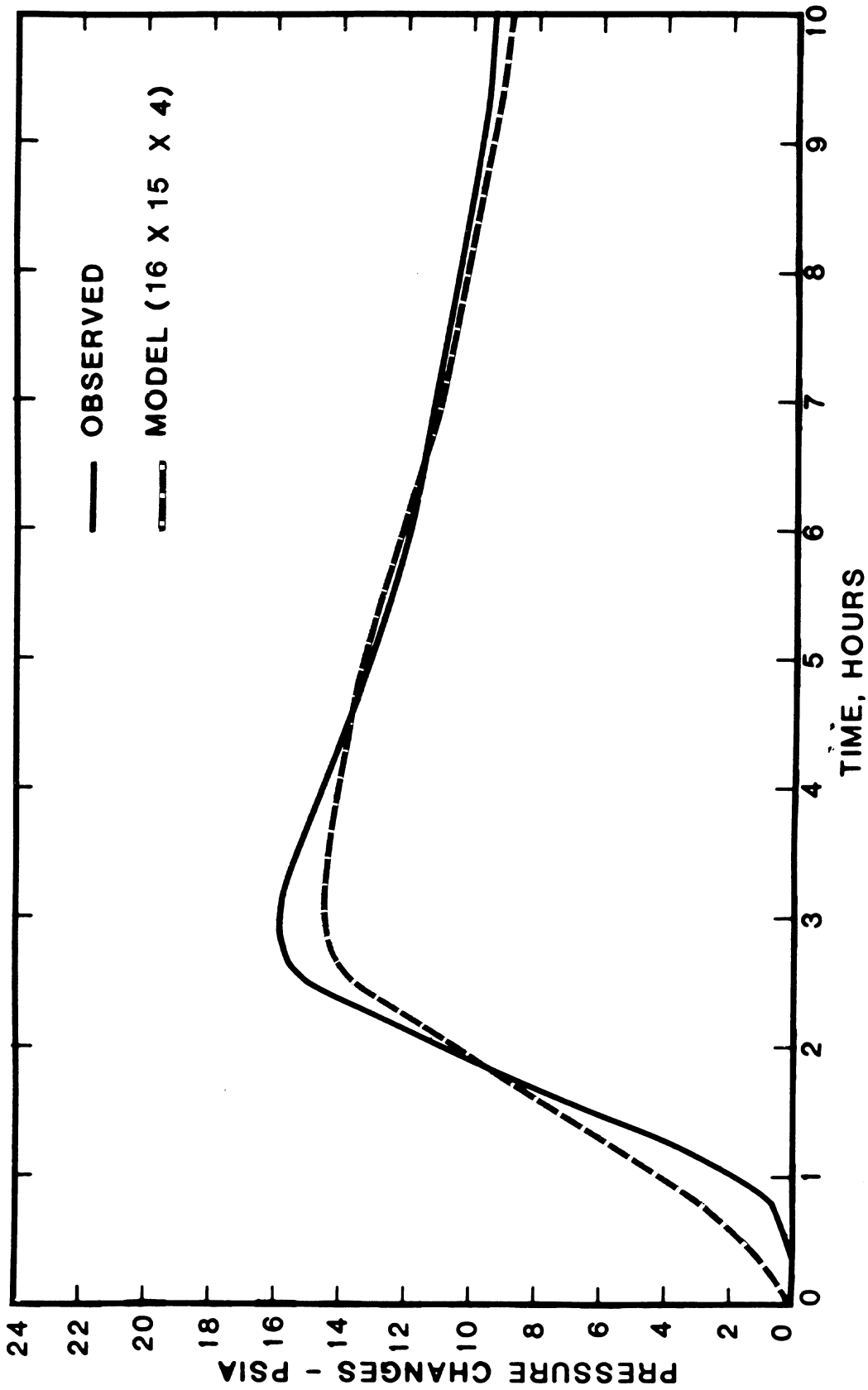


Fig. 105-Simulator match of the four-well multi-well pulse test response, solid line is observed data and dashed line is the simulation model match, at observation well no. 2, November 15, 1980.

FOUR-WELL PULSE TEST RESPONSE AT OBSERVATION NO. 3

NOVEMBER 15, 1980

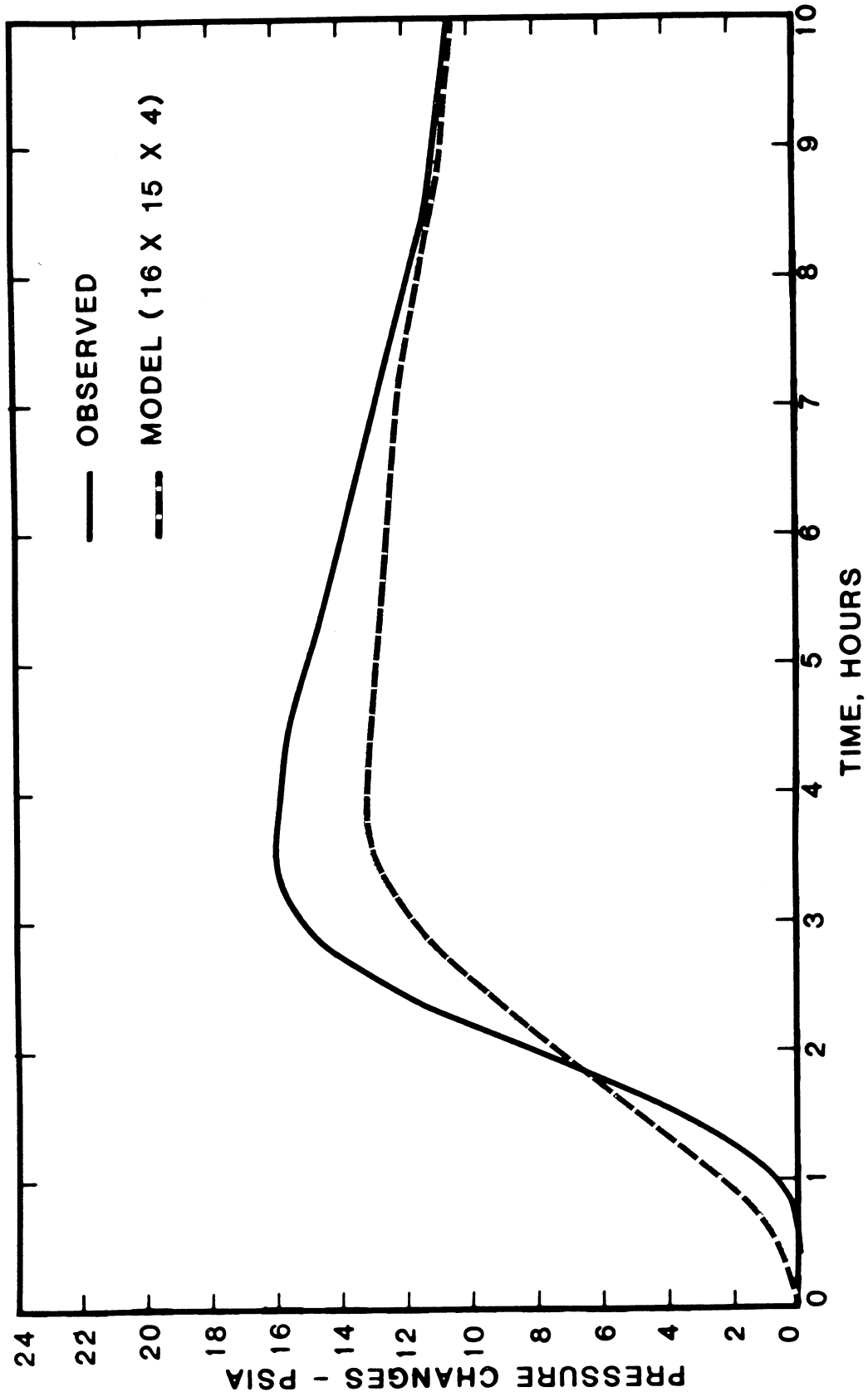


Fig. 106-Simulator match of the four-well multi-well pulse test response, solid line is observed data and dashed line is the simulation model match, at observation well no. 3, November 15, 1980.

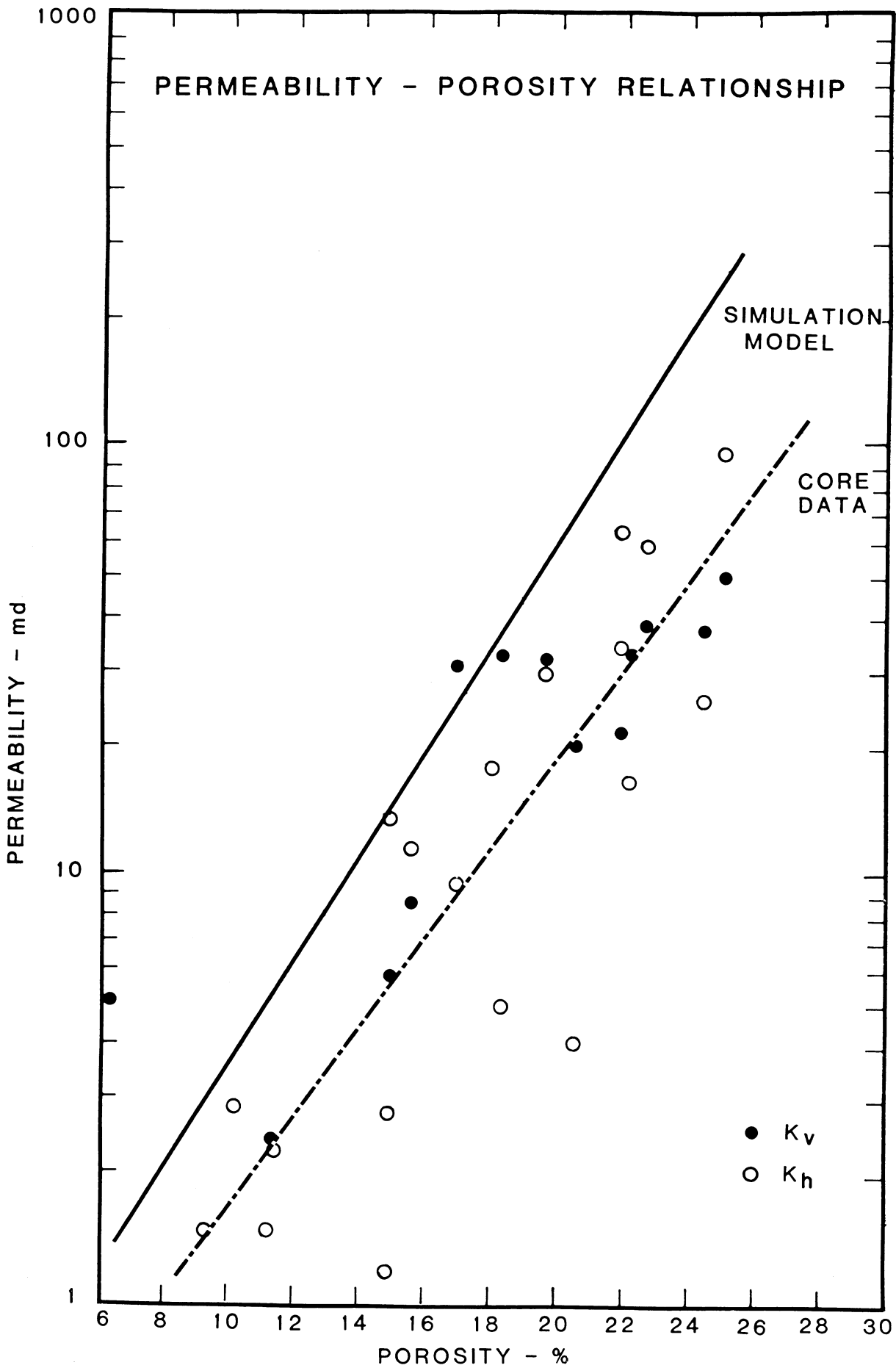


Fig. 107-Permeability-porosity relationship of core data and simulation data.

PRESSURE HISTORY MATCH (12-11-80 TO 10-7-81)
ZABOLOTNY INJECTION WELL NO. 1

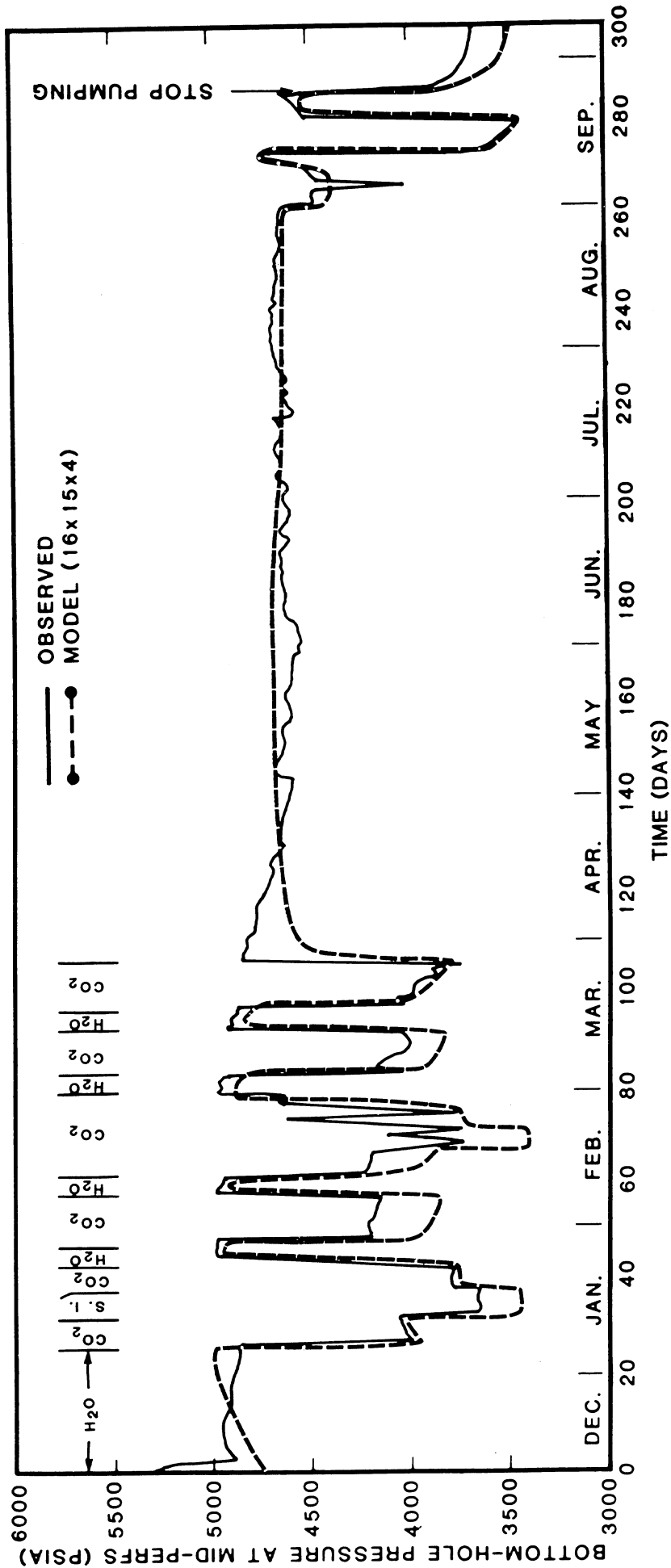


Fig. 108-Simulator match of bottom-hole pressure vs. time. Solid line is observed data and dashed line is the simulation model match, December 11, 1980 to October 7, 1981 at injection well no. 1.

PRESSURE HISTORY MATCH (12-11-80 TO 10-7-81)
 ZABOLOTNY OBSERVATION WELL NO. 1

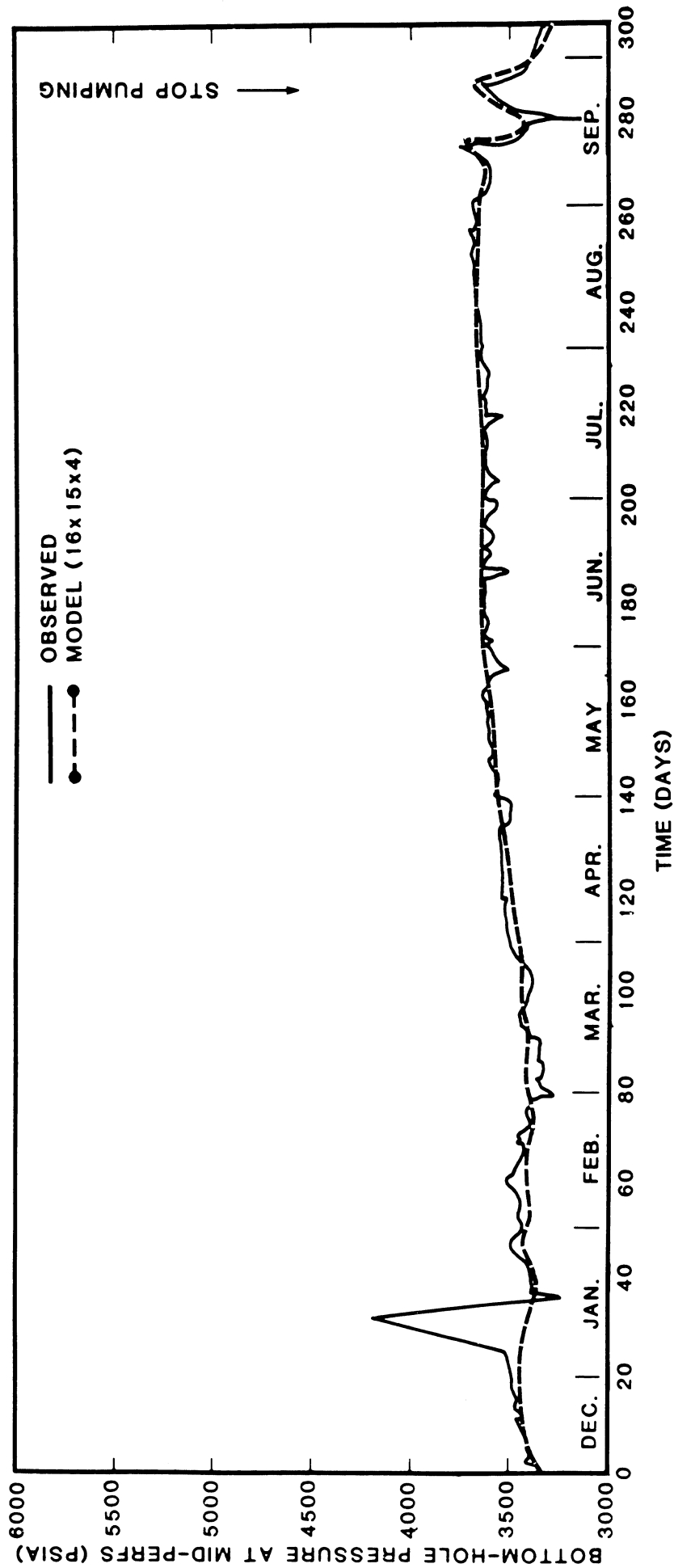


Fig. 109-Simulator match of bottom-hole pressure vs. time. Solid line is observed data and dashed line is the simulation model match, December 11, 1980 to October 7, 1981 at observation well no. 1.

PRESSURE HISTORY MATCH (12-11-80 TO 10-7-81)
 ZABOLOTNY OBSERVATION WELL NO. 2

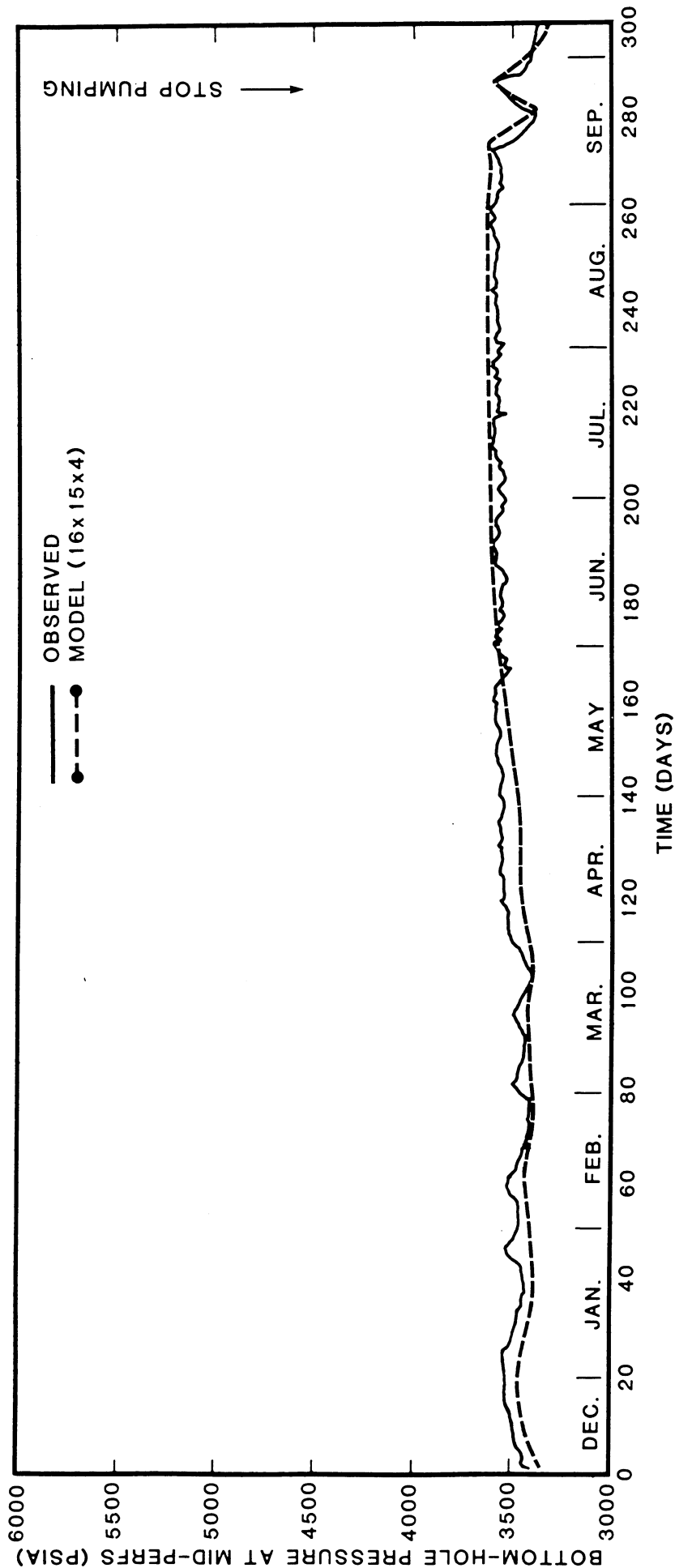


Fig. 110-Simulator match of bottom-hole pressure vs. time. Solid line is observed data and dashed line is the simulation model match, December 11, 1980 to October 7, 1981 at observation well no. 2.

PRESSURE HISTORY MATCH (12-11-80 TO 10-7-81)
 ZABOLOTNY OBSERVATION WELL NO. 3

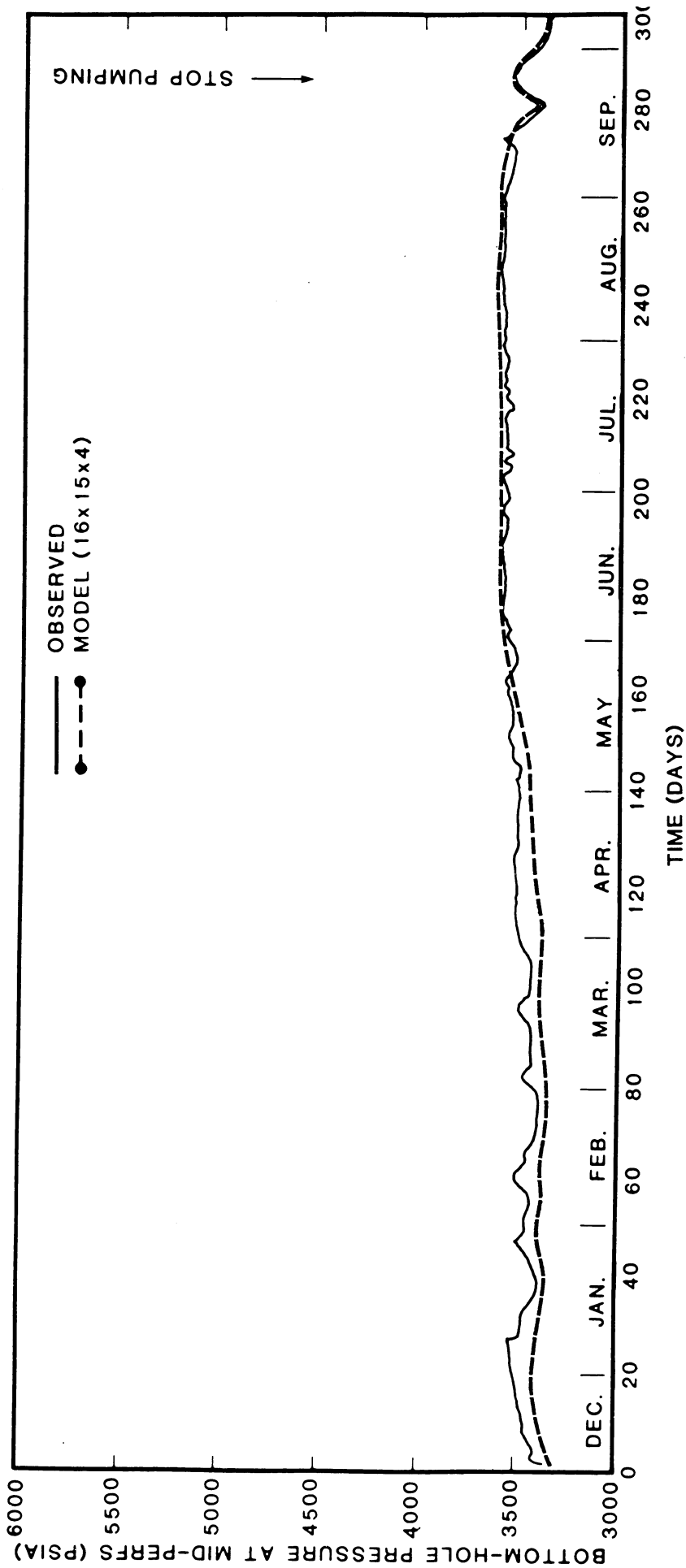


Fig. 111-Simulator match of bottom-hole pressure vs. time. Solid line is observed data and dashed line is the simulation model match, December 11, 1980 to October 7, 1981 at observation well no. 3.

WATER SATURATION HISTORY MATCH BY LAYERS (12-11-80 TO 9-17-81)
ZABOLOTNY OBSERVATION WELL NO. 1

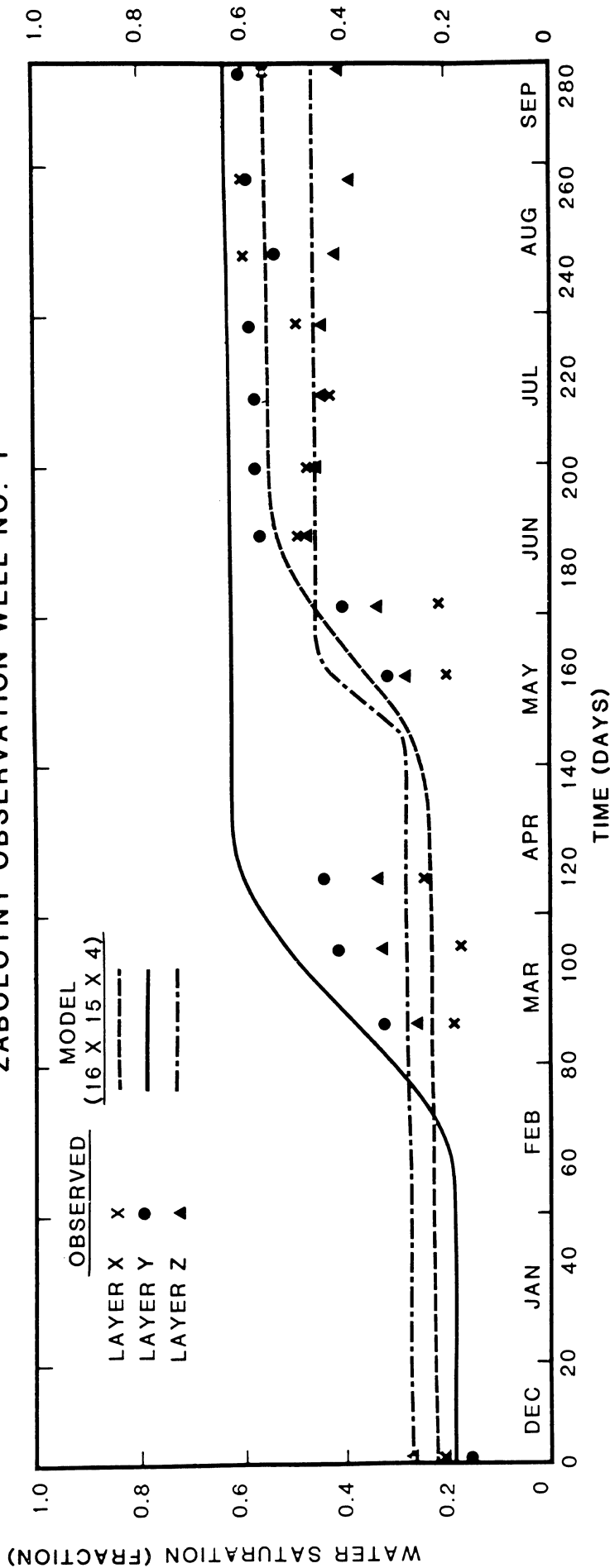


Fig. 112-Water saturation history match for layers X, Y and Z. X's, dots, and triangles are observed data and lines are simulation model matches, December 11, 1980 to September 17, 1981 at observation well no. 1.

WATER SATURATION HISTORY MATCH BY LAYERS (12-11-80 TO 9-17-81)
ZABOLOTNY OBSERVATION WELL NO. 2

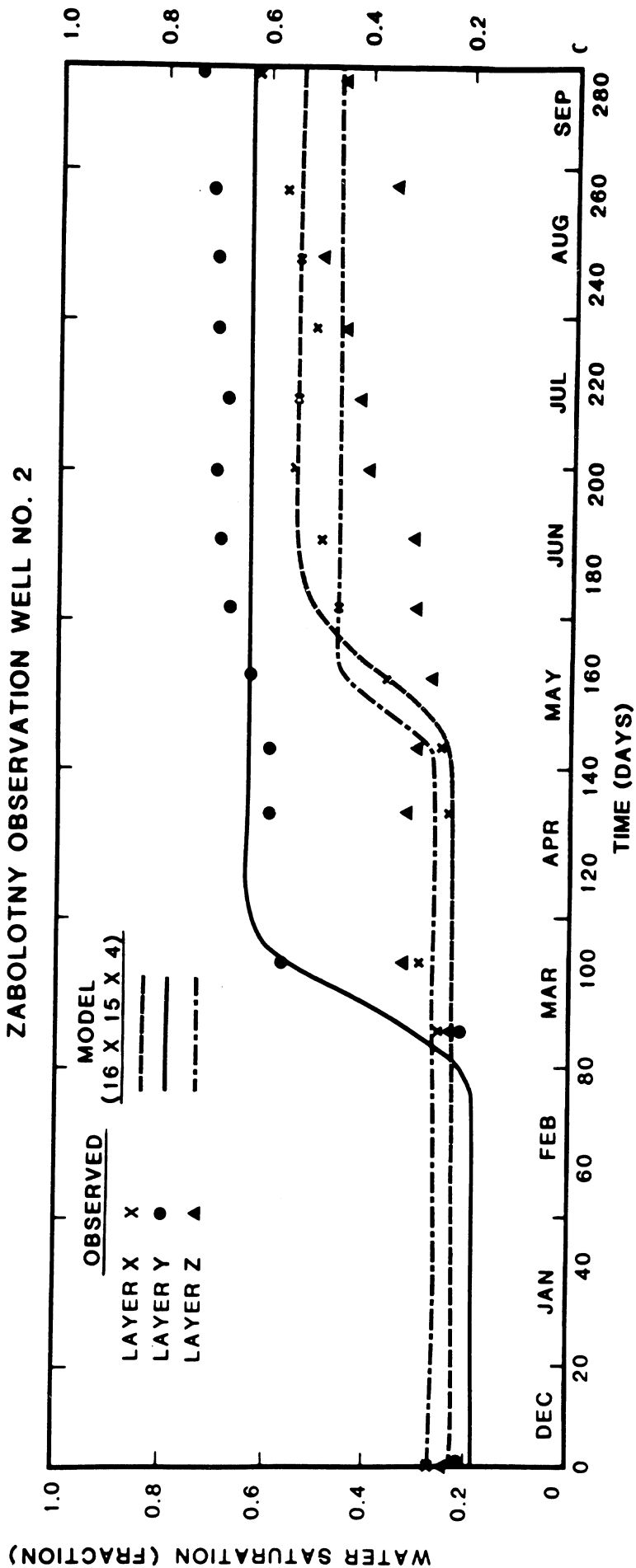


Fig. 113-Water saturation history match for layers X, Y and Z. X's, dots and triangles are observed data and lines are simulation model matches, December 11, 1980 to September 17, 1981 at observation well no. 2.

WATER SATURATION HISTORY MATCH BY LAYERS (12-11-80 TO 9-17-81)
ZABOLOTNY OBSERVATION WELL NO. 3

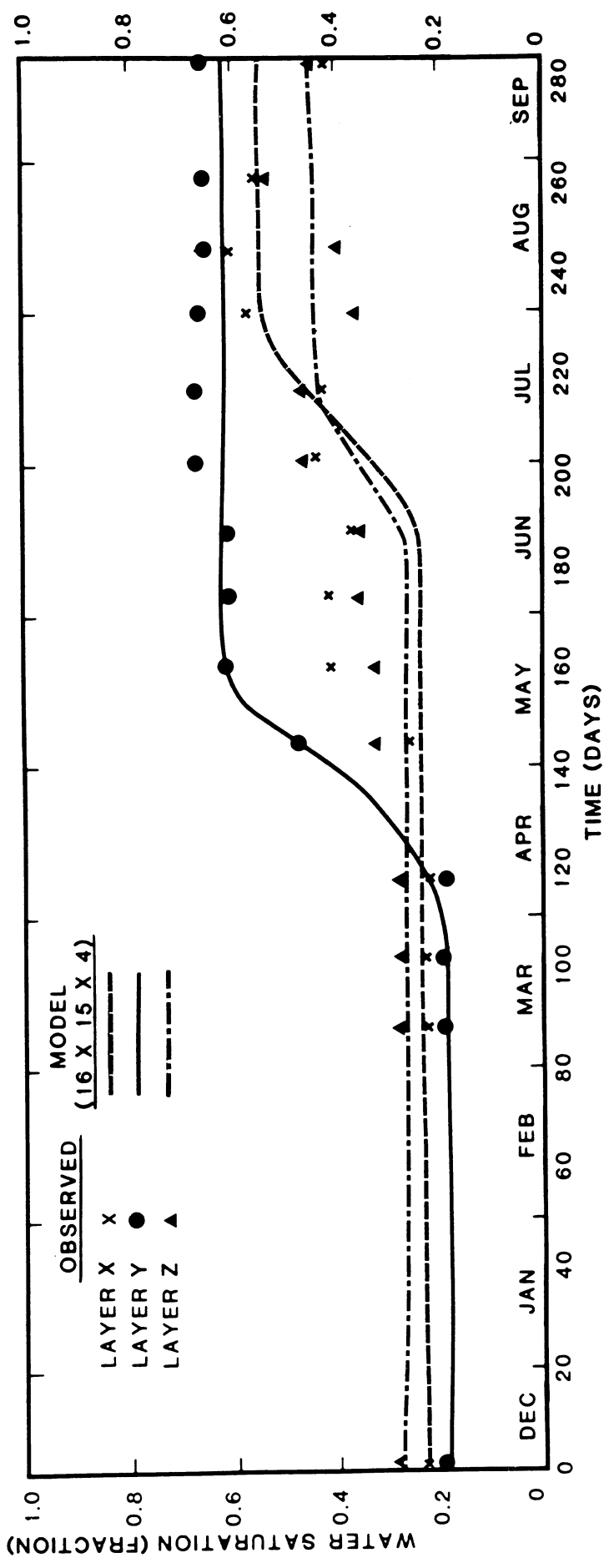


Fig. 114-Water saturation history match for layers X, Y and Z. X's, dots and triangles are observed data and lines are simulation model matches, December 11, 1980 to September 17, 1981 at observation well no. 3.

WATER SATURATION HISTORY MATCH FOR ZONE D (12-11-80 TO 9-17-81)
ZABOLOTNY OBSERVATION WELL NO. 1

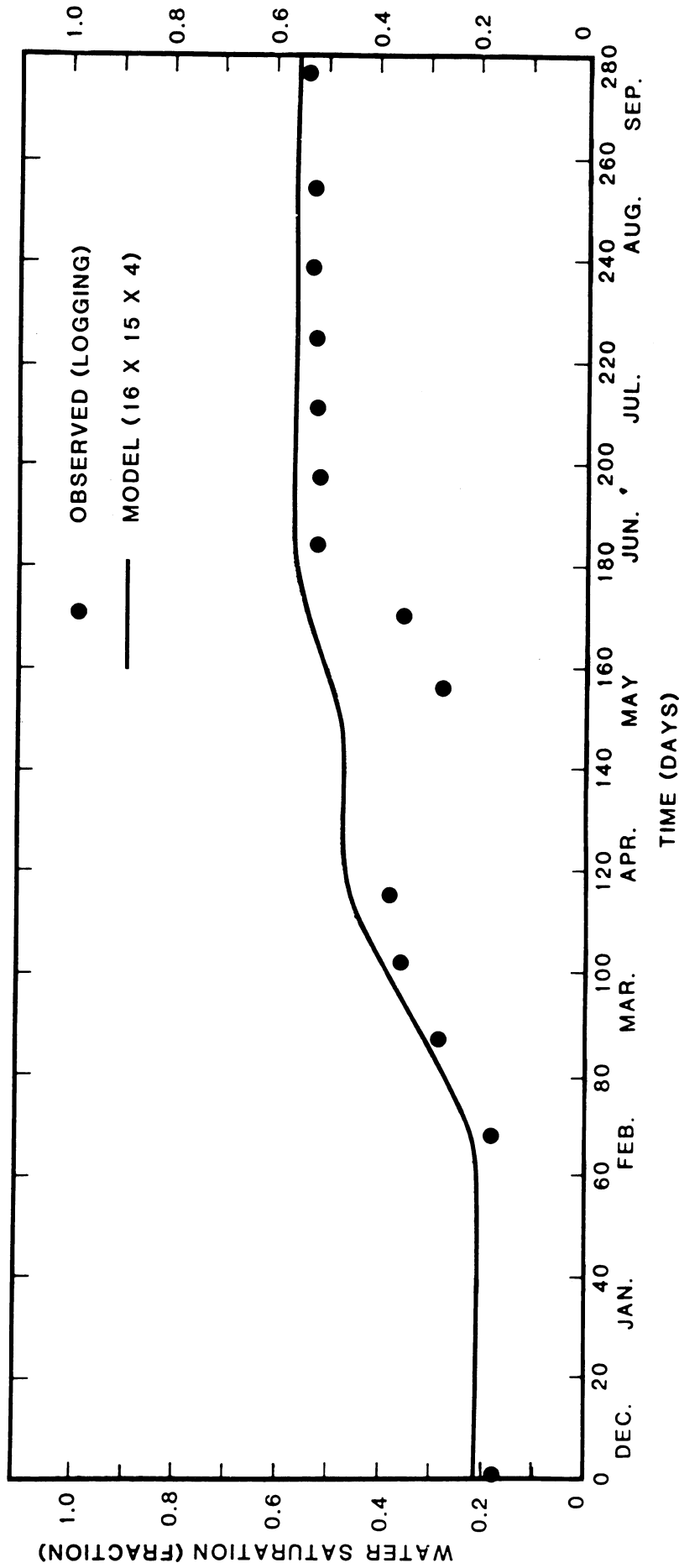


Fig. 115-Simulator match of water saturation history for zone D, layers X, Y and Z combined. Dots are observed logging data and the line is the simulation model match, December 11, 1980 to September 17, 1981 at observation well no. 1.

WATER SATURATION HISTORY MATCH FOR ZONE D (12-11-80 TO 9-17-81)
 ZABOLOITNY OBSERVATION WELL NO. 2

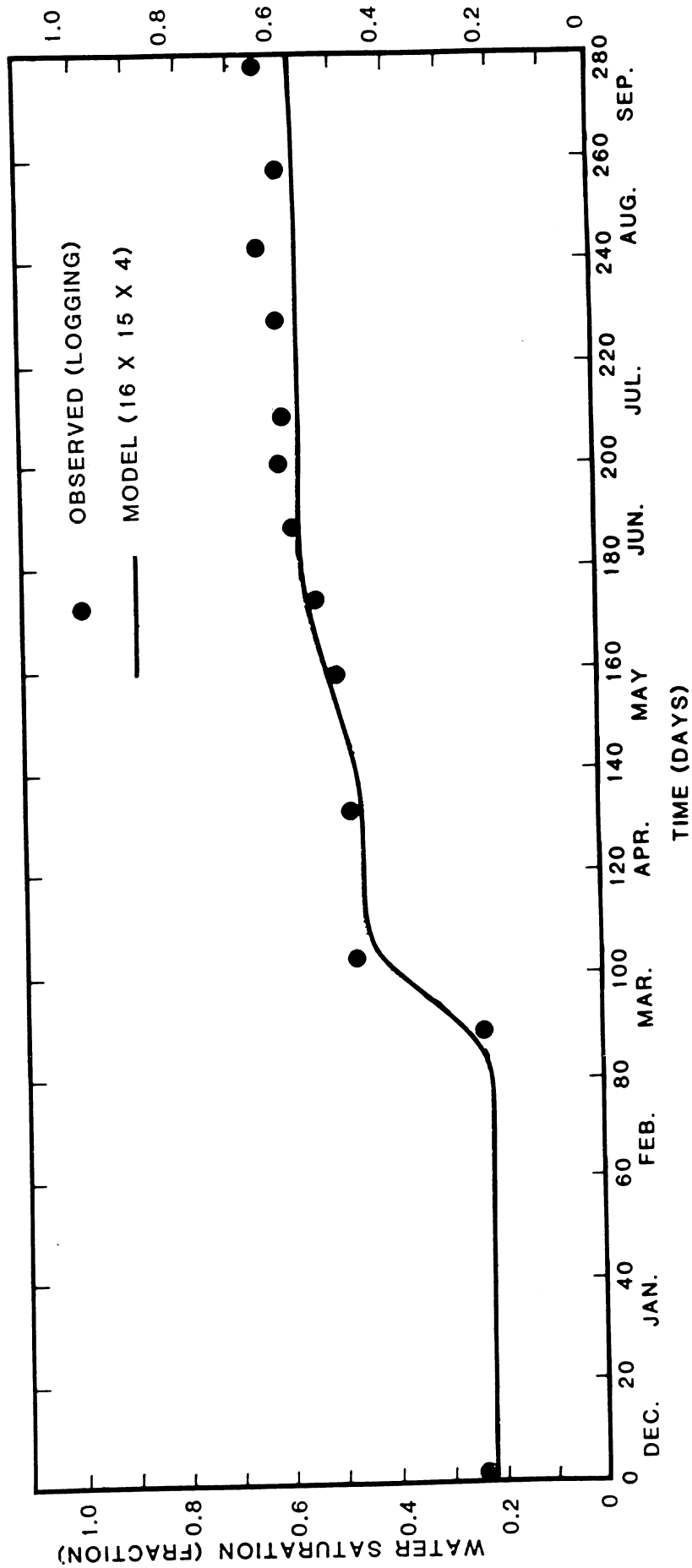


Fig. 116-Simulator match of water saturation history for zone D, layers X, Y and Z combined. Dots are observed logging data and the line is the simulation model match, December 11, 1980 to September 17, 1981 at observation well no. 2.

WATER SATURATION HISTORY MATCH FOR ZONE D (12-11-80 TO 9-17-81)
 ZABOLOTNY OBSERVATION WELL NO. 3

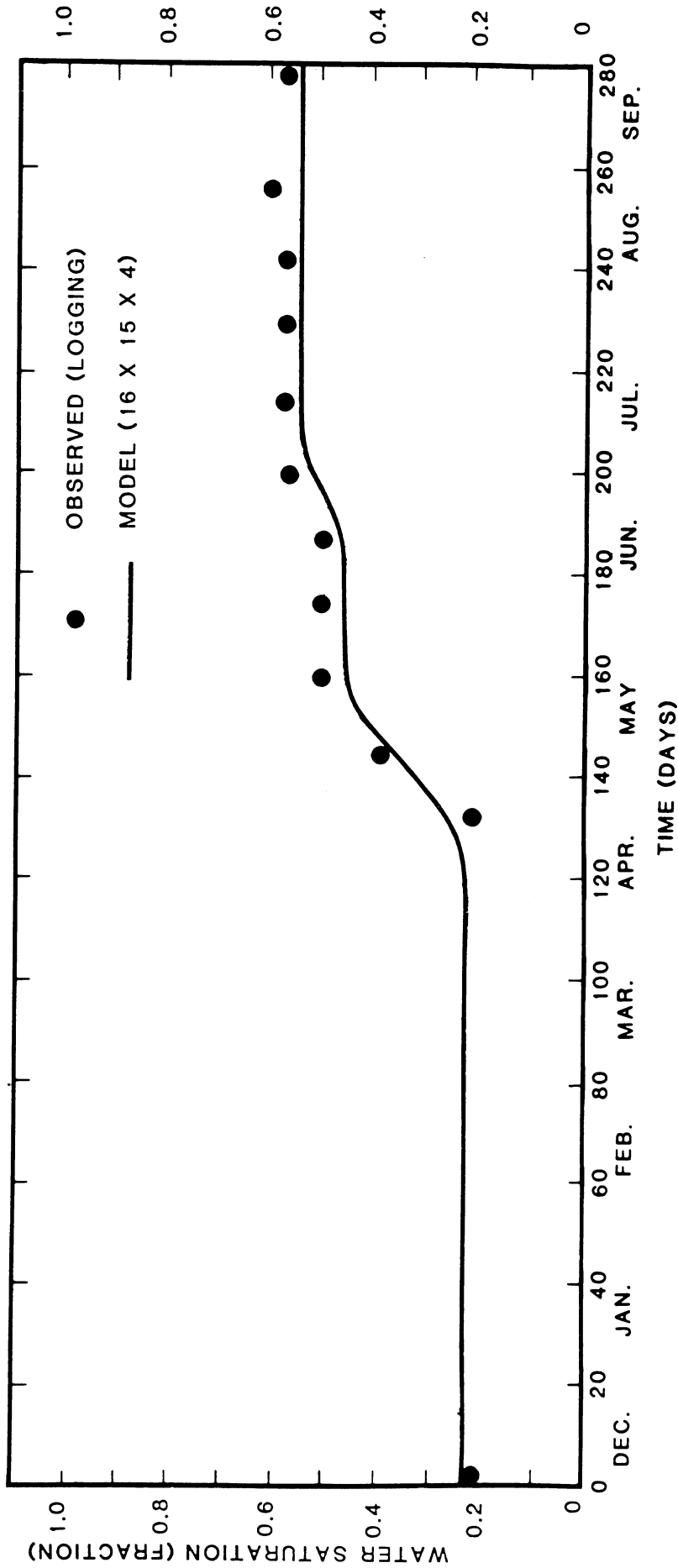


Fig. 117-Simulator match of water saturation history for zone D, layers X, Y and Z combined. Dots are observed logging data and the line is the simulation model match, December 11, 1980 to September 17, 1981 at observation well no. 3.

CO₂ CONTENT OF SEPARATOR GASES (N₂ & H₂S FREE BASIS)
(MOLE %)

MEASURED CARBON DIOXIDE CONTENTS FROM
LOGS, SEPARATOR GAS ANALYSIS, AND ISOTOPE ANALYSIS
ZABOLOTNY OBSERVATION WELL NO. 1
(12-11-80 TO 9-17-81)

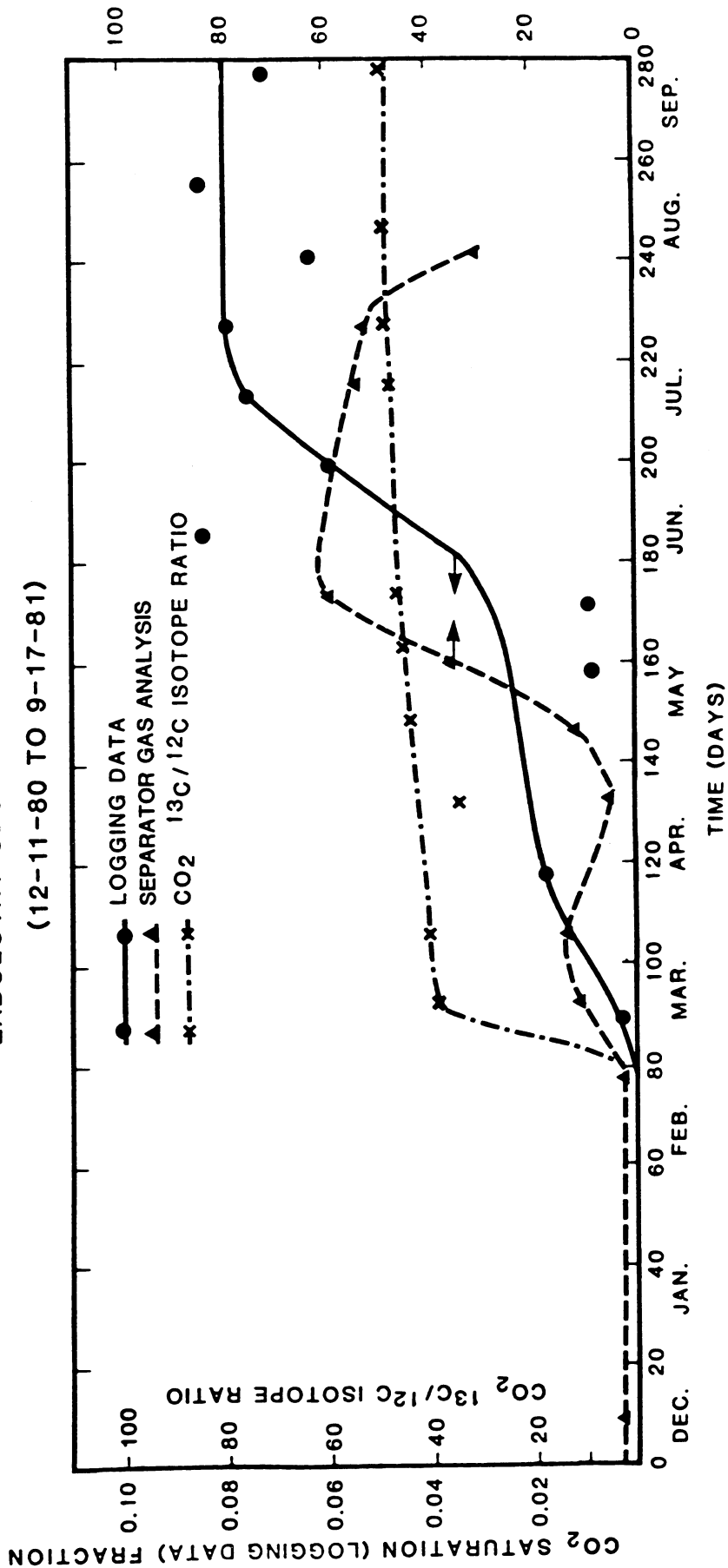


Fig. 118-Measured CO₂ contents from logs, separator gas analysis and isotope analysis vs. time, December 11, 1980 to September 17, 1981 at observation well no. 1.

MEASURED CARBON DIOXIDE CONTENTS FROM
LOGS, SEPARATOR GAS ANALYSIS, AND ISOTOPE ANALYSIS
ZABOLOTNY OBSERVATION WELL NO. 2
(12-11-80 TO 9-17-81)

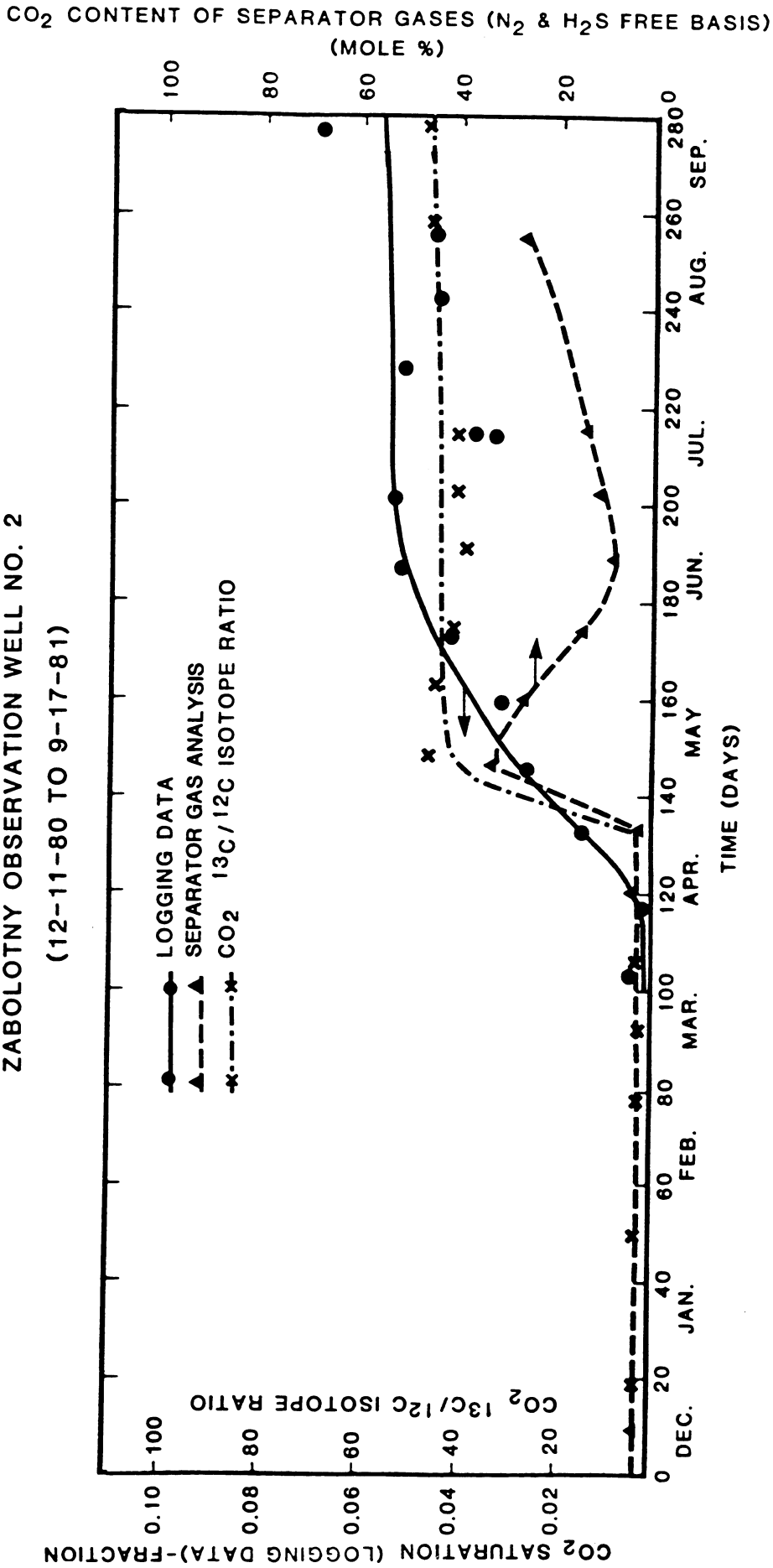


Fig. 119-Measured CO₂ contents from logs, separator gas analysis and isotope analysis vs. time, December 11, 1980 to September 17, 1981 at observation well no. 2.

MEASURED CARBON DIOXIDE CONTENTS FROM
 LOGS, SEPARATOR GAS ANALYSIS, AND ISOTOPE ANALYSIS
 ZABOLOTNY OBSERVATION WELL NO. 3
 (12-11-80 TO 9-17-81)

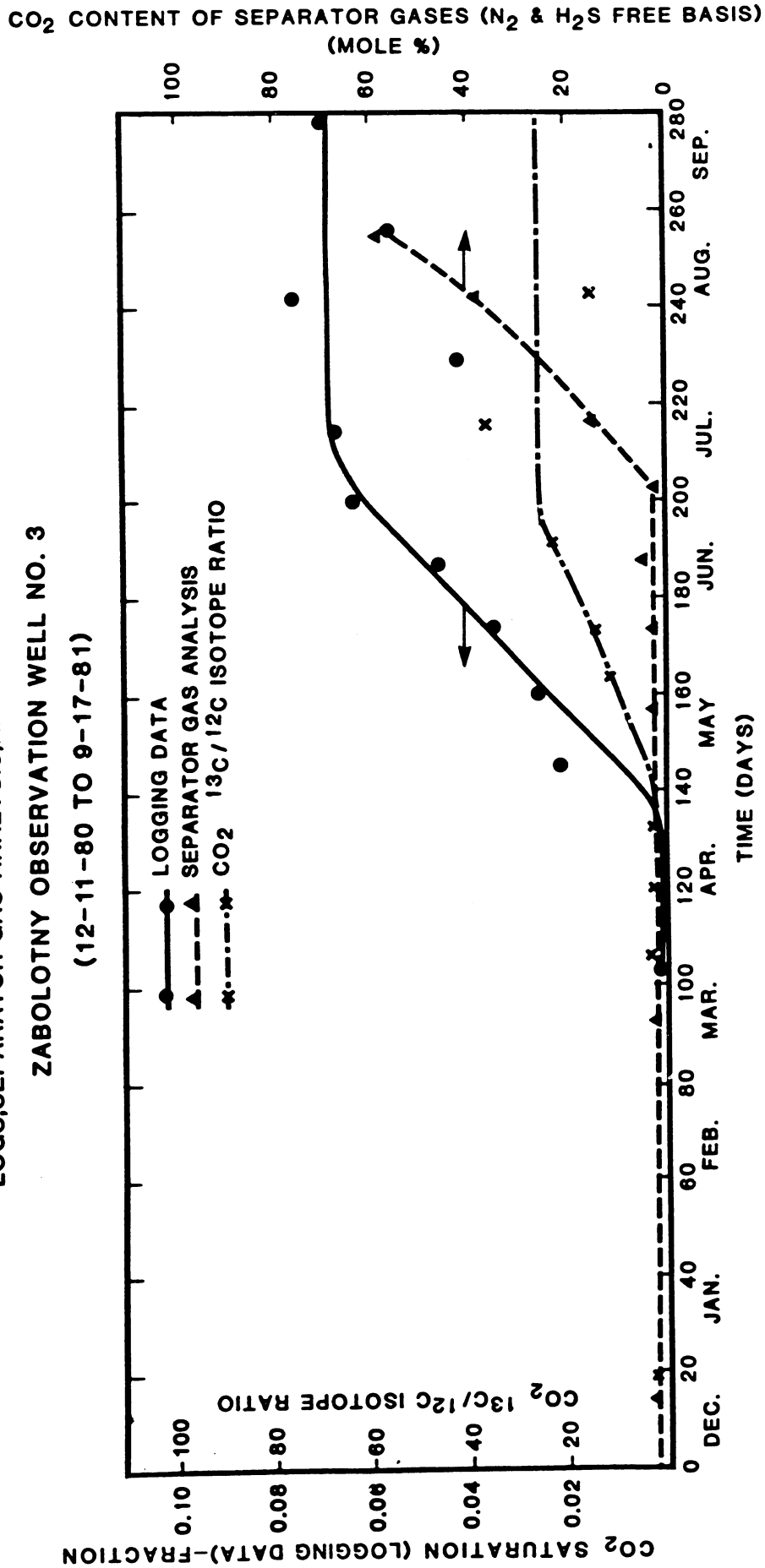


Fig. 120-Measured CO₂ contents from logs, separator gas analysis and isotope analysis vs. time, December 11, 1980 to September 17, 1981 at observation well no. 3.

CO₂ SATURATION HISTORY MATCH (12-11-80 TO 9-17-81)
 ZABOLOITNY OBSERVATION WELL NO. 1

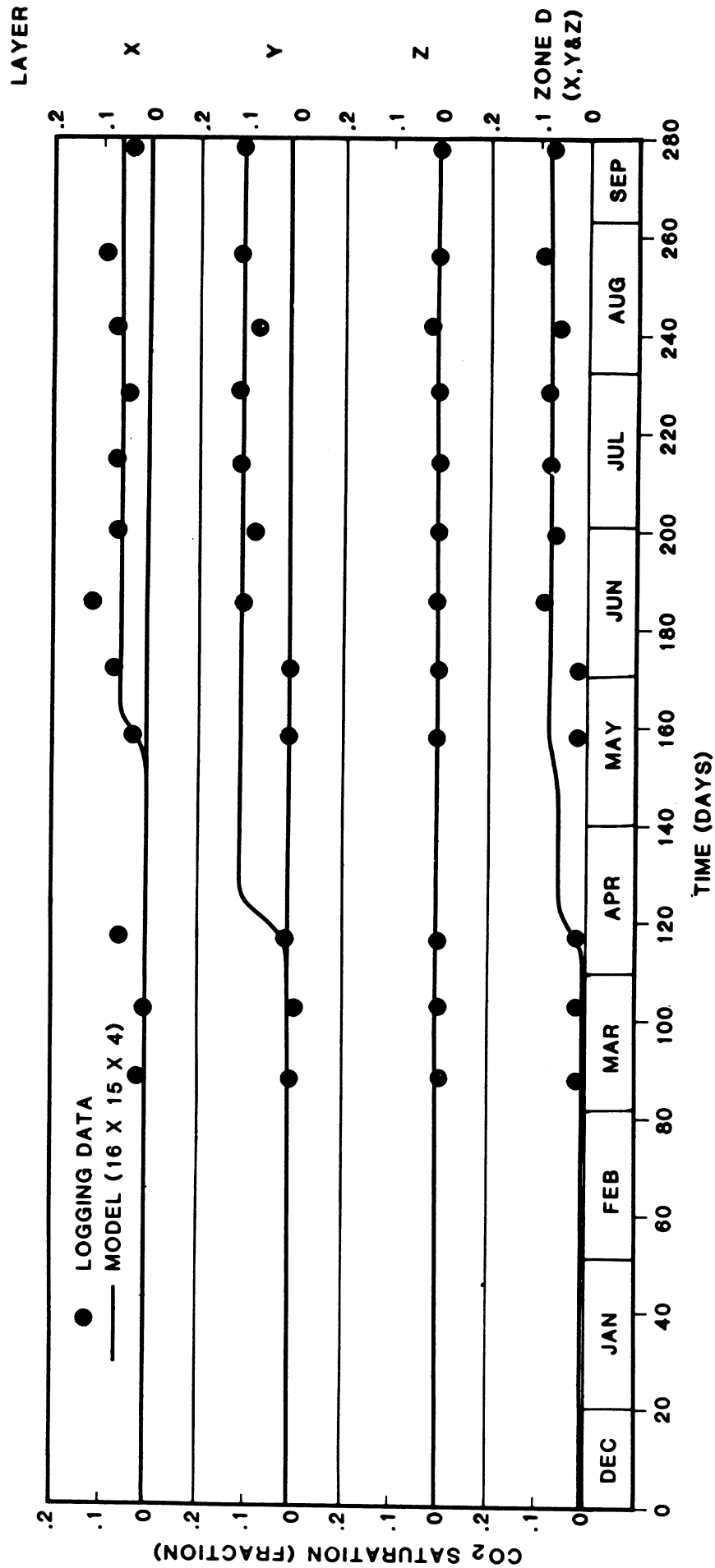


Fig. 121-CO₂ saturation history match. Dots are observed logging data and lines are the simulation model matches for layers X, Y and Z and zone D with layers X, Y and Z combined, December 11, 1980 to September 17, 1981 at observation well no. 1.

CO₂ SATURATION HISTORY MATCH (12-11-80 TO 9-17-81)
ZABOLOTNY OBSERVATION WELL NO. 2

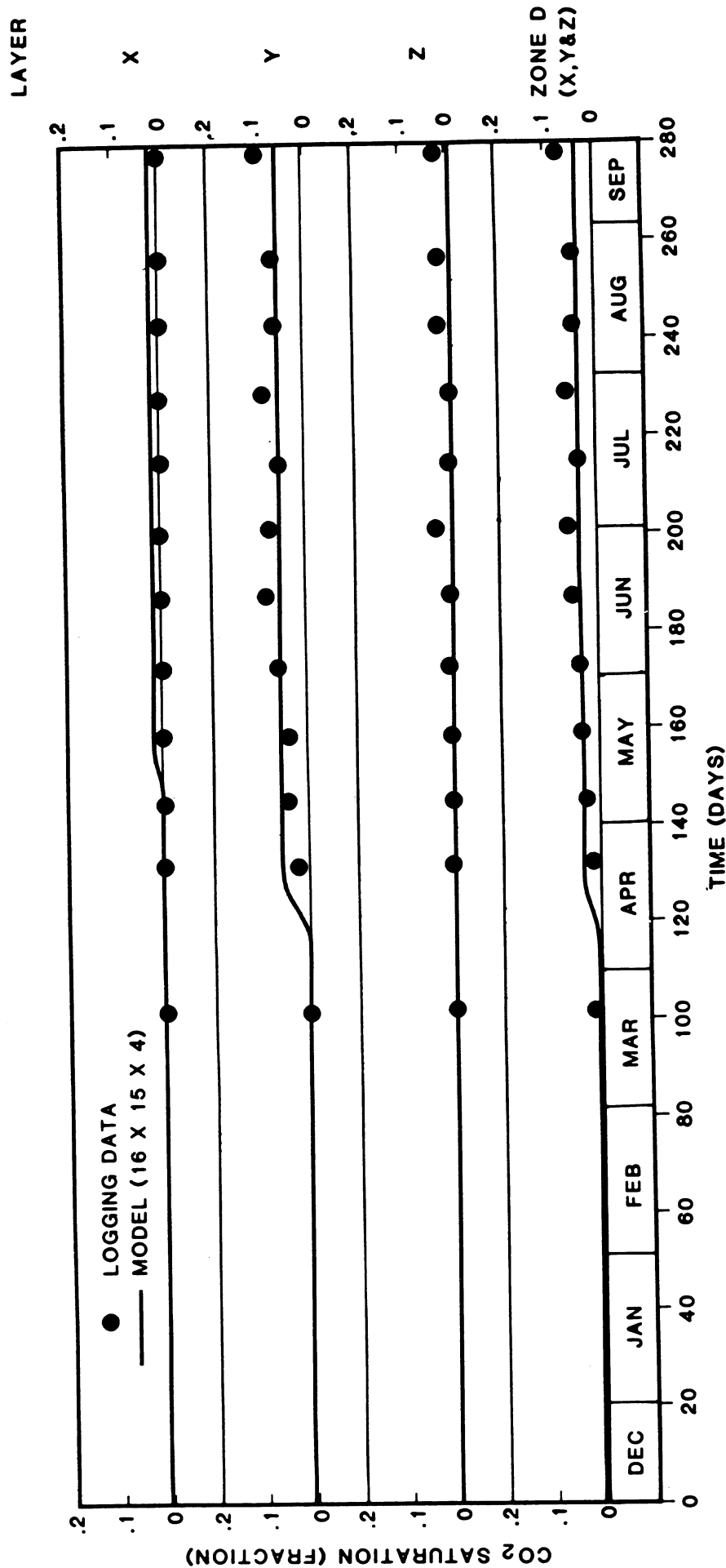


Fig. 122-CO₂ saturation history match. Dots are observed logging data and lines are the simulation model matches for layers X, Y and Z and zone D with layers X, Y and Z combined, December 11, 1980 to September 17, 1981 at observation well no. 2.

**CO₂ SATURATION HISTORY MATCH (12-11-80 TO 9-17-81)
ZABOLOTNY OBSERVATION WELL NO. 3**

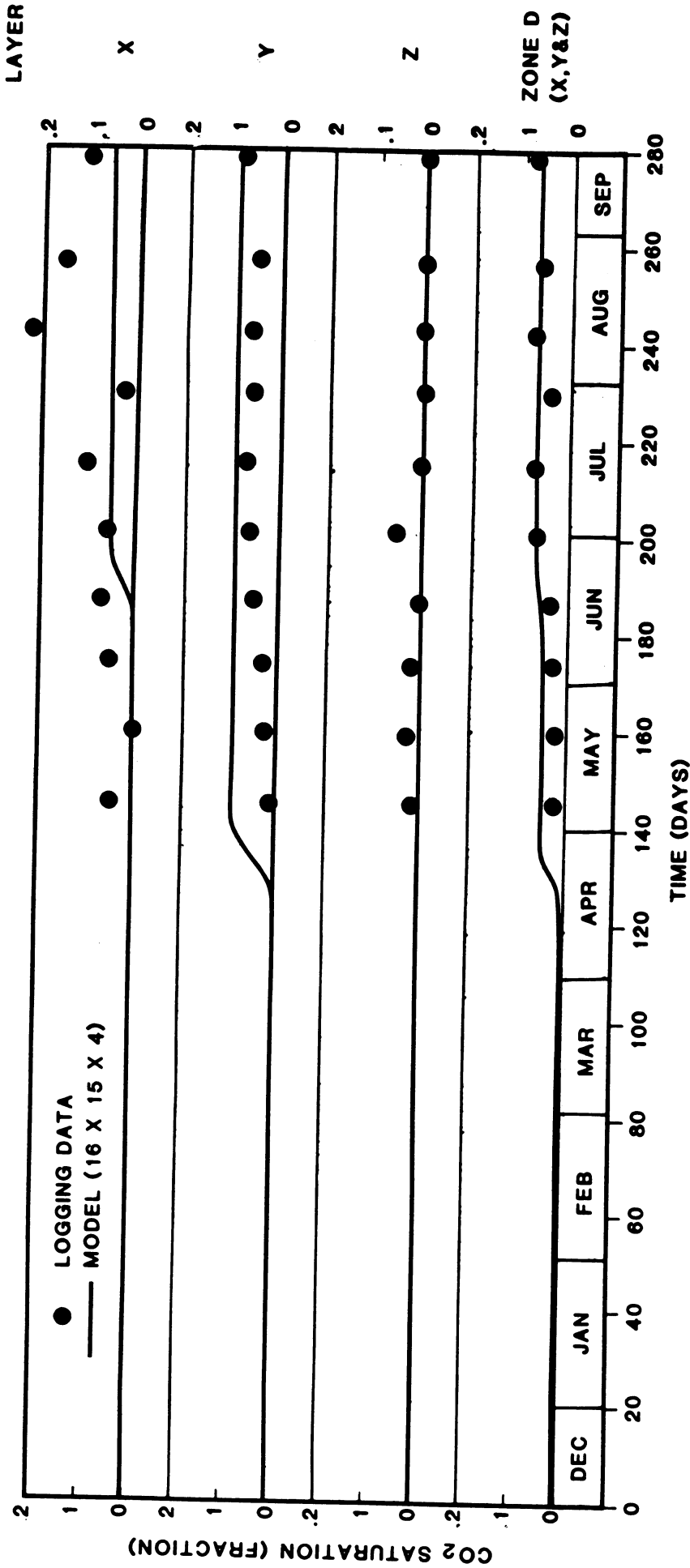


Fig. 123-CO₂ saturation history match. Dots are observed logging data and lines are the simulation model matches for layers X, Y and Z and zone D with layers X, Y and Z combined, December 11, 1980 to September 17, 1981 at observation well no. 3.

**SWELLING FACTORS OF OIL-CO₂ MIXTURES AT 245°F
ZABOLOTNY 1-3-4A WELL**

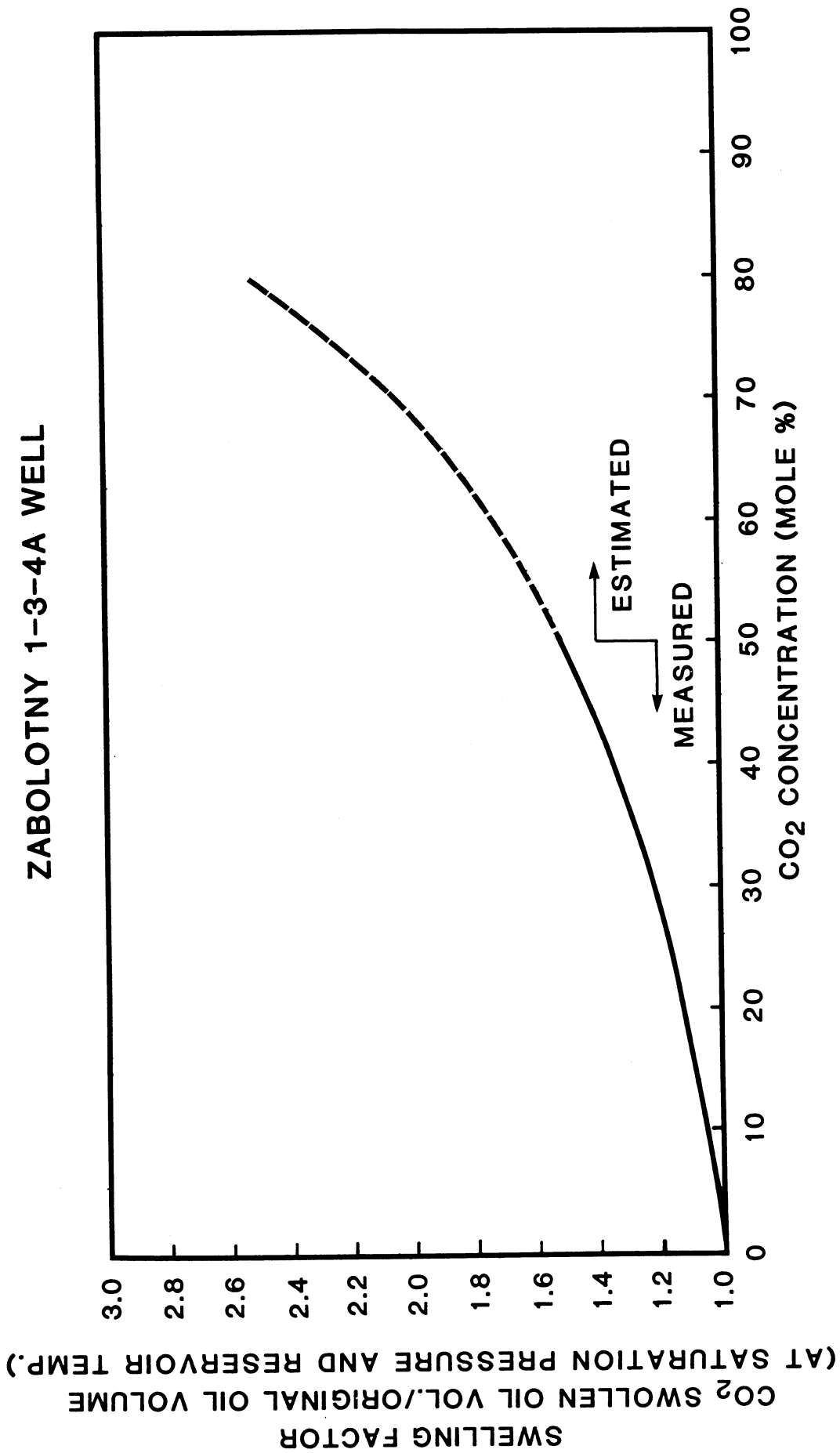


Fig. 124-Swelling factors of oil-CO₂ mixtures. CO₂ swollen oil volume/original oil volume vs. CO₂ concentration (mole percent) at 245°F, Zabolotny 1-3-4A.

OIL SATURATION HISTORY MATCH BY LAYERS (12-11-80 TO 9-17-81)
ZABOLOTNY OBSERVATION WELL NO. 1

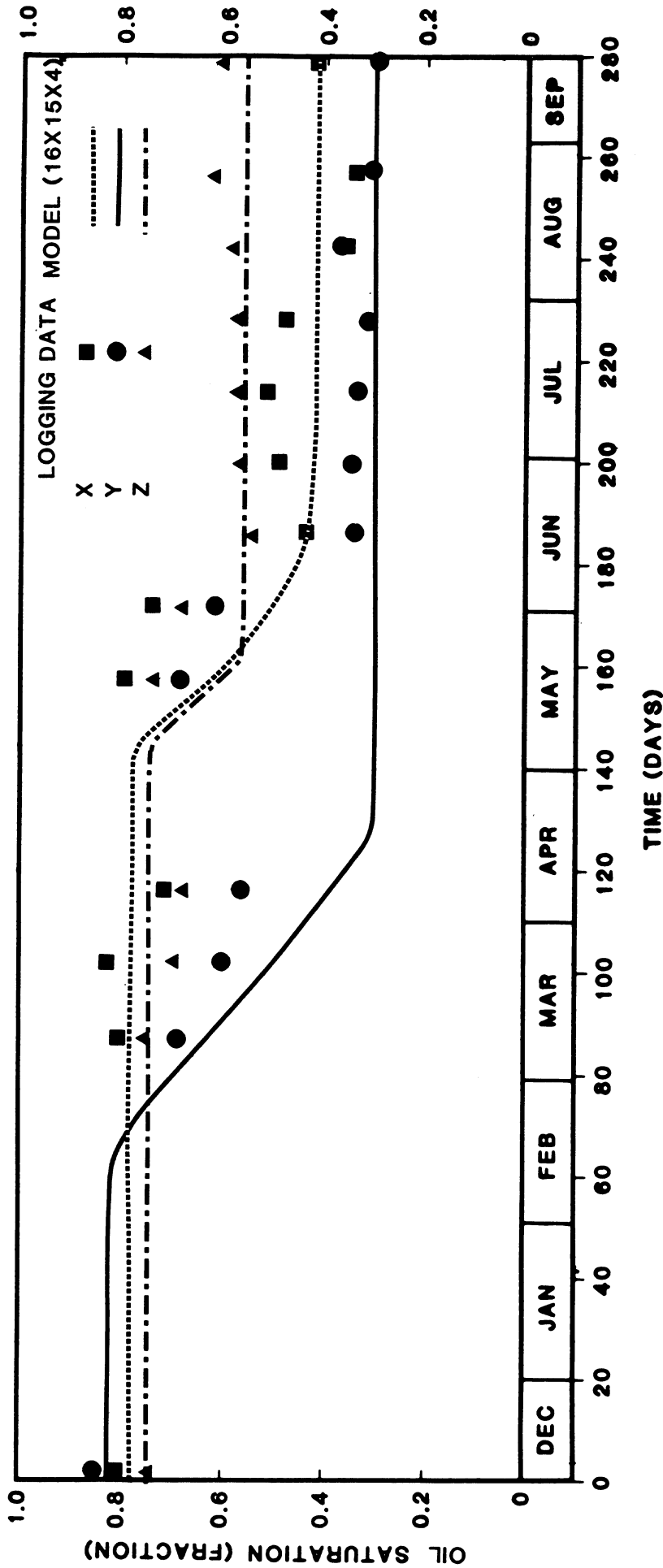


Fig. 125-011 saturation history match for layers X, Y and Z. Dots, squares and triangles are logging data and lines are the simulation model matches, December 11, 1980 to September 17, 1981 at observation well no. 1.

OIL SATURATION HISTORY MATCH BY LAYERS (12-11-80 TO 9-17-81)
ZABOLOTNY OBSERVATION WELL NO. 2

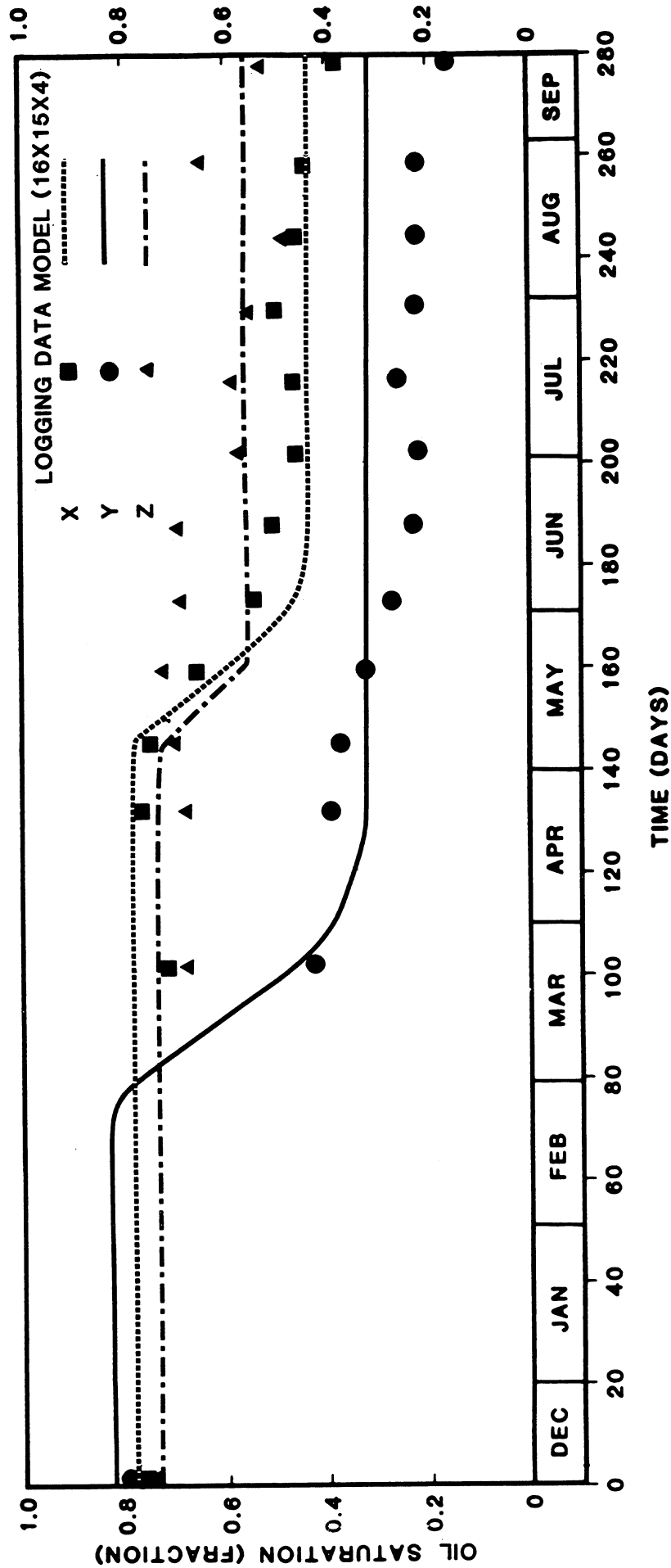


Fig. 126-Oil saturation history match for layers X, Y and Z. Dots, squares and triangles are logging data and lines are the simulation model matches, December 11, 1980 to September 17, 1981 at observation well no. 2.

OIL SATURATION HISTORY MATCH BY LAYERS (12-11-80 TO 9-17-81)
ZABOLOTNY OBSERVATION WELL NO. 3

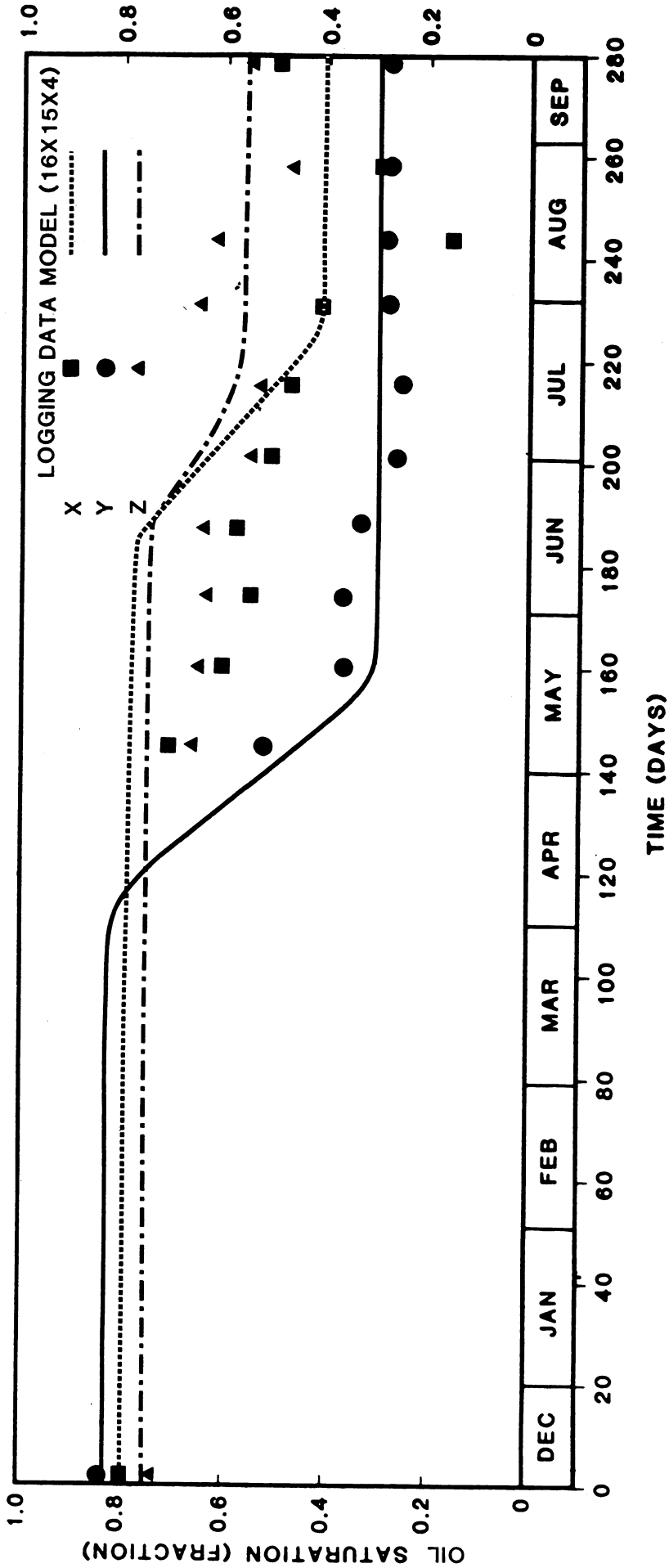


Fig. 127-Oil saturation history match for layers X, Y and Z. Dots, squares and triangles are logging data and lines are the simulation model matches, December 11, 1980 to September 17, 1981 at observation well no. 3.

**OIL SATURATION HISTORY MATCH FOR ZONE D (12-11-80 TO 9-17-81)
ZABOLOTNY OBSERVATION WELL NO. 1**

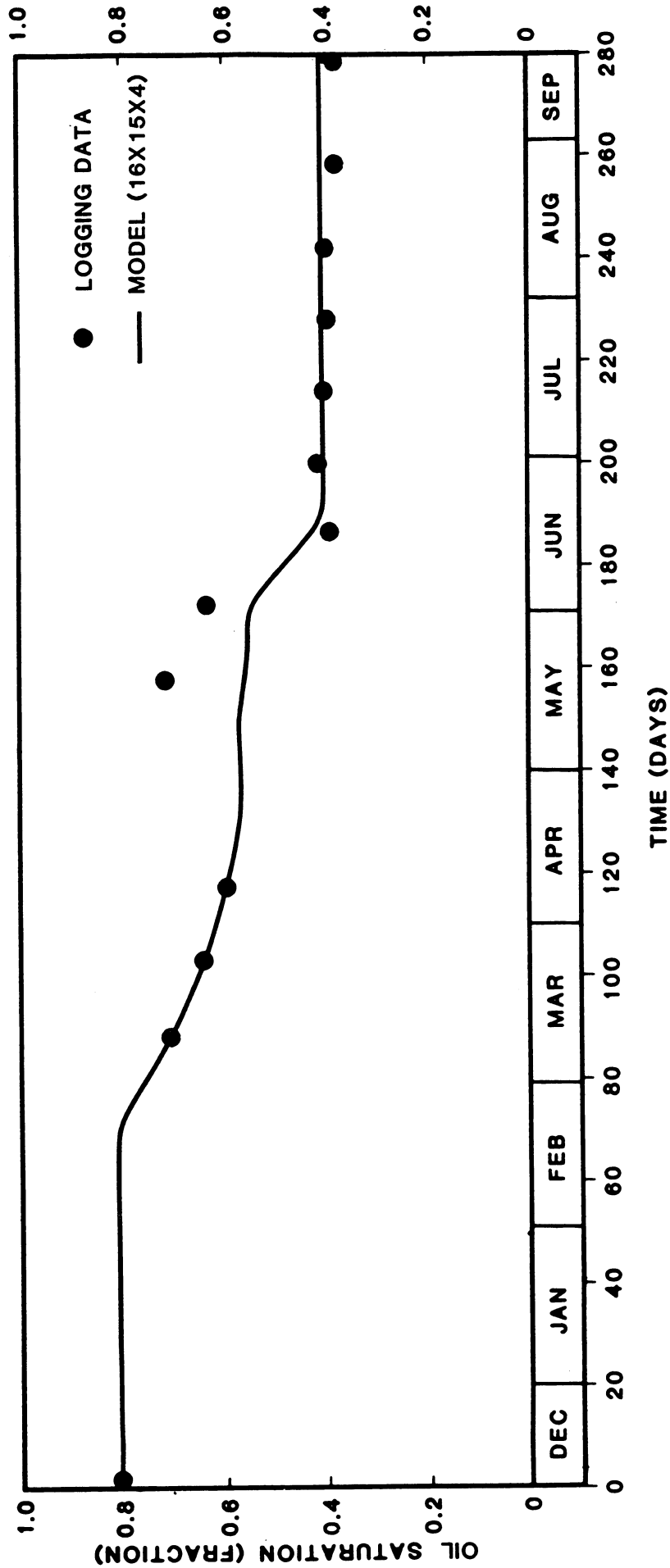


Fig. 128--Oil saturation history match for zone D, layers X, Y and Z combined. Dots are logging data and the line is the simulation model match, December 11, 1980 to September 17, 1981 at observation well no. 1.

OIL SATURATION HISTORY MATCH FOR ZONE D (12-11-80 TO 9-17-81)
 ZABOLOTNY OBSERVATION WELL NO. 2

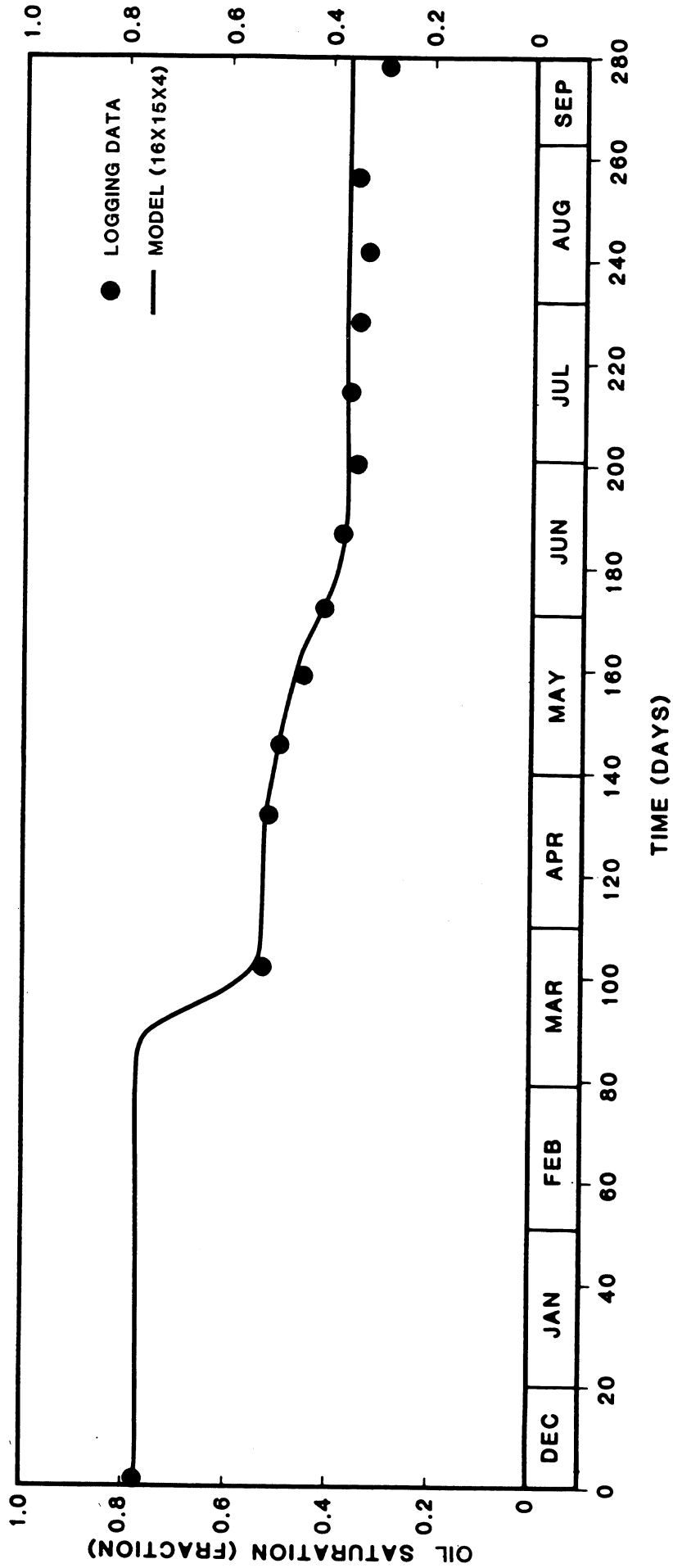


Fig. 129-Oil saturation history match for zone D, layers X, Y and Z combined. Dots are logging data and the line is the simulation model match, December 11, 1980 to September 17, 1981 at observation well no. 2.

OIL SATURATION HISTORY MATCH FOR ZONE D (12-11-80 TO 9-17 -81)

ZABOLOTNY OBSERVATION WELL NO. 3

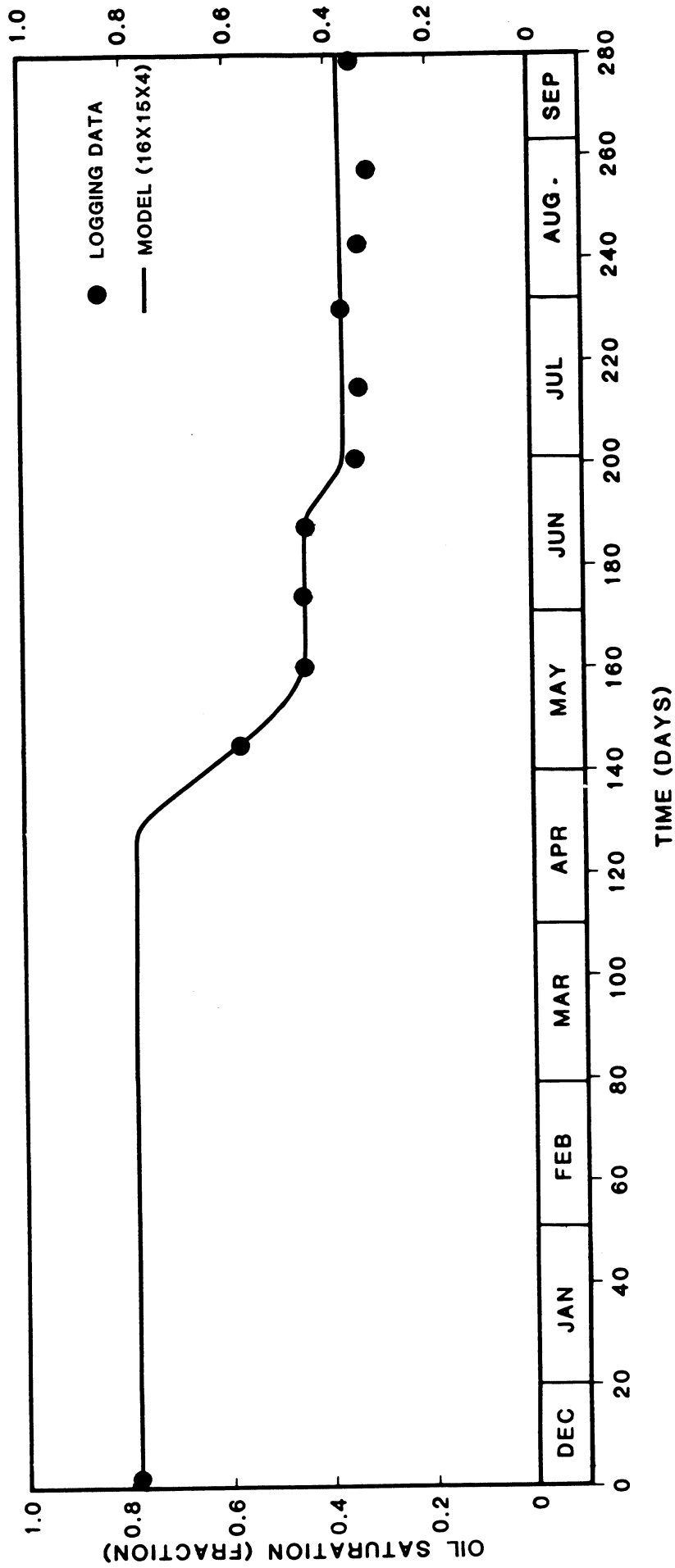


Fig. 130-Oil saturation history match for zone D, layers X, Y and Z combined. Dots are logging data and the line is the simulation model match, December 11, 1980 to September 17, 1981 at observation well no. 3.

CO₂-FREE OIL SATURATION (AT RESERVOIR CONDITIONS)
PROFILE ON JULY 17, 1981
FOUR LAYER MODEL
ZABOLOTNY OBSERVATION WELL NO. 4

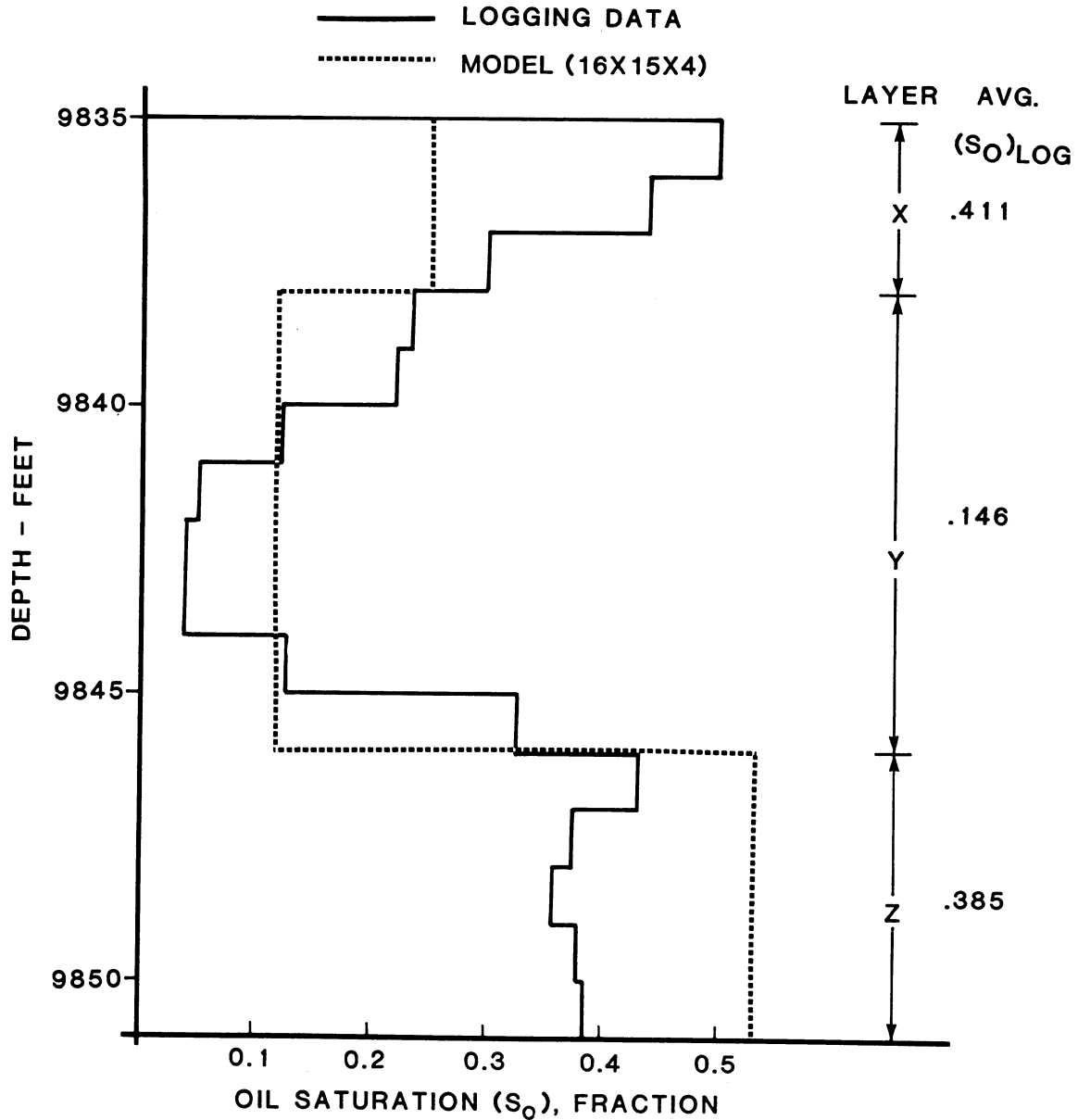


Fig. 131-CO₂-free oil saturation profile at reservoir conditions for layers X, Y and Z. Solid line is logging data and dashed line is simulation modeling, on July 17, 1981 at observation well no. 4.

**OIL SATURATION (AT STOCK TANK CONDITIONS)
 JULY 17, 1981
 FOUR LAYER MODEL
 ZABOLOTNY OBSERVATION WELL NO. 4**

PRESSURE CORE DATA
 MODEL (16 X 15 X 4)

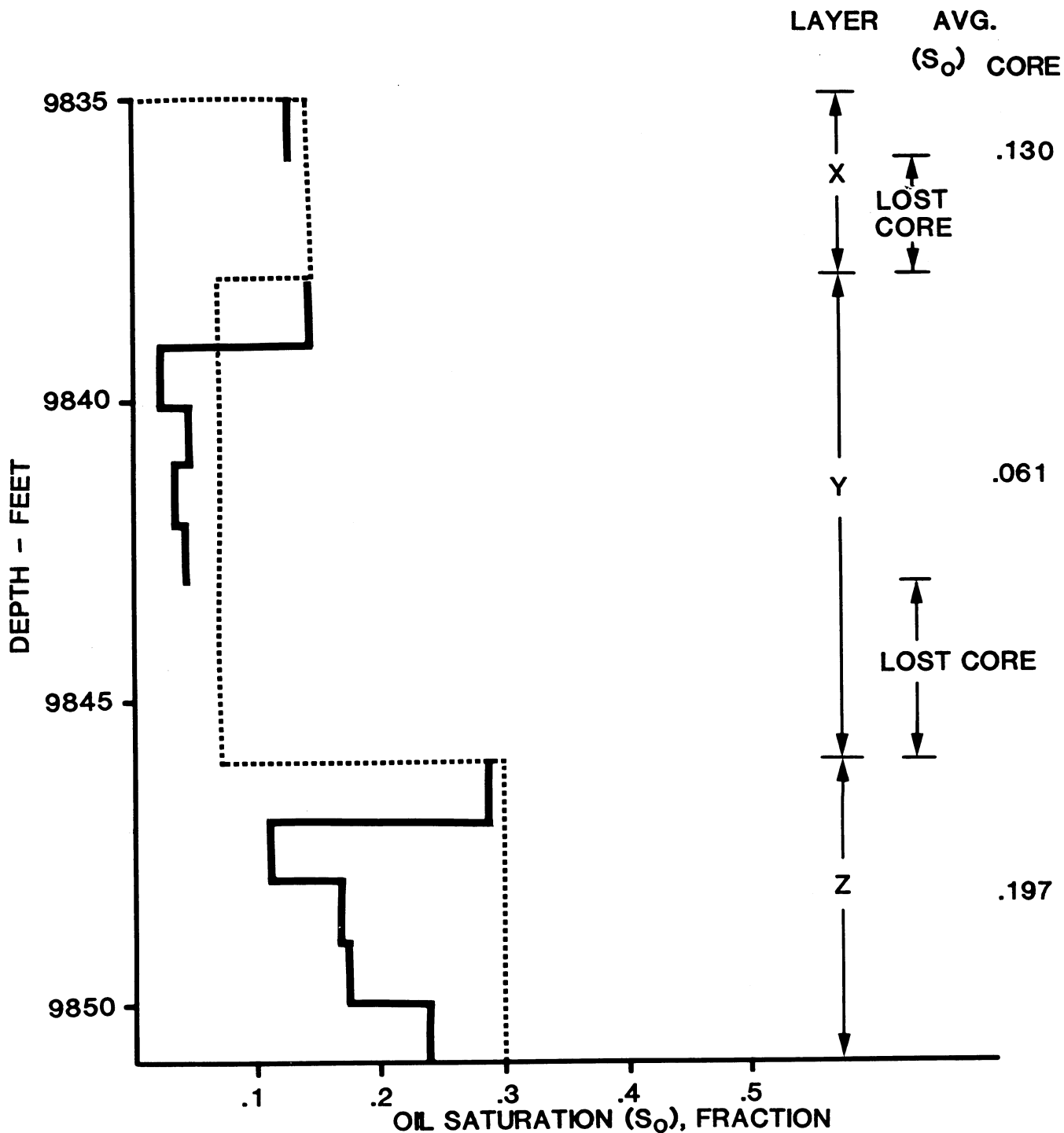


Fig. 132-Oil saturation profile at stock tank conditions for layers X, Y and Z. Solid line is pressure core data and dashed line is simulation modeling, on July 17, 1981 at observation well no. 4.

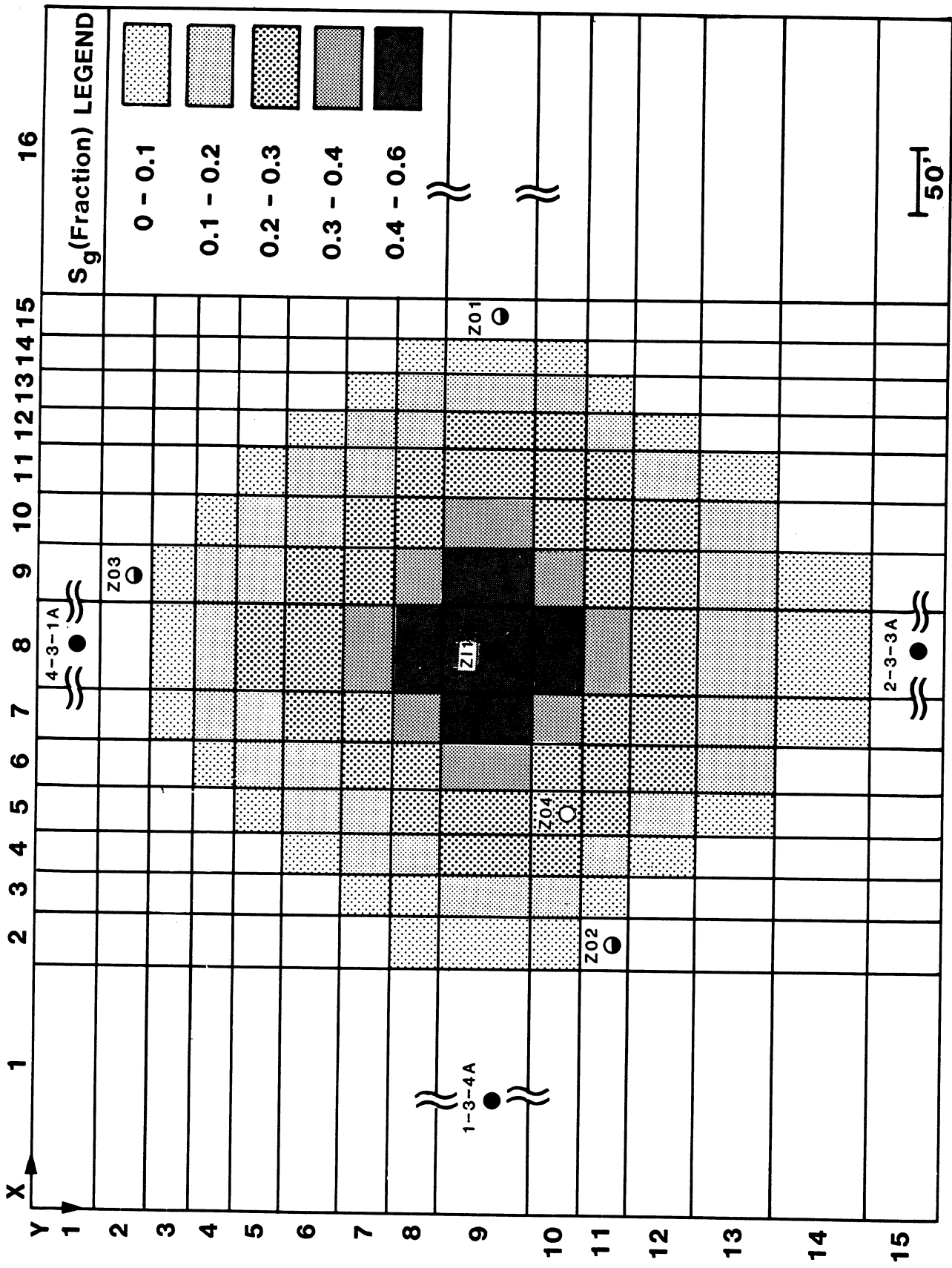


Fig. 133-Gas saturation distribution for layer Y at the end of CO₂ injection, March 25, 1981.

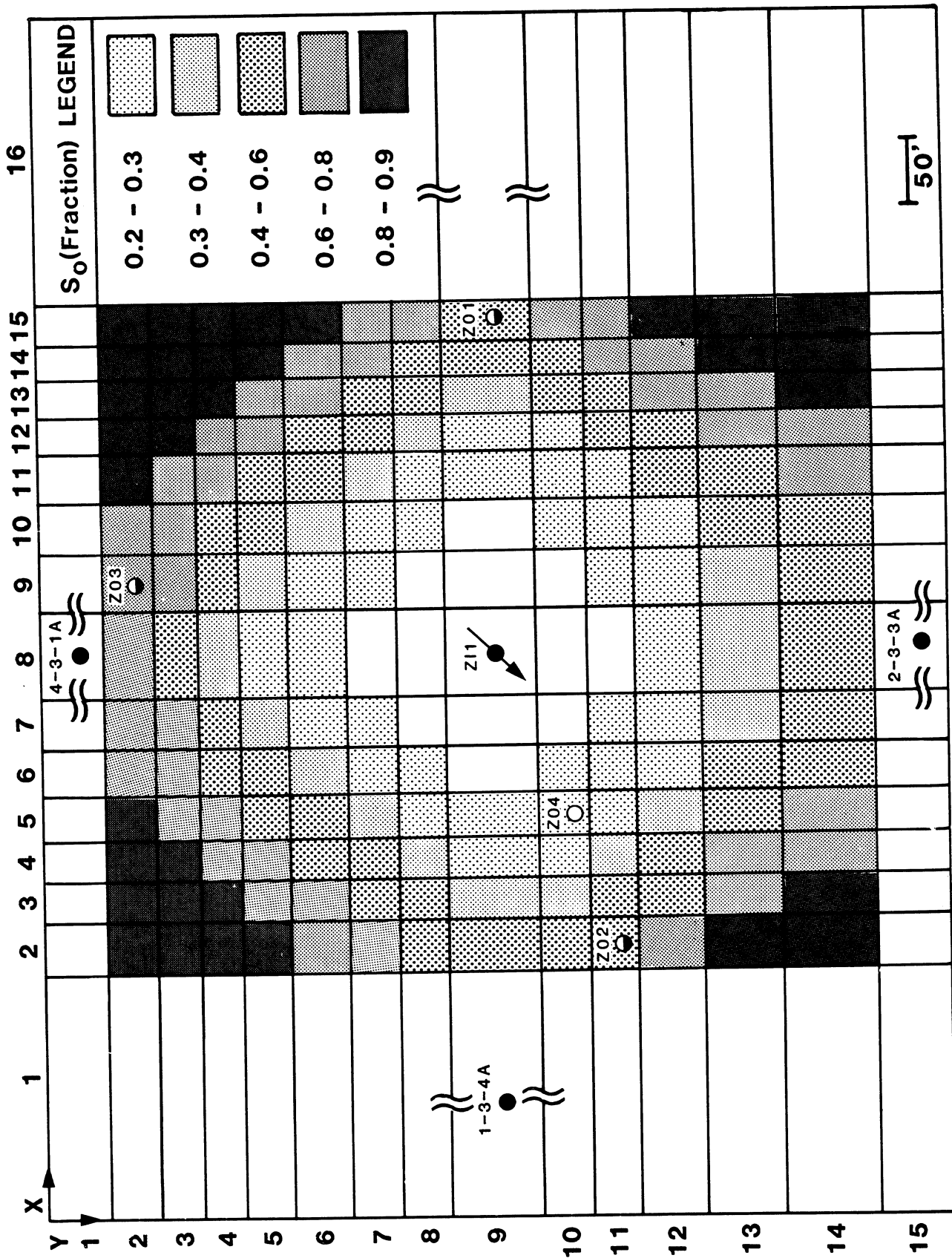


Fig. 134-Oil saturation distribution for layer Y at the end of CO₂ injection, March 25, 1981.

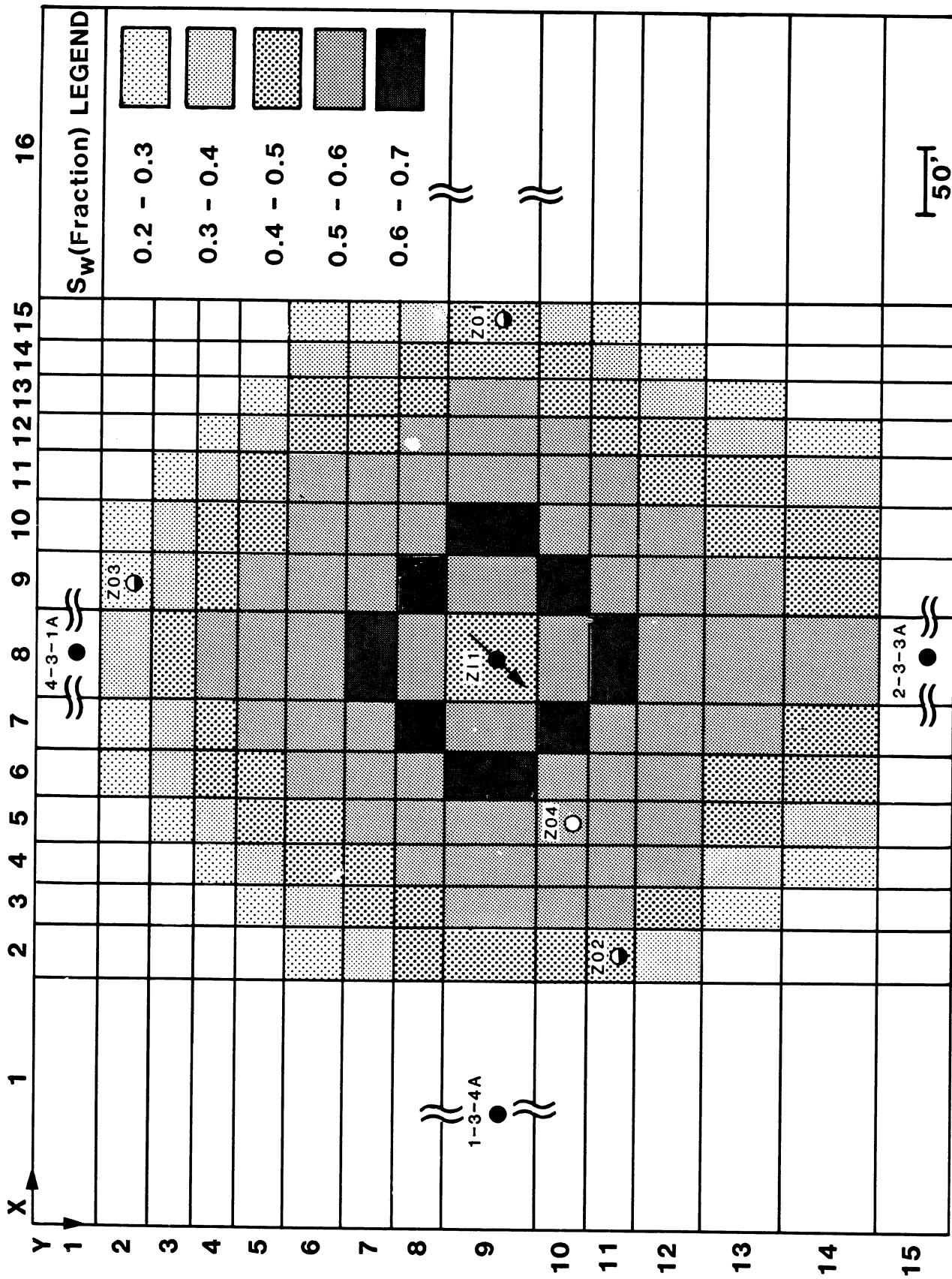


Fig. 135-Water saturation distribution for layer Y at the end of CO₂ injection, March 25, 1981.

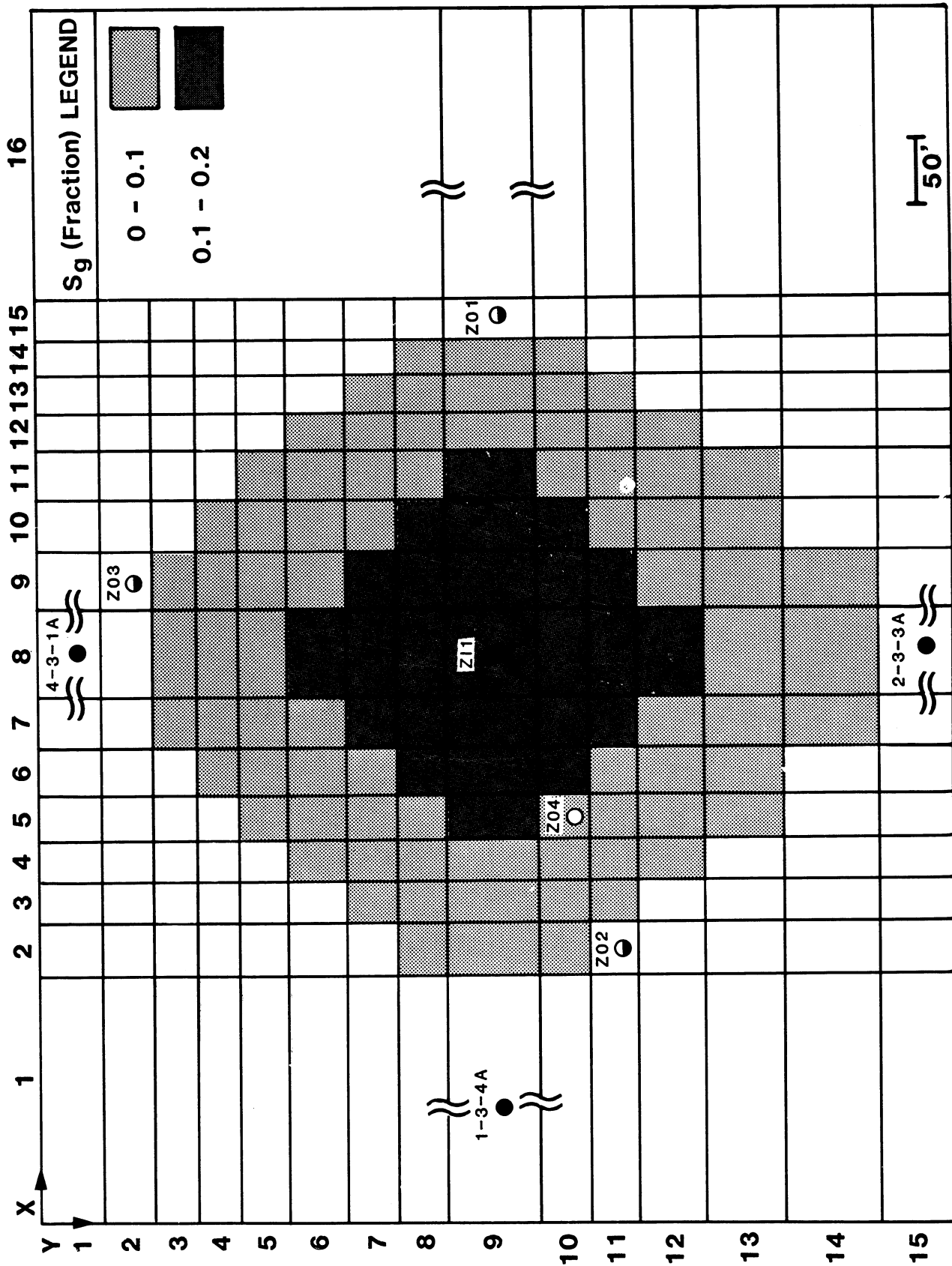


Fig. 136-Gas saturation distribution for layer Y on July 17, 1981.

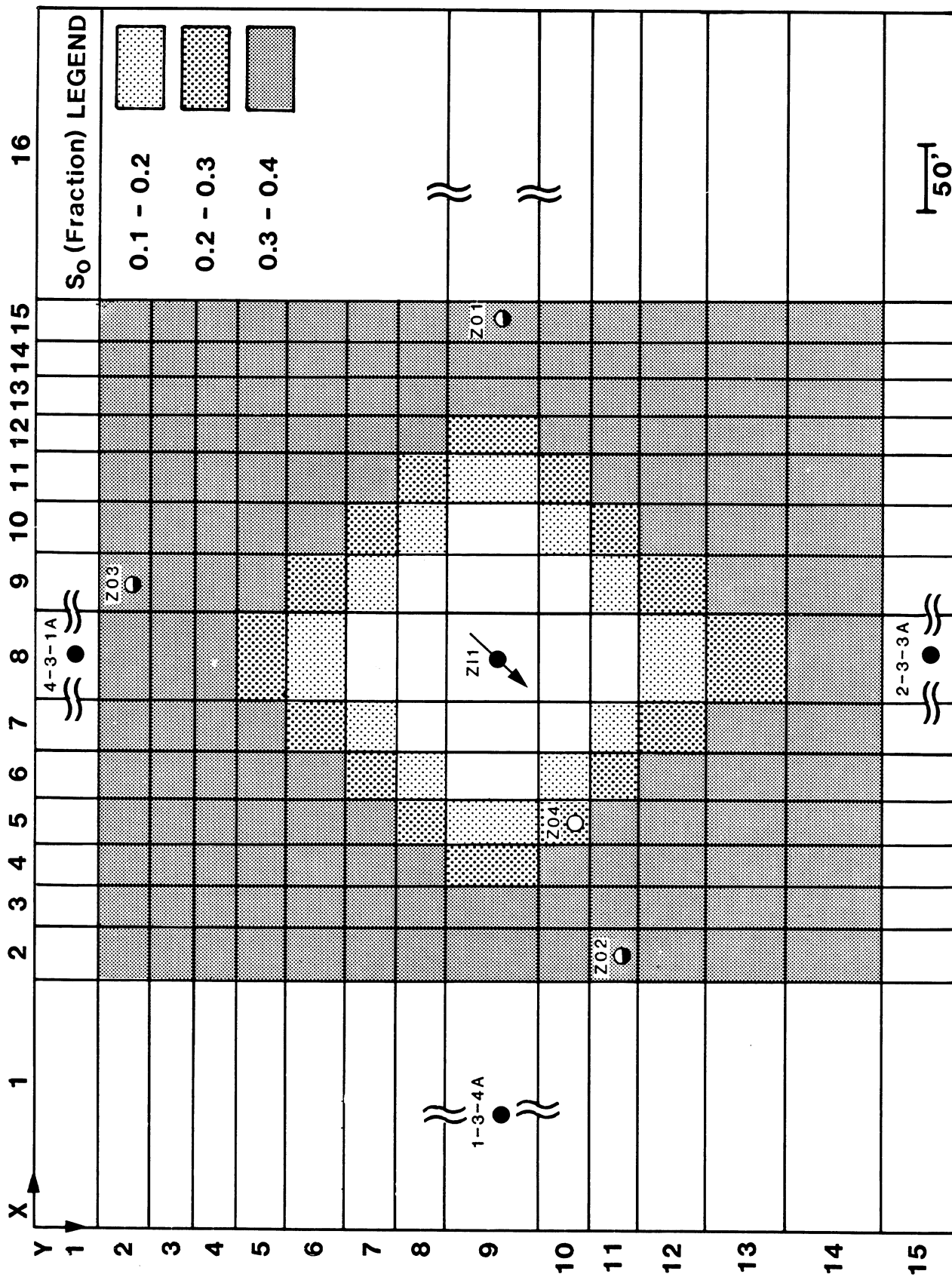


Fig. 137-Oil saturation distribution for layer Y on July 17, 1981.

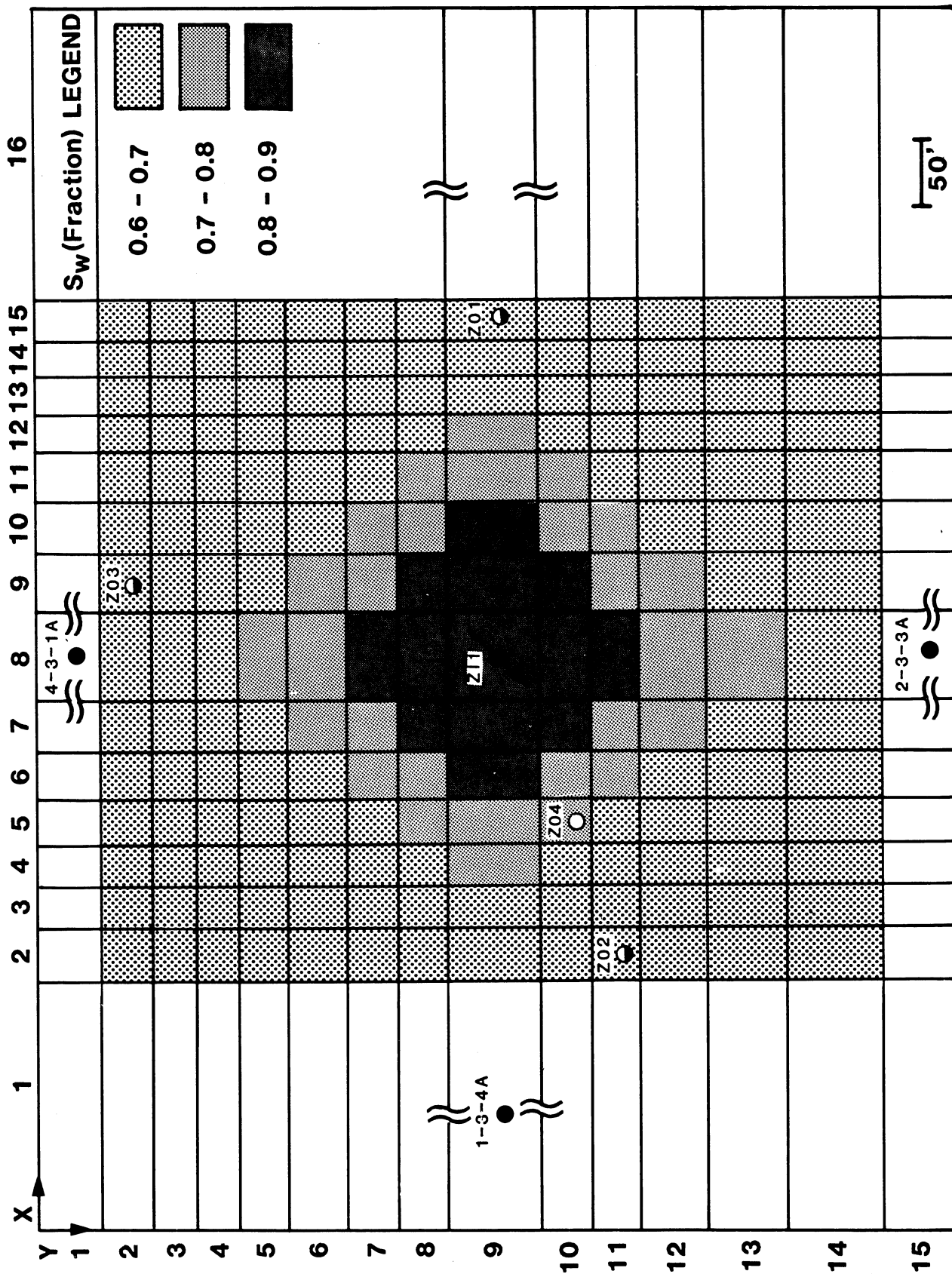


Fig. 138-Water saturation distribution for layer Y on July 17, 1981.

**OIL RECOVERY FROM THE MINITEST AREA
BY PRODUCING ALL THREE OBSERVATION WELLS**

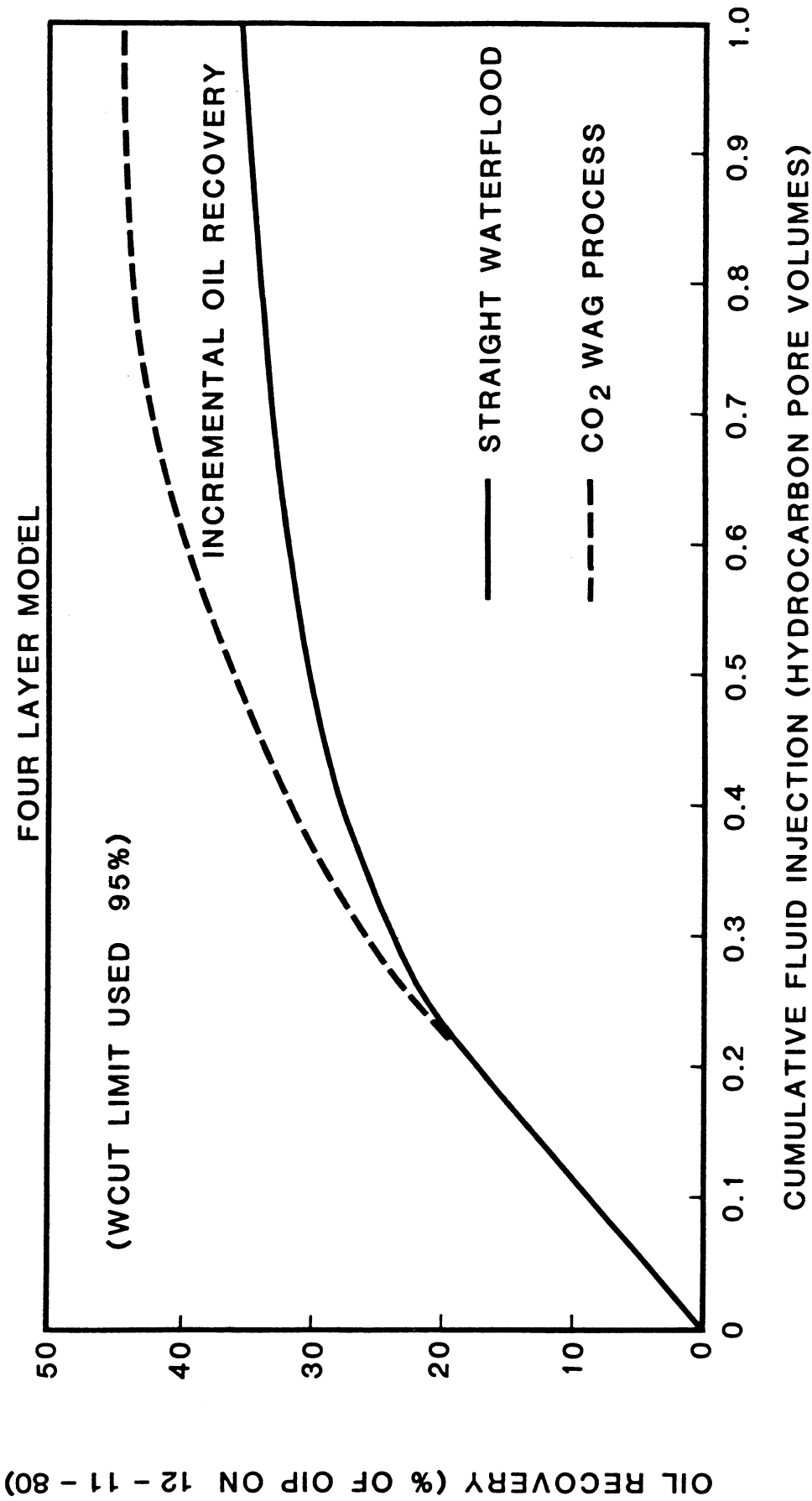


Fig. 140-Oil recovery from the minitest area by simulating production at observation wells no. 1, 2 and 3. Solid line for a straight waterflood and dashed line for the CO₂ WAG process (four-layer model).

WATER SATURATION HISTORY MATCH FOR LAYER Y (12-11-80 TO 9-17-81)

SIX LAYER MODEL

ZABOLOTNY OBSERVATION WELL NO. 2

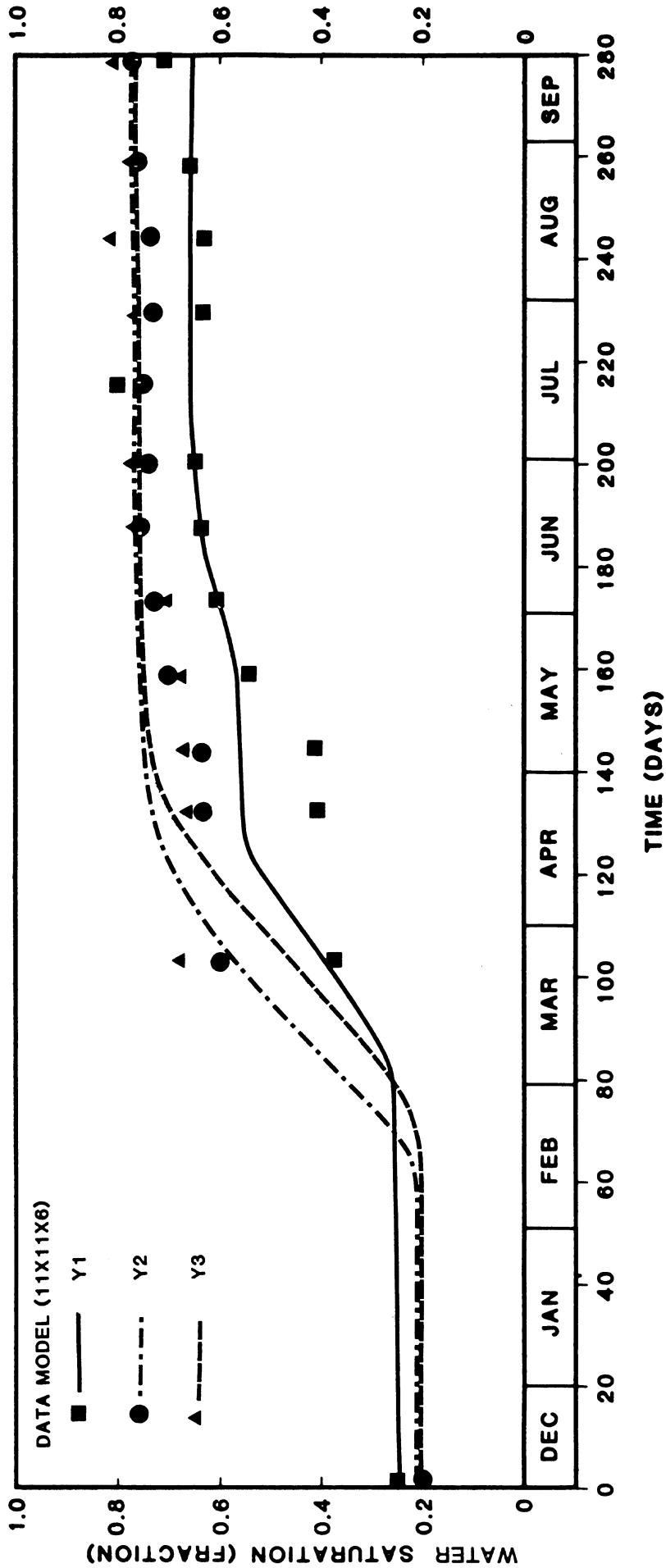


Fig. 141-Water saturation history match for layer Y, divided into sub-layers Y₁, Y₂ and Y₃. Six-layer model. December 11, 1980 to September 17, 1981 at observation well no. 2.

CARBON DIOXIDE SATURATION HISTORY MATCH FOR LAYER Y (12-11-80 TO 9-17-81)
 ZABLOTNY OBSERVATION WELL NO. 2

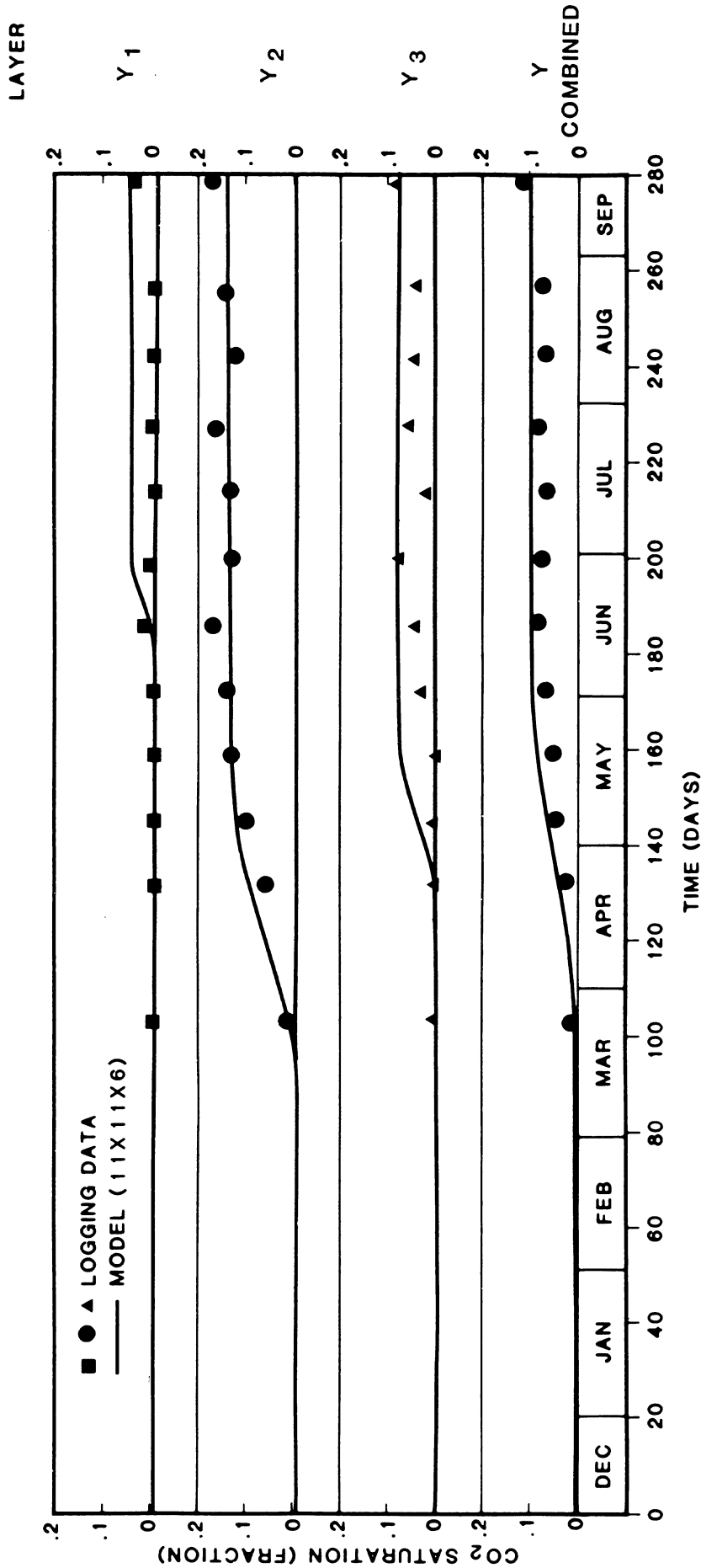


Fig. 142-CO₂ saturation history match for layer Y, divided into sub-layers Y₁, Y₂ and Y₃. Six-layer model. December 11, 1980 to September 17, 1981 at observation well no. 2.

OIL SATURATION HISTORY MATCH FOR LAYER Y (12-11-80 TO 9-17-81)

SIX LAYER MODEL

ZABOLOTNY OBSERVATION WELL NO. 2

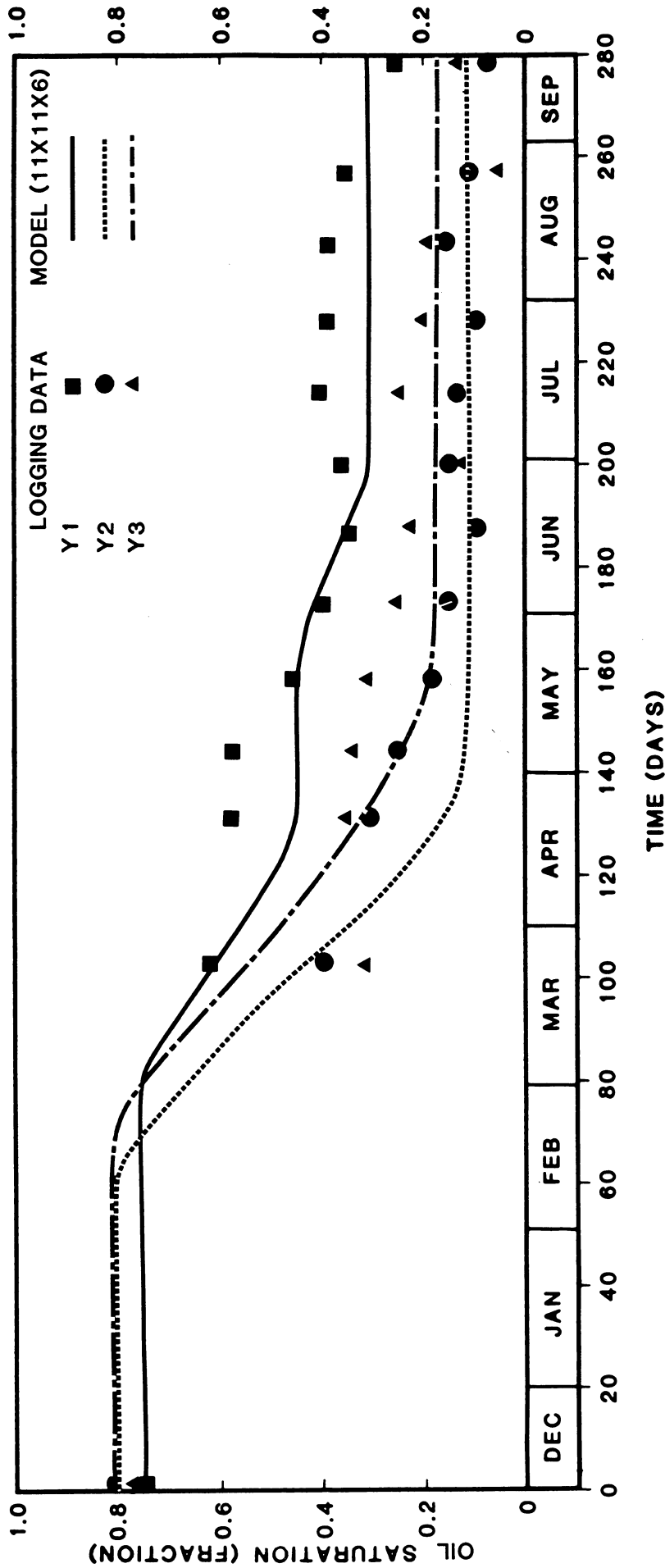


Fig. 143-Oil saturation history match for layer Y, divided into sub-layers Y₁, Y₂ and Y₃. Six-layer model. Squares, dots and triangles are logging data and lines are simulation model matches, December 11, 1980 to September 17, 1981 at observation well no. 2.

WATER SATURATION HISTORY MATCH FOR LAYER Y (12-11-80 TO 9-17-81)

SIX LAYER MODEL

ZABOLOTNY OBSERVATION WELL NO. 2

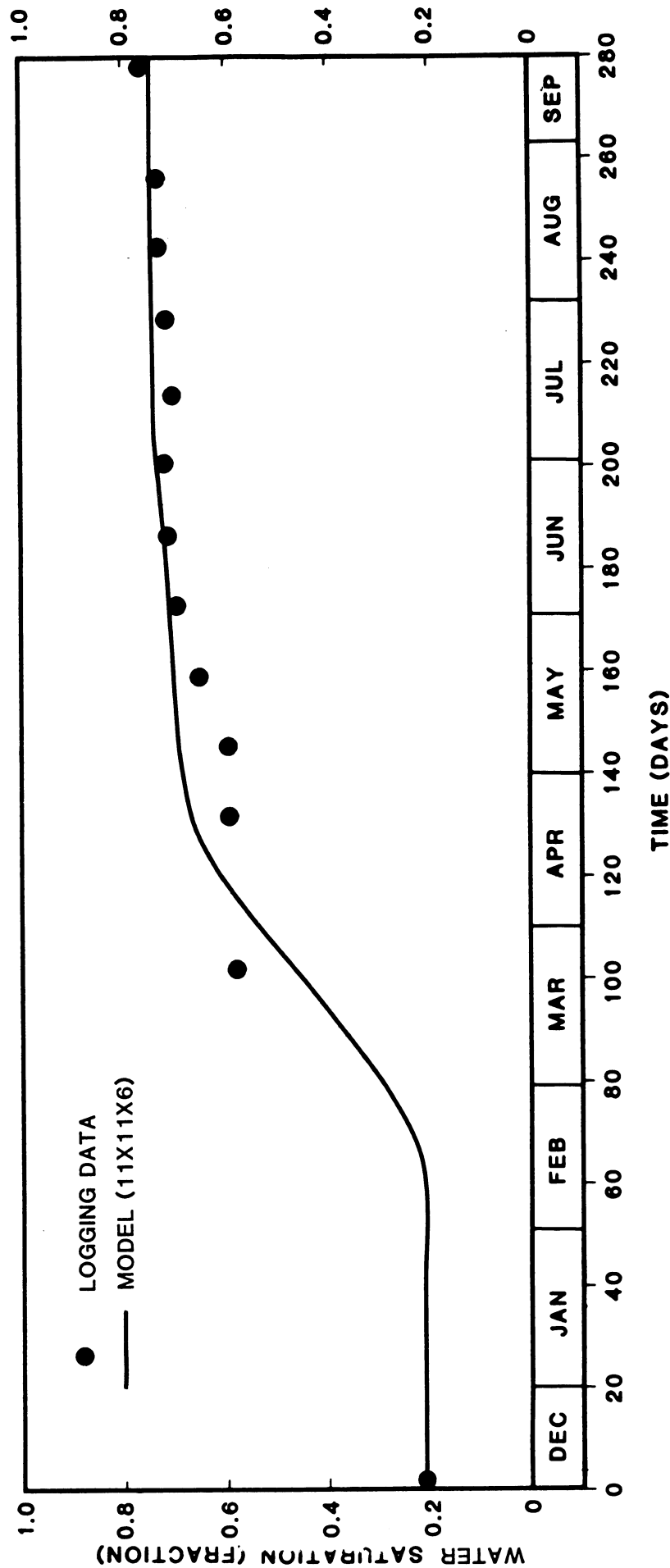


Fig. 144-Water saturation history match for layer Y, divided into sub-layers Y_1 , Y_2 and Y_3 . Six-layer model. Dots are logging data and line is simulation model match, December 11, 1980 to September 17, 1981 at observation well no. 2.

OIL SATURATION HISTORY MATCH FOR LAYER Y (COMBINED) (12-11-80 TO 9-17-81)

SIX LAYER MODEL

ZABOLOTNY OBSERVATION WELL NO. 2

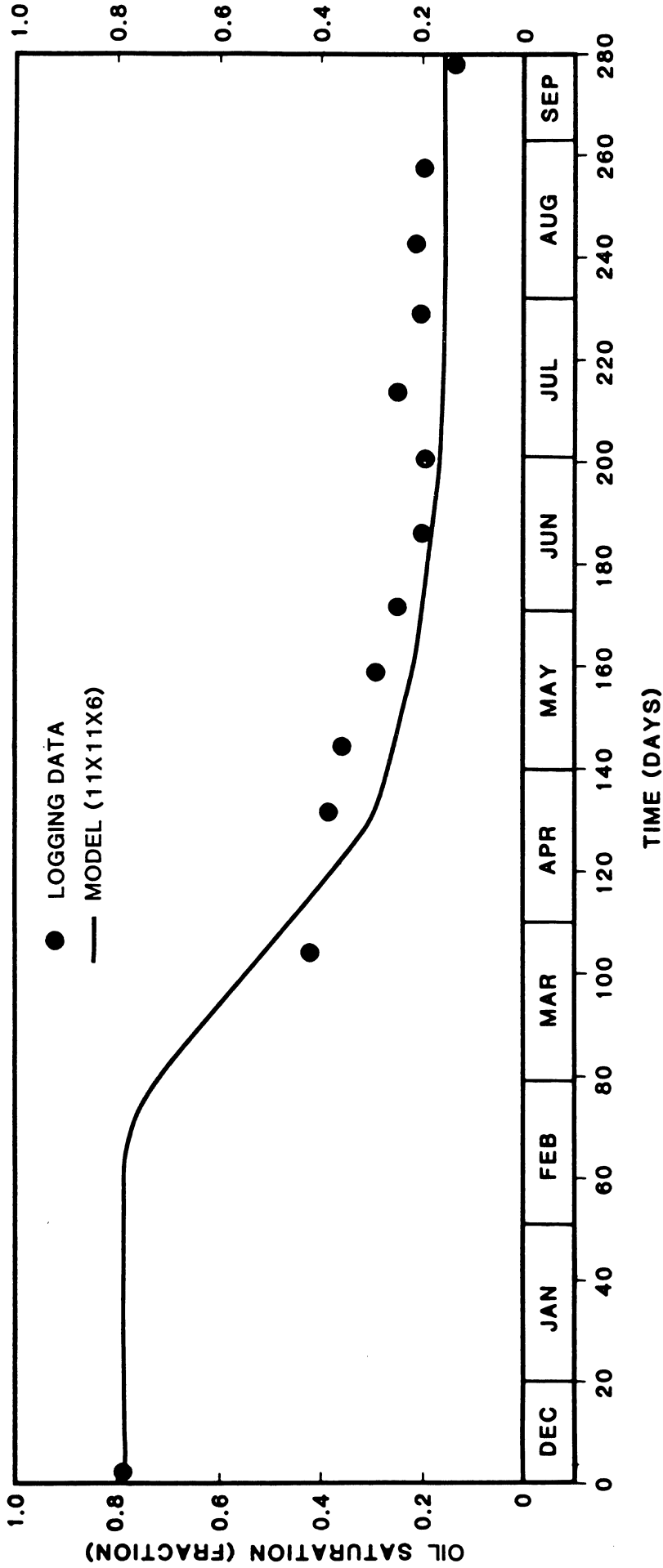


Fig. 145-Oil saturation history match for layer Y. Six-layer model. Dots are logging data and the line is simulation model match, December 11, 1980 to September 17, 1981 at observation well no. 2.

**CO₂-FREE OIL SATURATION (AT RESERVOIR CONDITIONS)
ON JULY 17, 1981
SIX LAYER MODEL**

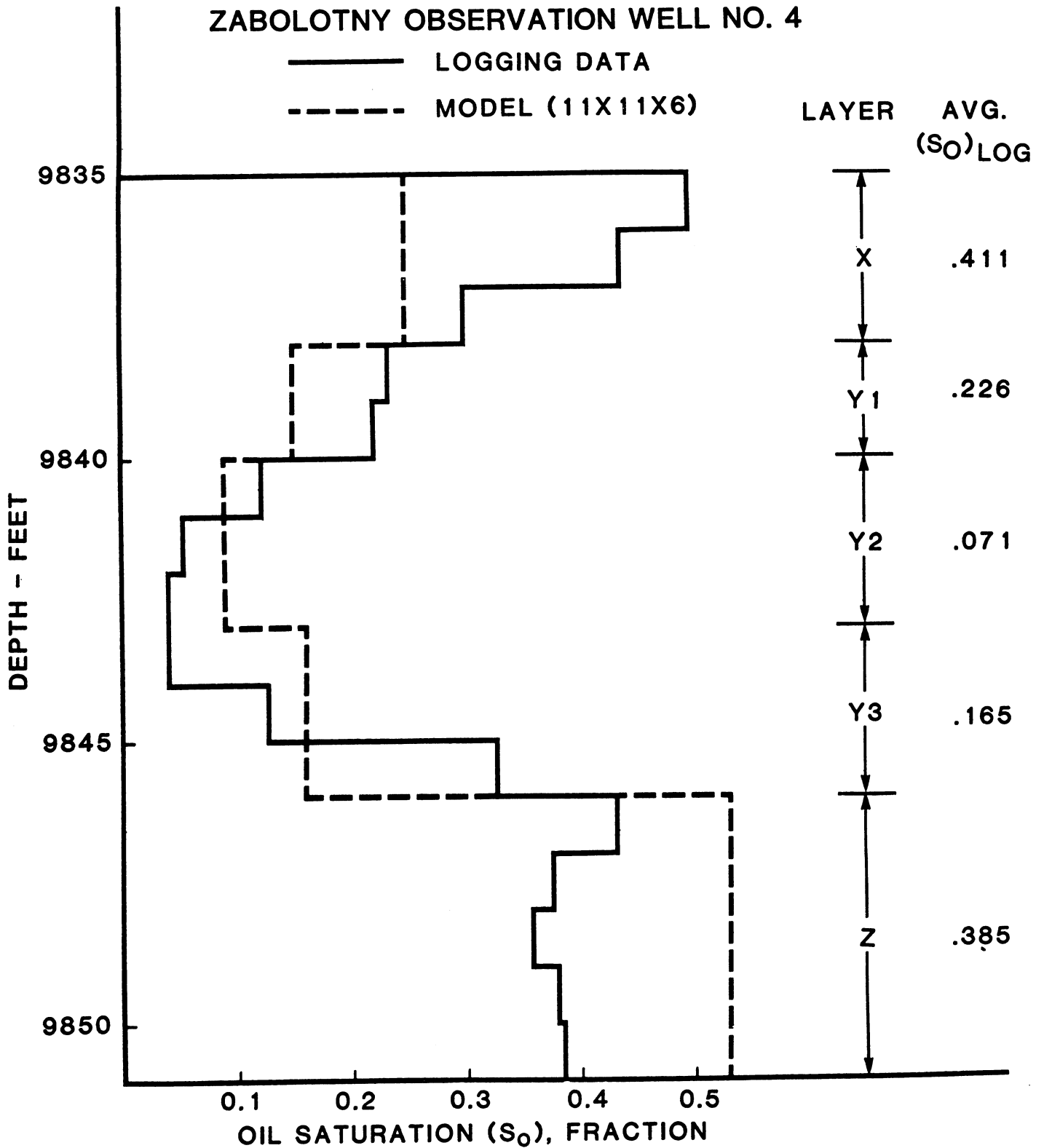


Fig. 146-CO₂-free oil saturation profiles. Six-layer model at reservoir conditions, for layer X, sub-layers Y₁, Y₂ and Y₃ and layer Z. Solid line is logging data and dashed line is the simulation model match. July 17, 1981 at observation well no. 4.

**OIL SATURATION (AT STOCK TANK CONDITIONS)
 JULY 17, 1981
 SIX LAYER MODEL
 ZABOLOTNY OBSERVATION WELL NO. 4**

PRESSURE CORE DATA
 MODEL (11 X 11 X 6)

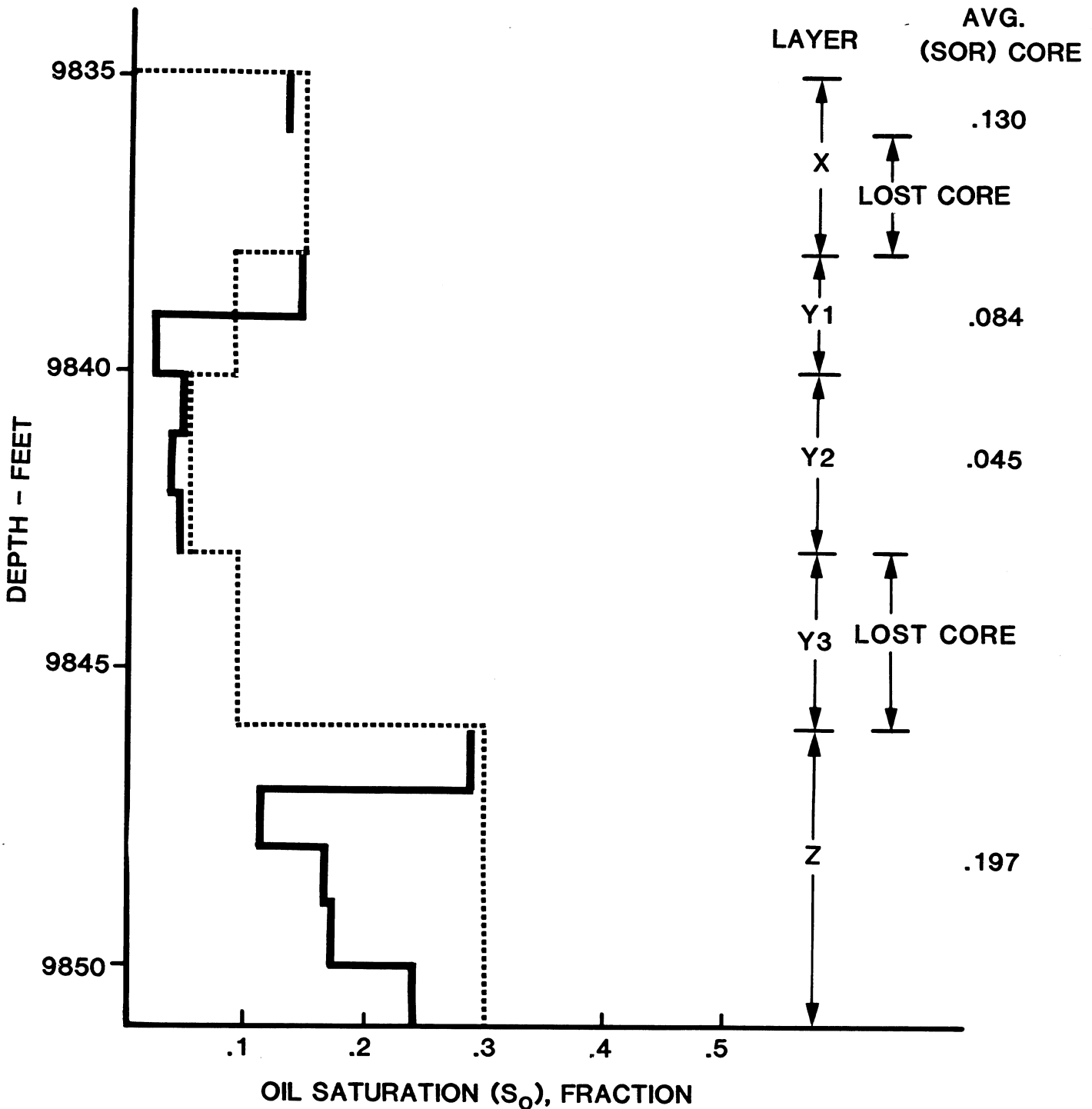


Fig. 147-Oil saturation profile. Six-layer model at stock tank conditions, for layer X, sub-layers Y₁, Y₂ and Y₃ and layer Z. Solid line is pressure-core data and dashed line is the simulation model match. July 17, 1981 at observation well no. 4.

Zabolotny Observation - 1 8/25/81

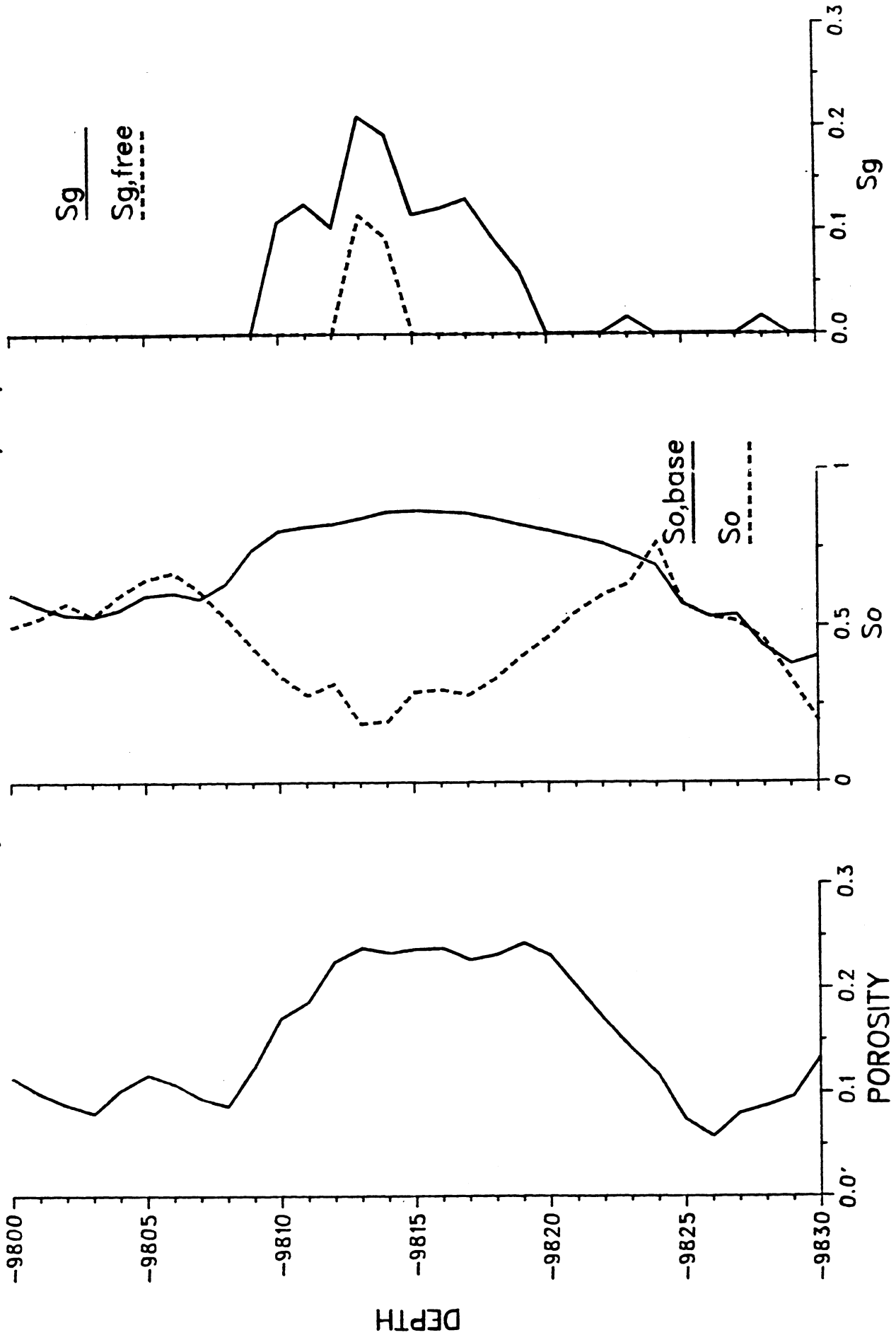


Fig. 148-Final monitor log of porosity, oil saturation and gas saturation, August 25, 1981, at observation well no. 1.

Zabolotny Observation - 2 9/16/81

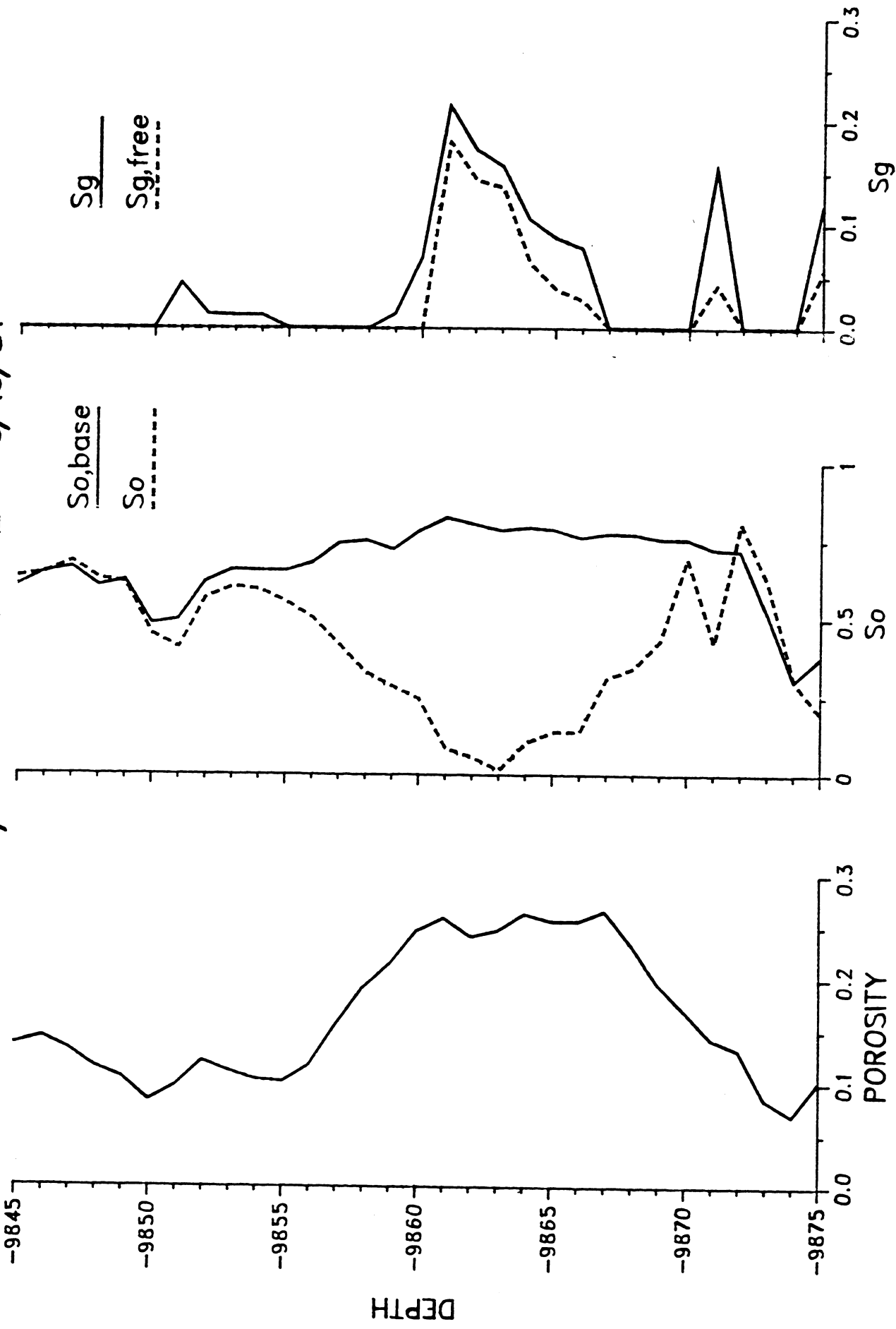


Fig. 149-Final monitor log of porosity, oil saturation and gas saturation, September 17, 1981, at observation well no. 2.

Zabolotny Observation - 3 9/17/81

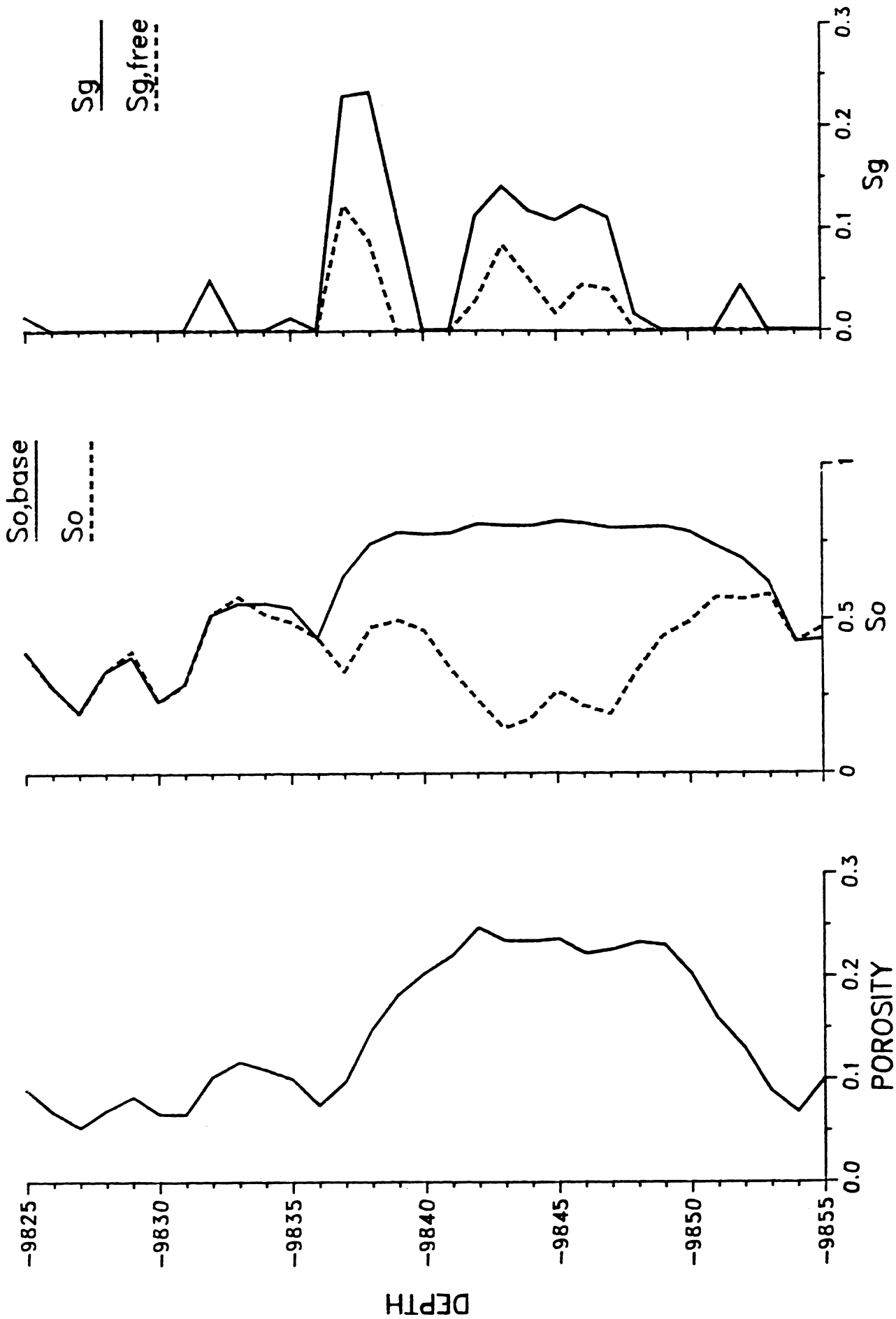


Fig. 150-Final monitor log of porosity, oil saturation and gas saturation, September 17, 1981, at observation well no. 3.

OBSERVATION NO. 1 9810 FEET

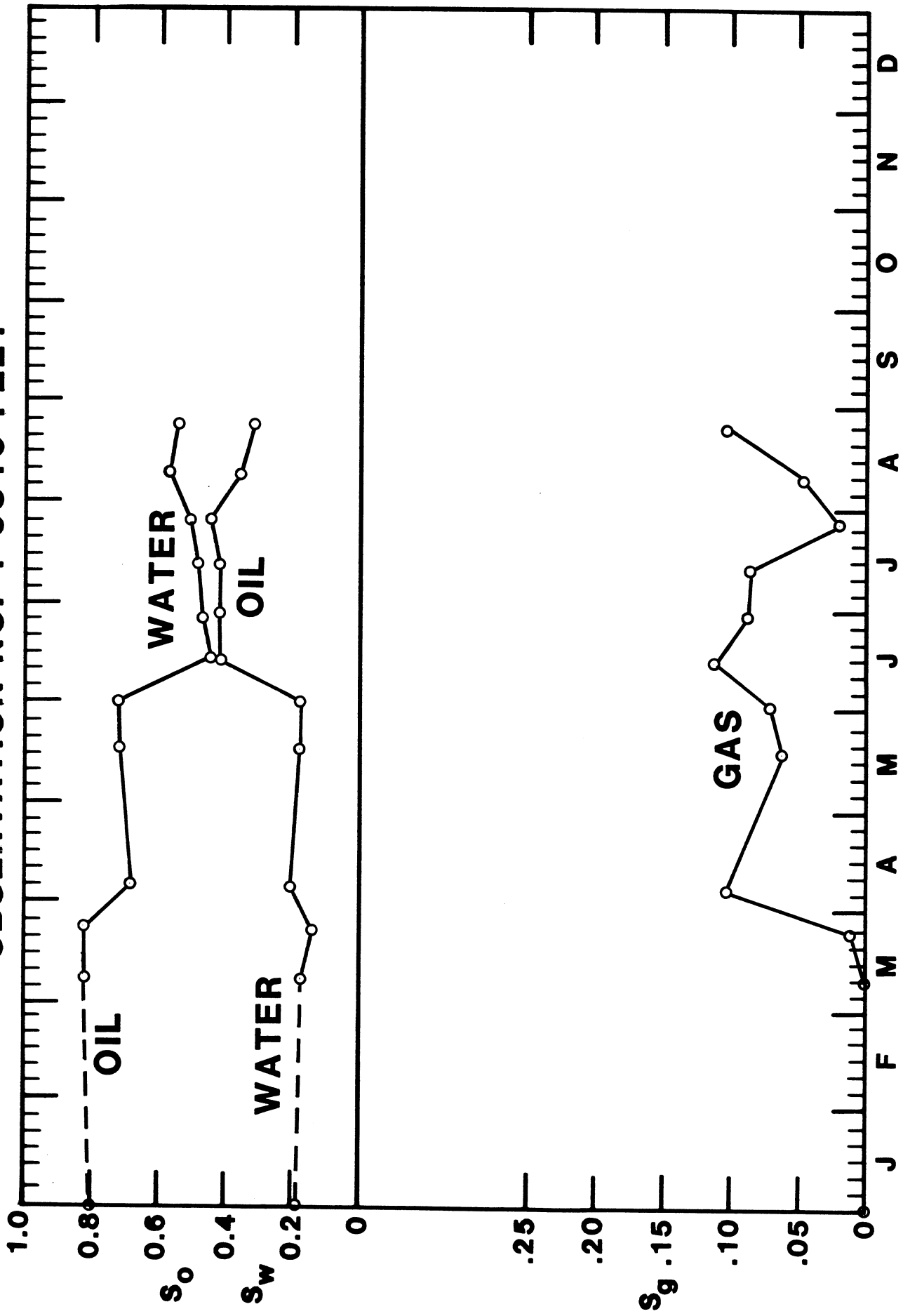


Fig. 151-Monitor log data of oil saturation, water saturation and gas saturation vs. time at 9810 feet in observation well no. 1.

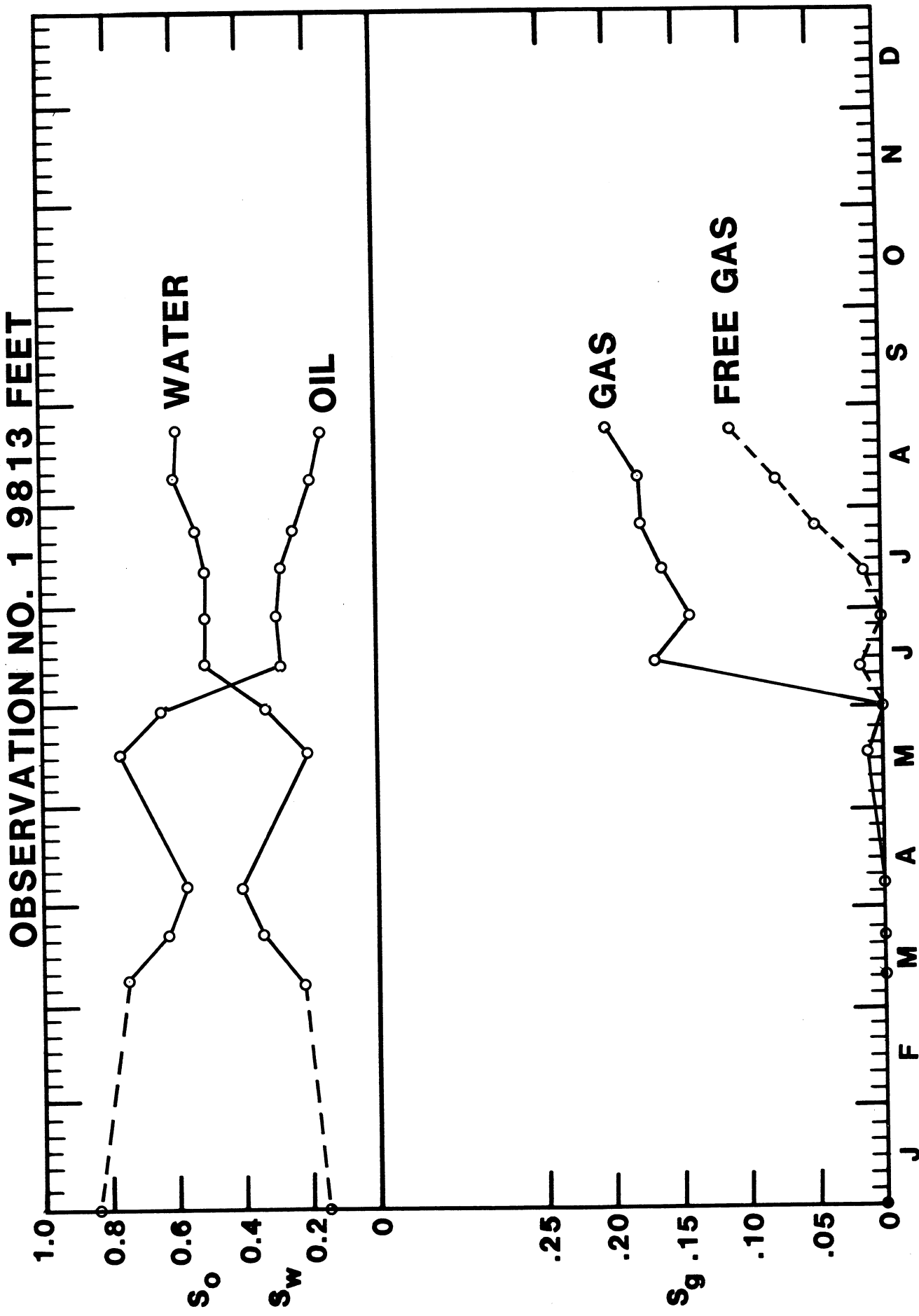


Fig. 152-Monitor log data of oil saturation, water saturation, gas saturation and free-gas saturation vs. time at 9813 feet in observation well no. 1.

OBSERVATION NO. 1 9817 FEET

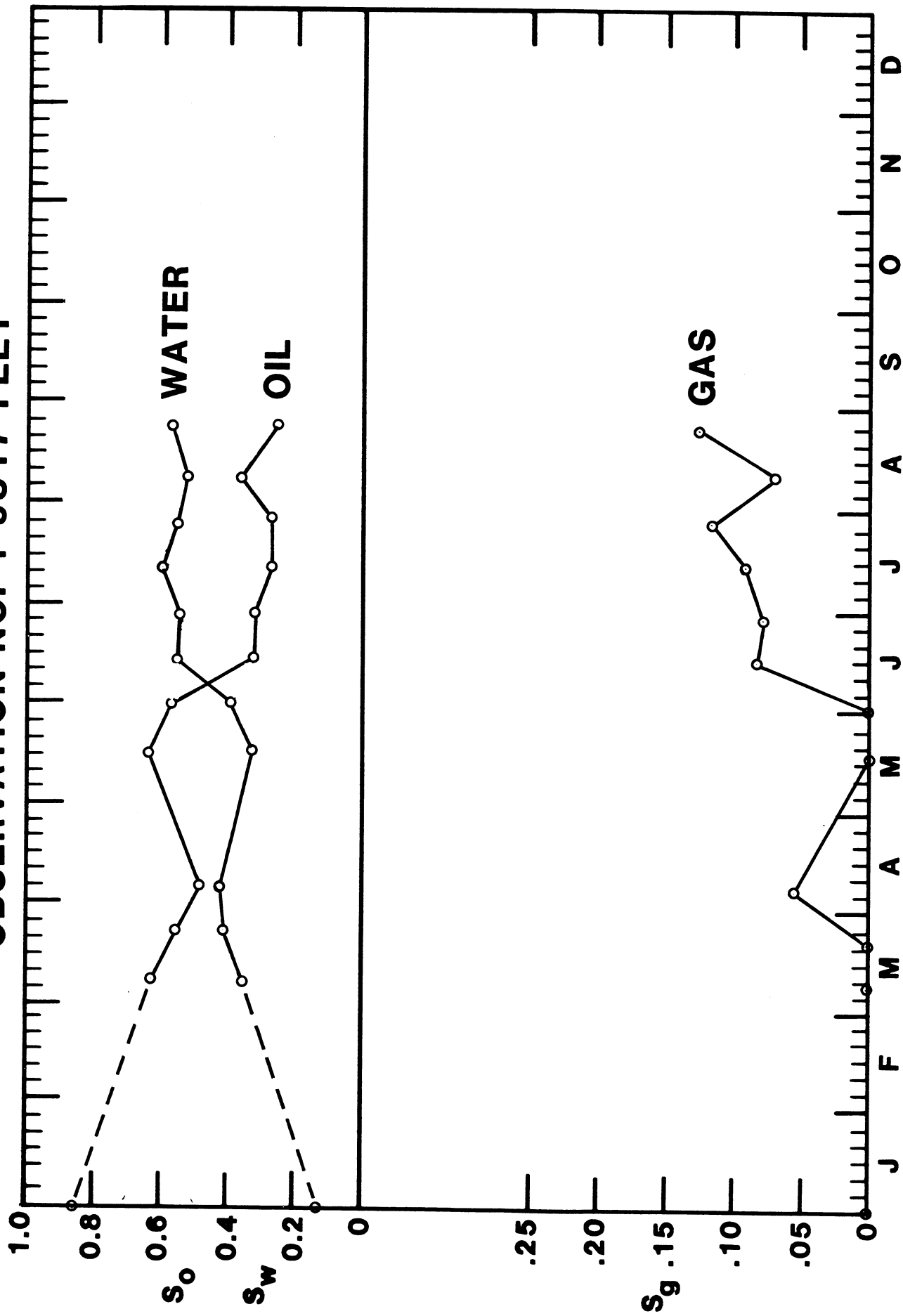


Fig. 153-Monitor log data of oil saturation, water saturation and gas saturation vs. time at 9817 feet in observation well no. 1.

OBSERVATION NO. 2 9860 FEET

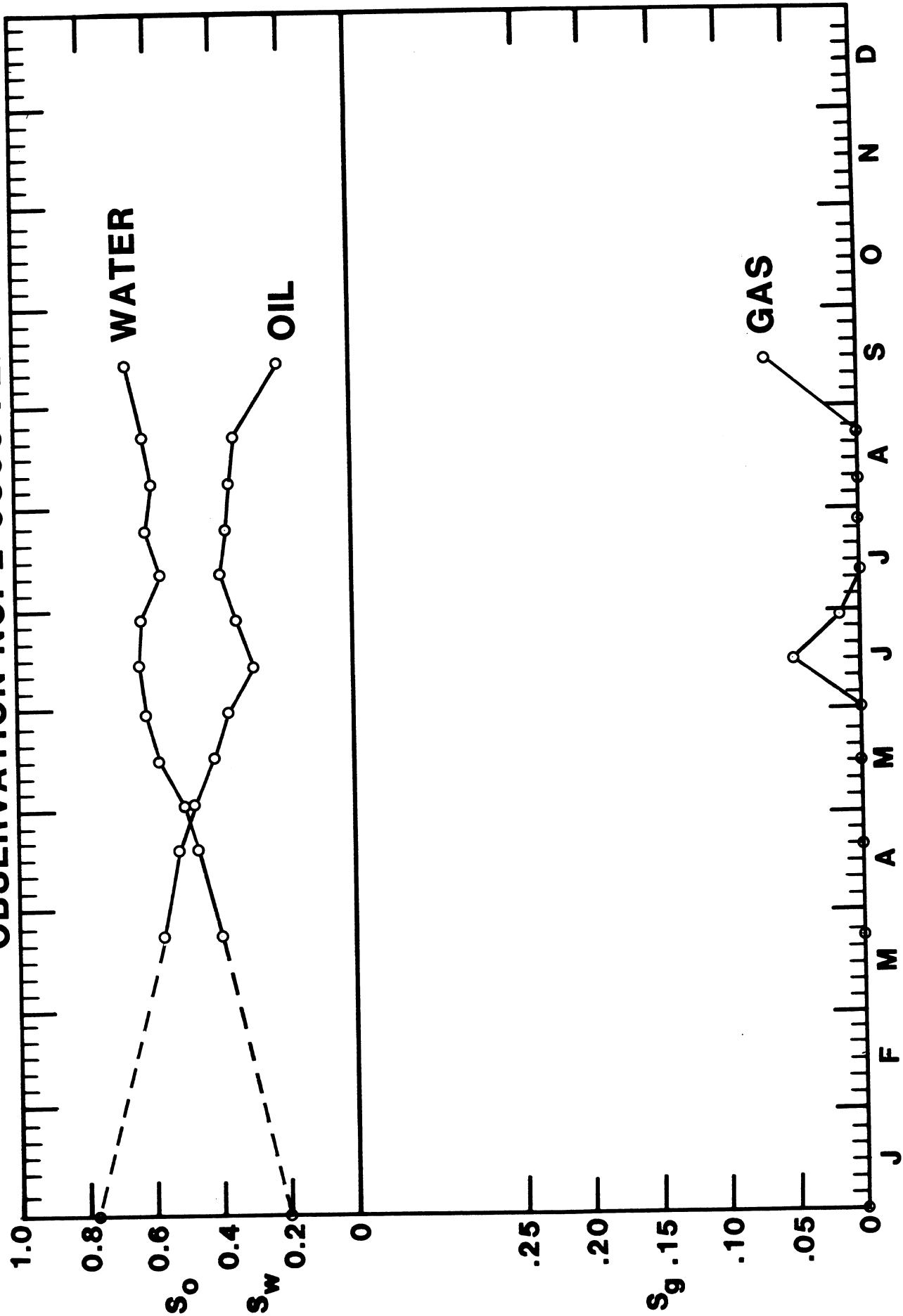


Fig. 154-Monitor log data of oil saturation, water saturation and gas saturation vs. time at 9860 feet in observation well no. 2.

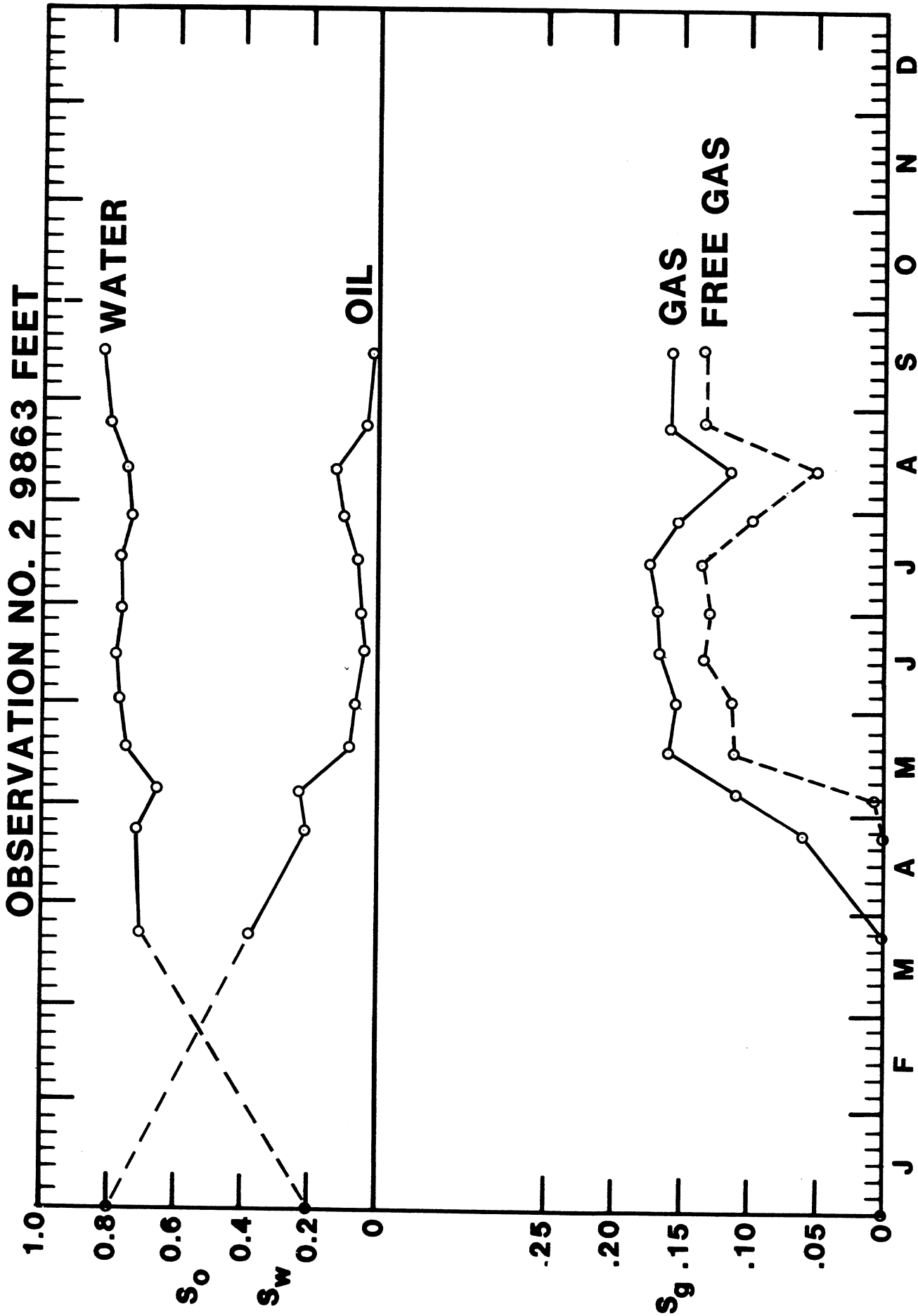


Fig. 155-Monitor log data of oil saturation, water saturation, gas saturation and free-gas saturation vs. time at 9863 feet on observation well no. 2.

OBSERVATION NO. 2 9867 FEET

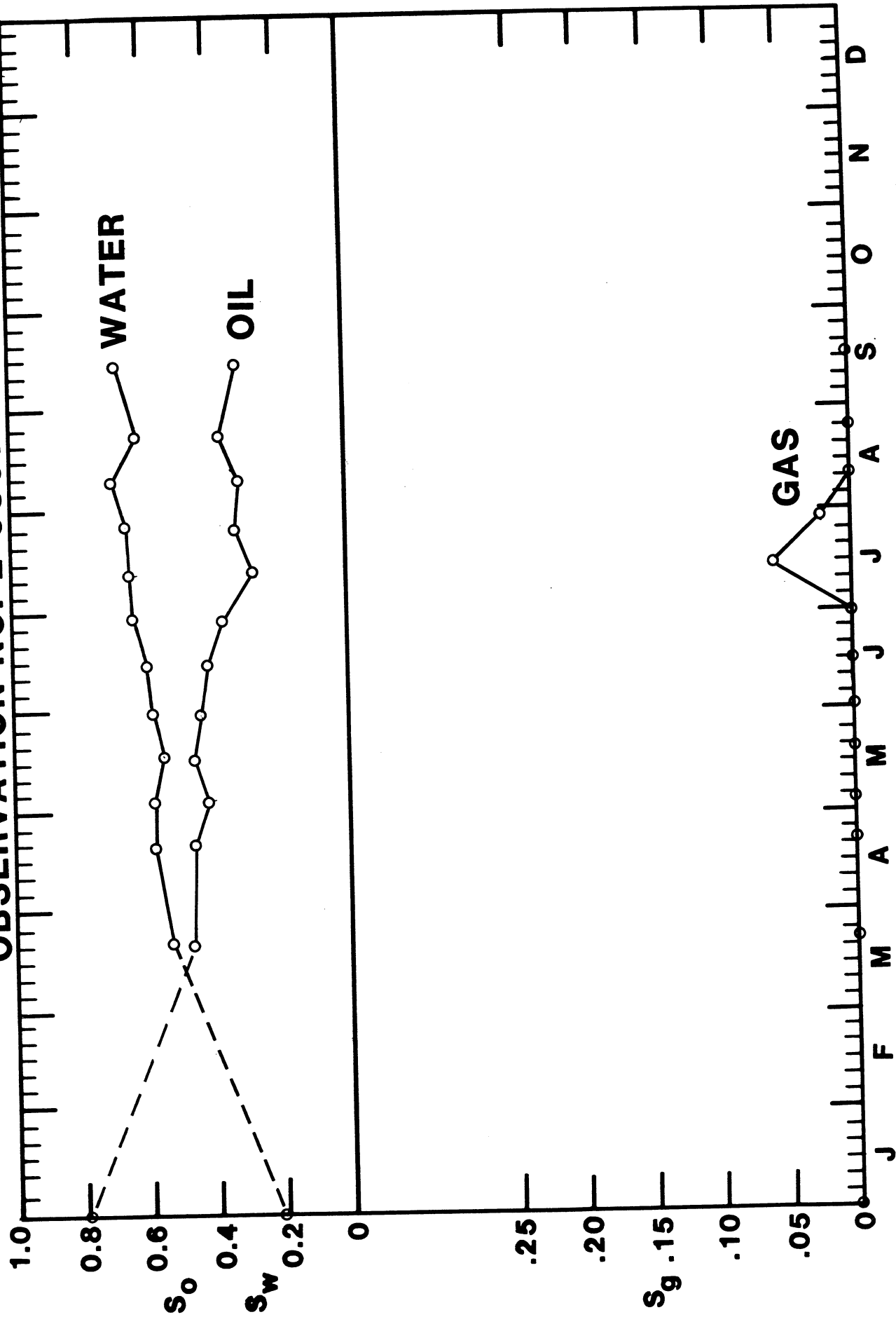


Fig. 156-Monitor log data of oil saturation, water saturation and gas saturation vs. time at 9867 feet in observation well no. 2.

OBSERVATION NO. 3 9840 FEET

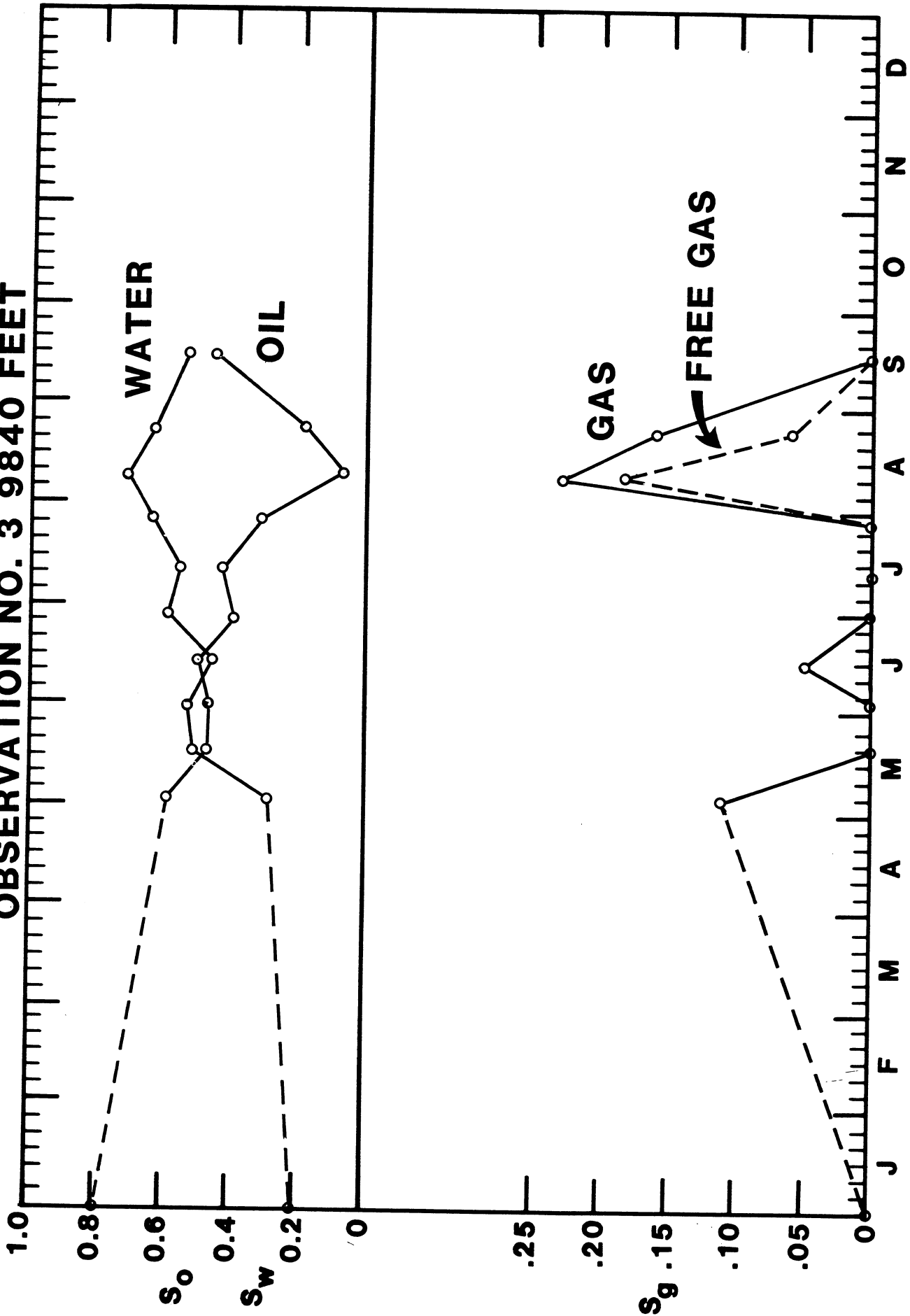


Fig. 157-Monitor log data of oil saturation, water saturation, gas saturation and free-gas saturation vs. time at 9840 feet in observation well no. 3.

OBSERVATION NO. 3 9843 FEET

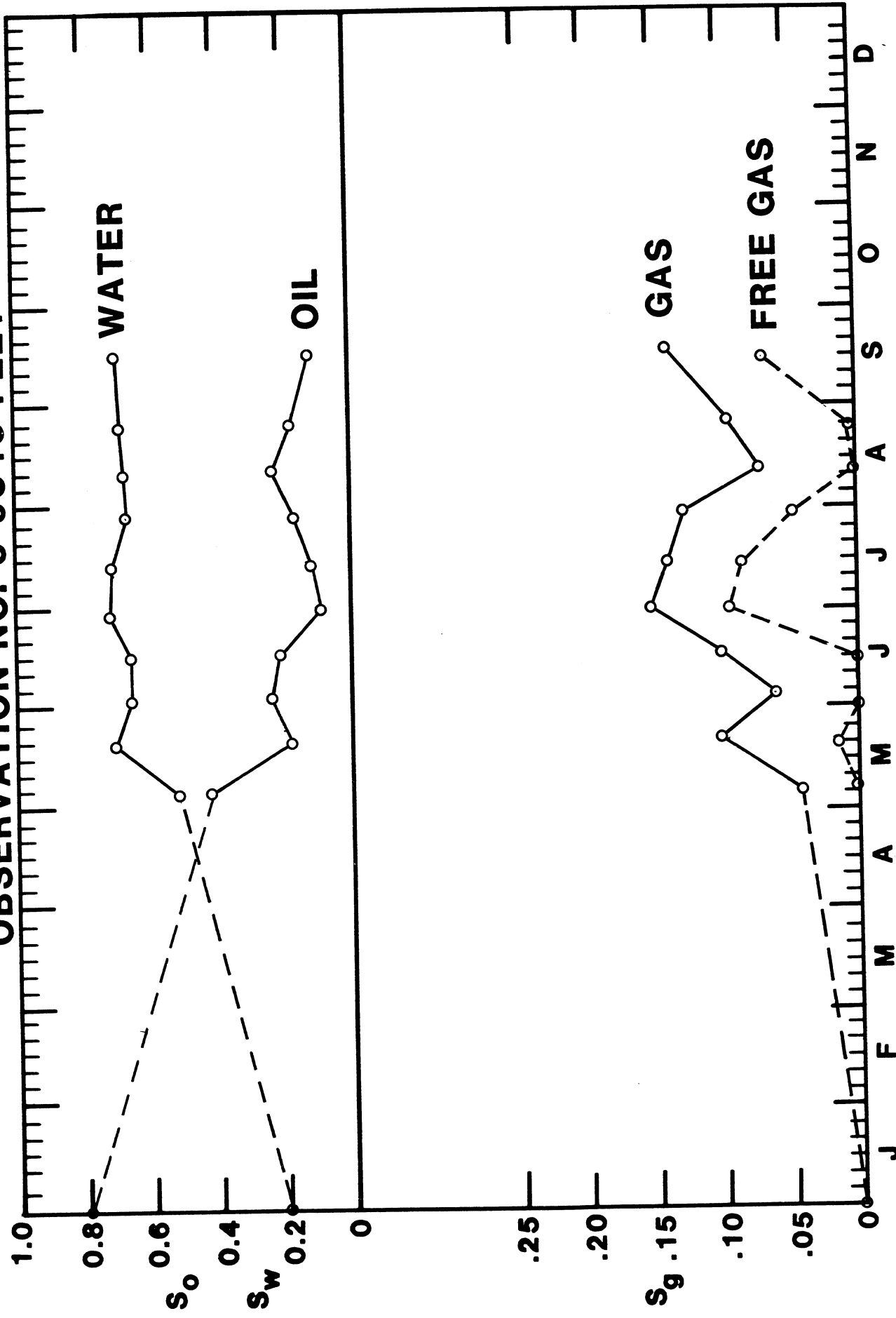


Fig. 158—Monitor log data of oil saturation, water saturation, gas saturation and free-gas saturation vs. time at 9843 feet in observation well no. 3.

OBSERVATION NO. 3 9847 FEET

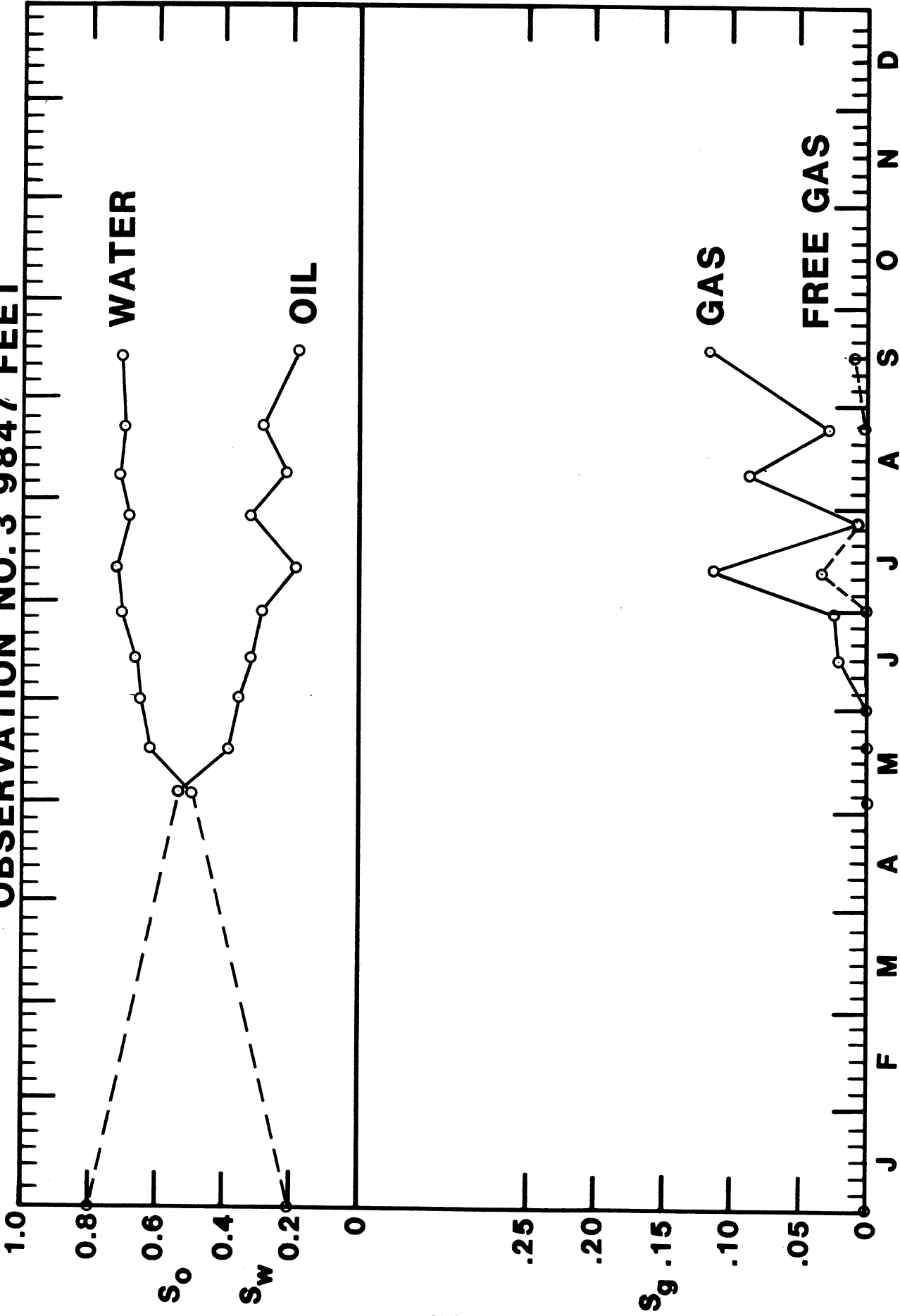


Fig. 159-Monitor log data of oil saturation, water saturation, gas saturation and free-gas saturation vs. time at 9847 feet in observation well no. 3.

Table 1-CO₂-water, residual-oil saturation and relative permeability, injection well no. 1, at 3,500 psi and 245°F.

Core Data	Water-CO ₂ Ratio			Final Conditions*		
	Depth (ft)	K (md)	φ (%)	(RBbl/RBbl)	S _o (% PV)	S _w (% PV)
9823	7.3	23	0	3.1	20.0	76.9
9826-27	5.3	22	1.5	3.1	61.5	35.4
9814-15	39	26	3.0	0.8	63.5	35.7
9814-15	39	26	0	--	29.9	70.1
9814-15	39	26	1.35	--	80.3	19.7
9814-15	39	26	2.7	--	87.3	12.7

(The following were obtained after extraction of residual oil.)

* Oil saturations are obtained gravimetrically assuming original oil density. Water and CO₂ saturations and relative permeabilities are calculated from pure component material balances and do not allow for mutual solubility.

Table 2-Little Knife CO₂ minitest fluid-injection schedule.

FLUID INJECTION SCHEDULE

<u>PHASE</u>	<u>VOLUME</u>	<u>DATES</u>	<u>DAYS</u>
PREFLUSH	29,539 BBLS	12/11/80-1/7/81	27
1ST CO ₂	420 TONS	1/7/81-1/24/81	17
WATER	5007 BBLS	1/24/81-1/27/81	3
2ND CO ₂	420 TONS	1/27/81-2/5/81	9
WATER	4964 BBLS	2/5/81-2/9/81	4
3RD CO ₂	432 TONS	2/9/81-2/26/81	17
WATER	4874 BBLS	2/26/81-3/2/81	4
4TH CO ₂	403 TONS	3/2/81-3/11/81	9
WATER	5776 BBLS	3/11/81-3/16/81	5
5TH CO ₂	419 TONS	3/16/81-3/25/81	9
FLUSH WATER	198,794 BBLS	3/25/81-9/24/81	182

Table 3-Pre-injection waterflood residual oil analysis, injection well no. 1, for layers X, Y and Z vs. depth.

PRE-INJECTION WATER FLOOD RESIDUAL OIL ANALYSIS

ZABOLOTNY INJECTION NO. 1

Layer	Depth	1 φ GULFLOG %	2 φ Core %	3 SwGULFLOG %	4 SwTDT %	5 GULFLOG Residual Oil	6 TDT Residual Oil	7 TDT Residual Oil
					$\Sigma_w2=163$ $\Sigma_m=16$		$\Sigma_m=16$ $\Sigma_w5=147$	w/o Σ_m
X	9824	15.2	13.3	25.3	23.7	40.4	53.8	52.3
	9825	18.7	20.9	19.3	23.9	49.7	43.7	48.8
	9826	20.5	16.8	17.2	23.1	37.2	37.4	42.7
	9827	21.2	22.2	18.4	22.5	32.5	37.2	41.8
	9828	21.7	22.7	16.2	21.0	35.8	33.4	38.8
	9829	22.1	21.9	14.7	19.2	43.8	30.8	35.7
	9830	22.5	21.9	14.6	19.2	44.9	29.1	34.3
	9831	22.6	23.3	15.5	19.8	39.4	27.9	32.8
	9832	22.1	23.3	16.8	22.0	33.6	27.7	33.5
	9833	22.0	22.0	20.4	23.7	40.7	30.5	34.2
	9834	22.6	23.5	23.5	24.0	39.2	31.4	31.9
	9835	23.1	21.4	23.4	21.0	46.7	36.4	33.7
	9836	20.1	18.4	26.1	22.9	50.7	35.6	32.0
	9837	17.1	15.8	30.2	22.2	46.2	35.5	26.5
	9838	16.1	13.6	29.9	21.4	54.6	44.8	36.5
	9839	13.1	13.8	35.9	22.6	50.6	48.2	33.2
Z	Average	18.1	17.0	20.2	23.6	42.5	44.2	47.6
	9824-9826 X	22.2	22.5	18.2	21.4	39.7	31.6	35.1
	9827-9835 Y	16.6	15.4	30.0	22.3	50.5	40.3	31.9

Table 4--Time-lapse monitor log oil, water and gas saturations for layers X, Y and Z at observation wells no. 1, 2 and 3.

TIME-LAPSE MONITOR WELL SATURATIONS
ZABOLOTNY OBSERVATION NO. 1

Layers	03-09-81			03-26-81			04-07-81			05-18-81			06-01-81			06-15-81			06-29-81			07-13-81			07-27-81			08-10-81			08-25-81			09-16-81		
	S _o	S _w	S _{CO2}	S _o	S _w	S _{CO2}	S _o	S _w	S _{CO2}	S _o	S _w	S _{CO2}	S _o	S _w	S _{CO2}	S _o	S _w	S _{CO2}	S _o	S _w	S _{CO2}	S _o	S _w	S _{CO2}	S _o	S _w	S _{CO2}	S _o	S _w	S _{CO2}						
X(9809-9811)	79.7	18.5	1.8	82.1	17.5	0.0	70.0	23.9	6.1	77.6	19.6	2.8	72.6	21.1	6.4	42.3	46.9	10.8	48.0	46.0	6.0	50.0	43.3	6.7	47.1	48.2	4.6	34.5	59.0	6.5	33.9	57.4	8.7	40.9	55.3	3.9
Y(9812-9820)	67.4	32.4	0.0	59.1	40.8	0.0	55.2	43.4	1.4	68.2	31.2	0.7	60.5	39.5	0.0	33.3	55.8	10.9	34.8	56.4	8.0	32.9	56.7	10.4	30.7	57.8	11.5	34.3	51.9	7.8	30.7	58.0	11.3	29.7	59.8	10.5
Z(9821-9825)	74.1	25.9	0.0	68.2	31.8	0.0	66.8	33.2	0.0	72.5	27.5	0.0	67.0	33.0	0.0	53.6	46.4	0.0	55.1	44.9	0.0	56.4	43.6	0.0	56.2	43.8	0.0	57.7	40.4	1.9	61.5	38.2	0.3	59.6	40.1	0.0

222

ZABOLOTNY OBSERVATION NO. 2

Layers	03-23-81			04-22-81			05-05-81			05-19-81			06-02-81			06-16-81			06-30-81			07-14-81			07-28-81			08-11-81			08-25-81			09-16-81		
	S _o	S _w	S _{CO2}	S _o	S _w	S _{CO2}	S _o	S _w	S _{CO2}	S _o	S _w	S _{CO2}	S _o	S _w	S _{CO2}	S _o	S _w	S _{CO2}	S _o	S _w	S _{CO2}	S _o	S _w	S _{CO2}	S _o	S _w	S _{CO2}	S _o	S _w	S _{CO2}	S _o	S _w	S _{CO2}			
X(9857-9858)	69.9	30.1	0.0	75.6	24.4	0.0	73.8	26.2	0.0	63.9	36.1	0.0	53.8	46.2	0.0	49.7	50.3	0.0	44.9	55.1	0.0	45.8	54.2	0.0	48.7	51.3	0.0	46.1	53.9	0.0	42.5	57.5	0.0	36.9	63.1	0.0
Y(9859-9867)	41.9	57.5	0.6	38.6	59.1	2.3	36.5	59.4	4.1	31.6	63.7	4.7	28.0	67.8	6.2	22.4	69.6	8.1	21.7	70.6	7.6	25.4	68.8	5.8	21.5	70.3	8.2	22.0	71.8	6.2	21.6	71.8	6.6	15.2	74.8	10.0
Z(9868-9872)	66.5	33.5	0.0	67.2	32.8	0.0	68.9	31.1	0.0	71.5	28.2	0.3	67.9	31.2	0.9	67.9	31.9	0.2	57.1	40.4	2.4	57.5	42.5	0.0	54.5	45.5	0.0	47.4	50.5	2.2	63.0	35.6	1.5	51.7	45.8	2.5

ZABOLOTNY OBSERVATION NO. 3

Layers	05-05-81			05-20-81			06-03-81			06-16-81			06-30-81			07-14-81			07-29-81			08-11-81			08-25-81			09-17-81		
	S _o	S _w	S _{CO2}	S _o	S _w	S _{CO2}	S _o	S _w	S _{CO2}	S _o	S _w	S _{CO2}	S _o	S _w	S _{CO2}	S _o	S _w	S _{CO2}	S _o	S _w	S _{CO2}	S _o	S _w	S _{CO2}	S _o	S _w	S _{CO2}	S _o	S _w	S _{CO2}
X(9838-9840)	69.1	26.8	4.1	58.8	41.2	0.0	53.6	41.4	5.0	56.3	36.7	7.0	50.2	43.9	5.8	45.9	43.8	10.3	39.7	57.8	2.5	15.1	61.5	23.4	28.8	55.6	15.6	47.6	42.0	10.4
Y(9841-9849)	51.2	47.2	1.6	35.2	61.7	3.1	35.7	60.9	3.5	32.6	61.8	5.6	25.7	67.7	6.7	24.6	67.4	8.0	27.4	66.4	6.2	28.5	65.3	6.2	28.8	66.1	5.1	25.9	66.1	8.1
Z(9850-9853)	64.6	33.2	7.1	63.1	33.7	3.1	61.9	35.5	2.6	63.0	36.7	0.2	53.6	46.4	6.0	51.8	47.2	0.9	64.1	35.9	0.0	60.0	40.0	0.0	45.7	54.3	0.0	53.9	45.1	1.0

S_o = Oil Saturation
S_w = Water Saturation
S_{CO2} = CO₂ Saturation

Table 5-Final monitor log saturation data. Original oil saturation and final oil, water and gas saturations for layers X, Y and Z at observation wells no. 1, 2, 3 and 4.

FINAL MONITOR WELL SATURATIONS

	ZABOLOTNY OBSERVATION NO. 1				ZABOLOTNY OBSERVATION NO. 2				ZABOLOTNY OBSERVATION NO. 3				ZABOLOTNY OBSERVATION NO. 4						
	Porosity	Original Oil Sat.	Final Saturatons Oil	Final Saturatons Water	CO2	Porosity	Original Oil Sat.	Final Saturatons Oil	Final Saturatons Water	CO2	Porosity	Original Oil Sat.	Final Saturatons Oil	Final Saturatons Water	CO2	Porosity	Gulflog Oil Saturation	Core Oil Saturation	
X	1	12.4	74.7	48.3	51.7	0.0	15.6	74.3	41.3	58.2	0.0	14.8	74.4	47.3	29.5	23.2	14.4	49.7	13.0
	2	17.1	80.7	48.2	51.8	0.0	19.2	75.2	32.8	67.2	0.0	18.2	78.0	49.5	39.0	11.5	16.1	43.6	Lost Core
	3	18.6	82.0	29.2	60.9	9.9		Not Present				20.3	77.3	46.1	53.9	0.0	16.8	29.9	Lost Core
Zone Averages		16.0	79.6	40.9	55.3	3.8	17.4	74.8	36.9	63.1	0.0	17.8	76.8	47.6	42.0	10.4	15.8	40.5	
	1	22.5	82.8	33.6	55.2	11.1	21.5	72.3	28.3	70.4	1.4	21.9	77.7	33.6	66.4	0.0	18.6	23.3	14.4
	2	23.8	84.5	29.6	56.7	13.7	24.7	78.4	24.4	68.8	6.8	24.6	80.6	23.7	65.0	11.2	21.6	22.1	2.4
	3	23.3	86.6	17.9	61.5	20.6	25.9	82.5	8.5	69.9	21.5	23.3	79.9	14.3	71.7	14.0	22.9	12.2	4.9
	4	23.7	86.9	20.2	65.2	14.6	24.1	80.4	5.6	77.2	17.2	23.3	79.8	17.5	70.9	11.6	24.3	5.2	4.0
	5	23.8	86.4	31.7	60.7	7.6	24.7	78.4	1.5	82.9	15.6	23.5	81.4	26.4	62.9	10.7	24.6	4.0	4.6
	6	22.7	85.9	19.1	63.2	17.7	26.3	79.3	10.5	78.9	10.5	22.1	80.6	21.5	66.4	12.1	24.5	4.1	Lost Core
	7	23.2	84.1	30.7	61.4	7.8	24.6	78.6	13.8	77.5	8.7	22.5	79.0	18.9	70.2	10.9	24.7	12.8	Lost Core
	8	24.3	82.1	40.4	58.2	1.4	25.6	76.0	13.9	78.4	7.7	23.2	79.2	33.0	65.5	1.5	25.3	32.7	Lost Core
9	23.1	80.3	44.1	55.9	0.0	26.6	77.4	31.2	68.8	0.0	22.9	79.5	44.3	55.7	0.0	24.4	43.1	28.7	
Zone Averages		23.4	84.4	29.7	59.8	10.5	25.0	78.2	15.2	74.8	10.0	23.0	79.8	25.9	66.1	8.1	23.4	17.6	
	1	20.0	78.3	51.3	48.7	0.0	23.3	77.1	34.5	65.5	0.0	20.1	77.6	48.9	51.1	0.0	18.9	37.5	11.2
	2	16.9	76.2	58.5	41.5	0.0	19.5	75.6	43.5	56.5	0.0	15.7	73.1	56.7	43.3	0.0	14.8	35.6	16.9
Z	3	14.1	72.8	66.4	33.6	0.0	16.9	75.6	69.8	30.2	0.0	12.9	69.0	56.0	39.7	4.3	12.4	37.8	17.4
	4	11.6	69.2	69.1	29.2	1.8	14.2	72.4	42.2	42.3	15.5	8.7	61.3	57.6	42.4	0.0	11.2	38.3	24.2
	5	7.3	56.8	56.8	43.2	0.0	13.2	71.9	81.1	18.9	0.0		Not Present					Not Present	
Zone Averages		14.0	72.9	59.6	40.1	0.0	17.4	74.9	51.7	45.8	2.5	14.4	71.9	53.9	45.1	1.0	14.3	37.3	

W-9785-9808
X-9809-9811
Y-9812-9820
Z-9821-9825

W-9827-9856
X-9857-9858
Y-9859-9867
Z-9869-9872

W-9823-9837
X-9838-9840
Y-9841-9849
Z-9850-9853

W-9819-9824
X-9825-9827
Y-9828-9836
Z-9837-9840
Coring Depth
(See Figure 83)

Table 6-Final monitor log saturation data. Original oil saturation and final oil, water and gas saturations, for layer W at observation wells no. 1, 2, 3 and 4.

FINAL MONITOR WELL SATURATIONS																								
	ZABOLOTNY OBSERVATION NO. 1				ZABOLOTNY OBSERVATION NO. 2				ZABOLOTNY OBSERVATION NO. 3				ZABOLOTNY OBSERVATION NO. 4											
	Porosity	Original Oil Sat.	Final Sat. Oil	Final Sat. Water	CO ₂	Porosity	Original Oil Sat.	Final Sat. Oil	Final Sat. Water	CO ₂	Porosity	Original Oil Sat.	Final Sat. Oil	Final Sat. Water	CO ₂	Porosity	Original Oil Sat.	Final Sat. Oil	Final Sat. Water	CO ₂	Porosity	Gulflog Oil Saturation	Core Oil Saturation	
1	11.4	71.6	66.1	33.9	0.0	8.6	60.3	51.9	46.7	1.4	6.5	39.6	39.6	60.4	0.0	7.4	25.5	25.5	29.7			25.5	29.7	
2	9.4	68.2	63.3	36.7	0.0	13.8	68.4	65.1	33.1	1.8	8.9	43.2	50.1	48.8	1.1	11.5	51.5	51.5	Lost Core			51.5	Lost Core	
3	6.4	60.8	60.8	39.2	0.0	18.9	74.9	81.2	18.8	0.0	6.7	39.3	39.0	59.7	1.4	12.8	48.6	48.6	Lost Core			48.6	Lost Core	
4	9.6	67.2	47.0	44.1	8.9	18.9	78.1	83.6	16.4	0.0	6.7	28.0	28.0	72.0	0.0	12.6	40.1	40.1	9.2			40.1	9.2	
5	11.8	72.7	53.4	39.0	7.6	16.3	76.2	77.5	22.5	0.0	5.2	19.6	19.6	80.4	0.0	12.3	34.4	34.4	23.5			34.4	23.5	
6	10.5	73.4	65.9	34.1	0.0	17.4	75.9	75.6	24.4	0.0	6.9	33.0	33.0	67.0	0.0	10.9	22.4	22.4	24.7			22.4	24.7	
7	9.0	71.3	75.0	25.0	0.0	14.7	75.8	74.8	25.2	0.0	8.2	37.7	39.6	60.4	0.0	9.1	4.4	4.4	26.6			4.4	26.6	
8	9.5	72.0	57.2	31.9	10.9	10.3	66.4	63.2	36.8	0.0	6.5	23.2	23.2	76.8	0.0	8.1	0.0	0.0	26.7			0.0	26.7	
9	8.5	71.6	60.5	29.5	10.0	12.9	70.7	67.2	32.8	0.0	6.5	28.9	28.9	71.1	0.0	7.0	0.0	0.0	23.9			0.0	23.9	
10	7.1	66.8	66.8	33.2	0.0	13.1	74.3	75.4	24.6	0.0	10.2	51.2	51.3	43.8	4.9	7.3	0.0	0.0	Lost Core			0.0	Lost Core	
11	9.1	58.2	29.5	70.5	0.0	10.8	70.1	74.1	25.9	0.0	11.6	54.8	57.0	43.0	0.0	9.6	23.5	23.5	Lost Core			23.5	Lost Core	
12	14.2	66.7	38.0	62.0	0.0	8.9	67.0	70.3	29.7	0.0	10.8	54.8	51.3	48.7	0.0	10.0	27.8	27.8	13.4			27.8	13.4	
13	15.6	67.3	42.2	57.8	0.0	9.5	71.0	65.4	30.0	0.0	9.9	53.3	48.7	50.1	1.2	9.5	22.1	22.1	11.0			22.1	11.0	
14	13.7	60.5	35.9	63.1	1.0	9.9	74.6	78.6	21.4	0.0	7.4	43.5	43.5	56.5	0.0	8.1	4.0	4.0	7.5			4.0	7.5	
15	12.8	59.0	41.8	58.2	0.0	8.0	58.1	66.5	33.5	0.0	9.7	64.0	32.8	44.3	22.8	7.7	0.0	0.0	10.2			0.0	10.2	
16	11.3	60.3	46.5	53.5	0.0	9.4	52.7	48.6	51.4	0.0	9.7	64.0	32.8	44.3	22.8	9.5	22.1	22.1	7.5			22.1	7.5	
17	9.8	56.6	38.0	57.7	4.3	15.5	68.6	66.6	33.4	0.0	9.7	64.0	32.8	44.3	22.8	7.7	0.0	0.0	10.2			0.0	10.2	
18	8.7	53.9	51.3	48.7	0.0	15.5	67.6	71.4	28.6	0.0	8.3	43.5	43.5	56.5	0.0	8.1	4.0	4.0	7.5			4.0	7.5	
19	7.9	53.2	53.2	46.8	0.0	13.7	60.6	63.4	36.6	0.0	8.3	43.5	43.5	56.5	0.0	8.1	4.0	4.0	7.5			4.0	7.5	
20	10.2	55.4	37.8	53.9	6.3	14.4	65.0	64.8	35.2	0.0	9.7	64.0	32.8	44.3	22.8	9.5	22.1	22.1	7.5			22.1	7.5	
21	11.6	60.0	56.0	44.0	0.0	13.2	66.4	68.4	31.6	0.0	9.7	64.0	32.8	44.3	22.8	9.5	22.1	22.1	7.5			22.1	7.5	
22	10.7	60.8	52.2	42.6	5.2	11.5	60.4	62.8	37.2	0.0	9.7	64.0	32.8	44.3	22.8	9.5	22.1	22.1	7.5			22.1	7.5	
23	9.3	58.9	44.6	48.4	7.0	10.5	62.3	61.5	38.5	0.0	8.3	43.5	43.5	56.5	0.0	8.1	4.0	4.0	7.5			4.0	7.5	
24	8.6	63.7	54.3	45.7	0.0	8.3	48.4	45.0	55.0	0.0	9.7	64.0	32.8	44.3	22.8	9.5	22.1	22.1	7.5			22.1	7.5	
25						9.7	49.8	40.7	55.1	4.3	12.1	62.0	56.9	41.8	1.3	12.1	62.0	56.9	41.8	1.3				
26						12.1	62.0	56.9	41.8	1.3	11.1	65.7	60.4	38.4	1.2	11.1	65.7	60.4	38.4	1.2				
27						11.1	65.7	60.4	38.4	1.2	10.3	65.4	59.3	39.6	1.2	10.3	65.4	59.3	39.6	1.2				
28						10.3	65.4	59.3	39.6	1.2	10.1	65.5	55.4	44.6	0.0	10.1	65.5	55.4	44.6	0.0				
29						10.1	65.5	55.4	44.6	0.0	11.7	68.1	50.3	49.7	0.0	11.7	68.1	50.3	49.7	0.0				
30						11.7	68.1	50.3	49.7	0.0														
Zone Averages		10.3	63.9	50.6	47.0	2.5	12.3	67.6	66.5	33.0	0.4	8.3	43.4	41.1	56.4	2.5	9.59	20.4						

W

Table 7-Subsurface sample analysis vs. time at observation wells no. 2 and 3.

LITTLE KNIFE - CO₂ MINITEST
ANALYSIS - SUBSURFACE SAMPLES

Date:	Mole Percent					
	<u>12/17/80</u>	<u>1/28/81</u>	<u>2/25/81</u>	<u>3/12/81</u>		
Component				<u>3/25/81</u>	<u>4/9/81</u>	<u>4/28/81</u>
N ₂	0.89	0.92	0.92	0.77		
CO ₂	1.28	1.27	1.22	1.45		
H ₂ S	4.82	5.63	6.63	5.20		
C ₁	35.47	34.51	34.57	33.90		
C ₂	10.50	11.43	10.20	9.90		
C ₃	6.99	7.23	7.03	6.75		
iC ₄	1.37	1.58	1.12	1.09		
nC ₄	3.92	4.10	4.06	3.85		
iC ₅	1.60	1.66	1.37	1.25		
nC ₅	1.85	1.85	2.01	2.13		
C ₆	5.26	4.81	4.20	3.30		
C ₇ +	26.05	25.01	26.67	30.41		
Mole wt.	223	225	220	193		
Sp. Gr.	0.8433	0.8488	0.8460	0.8407		
P(SAT)	1870 @ 76°	1850 @ 76°	1820 @ 76°	1825 @ 67°		
N ₂	2.30			0.73		0.79
CO ₂	1.36			1.48		1.48
H ₂ S	4.07			5.22		5.15
C ₁	45.28		No Sample Taken	33.66		33.58
C ₂	8.86			9.89		9.94
C ₃	4.56			6.58		6.75
iC ₄	0.80			1.01		1.32
nC ₄	2.22			3.71		3.81
iC ₅	0.80			1.30		1.28
nC ₅	0.97			1.94		1.91
C ₆	9.47			3.31		2.38
C ₇ +	19.28			31.17		31.61
Mole wt.	198			190		190
Sp. Gr.	0.8382			0.8392		0.8338
P(SAT)	5100+ @ 76°			1840 @ 65°		1821 @ 68°
				1757 @ 70°		1842 @ 69°

No samples taken
Water breakthrough occurred
between 3/12 and 3/25/81

Obs.
Well
No.2

Obs.
Well
No.3

Table 8- Separator gas analysis vs time, N₂ and H₂S free (mole percent), for observation well no. 1.

LITTLE KNIFE - CO₂ MINITEST

Separator Gas Analysis (N₂ and H₂S Free, Mole Percent)
Observation Well No. 1

Date	12/17/80	1/28/81	2/25/81	3/12/81	3/26-27/81
Sep. Press.				96	50
CO ₂				11.67	13.20
C ₁				59.81	46.48
C ₂				16.03	20.24
C ₃	No	No	No	8.40	13.49
iC ₄	Sample	Sample	Sample	1.07	1.10
nC ₄				2.36	3.01
iC ₅				0.35	1.07
nC ₅				0.31	1.43
Date	4/9/81	4/22-29/81	5/6-11/81	5/20-26/81	6/2-4/81
Sep. Press.		30	30	10	18
CO ₂		5.84	12.09	46.99	60.21
C ₁		43.44	53.42	38.61	19.15
C ₂		23.92	27.59	8.04	9.31
C ₃	All	21.39	5.48	3.38	6.92
iC ₄	Nitrogen	2.27	0.48	0.62	1.19
nC ₄		2.50	0.79	1.84	3.21
iC ₅		0.28	0.09	0.26	-
nC ₅		0.37	0.05	0.26	-

Table 9-Separator gas analysis vs time, N₂ and H₂S free (mole percent), for observation well no. 1 (continued).

LITTLE KNIFE - CO₂ MINITEST

Separator Gas Analysis (N₂ and H₂S Free, Mole Percent)
Observation Well No. 1

Date	6/20/81	7/2/81	7/16/81	7/28/81	8/11-13/81
Sep. Press.	5		38	20	30
CO ₂	2.85*		53.34	52.92	31.34
C ₁	4.13		33.44	33.25	49.35
C ₂	2.28		7.19	6.45	10.23
C ₃	-	All	3.16	3.66	5.62
iC ₄	23.79	Nitrogen	0.53	1.12	0.95
nC ₄	44.02		1.39	1.80	2.84
iC ₅	10.68		0.32	0.42	0.29
nC ₅	12.25		0.18	0.38	0.18

Date	8/25-27/81	9/13-21/81
Sep. Press.	10	-
CO ₂		94.6*
C ₁		4.56
C ₂		0.80
C ₃	All	
iC ₄	Nitrogen	
nC ₄		
iC ₅		
nC ₅		

* Extremely high nitrogen concentration before calculating nitrogen free basis.

Table 10-Separator gas analysis vs time, N₂ and H₂S free (mole percent), for observation well no. 2.

LITTLE KNIFE - CO₂ MINITEST

Separator Gas Analysis (N₂ and H₂S Free, Mole Percent)
Observation Well No. 2

Date	12/17/80	1/28/81	2/25/81	3/12/81	3/26-27/81
Sep. Press.	-	58	110	100	41
CO ₂	2.55	2.49	2.52	2.49	2.68
C ₁	67.49	69.78	72.30	64.79	64.70
C ₂	17.33	16.91	15.57	16.08	18.27
C ₃	8.57	7.05	6.70	10.84	9.70
iC ₄	1.04	0.84	0.91	1.62	1.69
nC ₄	2.29	2.23	1.63	2.88	1.96
iC ₅	0.37	0.28	0.24	0.57	0.49
nC ₅	0.35	0.25	0.18	0.73	0.51

Date	4/9/81	4/22-29/81	5/6-11/81	5/20-26/81	6/2-4/81
Sep. Press.	30	40	40	40	12
CO ₂	4.75*	1.04	32.08	26.40	13.93
C ₁	62.76	84.09	42.13	44.06	59.14
C ₂	9.65	0.52	16.88	6.20	9.16
C ₃	14.20	3.19	7.23	6.14	5.90
iC ₄	2.34	3.64	0.58	2.91	1.79
nC ₄	5.25	4.81	0.89	9.36	5.89
iC ₅	0.52	1.27	0.13	2.43	2.46
nC ₅	0.53	1.44	0.08	2.52	1.74

* Extremely high nitrogen concentration before calculating nitrogen free basis.

Table 11-Separator gas analysis vs time, N₂ and H₂S free (mole percent), for observation well no. 2 (continued).

LITTLE KNIFE - CO₂ MINITEST

Separator Gas Analysis (N₂ and H₂S Free, Mole Percent)
Observation Well No. 2

Date	6/20/81	7/2/81	7/16/81	7/28/81	8/11-13/81
Sep. Press.	11	30	-		
CO ₂	7.41	11.91	13.92		
C ₁	63.91	69.99	68.43		
C ₂	7.96	9.26	9.13		
C ₃	4.16	4.53	4.67	Sample	Sample
iC ₄	3.40	1.61	1.07	Container	Container
nC ₄	9.18	2.25	2.41	Empty	Empty
iC ₅	1.75	0.28	0.25		
nC ₅	2.24	0.17	0.12		

Date	8/25-27/81	9/13-21/81
Sep. Press.	20	
CO ₂	26.53	25.3*
C ₁	50.60	18.3
C ₂	5.99	16.0
C ₃	7.08	13.5
iC ₄	2.79	7.8
nC ₄	5.68	12.0
iC ₅	0.70	3.3
nC ₅	0.63	3.8

* Extremely high nitrogen concentration before calculating nitrogen free basis.

Table 12-Separator gas analysis vs time, N₂ and H₂S free (mole percent), for observation well no. 3.

LITTLE KNIFE - CO₂ MINITEST

Separator Gas Analysis (N₂ and H₂S Free, Mole Percent)
Observation Well No. 3

Date	12/17/80	1/28/81	2/25/81	3/12/81	3/26-27/81
Sep. Press.	42			100	46
CO ₂	2.61			2.33	2.51
C ₁	61.26			69.90	62.38
C ₂	18.42			16.30	17.64
C ₃	10.31	No	No	6.77	10.88
iC ₄	1.65	Sample	Sample	1.22	1.73
nC ₄	4.26			2.99	3.29
iC ₅	0.49			0.37	0.76
nC ₅	0.70			0.13	0.80
C ₆	0.30				

Date	4/9/81	4/22-29/81	5/6-11/81	5/20-26/81	6/2-4/81
Sep. Press.	30	100	98	44	14
CO ₂	2.36	2.65	3.43	2.84	3.85
C ₁	85.10	69.57	68.68	78.60	73.13
C ₂	8.02	17.27	17.20	8.76	11.03
C ₃	3.39	6.79	7.18	5.65	4.62
iC ₄	0.06	0.87	0.73	1.84	1.75
nC ₄	0.47	1.84	2.10	2.31	2.59
iC ₅	0.33	0.38	0.34	-	1.67
nC ₅	0.28	0.64	0.33	-	1.36

Table 13—Separator gas analysis vs time, N₂ and H₂S free (mole percent), for observation well no. 3 (continued).

LITTLE KNIFE - CO₂ MINITEST

Separator Gas Analysis (N₂ and H₂S Free, Mole Percent)
Observation Well No. 3

Date	6/20/81	7/2/81	7/16/81	7/28/81	8/11-13/81
Sep. Press.	12	10	22		10
CO ₂	4.77	1.95	15.31		30.84
C ₁	49.80	28.87	61.90		36.08
C ₂	28.76	0.89	13.20		15.05
C ₃	11.29	-	5.66	All	-
iC ₄	1.83	-	-	Nitrogen	-
nC ₄	3.00	8.09	0.89		4.39
iC ₅	0.39	34.77	2.25		10.74
nC ₅	0.17	9.55	0.49		0.97
C ₆		15.88	0.30		1.93

Date	8/25-27/81	9/13-21/81
Sep. Press.	10	
CO ₂	58.01	
C ₁	32.01	
C ₂	4.64	
C ₃	-	All
iC ₄	-	Nitrogen
nC ₄	-	
iC ₅	3.83	
nC ₅	1.51	
C ₆	-	

Table 14-Water tracer analysis, isopropyl and n-propyl alcohols, for observation wells no. 1, 2 and 3.

LITTLE KNIFE - CO₂ MINITEST
WATER TRACER ANALYSIS (ppm)

<u>Date</u> <u>1981</u>	<u>Obs. No. 1</u>		<u>Obs. No. 2</u>		<u>Obs. No. 3</u>	
	<u>IPA</u>	<u>NPA</u>	<u>IPA</u>	<u>NPA</u>	<u>IPA</u>	<u>NPA</u>
3-4	41	0	-	-	-	-
3-27	43	1	52	1	-	-
4-9	72	1	41	1	-	-
4-28	108	1	56	1	-	-
5-8	107	67	107	0	27	0
5-22	42	108	98	61	70	0
6-5	44	102	94	87	127	0
6-18	25	61	45	180	36	0
7-3	25	74	27	144	76	61
7-20	23	40	19	74	35	107
7-31	17	3	18	35	28	120
8-14	18	0	18	28	24	65
8-28	2	1	12	1	11	18
9-21	7	1	13	8	14	37

IPA - isopropyl Alcohol

NPA - normal propyl Alcohol

Table 15-CO₂ isotope ratio analysis for injected CO₂ at observation wells no. 1, 2 and 3, and Zabolotny 1-3-4A, 2-3-3A, 3-3-2B and 4-3-1A production wells surrounding the minitest.

LITTLE KNIFE CO₂ MINITEST
CO₂ ¹³C/¹²C ISOTOPE RATIO

<u>Date</u>	<u>Inj. CO₂</u>	<u>Obs. No.1</u>	<u>Obs. No.2</u>	<u>Obs. No.3</u>	<u>Well Z1</u>	<u>Well Z2</u>	<u>Well Z3</u>	<u>Well Z4</u>
12-17-80	-48.8	NS	-2.3	-2.4	-1.6	-1.7	-1.7	-1.6
1-28-81	-48.9	NS	-2.5	NS	-1.8	-2.1	-1.5	-2.2
2-25-81	NS	NS	-2.1	NS	NS	NS	NS	NS
3-12-81	NS	-38.3	-1.6	-2.1	NS	-0.1	NS	NS
3-26-81	NS	-40.3	-2.7	-2.8	NS	NS	NS	-2.3
4-9-81	NS	NS	NA	-1.6	NS	-2.0	NS	NS
4-22-81	NS	-34.6	0.4	-2.1	NS	NS	-1.4	NS
5-8-81	NS	-43.6	-45.2	-12.7	-1.9	NS	NS	NS
5-23-81	NS	-45.6	-43.7	-11.8	NS	NS	-1.4	NS
6-3-81	NS	-46.8	-40.1	-14.8	NS	NS	-2.1	NS
6-20-81	NS	Insuf	-37.5	-22.8	NS	NS	-1.2	NS
7-2-81	NS	Insuf	-39.6	Insuf	NS	-1.6	NS	NS
7-15-81	NS	-47.8	-39.2	-36.3	NS	NS	-0.9	NS
7-28-81	NS	-49.9	Insuf	Insuf	NS	NS	-1.0	NS
8-11-81	NS	-49.2	Insuf	-15.2	NS	NS	-1.0	NS
8-27-81	NS	Insuf	-44.8	Insuf	NS	NS	-1.4	NS
9-17-81	NS	-49.6	-45.9	Insuf	NS	NS	-1.5	NS

Z1 - Zabolotny 1-3-4A

Z2 - Zabolotny 2-3-3A

Z3 - Zabolotny 3-3-2B

Z4 - Zabolotny 4-3-1A

NS - No sample taken

NA - Not analyzed

Insuf - Insufficient sample for analysis

Table 16-Fluid properties of various coring fluid compositions with low slurry weights.

	<u>Sample #1</u>	<u>Sample#2</u>	<u>Sample #3</u>	<u>Sample #4</u>	<u>Sample #5</u>
<u>lb/bbl</u>					
Bentonite	12.5	12.5	12.5	12.5	7
Modified Starch	4	---	---	---	---
Carboxymethyl Cellulose	1	---	---	---	---
Sodium Polyacrylate	---	---	---	---	1
Partially Hydrolyzed Polyacrylamide	---	---	---	---	---
Shredded Paper	---	---	---	---	2
Low-Viscosity Polyanionic Cellulosic Polymer	---	2	1	2	---
Inert Clay Solids	40	**60	---	---	60
Slurry Weight, ppg	9.1	9.3	8.5	8.5	9.3
Plastic Viscosity, cps	32	48	15	28	12
Yield Point, lbs/100 ft ²	30	35	9	19	5
10 Sec Gel Strength, lbs/100 ft ²	12	13	4	5	1
10 Min Gel Strength, lbs/100 ft ²	53	35	6	14	2
Temp. °F	110	112	110	112	108
pH	8.0	8.1	8.5	8.7	7.6
30 Min. API F.L., cm ³	5.8	6.8	13.6	10.4	10.7
API F.L. @ 210°F, cm ³	7.6	8.5	15.4	14.3	13.5

**Recommendation: Use 40 lb/bbl inert clay solids rather than 60 lb/bbl.

Table 17-Apparent spurt loss calculations for coring fluids mentioned in Table 16.

**APPARENT SPURT LOSS CALCULATED @ T=1 SECOND
FOR FLUIDS SHOWN ON TABLE 16**

@ 110°F

Time	Volume, cm ³				
	Sample #1	Sample#2	Sample #3	Sample #4	Sample #5
30 sec	0	0	.438	.183	.055
1 min	.039	.052	.387	.207	.090
2 min	.082	.082	.374	.210	.146
5 min	.104	.121	.352	.231	.196
7½ min	.113	.132	.344	.236	.217
10 min	---	---	---	---	---
15 min	.130	.152	.331	.243	---
16 min	---	---	---	---	.236
30 min	.137	.160	.321	.245	.252

APPARENT SPURT LOSS CALCULATED @T=1 SECOND

@ 210°F

Time	Volume, cm ³				
	Sample #1	Sample#2	Sample #3	Sample #4	Sample #5
30 sec	.055	---	---	---	.164
1 min	.090	.103	.478	.465	.207
2 min	.119	.137	.411	.411	.246
5 min	.156	.173	.393	.381	.294
7½ min	---	.184	.391	.372	---
10 min	.176	---	---	---	---
15 min	.173	.201	.377	.363	---
16 min	---	---	---	---	---
24 min	---	---	---	---	.319
30 min	.179	.200	.363	.337	.318

Apparent Spurt Loss Formula: $Q_2 = Q_1 \sqrt{\frac{T_2}{T_1}}$

Q_1 = known filtrate @ time T_1

Q_2 = unknown filtrate @ time T_2

Table 18-Rheological and fluid-loss properties for various coring fluid compositions.

Purpose: Determine rheological and fluid-loss effects of H₂S scavenger

	<u>Sample #1</u>	<u>Sample#2</u>	<u>Sample #3</u>	<u>Sample #4</u>
<u>lb/bbl</u>				
Bentonite	12.5	12.5	12.5	12.5
Modified Starch	4	4	4	4
Carboxymethyl Cellulose	1	2	1	2
Inert Clay Solids	40	40	40	40
Chelated Zinc Tannate	-	-	1	1
Zinc Lignosulfonate	.12 gal/bbl	.12 gal/bbl	---	---
Slurry Weight, ppg	9.1	9.1	9.1	9.1
Plastic Viscosity, cps	25	40	22	35
Yield Point, lbs/100 ft ²	22	51	22	47
10 Sec Gel Strength, lbs/100 ft ²	9	28	15	35
10 Min Gel Strength, lbs/100 ft ²	45	80	60	95
Temp., °F	119	122	118	123
30 Min. API F.L., cm ³	6.0	5.2	5.3	4.6

Table 19-Apparent spurt loss calculations for coring fluids mentioned in Table 18.

APPARENT SPURT LOSS CALCULATED @ T=1 SECOND
FOR FLUIDS SHOWN ON TABLE 18
@ 110°F

Time	Volume, cm ³			
	Sample #1	Sample #2	Sample #3	Sample #4
30 sec	0	Sample too	0	Sample too
1 min	.039	viscous for	.026	viscous for
2 min	.091	accurate	.082	accurate
5 min	.115	results	.104	results
7½ min	.123	"	.108	"
10 min	.127	"	---	"
15 min	.133	"	---	"
18 min	.134	"	.125	"
24 min	.137	"	.124	"
30 min	.141	5.2	.125	4.6

Apparent Spurt Loss Formula: $Q_2 = Q_1 \sqrt{\frac{T_2}{T_1}}$

Q_1 = known filtrate @ time T_1

Q_2 = unknown filtrate @ time T_2

Table 20-Plug and donut analysis data from the pressure core in observation well
no. 4.

ZABOLOTNY OBSERVATION #4
ANALYSES OF PLUGS AND DONUTS

Sample No.	Core No.	Layer	Depth Ft.	Confining Pressure psi	Vertical Permeability md	Porosity	Average Water Saturation	Sample Position In Core	Is Filtrate Concentration Difference Within Maximum Experimental Error
2	1	W	9806.7-9806.9	3,550	1.3	.13	.55	Center	Yes
4	3	W	9819.6-9819.8	2,000	.13	.13	.64	Top	No
6	4	Y	9827.2-9827.4	3,100	4.5	.16	.80	Top	Yes
7	4	Y	9830.1-9830.3	3,100	26.00	.22	.69	Center	Yes
8	5	Y	9837.0-9832.2	0	39.00	.23	.34	Top	No

ANALYSES OF NEAREST CORES

Sample No.	Depth Ft.	Maximum Permeability md	Porosity	Oil Saturation	Water Saturation	Voilage
2	9806-07	1.3	.164	.192	.749	.059
4	9819-20	2.6	.140	.134	.634	.232
6	9827-28	454.00	.233	.144	.822	.034
7	9830-31	567.00	.262	.040	.812	.148
8	9837-38	46.00	.213	.169	.354	.477

Table 21-Pressure core analysis data, for layers W, X, Y and Z, observation well no. 4.

	Depth (ft)	k _{max} (md)	φ (%)	S _o ^a (%PV)	S _w ^b (%PV)	S _{CO₂} ^c (%PV)	CO ₂ in gas (mol %) (N ₂ -free basis)	LAYER
Core #1 3550 psi	9803.0-04.0	12.	15.1	16.6	85.3	0.1	2.00	W
	9804.0-05.0	4.2	6.6	37.5	53.6	0.5	2.45	
	9805.0-06.0	0.58	9.2	27.7	75.5	0.3	1.94	
	9806.0-07.0	1.3	16.4	31.9	79.2	0.4	2.27	
	9807.0-08.0	3.3	12.9	32.0	72.5	0.3	1.65	
	9808.0-09.0	1.9	15.8	49.3	48.3	--	--	
	9809.0-10.0							
9810.0-11.0			lost					
Core #2 3200 psi	9811.0-12.0	0.7	6.6	15.3	91.2		3.09	
	9812.0-13.0	3.4	10.1	39.0	65.6	0.6	2.38	
	9813.0-14.0	2.2	15.5	41.0	72.4	--	--	
	9814.0-15.0	0.42	6.7	44.2	65.7	1.3	8.56	
	9815.0-16.0	0.34	6.1	44.3	74.2	0.4	4.06	
	9816.0-16.7	1.2	9.9	39.7	67.6	0.6	2.07	
	9816.7-18.0			lost				
9818.0-19.0								
Core #3 2000 psi	9819.0-20.0	2.6	14.0	22.2	67.0	--	--	
	9820.0-21.0	1.2	9.6	18.3	85.3	1.6	8.51	
	9821.0-22.0	1.3	6.2	12.5	89.1	1.4	9.61	
	9822.0-23.0	0.47	7.2	16.9	78.9	4.6	22.39	
	9823.0-24.0	1.6	8.5	15.6	79.5	1.6	8.05	
	9824.0-24.5	1.8	7.9	21.6	81.4	--	--	
	9824.5-26.0			lost				
9826.0-27.0								
Core #4 3100 psi	9827.0-28.0	454.	23.3	23.7	86.8	--	--	
	9828.0-29.0	63.	20.6	4.0	89.8	--	--	
	9829.0-30.0	117.	23.4	8.3	84.0	18.5	79.03	
	9830.0-31.0	567.	26.2	6.8	85.7	5.6	97.72	
	9831.0-32.0	233.	27.8	7.8	84.1	0.6	77.19	
	9832.0-33.0							
	9833.0-34.0			lost or broken				
9834.0-35.0								
Core #5 0 psi	9835.0-36.0	617.	24.0	47.6	49.7	--	--	
	9836.0-37.0	1971.	23.6	18.6	49.9	--	--	
	9837.0-38.0	46.	21.3	28.1	37.4	--	--	
	9838.0-39.0	26.	11.8	28.9	44.1	--	--	
	9839.0-40.0	6.2	17.7	40.2	41.8	--	--	
9840.0-41.0								
9841.0-42.0			lost or broken					
9842.0-43.0								
Core #6 3800 psi	9843.0-44.0	0.01	5.4	21.2	87.2	0.2	3.91	
	9844.0-45.0	0.38	10.5	20.6	89.4	0.1	4.38	
	9845.0-46.0	0.33	10.9	28.7	83.1	0.2	3.21	
	9846.0-47.0	0.03	9.7	6.5	96.0	0.2	12.56	
	9847.0-48.0	0.94	10.6	28.7	78.6	0.3	3.27	
	9848.0-49.0	3.9	16.7	30.9	78.6	--	--	
	9849.0-50.0	5.5	15.5	22.1	82.9	0.3	3.13	
	9850.0-51.0	3.6	10.4	20.9	89.7	0.1	3.66	
	9851.0-52.0	0.14	8.3	20.1	89.5	0.5	7.16	
	9852.0-53.0	0.03	5.6	11.5	97.3	0.3	5.4	
Core #7 3000 psi	9853.0-54.0	0.23	7.3	18.3	91.1	0.1	4.38	
	9854.0-55.0	0.24	7.3	35.7	78.7	--	--	
	9855.0-56.0	0.35	11.7	38.0	79.3	0.3	2.98	
	9856.0-57.0	0.10	4.9	16.6	85.0	--	--	
	9857.0-58.0	2.9	12.7	39.2	70.0	0.3	1.88	
	9858.0-59.0	0.67	9.5	93.3	40.3	0.3	2.32	

^aFVF for oil at 3800 psi and 245°F ~1.66

^bFVF for water at 3800 psi and 245°F ~1.056

^ccalculated assuming CO₂ density at retained pressure

Table 22-Gulflog and core analyses comparisons for injection well no. 1 and observation wells no. 1, 2, 3 and 4.

<u>Layer</u>	<u>Log Depth (ft)</u>	<u>Thickness (ft)</u>	<u>Core Φ(%)</u>	<u>Log Φ(%)</u>	<u>K_h (md)</u>	<u>K_v (md)</u>	<u>S_{oi} (%)</u>	<u>S_{orw}* (%)</u>
<u>Zabolotny Inj. No. 1</u>								
W	9809-24	15	11.4	9.6	2.3	2.4	---	---
X	9824-27	3	17.0	18.1	9.5	30.6	79.8	42.5
Y	9827-35	8	22.7	22.2	58.7	38.1	81.8	39.7
Z	9835-40	5	15.6	16.6	11.7	8.5	70.0	50.5
		<u>31</u>						
<u>Zabolotny Obs. No. 1</u>								
W	9798-10	12	10.2	8.4	2.9	.9	---	---
X	9810-13	3	18.3	16.0	5.0	32.0	79.6	44.7
Y	9813-21	8	22.2	23.4	16.5	32.3	84.4	40.2
Z	9821-25	4	14.9	14.0	1.2	5.8	72.9	59.9
		<u>27</u>						
<u>Zabolotny Obs. No. 2</u>								
W	9842-57	15	11.2	10.9	1.5	.8	---	---
X	9857-59	2	20.5	17.4	4.1	20.0	74.8	47.9
Y	9859-68	9	24.4	25.0	25.6	36.9	78.2	38.2
Z	9868-73	5	14.9	17.4	2.8	4.2	74.9	54.7
		<u>31</u>						
<u>Zabolotny Obs. No. 3</u>								
W	9823-38	15	9.6	5.5	.9	.4	---	---
X	9838-41	3	18.0	17.8	18.0	---	76.8	---
Y	9841-50	9	21.9	23.0	34.0	21.2	79.8	37.1
Z	9850-54	4	14.9	14.4	13.8	.7	71.9	49.2
		<u>31</u>						
<u>Zabolotny Obs. No. 4</u>								
W	9821-35	14	9.3	---	1.5	.3	---	---
X	9835-38	3	21.9**	15.8	63.0	---	---	---
Y	9838-46	8	25.0**	23.4	96.0	50.0	---	---
Z	9846-51	5	19.6**	14.3	29.6	31.0	---	---
		<u>30</u>						

* Based upon flushed zone water saturation correlation (micro-resistivity logs).

** Portions of the core samples were broken and hence not analyzed or pressure was too low.

Table 23-Oil composition and component parameters for the Peng-Robinson equation of state used in simulation studies.

<u>Component</u>	<u>Mole Fraction</u>	<u>Molecular Weight</u>	<u>Critical Pressure (psi)</u>	<u>Critical Temperature (°R)</u>	<u>Critical Volume (Cu Ft/Lb-Mole)</u>	<u>Accentric Factor</u>
CO ₂	.0120	44.010	1070.94	547.59	1.5051	.2250
H ₂ S	.0491	34.076	1305.92	672.39	1.5641	.1000
C ₁ N ₂	.3494	16.362	663.10	339.98	1.5860	.0112
C ₂	.0987	30.070	707.76	549.78	2.3695	.0986
C ₄ *	.1464	54.809	565.12	733.36	3.5420	.1860
C ₁₀ *	.0668	135.000	375.22	1149.90	8.6030	.3705
C ₁₄ *	.2776	192.000	292.49	1298.30	12.5000	.5485

Nitrogen was included in methane. Propane, butanes, and pentanes were combined as C₄*. Hexane and heptanes plus were lumped together and then divided into C₁₀* and C₁₄*.

Table 24-Binary interaction parameters for the Peng-Robinson equation of state used in the three-dimensional simulator.

	<u>CO₂</u>	<u>H₂S</u>	<u>C₁N₂</u>	<u>C₂</u>	<u>C₄*</u>	<u>C₁₀*</u>	<u>C₁₄*</u>
CO ₂	0.						
H ₂ S	0.100	0.					
C ₁ N ₂	0.100	0.088	0.				
C ₂	0.130	0.080	0.001	0.			
C ₄ *	0.131	0.072	0.020	0.	0.		
C ₁₀ *	0.129	0.034	0.034	0.	0.	0.	
C ₁₄ *	0.127	0.003	0.065	0.	0.	0.	0.

Nitrogen was included in methane. Propane, butanes, and pentanes were combined as C₄*. Hexane and heptanes plus were lumped together and then divided into C₁₀* and C₁₄*.

Table 25-Basic reservoir characteristic data, zone D of the Mission Canyon Formation at Little Knife Field.

Reservoir Depth, feet	9800
Thickness, feet	16
Porosity, %	21
Core Permeability, md	30
Interstitial Water Saturation, %	21
Waterflood Residual Oil Saturation, %	40
Reservoir Temperature, °F	245
Initial Reservoir Pressure, psia	4409
BHP, Dec. 1980, psia	3345
Rock Compressibility, psi ⁻¹	2.63 × 10 ⁻⁶
Dip Angle, degree	0.5

Table 26-Physical properties of Little Knife Field reservoir fluids from Zabolotny 1-3-4A well.

Reservoir Temperature, °F	245
Saturation Pressure (P _s), psia	2698
Solution GOR at P _s , SCF/STB	1119.4
Oil Formation Volume Factor at P _s , RB/STB	1.769
Oil Viscosity at P _s , cp	0.20
Oil Gravity, °API	41.0
Oil Density at P _s , gm/ml	0.6043
Oil Compressibility at P _s , psi ⁻¹	28.95 × 10 ⁻⁶
Minimum Miscibility Pressure with CO ₂ , psig	3400
Water Formation Volume Factor, RB/STB	1.045
Water Viscosity, cp	0.456
Water Compressibility, psi ⁻¹	3.89 × 10 ⁻⁶

Table 27-Distances and orientations of production wells and observation wells relative to injection well no. 1.

<u>Well</u>	<u>Distance, feet</u>	<u>Azimuthal Angle θ, Degree</u>
Zabolotny 4-3-1A	2015	90
Zabolotny 1-3-4A	1915	180
Zabolotny 2-3-3A	1713	270
Observation No. 1	258	0
Observation No. 2	250	201
Observation No. 3	283	78.9
Observation No. 4	136	196.7

Table 28-Input data of reservoir rock properties of injection well no. 1 and observation wells no. 1, 2 and 3 as well pairs.

Well Pair	Distance (ft)	Layers	Thickness (ft)	Porosity	Permeability, md		Saturation, Fraction PV	
					k_h	k_v	S_{oi}	S_{orw}
ZI-ZO1	258	W	10	0.105	4.2	3.0	0.680	0.55
		X	3	0.180	34.0	3.0	0.796	0.45
		Y	8	0.223	112.0	3.0	0.844	0.41
		Z	4	0.149	14.2	1.0	0.729	0.60
		*XYZ	15	0.195	50.1	3.0	0.811	0.46
ZI-ZO2	250	W	20	0.112	5.0	3.0	0.680	0.55
		X	2	0.196	50.3	3.0	0.748	0.45
		Y	9	0.240	180.0	3.0	0.782	0.33
		Z	5	0.149	14.2	1.0	0.749	0.55
		*XYZ	16	0.206	70.0	3.0	0.770	0.40
ZI-ZO3	283	W	15	0.100	3.6	3.0	0.680	0.55
		X	3	0.178	32.0	3.0	0.768	0.45
		Y	9	0.221	105.0	3.0	0.798	0.37
		Z	4	0.149	14.2	1.0	0.719	0.50
		*XYZ	16	0.195	50.1	3.0	0.778	0.41
**Average		W	15.0	0.106	4.3	3.0	0.680	0.55
		X	3.0	0.184	38.8	3.0	0.771	0.45
		Y	8.5	0.228	132.3	3.0	0.808	0.38
		Z	4.5	0.149	14.2	1.0	0.732	0.55

*For 11x11x2 grid system.

**For 16x15x4 grid system.

Table 29-Percentages of oil displaced, at stock tank conditions, for layers W, X, Y and Z in the minutest area (radius = 283 feet).

OIL DISPLACED

(Radius = 283 Feet)

<u>Layer</u>	<u>OIP STB*</u>	<u>Oil Displaced, Percent OIP</u>		
		<u>Waterflood</u>	<u>CO₂ WAG=1:1</u>	<u>Incremental</u>
W	27,360	15	17	2
X	10,854	39	58	19
Y	39,740	57	79	22
Z	12,267	21	24	3
<hr/> TOTAL	<hr/> 90,221	<hr/> 37	<hr/> 50	<hr/> 13

*Oil-in-place on December 11, 1980

Table 30-Input data of reservoir rock properties for layer Y, divided into sub-layers Y₁, Y₂, Y₃ and combined, in the six-layer model.

INPUT DATA FOR RESERVOIR ROCK PROPERTIES
FOR LAYER Y (SIX-LAYER MODEL)

<u>Layers</u>	<u>Depth feet</u>	<u>Thickness feet</u>	<u>Porosity, fraction</u>	<u>Saturation, Fraction PV</u>			<u>Permeability, md</u>	
				<u>Soi</u>	<u>Sorw</u>	<u>So(9-16-81)</u>	<u>Kh</u>	<u>Kv</u>
Y1	9859	2	.241	.723	.370	.283	50	1
	9860		.240	.784	.244			
Y2	9861	3	.320	.825	.320	.085	200	100
	9862		.228	.804	.056			
	9863		.256	.784	.015			
Y3	9864	3	.255	.793	.105		100	3
	9865		.256	.786	.138			
	9866		.270	.760	.139			
Y (Combined)		8	.246	.782	.330	.133	125	

Table 31-Carbon dioxide sweep efficiency.

<u>LAYER</u>	<u>AREAL MODE</u>	
	<u>AREAL SWEEP EFFICIENCY, %</u>	
	<u>x = 3%*</u>	<u>x = 10%*</u>
W	20	2
X	100	80
Y	100	100
Z	25	10

<u>x</u>	<u>VERTICAL SWEEP EFFICIENCY, %</u>
	3%
10%	52

*Where x equals carbon dioxide content in given grid block in the minitest simulation model.

Table 32-Water analysis data from eight field production wells at Little Knife Field.

Water Analysis - Little Knife Field, North Dakota

Well	P. Glovatski	Kostelnak- State	USA	Fed.Land BF-Gulf	Lind 2	Dolezal 1	Zabolotny 3-3-2B	Hlebechuk
Sample Date	3/24/78	3/24/78	3/24/78	3/24/78	3/24/78	3/24/78	3/24/78	3/24/78
pH	5.9	5.7	5.8	5.6	5.6	5.6	4.1	5.5
Dissolved Solids, ppm	376,000	313,000	346,000	349,000	346,000	341,000	259,000	292,000
Sodium, ppm	125,000	101,000	111,000	110,000	111,000	108,000	71,500	92,200
Calcium, ppm	16,400	18,000	20,000	21,600	18,800	20,400	18,400	17,200
Magnesium, ppm	2,920	1,700	2,190	1,940	2,670	2,190	6,560	2,430
Chlorides, ppm	231,000	192,000	212,000	214,000	212,000	209,000	162,000	180,000
Sulfate, ppm	135	131	135	135	131	135	155	135
Bicarbonates, ppm	307	254	293	259	405	444	(?)	268
Iron, ppm	18	4	10	8	8	8	12	12

Table 33-Physical properties and analysis of reservoir fluid from Zabolotny 1-3-4A well.

PHYSICAL PROPERTIES OF RESERVOIR FLUID
LITTLE KNIFE, ZABOLOTNY 1-3-4A

Saturation Pressure	2698 psia
Coefficient of thermal expansion at 4000 psia from 69°F to 245°F	7.2 x 10 ⁻⁴ vol/vol/°F
Density of oil at 2698 psia and 245°F	0.6043 g/ml
Specific volume at 2698 psia and 245°F	0.0265 cu. ft./lb.

Hydrocarbon Analysis

<u>Component</u>	<u>Mole %</u>	<u>Volume %</u>
Nitrogen	0.91	0.27
Carbon Dioxide	1.12	0.51
Hydrogen Sulfide	5.73	2.09
Methane	33.34	15.03
Ethane	9.85	7.01
Propane	6.66	4.88
iso-Butane	1.35	1.18
n-Butane	3.85	3.24
iso-Pentane	1.49	1.45
n-Pentane	1.96	1.89
Hexanes	3.42	3.74
Heptanes-plus	<u>30.32</u>	<u>58.71</u>
Total	100.00	100.00

Properties of Heptanes-plus Fraction

Sp. Gr. (60/60)	0.8390
API Gravity	37.2
Molecular Weight	192

Table 34-Results of autoclave tests performed on various materials for corrosior studies.

<u>Source of Water</u>	<u>Dunn Co., ND</u>	<u>McKensie Co., ND</u>	<u>Synthetic Brine¹</u>	<u>Dunn Co., ND</u>	<u>McKensie Co., ND</u>
<u>VAPOR COMPOSITION</u>					
Carbon Dioxide, %	35	35	35	85	85
Hydrogen Sulfide, %	15	15	15	15	15
Nitrogen, %	50	50	50	--	--
Temperature, °F	236	240	240	235	240
Pressure, psig	4000	3600	3550	2800	2750
<u>CORROSION RATES, MPY</u>					
17-4 PH	4.9	2.7	6.4	5.2	5.8
L-80 Casing	7.5	6.7	8.0	9.4	8.2
Incoloy 825	0.2	1.3	0.9	1.0	1.1
Hastelloy C-276	0.3	1.2	0.6	3.1	1.0
Inconel 625	0.0	0.8	0.5	1.1	0.9
Cast 410 SS	7.8	10.3	26.6	11.5	9.4
K-Monel	6.9	8.5	5.4	7.2	6.8
316 SS	1.3	4.3	3.1	6.5	1.9
L-80 Casing (Vapor)	--	--	--	--	11.1

1. Synthetic Brine Composition: NaCl 250,000 Mg/L, CaCl₂ 50,000 Mg/L, Distilled H₂O.

Table 35—Results of autoclave tests performed on various materials for corrosion studies (continued).

LITTLE KNIFE CO₂ MINITEST
AUTOCLAVE CORROSION TESTS

<u>Source of Water Vapor Composition</u>	<u>Dunn Co., ND diluted 1:1 w/distilled water*</u>	<u>Dunn Co., ND diluted 20:1 w/distilled water*</u>
Carbon Dioxide, %	85	85
Hydrogen Sulfide, %	15	15
Nitrogen, %	0	0
Temperature, °F	240	232
Pressure, psig	2250	2300
 <u>Corrosion Rates, MPY</u>		
17-4 PH	4.1	3.6
L-80 Casing	10.0	11.0
Incoloy 825	0.6	1.6
Hastelloy C-276	0.5	0.8
Inconel 625	0.4	0.6
Cast 410 SS	11.4	3.4
K-Monel	7.1	7.8
316 SS	3.6	1.6

* Autoclave O₂ purged w/CO₂

Table 36/37-Visual inspection results of surface and downhole tubulars and equipment at Little Knife Field.

Equipment	Material	Visual Inspection	Comments
Surface water injection line	2 in. schedule 80 line pipe internally coated with TK-75	Good condition	No visible pitting. Pipe used in field for other purposes.
Surface CO ₂ injection line	2 in. schedule 80 line pipe	Good condition	No visible pitting. Pipe used in field for other purposes*.
Injection and production wellheads	316 stainless steel internally clad w/Inconel, 17-4 PH valve trim	--	See Table 46.
Injection tubulars	2-7/8 in. OD C-75 Hydril CS-CB with TK-2	--	Tubing inspection report in Appendix 46.
Production tubulars	2-7/8 in. OD C-75 Hydril CS-CB with TK-7	Coating failure ³ in one string	Coating failure possible due to mechanical damage. Tubing inspection report in Appendix 46.
Landing nipples	Inconel 718	Excellent condition	No evidence of corrosion.
Downhole pressure monitor and chamber	Chamber containing tool joints internally coated with TK-2 in injector and TK-7 in producer	Good	No apparent evidence of corrosion. Inspected with tubing. Returned to stock.
Gas lift valve	Internally coated with TK-7, 303 SS valve, Viton O-rings, SS gasket, monel seat and latches	Good	Valves disassembled and visually examined by manufacturer. The valves were in good mechanical condition with no evidence of corrosion.

* Corrosion rates from coupons -- .03-.04 mpy

Table 38-Corrosion results of four (4) downhole flow-through racks, located through out Little Knife Field.

<u>Rack No.</u>	<u>Location</u>	<u>Material</u>	<u>Coating</u>	<u>Corrosion Rate (mils per year)</u>	<u>Remarks</u>
1	B. Zabolotny	C-75		0.2	One large blister. Good. No defects. Numerous blisters. Good. No defects.
		N-80		0.2	
		316 SS		0.0	
			TK-2 TK-7 TK-69 TK-77		
2	E. E. Miller	C-75		0.7	Blisters, some broken. Many small cracks, but intact. Numerous blisters, some broken. Coating missing over 4 large areas.
		N-80		0.3	
		316 SS		0.07	
			TK-2 TK-7 TK-69 TK-77		
3	Hurinenko	C-75		0.1	Numerous small blisters. Good. No defects. Numerous blisters, some broken. Evident disbonding.
		N-80		0.1	
		316 SS		0.0	
			TK-2 TK-7 TK-69 TK-77		
4	Sabrosky	C-75		0.1	Three small blisters. Good. No defects. Good. No defects. One large blister.
		N-80		0.1	
		316 SS		0.0	
			TK-2 TK-7 TK-69 TK-77		

Table 39-Corrosion results of two (2) downhole flow-through racks, located throughout Little Knife Field and two (2) four inch (4") surface racks at the minitest site.

Downhole Flow-Through Racks

<u>Rack No.</u>	<u>Location</u>	<u>Material</u>	<u>Coating</u>	<u>Corrosion Rate (mils per year)</u>	<u>Remarks</u>
5	Zabolotny	C-75		0.3	Blistered, one large holiday. Good. No defects. Blistered, disbonded. Good. No defects.
		N-80		0.5	
		316 SS		0.07	
			TK-2		
			TK-7		
			TK-69		
			TK-77		
6	J. Tachenko	C-75		0.1	Blistered, cracks. Good. No defects. A few small blisters. Several blisters, disbonding.
		N-80		0.1	
		316 SS		0.0	
			TK-2		
			TK-7		
			TK-69		
			TK-77		

4-inch Surface Racks

<u>Rack No.</u>	<u>Location</u>	<u>Material</u>	<u>Coating</u>	<u>Corrosion Rate (mils per year)</u>	<u>Remarks</u>
1	Downstream of high pressure Scrubber CTB#2	C-75		0.05	
		L-80		0.06	
		4140		0.03	
		316 SS		0.0	
2	Downstream of Treater #1 at CTB #2	C-75		0.1	
		L-80		0.2	
		4140		0.1	
		316 SS		0.0	

Table 40-Corrosion results of six (6) four inch (4") surface racks, located at a central production facility, Little Knife Field.

<u>Rack No.</u>	<u>Location</u>	<u>Material</u>	<u>Coating</u>	<u>Corrosion Rate (mils per year)</u>	<u>Remarks</u>
3	Bad oil (recycle) line at CTB #2	C-75		0.6	
		L-80		1.9	
		4140		0.8	
		316 SS		0.0	
4	Downstream of Treater #3 on Water Leg-CTB #2	C-75		0.2	
		L-80		0.3	
		4140		0.2	
		316 SS		0.0	
5	Downstream of Treaters on oil Line going into boot-CTB #2		TK-2		Good. No defects.
			TK-7		Good. No defects.
			TK-69		Good. No defects.
			TK-77		Good. Mechanical damage.
6	Downstream of Low Pressure Scrubber CTB #2		TK-2		Good. No defects.
			TK-7		Good. Mechanical damage.
			TK-69		Good. No defects.
			TK-77		Good. Color change.
7	Upstream of Pressure Scrubber CTB #2		TK-2		Good. No defects.
			TK-7		Good. No defects.
			TK-69		Good. No defects.
			TK-77		Good. Color change.
8	Downstream of Treater #2 on Water Leg-CTB #2		TK-2		Good. No defects.
			TK-7		Good. No defects.
			TK-69		Good. No defects.
			TK-77		Good. Mechanical damage.

Table 41-Corrosion results of seven (7) two inch (2") surface racks containing metal coupons, located throughout Little Knife Field.

<u>Rack No.</u>	<u>Location</u>	<u>Exposure Time (Days)</u>	<u>Material</u>	<u>Corrosion Rate (mils per year)</u>
164	Downstream of Casing Valve Tedrow 1-11-1A	518	C-75	0.4
			L-80	0.6
			4140	0.3
			316 SS	0.0
165	Downstream of casing choke on pumping well Tedrow 6-12-2A	225	L-80	0.0
			4140	0.0
			316 SS	0.0
167	CO ₂ injection system line	95	C-75	0.04
			L-80	0.04
			4140	0.03
			316 SS	0.00
168	Salt water injection line	341	C-75	0.9
			L-80	1.4
			4140	0.6
			316 SS	0.0
175	Recycle-Bad Oil Line - CTB #2	237	C-75	0.009
			L-80	0.009
			4140	0.03
			316 SS	0.00
176	Downstream of Casing Valve Tedrow 6-12-2A Gas Line	238	C-75	0.9
			L-80	1.2
			4140	1.0
			316 SS	0.0
177	Downstream of Casing Valve L. Kostelnak 2-29-ID Gas Line	238	C-75	0.008
			L-80	0.006
			4140	0.02
			316 SS	0.00

Table 42-Corrosion results of one (1) two inch (2") surface rack containing metal coupons and four (4) two inch (2") surface racks containing coated coupons, located throughout Little Knife Field.

2-inch Surface Racks (Metal Coupons)

<u>Rack No.</u>	<u>Location</u>	<u>Exposure Time (Days)</u>	<u>Material</u>	<u>Corrosion Rate (mils per year)</u>
178	Downstream of Casing Valve- Kostelnak State I-36-2B Gas Line	238	C-75	0.02
			L-80	0.02
			4140	0.03
			316 SS	0.00

2-inch Surface Racks (Coated Coupons)

<u>Rack No.</u>	<u>Location</u>	<u>Exposure Time (Days)</u>	<u>Coating</u>	<u>Remarks</u>
169	Downstream of Casing Valve- S. Burian I-22-1A	427	TK-2	Good. No defects.
			TK-7	Good. No defects.
			TK-69	Good. Mechanical damage.
			TK-77	Good. No defects.
170	Downstream of Casing Valve- D. Dolezal I-17-1A	517	TK-2	Good. Color change.
			TK-7	Good. No defects.
			TK-69	Good. No defects.
			TK-77	Poor. Failed at edges.
171	Downstream of Casing Valve- State I-16-2B	519	TK-2	Good. No defects.
			TK-7	Good. No defects.
			TK-69	Good. No defects.
			TK-77	Good. No defects.
172	Downstream of Casing Valve- A. Zabolotny I-4-4C	517	TK-2	Good. No defects.
			TK-7	Good. No defects.
			TK-69	Good. No defects.
			TK-77	Good. No defects.

Table 43-Corrosion results of two (2) two inch (2") surface racks containing coated coupons at the minitest site, Little Knife Field.

2-inch Surface Racks (Coated Coupons)

<u>Rack No.</u>	<u>Location</u>	<u>Exposure Time (Days)</u>	<u>Coating</u>	<u>Remarks</u>
173	CO ₂ injection system line	95	TK-2	Good. Minor mechanical damage.
			TK-7	Good. Minor mechanical damage.
			TK-69	Good. Minor mechanical damage.
			TK-77	Good. Minor mechanical damage.
174	Saltwater Injection Line	341	TK-2	Good. No defects.
			TK-7	Good. No defects.
			TK-69	Good. Color change.
			TK-77	Poor. Failed at one end.

Table 44-Visual inspection results of tubing nipples recovered from observation well no. 3.

2 7/8 in. O.D. tubing subs

<u>Material</u>	<u>Remarks</u>
C-75	Moderate corrosion, some pitting
L-80	Moderate corrosion, some pitting
N-80	Slight corrosion
N-80 w/ Ni plating	Very slight corrosion
316 SS w/ Ni plating	No corrosion evident
316 SS	No corrosion evident

Table 45-Independent laboratory results of pit-depth measurements made on corrosion nipples recovered from observation wells no. 2 and 3.

<u>SAMPLE</u>	<u>PIT DEPTH</u> <u>(INCHES)</u>	
	.017	
	.0004	
C-75	.0105	AVG. = .0101
	.010	
	.0125	
	.010	
	.0155	
L-80	.007	AVG. = .0123
	.013	
	.016	

NOTE: Depth was measured on the 5 deepest-appearing pits on the inside surface. Exposure time was approximately one year. General corrosion was not accounted for by localized measurements.

Table 46-Corrosion results of wellhead equipment from observation well no. 1.

<u>Quantity</u>	<u>Description</u>	<u>Condition</u>
1	Tubing Bnt, K, 2-7/8, 6 5M, 2½ 5M Std Top, Inconel clad bore, Type II LA NACE	Good - Minimum pits and corrosion in bore area; no other visual damage
2	Graygate, API Flg, 2-9/16 5M, B, 2½ 5M Flg ends, 17-4 PH Internals, Inconel clad bore NACE	Good - No substantial pitting or corrosion in bore areas. No visual damage.
1	Graygate, API Flg, 2-9/16 5M B, 2½ 5M Flg ends, 17-4 PH Internals, NACE w/Inconel clad bore w/PAll Actuator	Good - No substantial pitting or corrosion in bore areas. No visual defects.
1	Graygate, API Flg, 2-1/6 5M, B, 2 5M Flg ends, 17-4 PH Internals, LA NACE w/Inconel clad bore	Good - No substantial pitting or corrosion in bore areas. No visual damage.
1	Choke, 8746 Adj, 5M, 2 5M, Studded Inledt & Outlet, AISI 630 SS NACE	Good - No substantial pitting or corrosion in bore areas.
1	Lubricator Adapter, L, 2½ 5M, 2½ 5M Flg Btm 2-7/8 OD EU8RD lift thd, w/Blanking plug ½ IP Tap, w/Inconel clad ring grove, Type I	Good - No substantial pitting or corrosion. No visual damage.
1	Tee, Studded, 2½ x 2 5M, AISI 630SS	Good - No substantial pitting or corrosion in bore areas. No visual damage.
1	Flange, BW, 2 5M, 2Sch80, Type II LA NACE, w/Inconel clad ring groove	Good - No substantial pitting or corrosion. No visual damage.

